AD

USAAVLABS TECHNICAL REPORT 67-61A

GENERAL METHOD FOR DETERMINING THE AERODYNAMIC CHARACTERISTICS OF FAN-IN-WING CONFIGURATIONS

VOLUME I
THEORY AND APPLICATION

By

P. E. Rubbert
G. R. Saaris
M. B. Scholey
N. M. Standen
R. E. Wallace

December 1967

U. S. ARMY AVIATION MATERIEL LABORATORIES
FORT EUSTIS, VIRGINIA

CONTRACT DA 44-177-AMC-323(T)

THE BOEING COMPANY
RENTON, WASHINGTON

Disclaimers

The findings in this report are not to be construed as an official Department of the Army position unless so designated by other authorized documents.

When Government drawings, specifications, or other data are used for any purpose other than in connection with a definitely related Government procurement operation, the United States Government thereby incurs no responsibility nor any obligation whatsoever; and the fact that the Government may have formulated, furnished, or in any way supplied the said drawings, specifications, or other data is not to be regarded by implication or otherwise as in any manner licensing the holder or any other person or corporation, or conveying any rights or permission, to manufacture, use, or sell any patented invention that may in any way be related thereto.

Disposition Instructions

Destroy this report when no longer needed. Do not return it to originator.

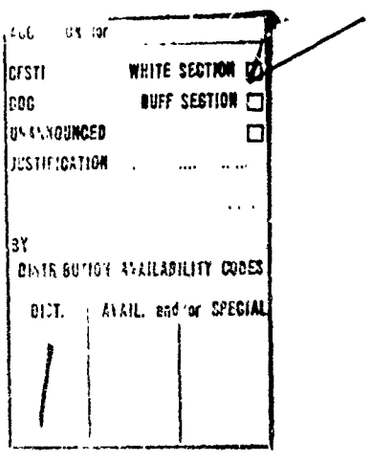

DEPARTMENT OF THE ARMY
U S ARMY AVIATION MATERIEL LABORATORIES
FORT EUSTIS, VIRGINIA 23604

This report has been reviewed by the U. S. Army Aviation Materiel Laboratories and is considered to be technically sound.

A study was made of the inlet flow to a fan-in-wing configuration as a function of various flow parameters as influenced by the geometry of the wing and of the fan inlet under various flight conditions. The theoretical results were compared with the available experimental data. The resulting computer program is a powerful tool for use in investigating not only fan-in-wing configurations but arbitrary wings with and without fans and with and without flaps.

The report is published for the dissemination of information and the stimulation of ideas in the application of theoretical aerodynamics.

Task 1F125901A14234
Contract DA 44-177-AMC-323(T)
USAAVLABS Technical Report 67-61A
December 1967

A GENERAL METHOD FOR DETERMINING THE AERODYNAMIC CHARACTERISTICS OF FAN-IN-WING CONFIGURATIONS

Volume I
Theory and Application

Final Report

By

P. E. Rubbert
G. R. Saaris
M. B. Scholey
N. M. Standen
R. E. Wallace

Prepared by

The Boeing Company
Renton, Washington

for

U. S. ARMY AVIATION MATERIEL LABORATORIES
FORT EUSTIS, VIRGINIA

SUMMARY

A general method has been developed to determine the aerodynamic characteristics of fan-in-wing configurations by means of incompressible potential-flow theory. The method is applicable to wings, flapped or unflapped, and to a wide variety of other potential-flow boundary-value problems. Arbitrary wing and inlet geometry, fan inflow distribution, thrust vectoring, angle of attack, angle of yaw, and flight speeds from hover through transition can be treated. The theoretical model is completely three dimensional, with no linearization of boundary conditions. The calculated results include pressure distributions, lift, induced drag and side force, pitching moment, rolling moment, and yawing moment. The method has been programed for use with a high-speed digital computer.

The numerical potential-flow solution is obtained with source and vortex distributions on the boundary surfaces. The representation is composed of small, constant-strength source sheet panels distributed over the exterior wing surfaces, internal vortex filaments that emanate from the wing trailing edge to provide circulation and to produce the trailing vortex sheet, and a vortex lattice across the fan face and along the periphery of the fan efflux. Source and vortex strengths are obtained by satisfying boundary conditions at a finite number of points on the boundary surfaces. From these, velocities and surface pressures, and flow properties at selected points in the flow field are found. Internal fan loads, based on pressure and momentum relations across the fan and an assumed fan exit flow distribution, are added to integrated wing surface pressures to determine total forces and moments on a fan-in-wing configuration.

Streamline paths on the wing and inlet surface are computed from the potential-flow surface velocity distribution. A boundary-layer theory is included to investigate the boundary layer along streamlines, particularly in the inlet region. The boundary-layer computations along streamlines include the three-dimensional effect of streamline divergence across wing surfaces. The aerodynamic effects of boundary-layer thickening or separation on the forces, moments, or pressure distributions, however, are not included in the theory.

Results of the method were compared with wind-tunnel data obtained by NASA on a fan-in-wing model having a fuselage and a single lift fan in each wing. Comparisons of results with NASA data were made in the flapped configuration with the fans operational at two thrust vector angles, and also with the inlets covered. Good agreement was found between the theoretical solution and experimental force data for both 0- and 30-deg deflected flaps with the inlets covered. Pitching moments did not agree as well, probably because of the fuselage on the NASA model, which was not included in the theoretical calculation.

Results with the fan thrust vectored and unvectored showed that the theoretical force calculations depend strongly on the fan forces, which were obtained from assumed inflow and fan exit flow distributions. The two inflow distributions investigated, uniform and with a sinusoidal variation around the fan face, produced values for lift below and above the experimental data, respectively. The

total inflow in both cases was the same, and the difference in lift between the two cases was due primarily to computed fan forces.

Comparisons of theoretical and experimental pressure distributions with the lift fans operational were in qualitative agreement. The most noticeable difference was in the overall pressure level everywhere on the wing, even near the tip regions. No experimental boundary-layer data were available for comparison with this model.

The results obtained to date indicate that the present method is a powerful tool for the evaluation of fan-in-wing aerodynamic characteristics. Its usefulness can be further extended by supplementing it with experimental data. Experimental determination of the fan thrust would eliminate the assumptions currently used and would lead to more accurate total force predictions. Entrainment along the fan efflux can also be simulated with this model if the entrainment distribution is known. Experimental determination of such entrainment could provide the required information.

FOREWORD

Development of the fan-in-wing analysis method described in this report was performed by the Commercial Airplane Division, Aerodynamic Research Unit of The Boeing Company, under contract to the U. S. Army Aviation Materiel Laboratories [Contract DA 44-177-AMC-323(T)]. The method is based on previous Boeing-sponsored research concerning the theoretical analysis of V/STOL wing configurations (References 1 and 2). It also incorporates many features developed by researchers at Douglas Aircraft Company (Reference 3) under Navy contract.

Volume I of this report presents the theory and application of the method and includes an explanation of the program usage. Volume II gives a detailed description of the computer program.

TABLE OF CONTENTS

TABLE OF CONTENTS (Continued)

LIST OF ILLUSTRATIONS

LIST OF ILLUSTRATIONS (Continued)

LIST OF ILLUSTRATIONS (Continued)

LIST OF ILLUSTRATIONS (Continued)

LIST OF ILLUSTRATIONS (Continued)

LIST OF ILLUSTRATIONS (Continued)

LIST OF SYMBOLS

A	Area of a source panel
A_{ij}	Influence coefficient of the j^{th} singularity at the i^{th} boundary point
a	Velocity derivative along a streamline at stagnation
B_i	Normal component of the disturbance velocity at the i^{th} boundary point
$\vec{b}$	Unit vector in panel plane normal to velocity
C_D	Drag coefficient
$\vec{C}_F$	Force coefficient
$C_{F_x}, C_{F_y}, C_{F_z}$	Components of the force coefficient parallel to the reference coordinate axes
C_f	Skin friction coefficient
C_{ij}	Influence coefficient
C_L	Lift coefficient
$\vec{C}_m$	Moment coefficient
$C_{m_x}, C_{m_y}, C_{m_z}$	Components of the moment coefficient parallel to the reference coordinate axes
C_p	Pressure coefficient
C_{p_c}	Centerbody base pressure coefficient
C_{p_e}	Fan exit pressure coefficient
C_S	Side force coefficient
c	Chord length
D	Displacement distance of panel corner
D_{fan}	Fan exit diameter
d	Length or distance
d_c	Diameter of centerbody

d_e	Length of the e^{th} panel edge
$\vec{F}$	Force vector
H	Boundary-layer shape factor, δ^*/θ
h	Distance between barrier and exit planes
$I_\eta, I_{\eta\xi}, I_\xi$	Second moments of inertia of a source panel about origin of a panel coordinate system
$\vec{i}, \vec{j}, \vec{k}$	Unit vectors parallel to the reference coordinate axes
K_1	Streamline divergence factor in plane of the surface
L_r	Reference length for moment coefficient
ℓ	Length or distance
$\vec{M}$	Moment vector
m	Source strength (per unit area)
$\vec{n}$	Outward unit normal vector to a surface
$\vec{n}_b$	Unit vector directed upward along a fan axis
p	Static pressure
$\vec{q}$	Dimensional velocity
R, Z, θ	Cylindrical coordinates
R_∞	Reyonlds number per foot
r	Radial distance; distance from a point to a surface
$\vec{r}$	Position vector measured from the moment center
$\vec{r}_c$	Vector from the moment center to the center of the fan exit
S	Surface
$\tilde{S}$	Exterior surface excluding wake
S_b	Barrier area (cf. Figure 12)
S_d	Surface represented by doublets
S_i'	Interior surface not adjacent to $\tilde{S}$

S_r	Planform reference area
S_s	Surface represented by sources
S_u'	Upper surface of S_l'
s	Distance along a streamline; segment lengths along the efflux tube centerline
t	Length of the maximum diagonal of a source panel
$\vec{t}$	Unit vector in fan efflux direction
U_R	Reference velocity
U_s	Specified inflow velocity, $\vec{V} \cdot \vec{n}$
$\vec{U}_\infty$	Free-stream velocity
$\vec{V} = \frac{\vec{q}}{U_\infty}, \frac{\vec{q}}{U_R}$	Nondimensional velocity
V_j	Volume flow into inlet per unit time divided by the inlet area (the inlet area is defined as the area of the fan face, and does not include the centerbody area)
W	Weight of a bound multihorseshoe vortex segment
x, y, z	Cartesian coordinates
x_b, y_b, z_b	Coordinates of the intersection of a fan axis with a barrier plane

Greek Symbols

α	Angle of attack in degrees
β	Streamline divergence angle measured along orthogonal trajectory (cf. Figure 8); thrust vector angle (cf. Figure 31)
Γ	Strength of line vortex
γ	Vorticity density; angular deflection of a sheared coordinate system
Δ	Increment or difference in a quantity
δ, ϵ	Small distance
δ^*	Boundary-layer displacement thickness
η	Semispan fraction, 2y/semispan

θ	Boundary-layer displacement thickness; angle around a fan
μ	U_∞ divided by fan tip speed; doublet strength per unit area
ξ, η, ζ	Local coordinate system
ρ	Fluid density
σ	Singularity strength
Φ	Velocity potential
φ	Disturbance velocity potential
ψ	Yaw angle in degrees
∇	Gradient operator

Superscripts

$()'$	Refers to the flow interior to a wing

Subscripts

b	Barrier; barrier center
bo	Point in the plane of a source panel used for calculation of the streamline divergence factor
bp	Boundary point
c	Centerbody; circumferential
e	Fan exit
I	Inboard
O	Outboard
	An arbitrary point in space
r	Reference quantities used to define the force and moment coefficients; radial direction
t	Directed in the plane of the surface normal to a streamline
te	Wing trailing edge
w	Wake

1. INTRODUCTION

Many investigators have attempted to analyze the flow field about fan-in-wing configurations. One of the more effective approaches has been the "vortex-lattice" method (References 1 and 2), which employs a vortex network to represent the wing, its trailing vorticity, and the boundary of the fan efflux. This method gives a nonplanar, three-dimensional, potential-flow representation, which is essential for a proper fan-in-wing theoretical model.

The promising results achieved earlier with the vortex lattice led to a proposed extension of this numerical procedure to provide the necessary detailed representation of thick-wing configurations, which was not included in the earlier model. The method described in this report utilizes source sheets on the exterior surface geometry, interior vortex distributions that emanate from the wing to produce lift and provide the trailing vortices, and a vortex-lattice representation of the fan face and jet efflux surfaces. Neumann boundary conditions are imposed on the wing and efflux tube surfaces and on the fan face. A method of constructing streamlines from the surface velocity field was developed for use in approximating the boundary-layer characteristics on a fan-in-wing configuration. The pressure distribution and streamline divergence given by the potential-flow solution are used in a turbulent boundary-layer theory incorporating the three-dimensional effect of streamline divergence.

The method described herein provides a substantial amount of information concerning the integrated fan-in-wing aerodynamic performance. The completeness of the theoretical model allows an accurate representation of wing and inlet geometry, including trailing-edge flaps, fan pressure ratio, efflux tube trajectory, and forward velocity. The influence of an arbitrarily specified unsymmetrical fan inflow distribution can be examined. Although an analysis of the fan blade characteristics or inlet guide vanes necessary to give this inflow distribution is beyond the scope of the present method, the current theory is valuable for determining the effect of inflow distribution on the pressure distribution on the inlet lip, an area prone to boundary-layer separation. The included boundary-layer theory, while incapable of accurately predicting boundary-layer separation, is very useful for indicating relative boundary-layer conditions on different inlet geometries, thus revealing where boundary-layer problems are likely to occur.

This method has proved feasible for computers with sufficient capacity to solve the large number of linear simultaneous equations required for accurate geometric representation of the configuration. The resulting computer program is divided into three basic packages called a geometry program, a potential-flow program, and a boundary-layer program. To enhance the versatility of the total computer package, the outputs of the first and second programs are directly usable in the second and third programs, respectively, or supplementary information or interpretation may be provided between programs. The computer time needed to solve a problem is a direct function of the number of singularities used in representing a configuration. For example, a simple wing solution with 500 singularities can be obtained in 10 minutes, whereas a sophisticated fan-in-wing problem, such as demonstrated in this report for a

NASA wind-tunnel model, may require an hour or more of central processor time on a CDC 6600 digital computer.

Volume I of this report describes the details of the aerodynamic theory underlying the computer program, shows how the method may be used in typical cases, and validates the method by comparison with experimental data. It is self-sufficient for instructing a program user. The second half of this report (Volume II, Reference 4) provides the details necessary for understanding the computer programing.

The aerodynamic work presented in these reports was accomplished by members of the Aerodynamic Research Unit, and the programing and checkout were accomplished by members of the Systems and Administrative Computing Staff, all of The Boeing Company, Commercial Airplane Division.

2. THEORY

2.1 DEVELOPMENT OF THE THEORETICAL MODEL

The primary goal of this investigation has been to develop a theory and computer program to predict the flow field about a finite wing containing an embedded lift fan. For this purpose, a theoretical model has been developed with the capability of simulating the effects of arbitrary wing and inlet geometry, angle of attack and yaw, forward velocity throughout the transition range, fan pressure ratio and mass flow, unsymmetrical inflow distributions at the fan face, and fan exit flow, including vectoring. The resulting theory predicts wing and inlet surface pressures, total lift, drag and side forces, including fan thrust, and moments about the three axes. Boundary-layer separation characteristics upstream of the fan are also calculated, but the effect of separated flow on forces, moments, and pressures is not included.

Flow fields about a fan-in-wing are adequately characterized by inviscid, incompressible potential flow everywhere except in the boundary layer adjacent to the wing surfaces, the trailing vortex sheets, the interior of the efflux emerging from the jets, and the region of turbulent mixing between the jet efflux and the surrounding potential flow. A theoretical model for this flow has been developed to take advantage of the powerful computational methods available for potential flow, while retaining the essential features of the complex viscous and rotational flow regions, as described below.

It is well known that the displacement effect of the boundary layer on the outer potential flow is usually small and can be neglected. Therefore, the potential flow must satisfy the usual Neumann boundary condition on the body surface. The behavior of the boundary layer itself is controlled by the static pressure distribution imposed on it by the surrounding potential flow. This representation, which is used in the present analysis, is normally an excellent approximation except in regions of extensive separated flow. Regions most likely to experience separation are the lower wing surface aft of the jet efflux, the upper surface of trailing-edge flaps without slots or boundary-layer control, and the inlet lip. The boundary-layer analysis will aid in determining regions of the inlet at which separation is likely to occur. However, the effects of separation are difficult to assess, and no attempt has been made in the current theory to do so.

The trailing vorticity shed by a lifting surface must also be excluded from the potential field. This has been done by enclosing the vorticity in an infinitely thin envelope across which there exists a discontinuity in the velocity potential. The position of this trailing sheet in real flow is controlled by the requirement that it be aligned with the local velocity. This nonlinear problem, which is beyond the scope of the present work, has been replaced by the usual approximation of an assumed location of the trailing sheet. The direction of the vorticity in the sheet must also be assumed. It is usual to suppose that it is directed longitudinally such that the discontinuity in potential across the sheet is a function only of the lateral or spanwise coordinate.

Previous experience with lifting wing theories using these assumptions (Reference 2) indicates that they are completely satisfactory for determination of the forces and pressure distributions on wings with moderately deflected flaps. The solution becomes sensitive to the assumed location of the trailing sheet only when large flap deflections (≥60 degrees) are encountered. In such cases, it is recommended that recourse to experimental data be made to ensure that the trailing sheet is properly oriented. The path of the trailing sheet is also somewhat questionable at very low forward speeds with large jet velocity ratios. However, in this case the strength of the trailing vortex sheet is usually small, and deviations from its true path will not significantly affect results.

A complete theoretical analysis of the turbulent mixing region and interior flow of the jet efflux is virtually impossible. In the present theory, the turbulent jet boundary is replaced by one along which Neumann boundary conditions are imposed. The exterior flow thus sees the efflux jet as a solid cylindrical surface in the flow field. The consequences of this representation of the efflux flow are twofold. One consequence is that the trajectory of the efflux tube is unknown, since in real flow this is strongly influenced by turbulent mixing phenomena. A method of obtaining an approximation to the jet trajectory is to assign an empirical drag coefficient to the jet tube and to compute the balance between the drag of the jet and the change in the direction of its momentum. Another method, which has been previously used at Boeing with excellent results, is to assume a jet trajectory based on experimental data of a jet emerging into a crossflow. This latter method has been used in the present analysis in view of the favorable results obtained previously for fan-in-wing studies (Reference 1). Also, it was concluded from this previous work that changing the trajectory of the jet for three-dimensional flow has relatively little influence on the flow pattern about the wing.

The other consequence of this type of jet efflux representation is that the flow near the lower surface of the wing aft of the jet, composed of viscous separation and mixing from the jet in forward flight, cannot be simulated. The effect of viscous entrainment on the jet boundary has also been neglected. These may affect the forces and moments on the wing and, in particular, the pressure distribution on the lower wing surface.

To complete the development of a properly posed boundary-value problem for the exterior potential flow, the inflow distribution must be specified on some plane across the inlet, commonly at the fan or compressor face. This inflow distribution is actually controlled by the interaction between the fan and the oncoming air, which cannot be predicted theoretically. Therefore, typical inflow distributions based on experiment must be used. One advantage of this treatment is that it allows a study of the effect of different inflow distributions on the inlet surface pressure distribution, which determines the boundary-layer separation characteristics in this critical area.

In summary, these approximations reduce the outer potential flow to a boundary-value problem governed by Laplace's equation as sketched in Figure 1. The flow everywhere outside the closed contour representing the wing, trailing vortex sheet, fan face, and jet efflux tube is considered incompressible and inviscid. Neumann boundary conditions are imposed on the actual nonplanar

wing surface and on the boundary of the jet efflux. The fan or compressor face is treated in a similar manner with a specified inflow distribution into the fan. The location of the efflux cube and trailing vortex sheet must be assumed, together with the direction of the vorticity ir the sheet.

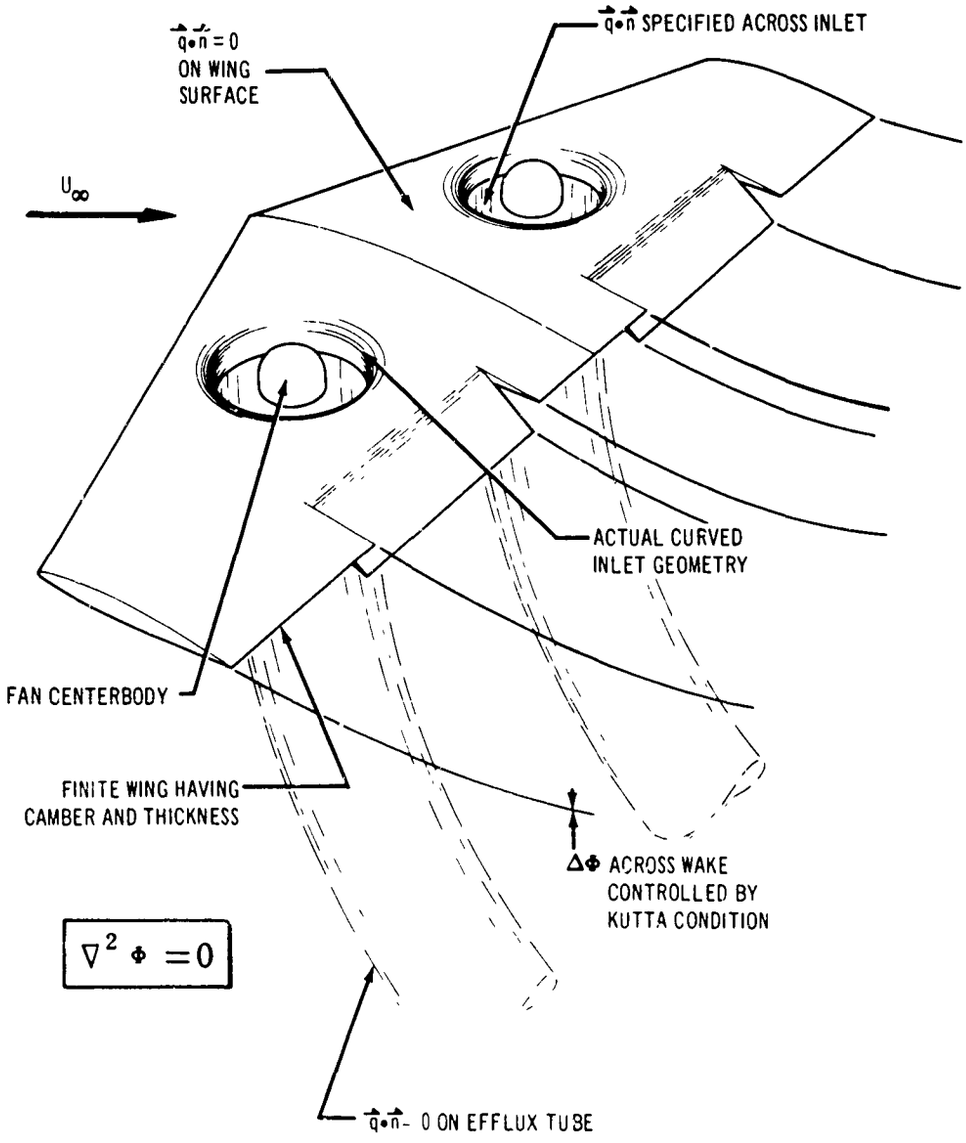

Figure 1. Typical Boundary-Value Problem.

This theoretical model represents a formidable boundary-value problem due to the complex three-dimensional geometry, but it cannot be further simplified without seriously compromising results. The outstanding asset of this theoretical model is its ability to represent arbitrary inlet and wing geometries, including fan centerbody, trailing-edge flaps, finite span effects, and general airfoil sections. The effects of arbitrary jet velocity ratios, thrust vectoring, and yawed and hovering flight are included. The solution produces surface pressure or velocity distributions controlling the behavior of the boundary layer. A three-dimensional boundary-layer theory is then used to predict the areas on the inlet surface where separation can be expected to occur.

2.2 POTENTIAL-FLOW THEORY

The foundation of the basic theory used to formulate the potential-flow problem is classical and may be found in many texts. The presentation given here is taken mainly from Lamb (Reference 5). The flow is governed by Laplace's equation,

$$\nabla^2 \Phi = 0 \tag{1}$$

subject to the proper boundary conditions prescribed on closed boundaries. Classically, these boundary conditions should be one of the following:

- The Neumann problem, in which $\partial\Phi/\partial n$ is given
- The Dirichlet problem, in which the value of Φ itself is given
- The mixed (Poincaré) problem, in which a linear combination of Φ and $\partial\Phi/\partial n$ is specified

The present analysis is concerned with three typically different types of boundaries encountered with nonlifting wings, lifting wings, and fan-in-wing configurations. For nonlifting wings, the closed boundary surrounding the outer flow of interest consists of the exterior surface of the wing and the boundary at infinity at which free-stream conditions are specified. The lifting wing case differs in that the boundary on the exterior surface of the wing must be extended to enclose also the trailing vortex sheet, thus rendering the flow field outside this boundary everywhere irrotational. The addition of a fan in the wing requires that the boundary on the exterior wing surface be extended to enclose also the exterior surface of the efflux tube and the fan face.

If a hypothetical flow field interior to the wing is also considered, an interior boundary can be defined on which the boundary conditions governing the interior flow are applied. The specification of boundary conditions on only the exterior boundaries is sufficient to produce a unique solution for the exterior flow field of interest. As will be seen below, however, different interior boundaries and boundary conditions may be defined to produce solutions that differ only in the interior of the body and that are of no physical consequence. This device of considering the interior flow field as well as the exterior one will be used to formulate the problem in a manner particularly suited to numerical analysis.

It is convenient to write Φ in terms of a disturbance potential φ, defined as

$$\Phi = \vec{U}_\infty \cdot [\vec{i}x + \vec{j}y + \vec{k}z] + \varphi \tag{2}$$

where φ also satisfies Laplace's equation

$$\nabla^2 \varphi = 0 \tag{3}$$

The boundary conditions controlling the external φ field are the following:

$$\varphi \to 0 \text{ as } x, y, z \to \infty \tag{4}$$

On the exterior surface of the wing, efflux tube, and centerbody, the velocity must be parallel to the surface. This requirement is satisfied when

$$\left.\frac{\partial \varphi}{\partial n}\right|_S = -\vec{n} \cdot \vec{U}_\infty \tag{5}$$

where $\vec{n}$ is the unit outward normal to the surface S. A desired inflow distribution, $\vec{q} \cdot \vec{n}$ at the fan face, is achieved by specifying that

$$\left.\frac{\partial \varphi}{\partial n}\right|_{\text{fan}} = -\vec{n} \cdot (\vec{U}_\infty - \vec{q}) \tag{6}$$

The assumptions concerning the direction of the vorticity in the wake imply that

$$\Delta\varphi_w \equiv \varphi_{\substack{\text{wake} \\ \text{upper} \\ \text{surface}}} - \varphi_{\substack{\text{wake} \\ \text{lower} \\ \text{surface}}} = \Delta\varphi_{te} \tag{7}$$

where $\Delta\varphi_{te}$ is the potential jump at the wing trailing edge. These, together with the Kutta condition, are sufficient to ensure a properly posed boundary-value problem for φ.

The solution to this boundary-value problem is found by expressing φ in terms of surface distributions of source and doublet singularities. Imposing the boundary conditions produces an integral equation for the singularity strengths, which is solved numerically. From Green's theorem, it follows that any solution of Laplace's equation can be expressed in the form (Reference 5)

$$\varphi_p = -\frac{1}{4\pi} \iint_S \frac{1}{r} \frac{\partial \varphi}{\partial n}\, dS + \frac{1}{4\pi} \iint_S \varphi \frac{\partial}{\partial n}\left(\frac{1}{r}\right) dS \tag{8}$$

where φ_p = perturbation potential at an arbitrary point p in the external flow field

S = exterior boundary surfaces (wing, efflux tube, fan face, wake surfaces)

n = outward normal to the surface S

r = distance from the arbitrary point p to the surface S

Figure 2 displays the nomenclature used above. The first term on the right side of Equation (8) can be interpreted as a distribution of sources on S ($\varphi_{source} = -1/4\pi r$), while the last term represents a distribution of doublets ($\varphi_{doublet} = \partial/\partial n\,[1/4\pi r]$) with axes normal to the surface. The source and doublet strengths (density per unit area) are $\partial\varphi/\partial n$ and φ, respectively. This shows that any solution can be expressed simply in terms of surface doublet and source distributions. However, as appears below, this representation is not unique and is only one of an infinite number of surface distributions that will give the same value of φ throughout the exterior flow field.

If the interior flow field φ' is considered (see Figure 2), it can be shown from Green's theorem (Reference 5) that the interior potential φ' satisfies the relationship

$$0 = -\frac{1}{4\pi}\iint_{S'}\frac{1}{r}\frac{\partial\varphi'}{\partial n'}\,dS + \frac{1}{4\pi}\iint_{S'}\varphi'\,\frac{\partial}{\partial n'}\left(\frac{1}{r}\right)dS \qquad (9)$$

where r is the distance from S' to the arbitrary point p, which is external to the interior flow field φ'. In the limit, $S \rightarrow S'$ and $\partial/\partial n = -\partial/\partial n'$, and Equations (8) and (9) are added to obtain

$$\varphi_p = -\frac{1}{4\pi}\iint_{S_{\substack{\text{wing,}\\ \text{fan,}\\ \text{tube}}}}\frac{1}{r}\left(\frac{\partial\varphi}{\partial n}+\frac{\partial\varphi'}{\partial n'}\right)dS + \frac{1}{4\pi}\iint_{S_{\substack{\text{wing,}\\ \text{fan,}\\ \text{tube}}}}(\varphi-\varphi')\,\frac{\partial}{\partial n}\left(\frac{1}{r}\right)dS$$

$$-\frac{1}{4\pi}\iint_{S_{wake}}\frac{1}{r}\,\frac{\partial\varphi}{\partial n} + \frac{1}{4\pi}\iint_{S_{wake}}\varphi\,\frac{\partial}{\partial n}\left(\frac{1}{r}\right)dS \qquad (10)$$

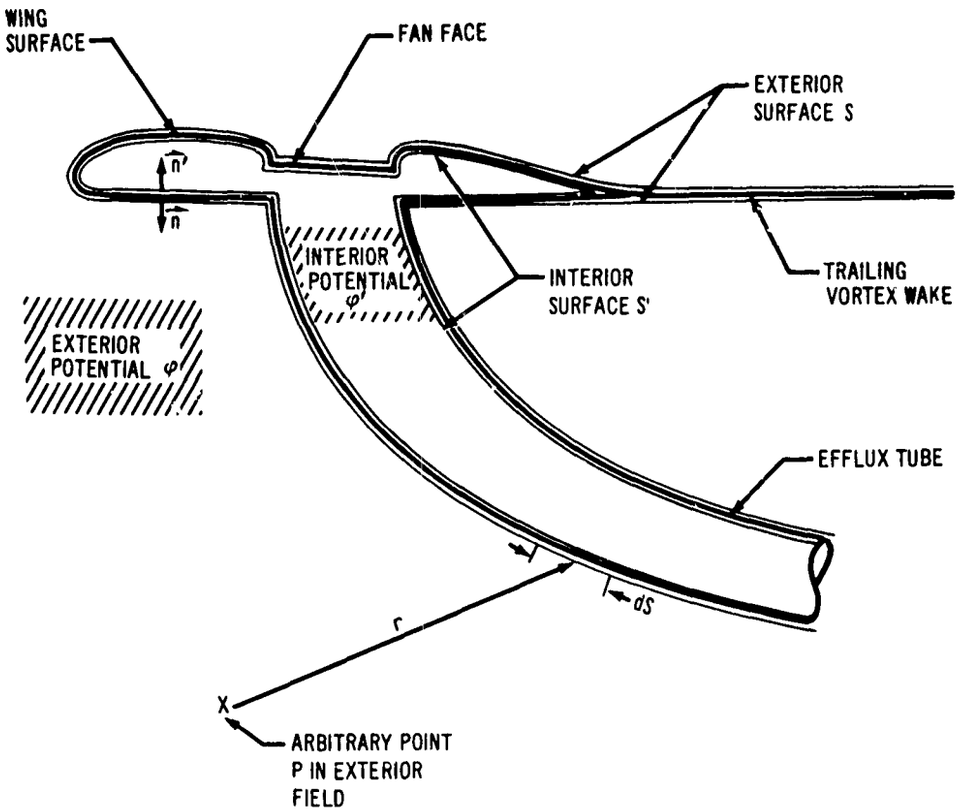

Figure 2. Boundaries of Fan-in-Wing Problem.

Since the normal velocity component must be continuous through the wake, the first integral over the wake is identically zero. The last wake integral can be converted to an integral over the upper surface of the wake only by noting that

$$\frac{\partial}{\partial n}\left(\frac{1}{r}\right)\Bigg|_{\substack{\text{upper}\\ \text{wake}\\ \text{surface}}} = -\frac{\partial}{\partial n}\left(\frac{1}{r}\right)\Bigg|_{\substack{\text{lower}\\ \text{wake}\\ \text{surface}}} \tag{11}$$

With these changes, the expression for the exterior potential field becomes

$$\varphi_p = -\frac{1}{4\pi}\iint_{\tilde{S}} \frac{1}{r}\left(\frac{\partial\varphi}{\partial n} + \frac{\partial\varphi'}{\partial n'}\right) dS + \frac{1}{4\pi}\iint_{\tilde{S}} (\varphi - \varphi')\,\frac{\partial}{\partial n}\left(\frac{1}{r}\right) dS$$

$$+ \frac{1}{4\pi}\iint_{S_w} \Delta\varphi_w\,\frac{\partial}{\partial n}\left(\frac{1}{r}\right) dS \qquad (12)$$

where $\tilde{S}$ = that portion of S not including the wake

S_w = upper surface only of the wake

$\Delta\varphi_w$ = jump in potential across the wake

Examining Equation (12), it is apparent that the surface $\tilde{S}$ can contain both source and doublet distributions, whereas S_w must be represented by a doublet sheet only. The function φ' is determined by the boundary conditions φ' or $\partial\varphi'/\partial n'$ imposed on the interior flow, which are yet at our disposal. Different choices for these interior boundary conditions will produce different surface singularity distributions giving the same exterior φ field. Once the interior boundary conditions are fixed, however, the singularity distribution becomes unique.

As a first example of one particular singularity distribution, consider an interior flow satisfying the boundary condition $\varphi' = \varphi$ on $\tilde{S}$. The tangential velocities on the two sides of $\tilde{S}$ are then continuous, but the normal velocities are discontinuous. With this choice, Equation (12) gives

$$\varphi_p = -\frac{1}{4\pi}\iint_{\tilde{S}} \frac{1}{r}\left(\frac{\partial\varphi}{\partial n} + \frac{\partial\varphi'}{\partial n'}\right) dS + \frac{1}{4\pi}\iint_{S_w} \Delta\varphi_w\,\frac{\partial}{\partial n}\left(\frac{1}{r}\right) dS \qquad (13)$$

where the first integral can be interpreted as a distribution of sources alone on $\tilde{S}$ of strength

$$\left(\frac{\partial\varphi}{\partial n} + \frac{\partial\varphi'}{\partial n'}\right) \qquad (14)$$

Doublets appear only in the wake.

Alternately, choosing $\partial\varphi'/\partial n = \partial\varphi/\partial n$ on $\tilde{S}$ leads to a flow having a continuous normal velocity across $\tilde{S}$, with the tangential velocity being discontinuous. For this case, Equation (12) gives

$$\varphi_p = \frac{1}{4\pi}\iint_{\tilde{S}} (\varphi - \varphi') \frac{\partial}{\partial n}\left(\frac{1}{r}\right) dS + \frac{1}{4\pi}\iint_{S_w} \Delta\varphi_w \frac{\partial}{\partial n}\left(\frac{1}{r}\right) dS \qquad (15)$$

demonstrating that the potential can also be expressed in terms of doublet sheets alone on the boundary surfaces.

It can be shown that both of the above representations are unique (Reference 5), except for an additive constant in the doublet strength on $\tilde{S}$ in Equation (15), whereas the representation of Equation (8) is indeterminate. This uniqueness resulted from fixing the boundary conditions on the interior flow as well as on the exterior flow.

The particular choices for the interior boundary conditions made in obtaining Equations (13) and (15) are completely equivalent to choosing a particular type of singularity on the surface. Choosing $\varphi' = \varphi$ on some portion of $\tilde{S}$ guarantees that sources only will appear on that part of the surface, while the choice $\partial\varphi'/\partial n = \partial\varphi/\partial n$ results in doublets alone. Hence, as an alternative to selecting boundary conditions for the interior flow, one can choose the type of singularity distribution to be placed on $\tilde{S}$ and be assured of a unique representation. The most important restriction seems to be that if both sources and doublets are chosen to represent the same part of $\tilde{S}$, a linear relationship between their strengths must be established. This corresponds to the choice of mixed (Poincaré) boundary conditions for the interior flow.

For the problems under consideration, it is convenient to restrict the choice of singularity distributions on $\tilde{S}$ to one type on any part. Thus, sources may be used on some parts of $\tilde{S}$, with doublets on the remainder, but the two are not superimposed. The particular arrangement of singularities used is primarily dictated by the geometry and requirements of the numerical solution procedure. With this restriction, the expression for the potential at any point p in the flow field becomes

$$\varphi_p = -\frac{1}{4\pi}\iint_{S_s} \frac{m(S)}{r} dS + \frac{1}{4\pi}\iint_{S_d} \mu(S) \frac{\partial}{\partial n}\left(\frac{1}{r}\right) dS + \frac{1}{4\pi}\iint_{S_w} \Delta\varphi_w \frac{\partial}{\partial n}\left(\frac{1}{r}\right) dS \qquad (16)$$

where S_s = portion of $\tilde{S}$ containing sources

S_d = portion of $\tilde{S}$ containing doublets

$m(S)$ = source strength per unit area

$\mu(S)$ = doublet strength per unit area

S_w = upper surface of the wake

$\Delta\varphi_w$ = jump in potential across the wake

Once the representation, Equation (16), has been established, the boundary-value problem is solved by constructing an integral equation for the desired singularity strengths, $m(S)$, $\mu(S)$, and $\Delta\varphi_w$, to be solved numerically. This integral equation is constructed by letting the field point p in Equation (16) approach the boundary $\tilde{S}$ and differentiating the equation with respect to the surface normal at p, and is

$$\left.\frac{\partial\varphi}{\partial n}\right|_{\tilde{S}} = -\hat{n}\cdot(\vec{U}_\infty - \vec{q}) = -\frac{1}{4\pi}\frac{\partial}{\partial n}\iint_{S_s}\frac{m(S)}{r}\,dS + \frac{1}{4\pi}\frac{\partial}{\partial n}\iint_{S_d}\mu(S)\,\frac{\partial}{\partial n}\left(\frac{1}{r}\right)dS$$

$$+\frac{1}{4\pi}\frac{\partial}{\partial n}\iint_{S_w}\Delta\varphi_{te}\,\frac{\partial}{\partial n}\left(\frac{1}{r}\right)dS \qquad (17)$$

where Equation (7) has been used to replace $\Delta\varphi_w$ by its value at the wing trailing edge. The left-hand side of Equation (17) is known at every point on $\tilde{S}$ from the boundary conditions, Equations (5) and (6). In addition, a Kutta condition is imposed at the wing trailing edge by the requirement that the velocity a small distance aft of the trailing edge be directed in the plane bisecting the wing trailing edge.

The numerical solution of this integral equation is the subject of Section 3. Once the singularity strengths are found, Equation (16) furnishes the desired flow properties.

There are two restrictions that occur when $\tilde{S}$ is represented by doublets alone. First, if $\tilde{S}$ is a closed surface not extending to infinity, then the doublet-alone representation is valid only if

$$\iint_{\tilde{S}}\vec{q}\cdot\hat{n}\,dS = 0 \qquad (18)$$

If Equation (18) is not satisfied, then there must be sources on some part of $\tilde{S}$ or in the interior. Second, the doublet strength on any closed surface $\tilde{S}$ with the type of boundary conditions imposed is unique within an arbitrary constant. Adding any constant to the doublet strength does not alter the exterior velocity field. Hence, to obtain a unique solution for the integral Equation (17), the doublet sheet strength must be fixed a priori at some point on $\tilde{S}$. The particular singularity distributions used in the present analysis were chosen to avoid these restrictions.

The arrangements of singularities used for various configurations are described in Section 6. The fundamental validity of such arrangements is discussed below.

Nonlifting configurations without trailing velocity are represented by sources alone on the boundary surfaces, which is quite straightforward. The integral Equation (17) is simplified in that only the first term on the right-hand side remains. For lifting wings without fans, part of the singularity distribution consists of sources on the wing surface with a trailing doublet sheet. This by itself is fundamentally acceptable, as shown by Equation (17), but would lead to numerical difficulties. The velocity induced by the trailing doublet sheet alone becomes infinite at the trailing edge. This is clearly seen by recognizing that this trailing sheet is equivalent to a vortex sheet emanating from a concentrated bound vortex at the wing trailing edge. The local velocities close to such a concentrated vortex are very large. To counteract these velocities, the source strength on the surface also must be large near the trailing edge. This causes the numerical difficulty. Maximum numerical accuracy is achieved when the singularity strengths vary smoothly over the surface without becoming excessively large anywhere.

To alleviate this difficulty, an additional interior surface is defined, as sketched in Figure 3. The interior boundary S' now must extend around the new interior surface. Let the portion of S' adjacent to the exterior wing surface be denoted as $\tilde{S}'$ and the portion surrounding the interior surface be S_i'. Equation (9) then becomes

$$0 = -\frac{1}{4\pi}\iint_{\tilde{S}'} \frac{1}{r}\frac{\partial \varphi'}{\partial n'}\,dS + \frac{1}{4\pi}\iint_{\tilde{S}'} \varphi'\frac{\partial}{\partial n'}\left(\frac{1}{r}\right)dS - \frac{1}{4\pi}\iint_{S_i'} \frac{1}{r}\frac{\partial \varphi'}{\partial n'}\,dS$$

$$+ \frac{1}{4\pi}\iint_{S_i'} \varphi'\frac{\partial}{\partial n'}\left(\frac{1}{r}\right)dS \qquad (19)$$

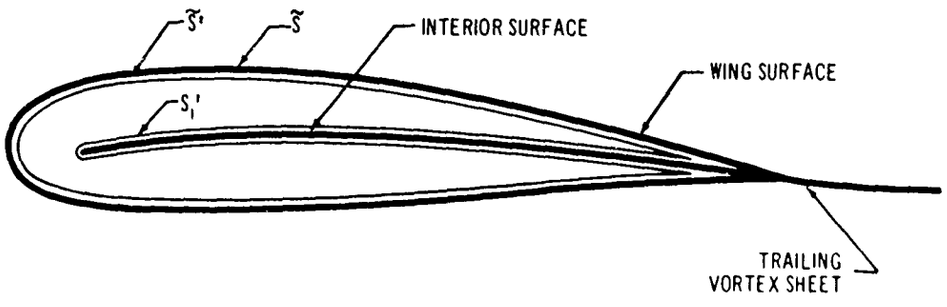

Figure 3. Interior Wing Surfaces.

If Equation (8) is added to this and the steps previously taken are again followed, the expression for the potential at an arbitrary point p in the external flow field becomes

$$\varphi_p = -\frac{1}{4\pi}\iint_{\tilde{S}} \frac{1}{r}\left(\frac{\partial\varphi}{\partial n} + \frac{\partial\varphi'}{\partial n'}\right) dS + \frac{1}{4\pi}\iint_{\tilde{S}} (\varphi - \varphi')\,\frac{\partial}{\partial n}\left(\frac{1}{r}\right) dS$$

$$+ \frac{1}{4\pi}\iint_{S_w} \Delta\varphi_w\,\frac{\partial}{\partial n}\left(\frac{1}{r}\right) dS - \frac{1}{4\pi}\iint_{S_i'} \frac{1}{r}\,\frac{\partial\varphi'}{\partial n'}\, dS + \frac{1}{4\pi}\iint_{S_i'} \varphi'\,\frac{\partial}{\partial n'}\left(\frac{1}{r}\right) dS \qquad (20)$$

Representing the wing surface by sources only, which corresponds to the boundary condition $\varphi' = \varphi$ on $\tilde{S}$, gives

$$\varphi_p = -\frac{1}{4\pi}\iint_{\tilde{S}} m(S)\,\frac{1}{r}\, dS + \frac{1}{4\pi}\iint_{S_w} \Delta\varphi_w\,\frac{\partial}{\partial n}\left(\frac{1}{r}\right) dS$$

$$- \frac{1}{4\pi}\iint_{S_i'} \frac{1}{r}\,\frac{\partial\varphi'}{\partial n'}\, dS + \frac{1}{4\pi}\iint_{S_i'} \varphi'\,\frac{\partial}{\partial n'}\left(\frac{1}{r}\right) dS \qquad (21)$$

The choice of boundary conditions for φ' on S_i' is still available and will be made to eliminate the troublesome infinite velocities induced at the trailing edge. First let the normal velocity be chosen to be continuous across S_i'. Equation (21) then becomes

$$\varphi_p = -\frac{1}{4\pi}\iint_{\tilde{S}} m(S)\,\frac{1}{r}\, dS + \frac{1}{4\pi}\iint_{S_w} \Delta\varphi_w\,\frac{\partial}{\partial n}\left(\frac{1}{r}\right) dS$$

$$+ \frac{1}{4\pi}\iint_{S_u'} \Delta\varphi_i'\,\frac{\partial}{\partial n}\left(\frac{1}{r}\right) dS \qquad (22)$$

where S_u' = upper surface of S_i'

$\Delta\varphi_i'$ = the jump in potential across S_i'

Setting $\Delta\varphi_i' = \Delta\varphi_w$ at the trailing edge eliminates the discontinuity in the doublet sheet strength causing the locally high velocities. Furthermore, $\Delta\varphi_i'$ can be specified over the remainder of S_u so as to minimize the velocity perturbations induced at $\tilde{S}$, resulting in well-behaved source strengths. This is accomplished by specifying that $\Delta\varphi_i'$ decrease by steps toward the front of

the interior surface S_u'. Thus, the fundamental quantities to be determined at any spanwise station remain the source sheet strength on $\tilde{S}$ and the strength of the trailing doublet sheet. The strength of the internal doublet sheet is specified a priori in terms of $\Delta\varphi_{te}$.

A typical example of the doublet sheet strength on S_u' is shown in Figure 4. In cross section, this is equivalent to a number of concentrated bound vortices located at the discontinuities of $\Delta\varphi_i'$. Obviously, this representation can be extended to include an arbitrary number of bound vortices located anywhere in the interior. Their relative strengths must be specified, as only their total strength is determinate from the exterior flow boundary conditions. In practice, the internal vortices, or doublet sheet discontinuities, are placed on the camber surface to keep them remote from the outer wing surface. Their relative strengths are chosen in accordance with the chordwise load distribution anticipated. The resultant surface source strengths then turn out to be well behaved, and good numerical solutions are produced.

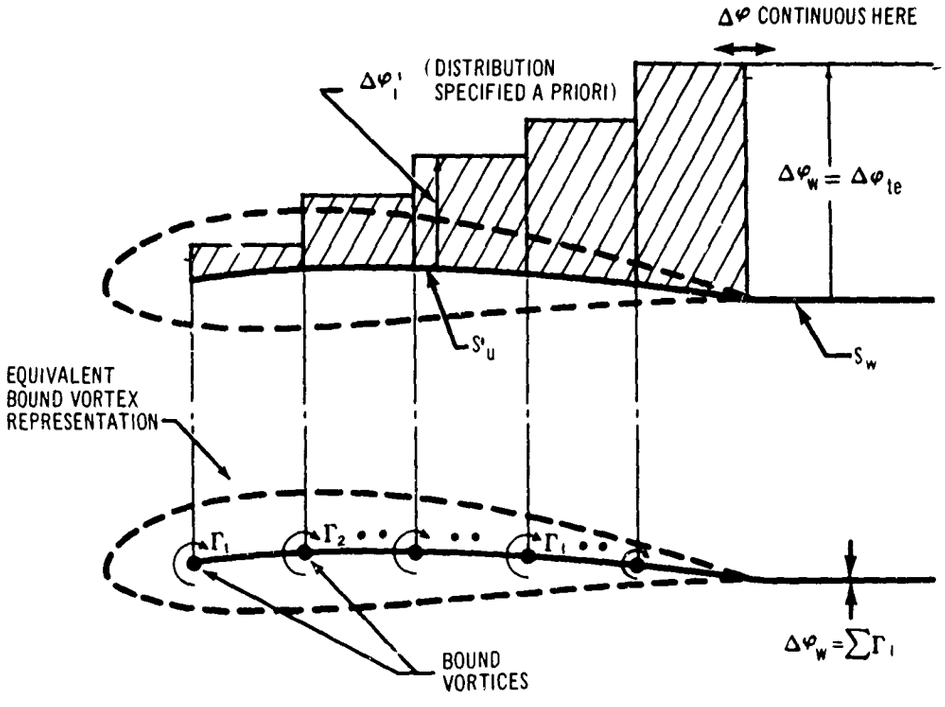

Figure 4. Internal Doublet Strength.

This same device is also used to provide better numerical results with a fan in the wing. Internal lifting systems—the name given to the internal vortex or doublet distributions—are used whenever doublet sheets intersect the wing surface. The surface singularity distribution chosen for a fan-in-wing configuration consists of sources on the wing surface and fan centerbody, and doublet sheets on the trailing wake, efflux tube, and fan face. The internal lifting system associated with the wake is routed behind the fan, as sketched in Figure 5. The internal lifting systems associated with the efflux tube and the fan face surface are usually located on the camber surface around the fan, as shown in Figure 6. It is important that these two systems be superimposed inside the wing, both geometrically and with respect to the specified relative strengths of the internal vortices. The bound vorticity strength of each system is large, but the strengths are of opposite sign and effectively cancel one another if properly superimposed, which minimizes their disturbance at the wing surface.

The forces and moments on a fan-in-wing configuration are given by the exterior surface pressures integrated over the wing plus the forces on the internal fan components. (Profile drag caused by the boundary layer is not included in this analysis.) The exterior surface pressures are furnished by the solution of the potential-flow problem, but the forces on the fan components downstream of the fan face are controlled by the internal flow, which is unknown. To obtain an approximate result for the total force and moment on the configuration, the fan forces are computed from momentum relations based on an assumed flow at the fan exit.

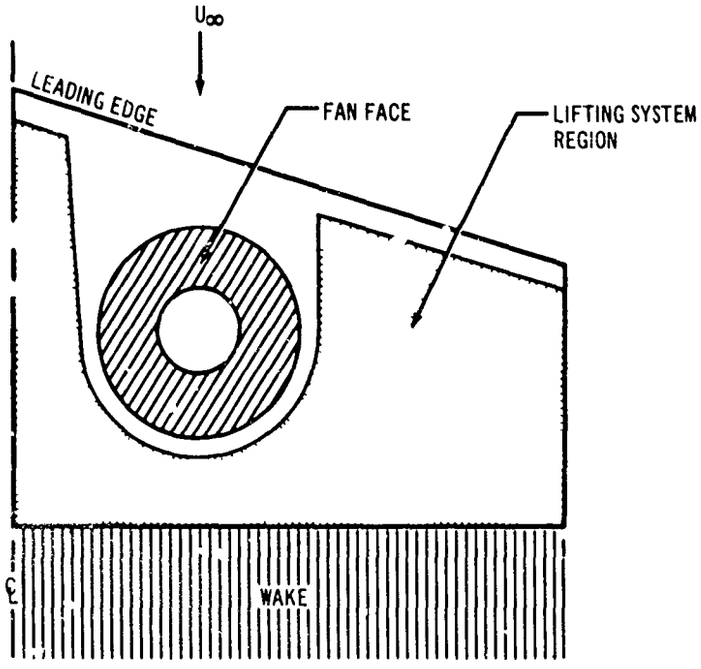

Figure 5. Internal Lifting System Associated Wake.

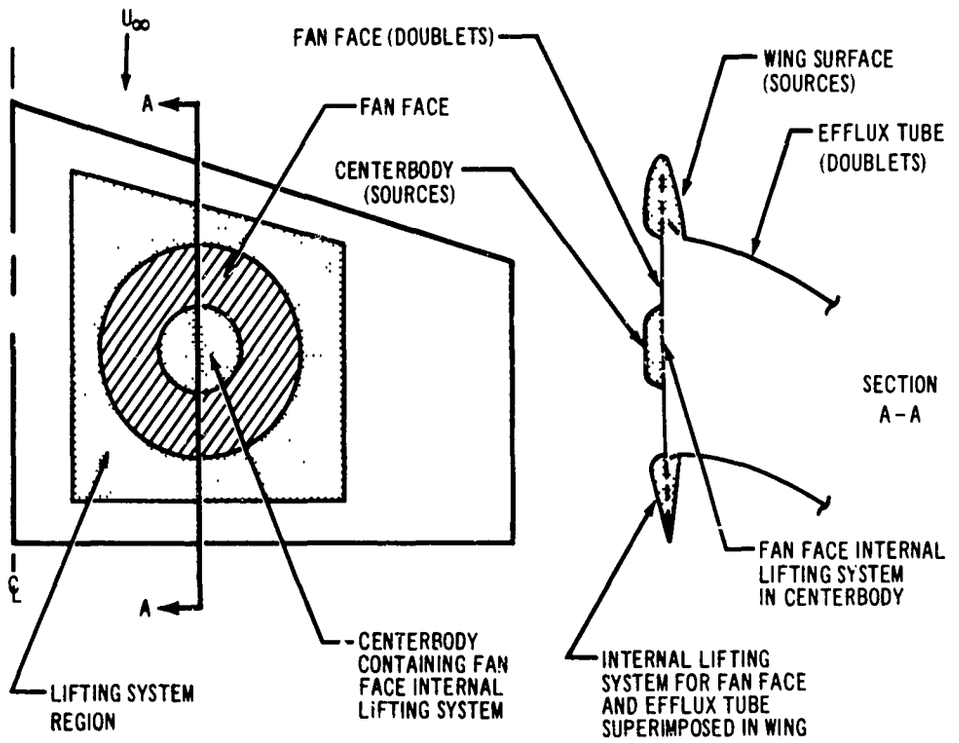

Figure 6. Internal Lifting System for Fan Face and Efflux Tube.

Consider the fan cross section shown in Figure 7. All forces acting on the internal fan assembly—including the rotor, stator, exit guide vanes, inlet and centerbody sidewalls, etc.—are determined from momentum considerations (Reference 6, p. 14) as

$$\vec{F}_{fan} = - \iint_{S_b + S_e} [\, p\vec{n} + \rho\vec{q}\,(\vec{q} \cdot \vec{n})\,]\, dS \qquad (23)$$

where S_b = mathematical barrier across the fan face

S_e = fan exit plane

$\vec{n}$ = outward normal

The corresponding expression for the moment is

$$\vec{M}_{fan} = - \iint_{S_b + S_e} [\, p\,(\vec{r} \times \vec{n}) + \rho(\vec{r} \times \vec{q})\,(\vec{q} \cdot \vec{n})\,]\, dS \qquad (24)$$

where $\vec{r}$ is a position vector measured from the point about which moments are taken.

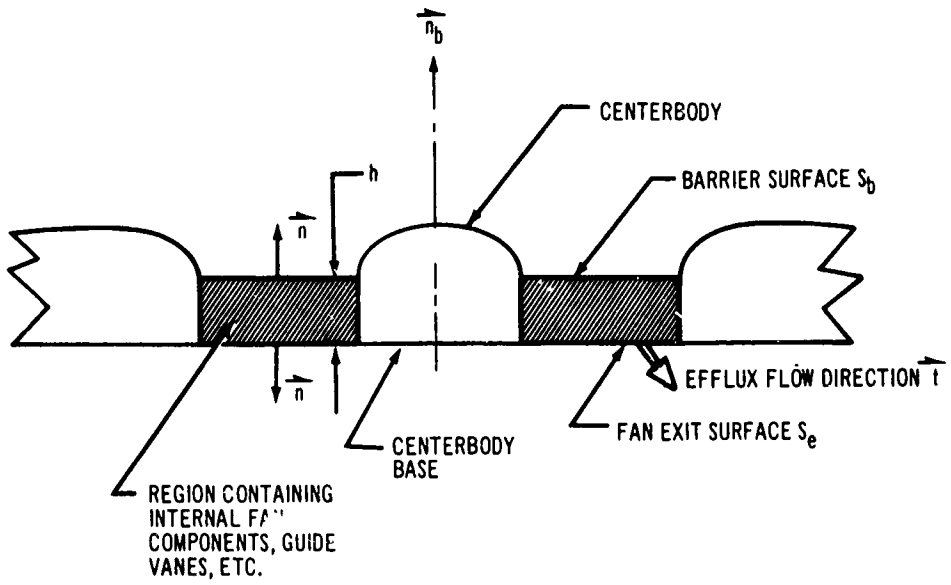

Figure 7. Cross Section of Fan.

The velocity and pressure on S_b are furnished by the potential-flow solution, which is governed by an assumed inflow distribution, $\vec{q} \cdot \vec{n}$, at the barrier. The velocity and pressure distribution at the exit plane must be determined experimentally or assumed. In this report, the internal force and moment are computed with the following assumptions concerning the exit flow:

- The fan exit is planar and parallel to the barrier across the inlet. It is the same size and shape as the barrier and lies a distance h below it.
- The exit flow is vectored in the known direction $\vec{t}$.
- The average exit static pressure p_e is known.
- The mass flow distribution $\vec{q} \cdot \vec{n}$ through the exit plane is the same as through the barrier.
- The fan flow is incompressible.

The relationships given below between quantities at corresponding points on the exit plane and barrier follow directly from these assumptions.

$$(\vec{q} \cdot \vec{n})_{\text{exit plane}} = -(\vec{q} \cdot \vec{n})_{\text{barrier}}$$

$$\vec{q}_{\text{exit plane}} = \frac{\vec{t}\,(\vec{q} \cdot \vec{n})_{\text{barrier}}}{\vec{t} \cdot \vec{n}_b} \tag{25}$$

$$\vec{r}_{\text{exit plane}} = \vec{r}_{\text{barrier}} - h\,\vec{n}_b$$

where $\vec{n}_b$ = unit vector directed upward along the fan axis.

With these relationships, Equations (23) and (24) can be converted to integrals over the barrier only. Introducing a reference area S_r and a reference length L_r, the expressions for the force and moment coefficients become

$$\vec{C}_{F_{fan}} = \frac{\vec{F}_{fan}}{1/2\,\rho U_\infty^2 S_r} = -\frac{\vec{n}_b}{S_r} \iint_{S_b} C_p\, dS + \frac{\vec{n}_b C_{p_e} S_b}{S_r}$$

$$-\frac{2}{S_r} \iint_{S_b} \vec{V}\,(\vec{V} \cdot \vec{n}_b)\, dS + \frac{2}{S_r} \frac{\vec{t}}{\vec{t} \cdot \vec{n}_b} \iint_{S_b} (\vec{V} \cdot \vec{n}_b)^2\, dS \tag{26}$$

$$\vec{C}_{m_{fan}} = \frac{\vec{M}_{fan}}{1/2\,\rho U_\infty^2 S_r L_r} = -\frac{1}{S_r L_r} \iint_{S_b} (\vec{r} \times \vec{n}_b)\, C_p\, dS + \frac{C_{p_e} (\vec{r}_b \times \vec{n}_b) S_b}{S_r L_r}$$

$$-\frac{2}{S_r L_r} \iint_{S_b} (\vec{r} \times \vec{V})\,(\vec{V} \cdot \vec{n}_b)\, dS + \frac{2}{S_r L_r} \iint_{S_b} \frac{(\vec{V} \cdot \vec{n}_b)^2}{\vec{n}_b \cdot \vec{t}} \left|(\vec{r} - h\,\vec{n}_b) \times \vec{t}\right| dS \tag{27}$$

where C_{p_e} = average pressure coefficient at the exit

$\vec{V} = \frac{\vec{q}}{U_\infty}$ = dimensionless velocity

The first and second right-hand terms in these expressions represent the force and moment contributed by the static pressure at the barrier and exit plane, respectively. The third and fourth terms give the momentum contributions. The total force and moment on a configuration are given by the sum of the exterior surface pressures from the potential-flow solution, the internal fan forces from Equations (26) and (27), and the force and moment on the center-body base, which can be computed from an assumed base pressure.

2.3 BOUNDARY-LAYER THEORY

This study is concerned with the prediction of the general trend of the boundary-layer growth and separation. Methods of analyzing three-dimensional boundary layers are at present only approximate, and they become exceedingly complex if many aspects of three-dimensional boundary-layer flow are considered. Consequently, certain simplifying assumptions have been made that reduce the problem to manageable proportions and allow the introduction of two-dimensional axisymmetric flow analyses.

Little experimental knowledge of three-dimensional transition and separation exists; accurate prediction of these phenomena is impossible at this time. Thus, the boundary-layer flow is assumed to be entirely turbulent, with only the initial boundary-layer properties at stagnation determined by laminar analyses. The usual two-dimensional separation criteria ($H > 2.5$, $dH/ds \gg 0$) is recommended in this study. However, as Cooke (Reference 7) carefully observes, the simplified boundary-layer model used becomes invalid near separation. An indication of separation based on two-dimensional axisymmetric criteria only suggests the probability of severe three-dimensional effects.

The boundary-layer growth along a surface streamline on a three-dimensional wing is described by first-order, nonlinear partial differential equations. At the outset the assumption was made that the local radius of curvature of the wing is much greater than the boundary-layer thickness. This allows the use of the equations of motion applicable to flow across a plane. The additional assumption is made that the boundary-layer crossflow is negligible, as well as the gradient of that crossflow. Then, the nondimensionalized momentum equation is reduced to the first-order, nonlinear ordinary differential equation given by Cooke (Reference 7)

$$\frac{d\theta}{ds} + \frac{1}{V}\frac{dV}{ds}(2\theta + \delta^*) - K_1\theta = \frac{C_f}{2} + \text{turbulence terms} \qquad (28)$$

where s is the distance along a surface streamline. The term K_1 denotes the potential-flow divergence in the plane of the wing surface. The additional turbulence terms are neglected, as is customary in two-dimensional analyses.

A more familiar form of this equation, similar to that for axisymmetric flow, is obtained by substituting the boundary-layer shape factor $H = \delta^*/\theta$.

$$\frac{d\theta}{ds} + \theta\left[\frac{1}{V}\frac{dV}{ds}(2 + H) - K_1\right] = \frac{C_f}{2} \qquad (29)$$

In this equation, the term K_1 occupies the same position as the term $-1/r\ dr/ds$ in Cooke's axisymmetric equation. Both of these variables describe the convergence or divergence of the potential-flow streamlines. If the streamlines are parallel curves in a plane so that their orthogonal trajectories are straight lines, then $K_1 = 0$ and Equation (29) reduces to two-dimensional form.

The value of K_1 is obtained from the potential-flow streamline pattern as the rate of change of the streamline direction with respect to the orthogonal distance s_t (see Figure 8). Thus,

$$K_1 = \lim_{\Delta s_t \to 0} \frac{\Delta\beta}{\Delta s_t} \tag{30}$$

The geometric relationship

$$-\Delta\beta = \sin^{-1}\frac{\Delta V_t}{V} \tag{31}$$

is used to compute the derivative in Equation (30), which then becomes

$$K_1 = \frac{-1}{V}\frac{dV_t}{ds_t} \tag{32}$$

The term ΔV_t is the component of the vector $(\vec{V}_2 - \vec{V})$ normal to the streamline.

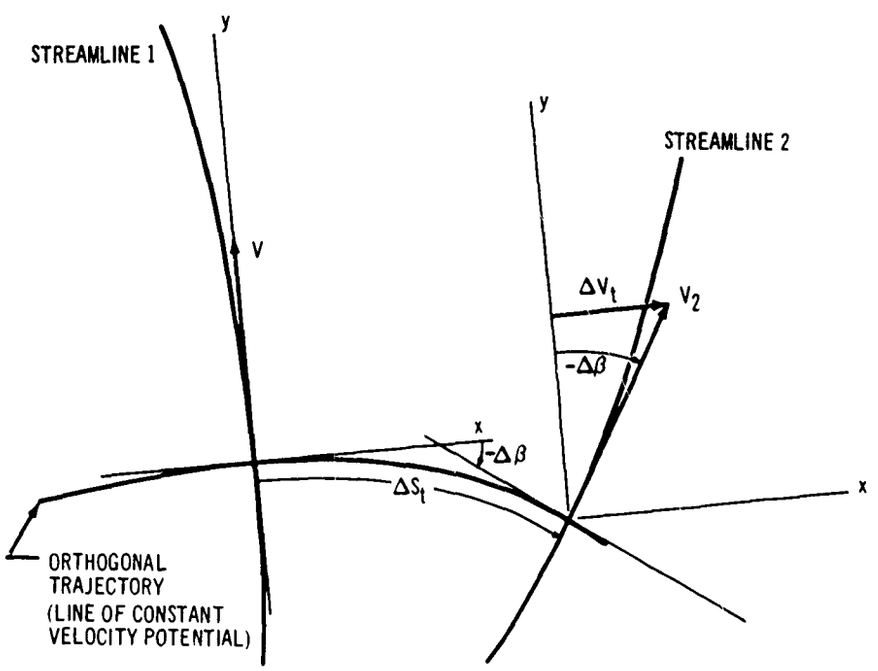

Figure 8. Streamline Velocity Diagram.

In Equation (29), then, there remain three unknown quantities: momentum thickness θ, shape factor H, and skin friction C_f. Past experience (Granville, Reference 8) in studying axisymmetric flows has shown that the combination of the Ludwig-Tillman law for C_f, the moment-of-momentum equation, and the axisymmetric momentum equation yields good results for the boundary-layer growth. The same equations are used in this study, with 1/r dr/ds replaced by $-K_1$. Following Granville, the simultaneous system of equations to be solved is

Momentum [See Equation (29).]

Moment-of-momentum

$$\frac{dH}{ds} = -\frac{1}{V}\frac{dV}{ds}\left[\frac{H(H+1)(H^2-1)}{2}\right] + \frac{H^2-1}{\theta}\left[H - (H-1)\left(\frac{H_0+1}{H_0-1}\right)I_0\right]\frac{C_f}{2} \tag{33}$$

Skin friction

$$\frac{C_f}{2} = 0.123\left(10^{-0.678H}\right) R_\infty^{-0.268} (V\theta)^{-0.268} \tag{34}$$

with

$$\text{Log}_{10} H_0 = 0.599 - 0.198\ \text{Log}_{10}(R_\infty V\theta) + 0.0189\left[\text{Log}_{10}(R_\infty V\theta)\right]^2 \tag{35}$$

$$I_0 = \frac{H_0}{H_0+1}\left[1 + 0.0378\ \frac{(52.9\ \text{Log}_{10} H - 4.18)^{\frac{1}{2}}}{(H_0^2 - 1)}\right] \tag{36}$$

The integration of these equations requires initial values of the boundary-layer parameters θ and H. If the boundary-layer calculation begins at some point along the streamline, then the turbulent momentum thickness must be known at that point. On the other hand, if the starting point of the boundary-layer calculation is at stagnation, then the initial θ must be obtained from a laminar value of momentum thickness at stagnation. Standard methods of describing the variation of boundary-layer parameters across transition set the turbulent momentum thickness equal to the laminar value, and this principle is used here. The initial value of the shape factor is always H = 1.5.

The laminar momentum thickness is obtained by considering the stagnation flow. For fan-in-wing configurations in vertical flight, a stagnation circle will exist on the upper surface around the fan. After transition from vertical to forward flight, stagnation occurs at the point of symmetry on the wing leading edge and

at a point downstream of the fan. A dividing streamline proceeds from the leading-edge stagnation point, approximately parallel to the leading edge, toward the wingtip. This dividing streamline is approximated by a two-dimensional stagnation line, which is valid if the velocity everywhere along the dividing streamline is small. The foregoing approximations are in accord with the condition of negligible crossflow in the boundary layer.

A comparison of an infinitesimally small section of the stagnation circle with an equally small section of the leading-edge stagnation line shows that the boundary layers at each of the two curves are similar. Rosenhead presents an analysis in Reference 9 (p. 231) of the laminar flow boundary layer in the neighborhood of a two-dimensional stagnation line. This analysis is applied to the fan-in-wing problem.

Numerical integration of Rosenhead's solution yields the laminar momentum thickness at the stagnation curve

$$\theta_0 = 0.2905 \ (aR_\infty)^{-\frac{1}{2}} \tag{37}$$

The constant a is the result of an approximation to the potential flow in the neighborhood of stagnation. It is calculated as $a = dV/ds$ at stagnation.

3. NUMERICAL PROCEDURE

This section describes the numerical procedure that forms the basis of the aerodynamic computations. Techniques and approximations used in the numerical procedure are described together with the computational methods.

The numerical procedure is divided into successive steps. First, the method of solving the basic integral equation for the singularity strengths is presented. This is followed by the computation of velocities and surface pressures. Later sections describe the computation of forces and moments, surface streamlines, and boundary-layer characteristics.

3.1 SOLUTION OF THE INTEGRAL EQUATION

The method of influence coefficients is used to solve the integral Equation (17) for the source and doublet strengths. The basic principles of the method are straightforward. Surface distributions of sources and doublets are approximated by networks of small quadrilateral panels with the singularity strength of each panel set equal to an arbitrary constant value σ_j. This reduces the problem to the determination of a finite number of discrete singularity strengths, one for each panel. The integrals in Equation (17) can then be evaluated in closed form over each panel. One point in each panel, the "boundary point," is selected as the point at which the integral equation is satisfied. The requirement that the integral equation be satisfied at all boundary points then produces a system of linear algebraic equations of the form

$$[A_{ij}] \{\sigma_j\} = \{B_i\} \tag{38}$$

where A_{ij} is the influence coefficient of the j^{th} singularity at the i^{th} boundary point, σ_j is the strength of the j^{th} singularity, and B_i is the normal component of the disturbance velocity at the i^{th} boundary point. This system of equations is solved for the singularity strengths σ_j by a process of reduction of the system to diagonal form.

The basic integral Equation (17) to be solved can be restated as

$$\left.\frac{\partial \varphi}{\partial n}\right|_{\tilde{S}} = -\vec{n} \cdot (\vec{U}_\infty - \vec{q}) = -\frac{1}{4\pi} \vec{n} \cdot \nabla \iint_{S_s} \frac{m(S)}{r} dS$$

$$+ \frac{1}{4\pi} \vec{n} \cdot \nabla \iint_{S_d} \mu(S) \frac{\partial}{\partial n} \left(\frac{1}{r}\right) dS + \frac{1}{4\pi} \vec{n} \cdot \nabla \iint_{S_{wake + \text{interior surfaces}}} \mu(S) \frac{\partial}{\partial n} \left(\frac{1}{r}\right) dS \tag{39}$$

where the boundary condition on the left-hand side is known and the source and doublet strengths, $m(S)$ and $\mu(S)$, are to be determined. As applied to the type of problem under consideration (fan-in-wing or ordinary lifting wing), $\tilde{S}$ denotes the exterior boundaries of the configuration where Neumann boundary conditions are applied. These include the exterior wing surface, the boundary or barrier

across the fan face, the fan centerbody surface protruding above the fan face, and the exterior surface of the efflux tube. The surface S_S is that portion of $\tilde{S}$ represented by a source distribution, which is normally the exterior wing and centerbody surfaces.

The doublet distributions have been written as two separate integrals that identify two basically different types of doublet surfaces. The first surface, S_d, is that portion of the exterior surface $\tilde{S}$ represented by doublets. For a fan-in-wing, S_d normally is composed of the fan face or barrier and the efflux tube surfaces. Together, S_S and S_d make up the boundary $\tilde{S}$.

The other doublet surface, $S_{\text{wake + interior surfaces}}$, denotes the wake and interior surfaces discussed on pp. 13-16. This type of doublet sheet is unique in that the variation of the doublet strength in one direction across the sheet has already been determined. For example, the assumption has been made for the trailing sheet that the doublet strength depends only on the lateral or spanwise coordinate and is independent of distance downstream. The variation in strength of the internal doublet sheets is also chosen a priori in one direction, which for the sheet shown in Figure 4 is chordwise. Furthermore, the strength of this sheet is related to the strength of the trailing doublet sheet by the requirement that $\Delta\varphi$ across the surfaces be continuous where they meet at the trailing edge. Hence, ultimately, the trailing and internal sheets of Figure 4 may be combined to form one continuous sheet whose chordwise doublet strength variation has been completely determined. This combined system is referred to as an "internal lifting system." With such a system, the requirement of smooth flow off the trailing edge (Kutta condition) must be imposed to furnish the boundary condition controlling the spanwise variation of the wake doublet strength.

Similarly, the radial variation in strength of the internal doublet sheets connecting to the fan face and efflux tube are specified a priori. Their circumferential variation is the same as that on the circumference of the fan face or efflux tube, which is controlled by the exterior boundary conditions. In the numerical representation, these internal sheets are combined with a narrow strip around the edge of the fan face or efflux tube. This forms doublet sheets whose strength to be determined varies only circumferentially, with exterior boundary conditions correspondingly applied on the narrow strips.

The numerical solution of Equation (39) proceeds as follows: The surface source sheets on S_S are divided arbitrarily into parts that may delineate separate physical regions or may be selected for other reasons. Each part is further subdivided into quadrilateral panels by the specification of a rectangular array (M x N) of (x, y, z) coordinates on the surface. A typical panel arrangement is shown in Figure 9.

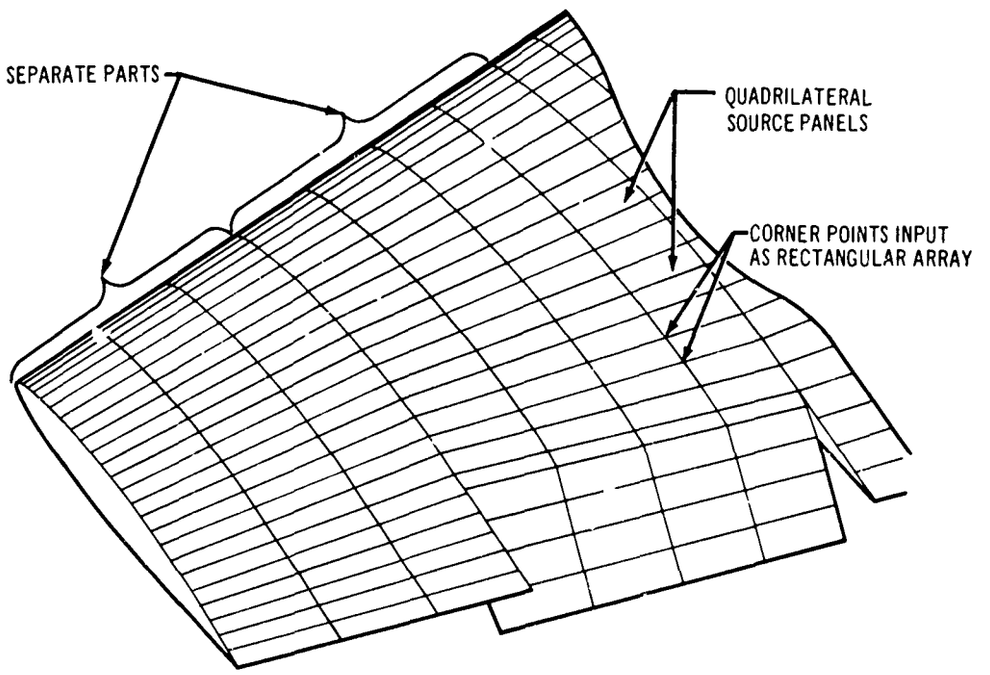

Figure 9. Typical Source-Panel Arrangement.

For the purpose of integrating the influence of sources over an individual panel, the panel is approximated as planar. This "near plane" passes through the midpoints of the four straight lines connecting the corner points of a panel. The four panel corner points on the actual surface are projected normally to the near plane. Thus, the surface is covered by a distribution of planar panels whose edges, depending on the surface curvature, may or may not be coincident. There is no practical limitation on the shape of an individual panel. If two successive corner points coincide, a panel degenerates into a triangle, which the computer program handles without difficulty.

The source strength m_j over each panel is approximated as constant, where the subscript j denotes the panel index. With this approximation, the integral of the source influence over an individual panel can be obtained in closed form (details are given in Appendix I) as

$$\frac{\vec{q}_{ij}}{U_\infty} = \vec{V}_{ij} = -\frac{m_j}{4\pi U_\infty} \nabla \iint_{\text{panel } j} \frac{1}{r}\, dS = \sigma_j C_{ij} \qquad (40)$$

where $\sigma_j = \dfrac{m_j}{4\pi U_\infty}$

$$\vec{C}_{ij} = -\nabla \iint_{\text{panel } j} \frac{1}{r}\, dS$$

$\vec{V}_{ij}$ = dimensionless velocity induced by the j^{th} source panel at the i^{th} point

The "influence coefficient" $\vec{C}_{ij}$ is determined entirely by the geometric relationship between the i^{th} influence point and the j^{th} panel.

The integral in Equation (39) over all surfaces represented by sources is obtained simply by summing the influence of all the source panels.

$$-\frac{1}{4\pi} \nabla \iint_{S_s} \frac{m(S)}{r}\, dS = U_\infty \left[\sum_j \vec{C}_{ij}\, \sigma_j \right]_{S_s} \tag{41}$$

The surface doublet sheets on S_d are similarly divided into parts with each part subdivided into quadrilateral panels by specifying a rectangular array of (x, y, z) coordinates on the surface. The individual panels are bounded by four straight lines connecting the corner points. The doublet strength μ_j over each panel is approximated as constant, but no assumption of a planar panel is needed. The integral over an individual doublet panel is evaluated by the well-known equivalence of a constant-strength doublet sheet and a concentrated vortex around the periphery of the sheet. Thus, each doublet panel is treated as a quadrilateral vortex around the periphery with its influence given by the simple Biot-Savart relationship. The term "quadrilateral vortex" refers to this type of singularity. The details of the integration are carried out in Appendix I, with the result expressed in a form analogous to that for a source panel.

$$\frac{\vec{q}_{ij}}{U_\infty} = \vec{V}_{ij} = \frac{\mu_j}{4\pi U_\infty} \nabla \iint_{\text{panel } j} \frac{\partial}{\partial n}\left(\frac{1}{r}\right) dS = \sigma_j\, \vec{C}_{ij} \tag{42}$$

where $\sigma_j = \dfrac{\mu_j}{U_\infty}$

$$\vec{C}_{ij} = \frac{1}{4\pi} \nabla \iint_{\text{panel } j} \frac{\partial}{\partial n}\left(\frac{1}{r}\right) dS$$

$\vec{V}_{ij}$ = dimensionless velocity induced by j^{th} quadrilateral vortex at the i^{th} point

With this terminology the integral in Equation (39) over S_d becomes

$$\frac{1}{4\pi} \nabla \iint_{S_d} \mu(S) \frac{\partial}{\partial n}\left(\frac{1}{r}\right) dS = U_\infty \left[\sum_j \tilde{C}_{ij}\, \sigma_j\right]_{S_d} \tag{43}$$

The numerical representation of the last integral in Equation (39) is similar, but the variation of the doublet strength on $S_{\text{wake + interior surfaces}}$ must be specified a priori in one direction. Constant-strength doublet panels are again defined by means of a rectangular array of (x, y, z) coordinates, but with the panel strengths now related in one direction. Making use again of the equivalence of a constant-strength doublet sheet and a concentrated vortex around the periphery, the resultant singularity network is termed a "multihorseshoe vortex network." Consider the typical multihorseshoe network shown in Figure 10. In addition to an array of corner points describing the network location, a system of weights, W_k, is assigned. These weights control the variation of the singularity strength in the vertical direction of Figure 10, so that only one singularity strength, σ_j, is associated with each column of bound vortices. The strengths of the individual bound vortices in a column are $W_k \sigma_j$. The strength of the trailing vortices are the sum of $W_k \sigma_j$'s through the requirement of continuity of vorticity.

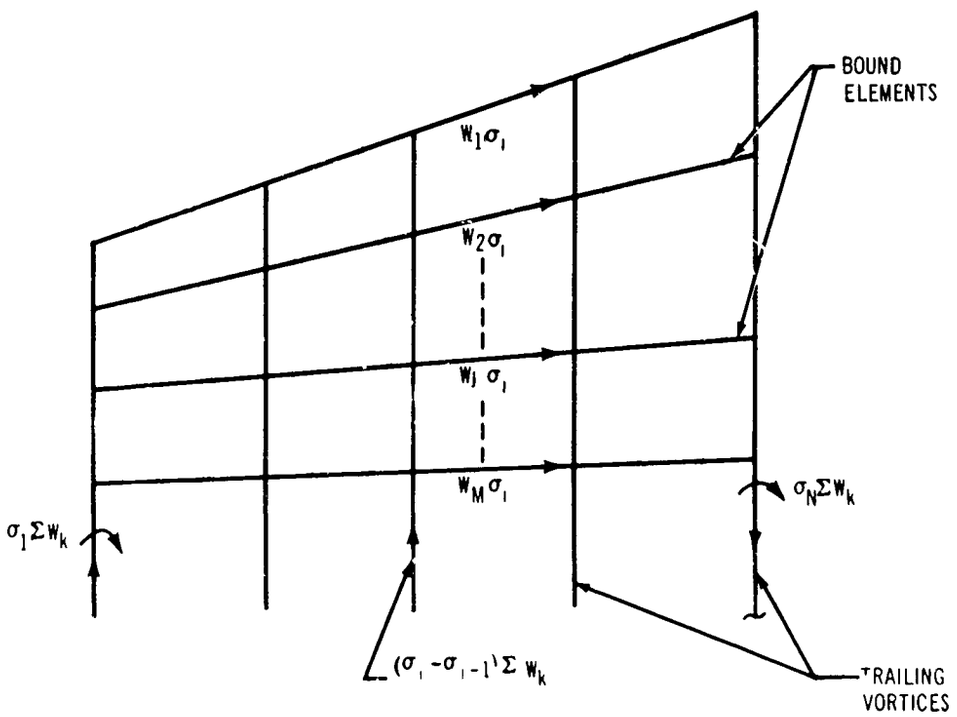

Figure 10. Multihorseshoe Vortex Network.

The versatility of a multihorseshoe network is sufficient to enable its use for both the internal lifting system that emanates from the wing to form the trailing sheet and the internal systems connecting the fan face and efflux tube. In the first application, the bound elements shown in Figure 10 are interior to the wing, with the trailing vortices emanating from the trailing edge. This network satisfies the requirement that the chordwise variation in singularity strength be specified a priori, which is accomplished by the specified weighting values, W_k. In the second application, the weights are selected so that their sum is zero. This eliminates the trailing vortices and gives a singularity sheet whose variation in one direction is fixed, as required.

The integration over a multihorseshoe vortex, described in Appendix I, is basically the same as for a quadrilateral vortex, Equation (42), except that the area of integration corresponding to each value of σ_j now includes a column of panels with the appropriate weights. The result for the induced velocity can be expressed in exactly the same form in terms of σ_j and a $\widehat{C}_{ij}$.

In summary, the three types of singularities used are source panels, quadrilateral vortices, and multihorseshoe vortices, which sufficiently represent all of the singularity distributions in integral Equation (39). The perturbation velocity at any point, i, in the field from the integrals over the various singularities on the body is expressed as

$$\frac{\nabla\varphi_i}{U_\infty} = -\frac{1}{4\pi}\,\nabla\iint_{S_s}\frac{m(S)}{r}\,dS + \frac{1}{4\pi}\,\nabla\iint_{S_d}\mu(S)\,\frac{\partial}{\partial n}\left(\frac{1}{r}\right)dS$$

$$+\frac{1}{4\pi}\,\nabla\iint_{\substack{S_{wake}+\\ interior\\ surfaces}}\mu(S)\,\frac{\partial}{\partial n}\left(\frac{1}{r}\right)dS = \left[\sum_j \widehat{C}_{ij}\;\sigma_j\right]_{\substack{all\\ surfaces}} \qquad (44)$$

The numerical representation of the integral Equation (39) is completed by approximating the boundary conditions on the left-hand side in a manner consistent with the approximations described for the singularity distributions. Since the singularities are represented by a finite number of discrete values, σ_j, a corresponding number of points on the surface, called boundary points, are selected. Equation (39) is satisfied at these discrete points.

A boundary point is located on each source panel at the centroid. The surface normal at the boundary point is taken normal to the near plane of that panel. The potential-flow program computes the location and normals of all source-panel boundary points. The user has the option of specifying the normal component of velocity at these boundary points, which is the Neumann boundary condition. If left unspecified, the program automatically sets the normal velocity component equal to zero, which is the usual condition for an impermeable surface.

For each quadrilateral vortex there must also be a corresponding boundary point. Unless otherwise specified, the program locates a boundary point at the average of the coordinates of the four panel corners, thus placing it near the middle of each panel. The surface normal is constructed as the vector product of the diagonals from opposite corners of the quadrilateral. The program also imposes the boundary condition of a zero normal velocity component at these boundary points. As an alternative, the user can specify the location of each boundary point, its normal direction, and the desired normal velocity component.

One boundary point is also needed for each multihorseshoe vortex. These are normally placed adjacent to the wing trailing edge (see Section 6) to furnish the Kutta condition or around the periphery of the fan or efflux tube. The location, normal direction, and specified normal-velocity component of each of these boundary points must be input to the program.

Denoting each boundary point by a subscript i, the integral Equation (39) finally reduces to the form

$$\frac{1}{U_\infty}\frac{\partial \varphi_i}{\partial n_i} = -\vec{n}_i \cdot \left(\frac{\vec{U}_\infty}{U_\infty} - \frac{\vec{q}_i}{U_\infty}\right) = \sum_j \vec{n}_i \cdot \vec{C}_{ij}\,\sigma_j, \quad (i = 1, \text{---all boundary points}) \tag{45}$$

where $\vec{n}_i$ is the unit normal at the i^{th} boundary point. The term $\vec{n}_i \cdot \vec{q}_i/U_\infty$, called U_{si} in the computer input description (Section 5), is the normal velocity component that must be specified in the input.

The system of Equation (45) is more conveniently written in matrix notation as

$$\left[A_{ij}\right]\left\{\sigma_j\right\} = \left\{B_i\right\} \tag{46}$$

where $A_{ij} = \vec{n}_i \cdot \vec{C}_{ij}$

$$B_i = -\vec{n}_i \cdot \left(\frac{\vec{U}_\infty}{U_\infty}\right) + U_{si}$$

Here σ_j denotes either source, quadrilateral, or multihorseshoe strength, and the influence coefficients A_{ij} depend only on the geometric relationships between the individual singularities and the i^{th} influence point. The B_i's depend only on the direction of the free stream and the specified normal velocities.

This system is solved for the singularity strengths σ_j by a technique of reduction of the A_{ij} matrix to diagonal form. The program is set up to perform this reduction process for up to five different sets of B_i's simultaneously. In this manner, five solutions, differing in the free-stream direction (yaw and angle of attack), specified normal velocities U_{si}, or perhaps with $U_\infty = 0$ can be obtained simultaneously. However, the geometry of the configuration, which enters into A_{ij}, must remain unchanged.

When the geometry is symmetric about the x-z plane and the free-stream velocity lies in this plane, the entire flow field and also the singularity strengths must be symmetric. In such a case, only the geometry on the positive y side of the symmetry plane is input. The program then computes each influence coefficient as the sum of a panel and its counterpart reflected about the x-z plane. The obvious advantage of this system is that the number of singularity strengths is reduced to those on half of the configuration.

3.2 VELOCITIES AND SURFACE PRESSURES

The program computes the velocity components and pressure coefficient at all of the boundary points. The velocity is given by the sum of the free stream and the perturbation velocities induced by the singularities (Equation 44).

$$\vec{V}_i = \frac{\vec{U}_\infty}{U_\infty} + \frac{\nabla\varphi_i}{U_\infty} = \frac{\vec{U}_\infty}{U_\infty} + \left[\sum_j \vec{C}_{ij}\,\sigma_j\right]_{\substack{\text{all}\\ \text{surfaces}}} \tag{47}$$

In the special case of a zero free-stream velocity, all quantities are nondimensionalized with respect to a reference velocity, U_R, instead of U_∞. The reference velocity enters the problem through the specified boundary conditions, U_{si}, which must be input as velocities nondimensionalized with respect to U_R.

The pressure coefficient is defined as

$$C_{p_i} = \frac{p_i - p_\infty}{\frac{1}{2}\rho U_\infty^2} = 1 - |V_i|^2, \quad U_\infty \neq 0$$

$$C_{p_i} = \frac{p_i - p_\infty}{\frac{1}{2}\rho U_R^2} = -|V_i|^2, \quad U_\infty = 0 \tag{48}$$

In addition to the pressure distribution on the wing and inlet surfaces given directly by the values at the source-panel boundary points, "off-body" points located anywhere in the field may be specified by the user, and the velocities and pressure coefficients will be determined at these points. There is one restriction, however: such points should not be placed directly on a source panel or vortex. They must be at least a small distance, 10^{-5}, away from any singularity because the integrals over the singularity sheets reduce to a special form or become singular when the influence point is on, or very close to, a singularity. The program does not recognize this special form for off-body points. Although the program will not malfunction if off-body points are located within this tolerance, the result at that point will be incorrect. If the off-body point is too close to a source panel, only the velocity component normal to the panel will be wrong. For vortices, the entire influence of the adjacent vortex will be neglected.

The velocities printed out at the quadrilateral and multihorseshoe boundary points generally cannot be interpreted as the correct surface velocities. As explained in Section 6.1, the tangential velocity components due to the local surface vorticity are not included. This is of little importance, since the main region of interest is the wing surface, where source panels are used.

On the barrier, however, a special procedure is used to produce correct velocities. The velocities at the barrier boundary points are computed by Equation (47), and they are incorrect. Corrected values are computed at the midpoints of the circumferential vortices by the following procedure: Consider a portion of the barrier network as shown in Figure 11. The radial velocity component at a point p located at the midpoint of a circumferential vortex segment due to the local vorticity density is

$$\vec{V}_{p_r} = \frac{1}{2} \frac{\sigma_c}{(\ell_1 + \ell_2)} \tag{49}$$

The circumferential component due to local vorticity is obtained by averaging the values at surrounding radial vortices and is

$$\vec{V}_{p_c} = \frac{1}{2} \frac{\sigma_1/d_1 + \sigma_2/d_2 + \sigma_3/d_3 + \sigma_4/d_4}{4} \tag{50}$$

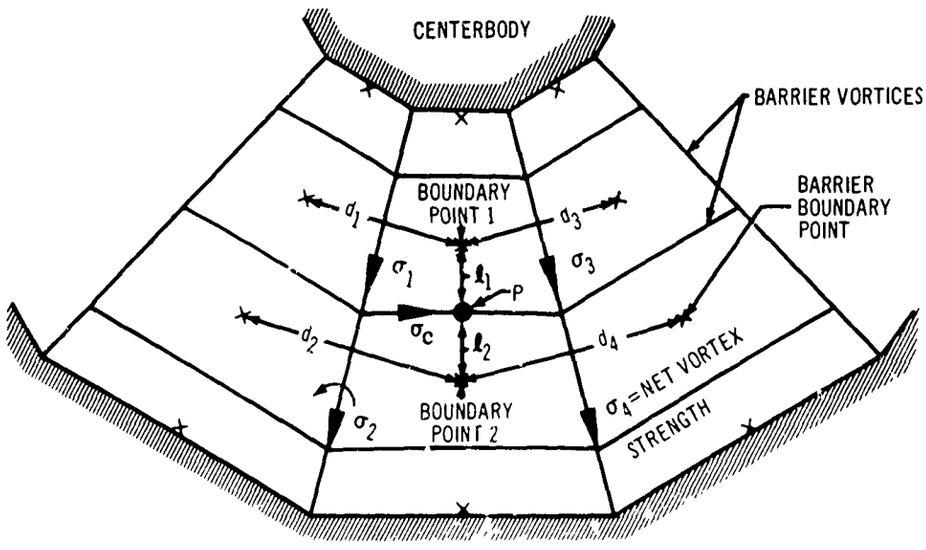

Figure 11. Velocity Computation on Fan Face.

The velocities calculated at boundary points 1 and 2 in the usual way do not include the effect of local vorticity. The corresponding velocity at point p is found by linear extrapolation from the expression

$$\vec{V}_p = \frac{\ell_2 \vec{V}_1 + \ell_1 \vec{V}_2}{\ell_1 + \ell_2} \tag{51}$$

The true velocity at point p is obtained by adding vectorially the components given by Equations (49), (50), and (51). This procedure is repeated to produce velocities at the midpoints of all circumferential vortex segments.

3.3 FORCES AND MOMENTS

The forces on a fan-in-wing configuration are the result of the pressure on the external surfaces and the internal forces on the fan assembly. External pressure forces are computed on all source panels by assuming the pressure on each source panel is constant over the panel and equal to the value computed at the boundary point. Expressions for the external force and moment coefficients are obtained by summing the force and moment contributions of all source panels

$$\vec{C}_{F_{\substack{\text{external}\\\text{surfaces}}}} = \frac{1}{S_r} \sum_{\substack{\text{source}\\\text{panels}}} C_p \vec{n} A$$

$$\vec{C}_{m_{\substack{\text{external}\\\text{surfaces}}}} = \frac{1}{S_r L_r} \sum_{\substack{\text{source}\\\text{panels}}} C_p (\vec{r} \times \vec{n}) A \tag{52}$$

where A is the area of a source panel. Partial sums consisting of the force and moment on the individual columns of source panels in each source network are also furnished.

This method produces the correct total pressure forces and moments if all surfaces on which pressure forces act are represented by source panels, and source panels are not used elsewhere. It is also restricted to source-paneled surfaces that are solid, with no flow through the surface. This is always the case for clean wings and fan-in-wings of the type under consideration, where the exterior wing surfaces are covered with source panels and other singularities are used for the fan face and efflux tube. It is conceivable, however, that an analysis of other types of configurations may be attempted in which singularity distributions not satisfying these criteria are used. If source panels are used for surfaces on which the pressures do not contribute to the desired forces, it is a simple matter to subtract from the total calculated force the partial sums due to these surfaces. On the other hand, if vortices are used to represent a surface on which pressures are desired, lengthy hand calculations would be required to produce these pressures. Also, if a source-paneled surface is not impermeable, an additional force due to the transfer of momentum across the surface must be added, which is not calculated by the program.

The force and moment on the fan assembly are given by Equations (26) and (27), involving integrals over the barrier surface. These integrals are evaluated

numerically with the approximation that the flow properties are constant over regions centered about the midpoints of the circumferential barrier vortices at which the velocity and pressure are computed (see Section 3.1). A typical region is shown in Figure 12. Its area is computed approximately as

$$S_{b_{ij}} = (\ell_1 + \ell_2)(\ell_i - \ell_{i-1})(r_{s_{j-1}} + r_{s_j})/2 \qquad (53)$$

where $r_{s_1} = r_1$

$$r_{s_2} = \frac{r_2 + r_3}{2}$$

$$\vdots$$

$$r_{s_j} = \frac{r_j + r_{j+1}}{2}$$

$$\vdots$$

$$r_{s_m} = r_{m+1}$$

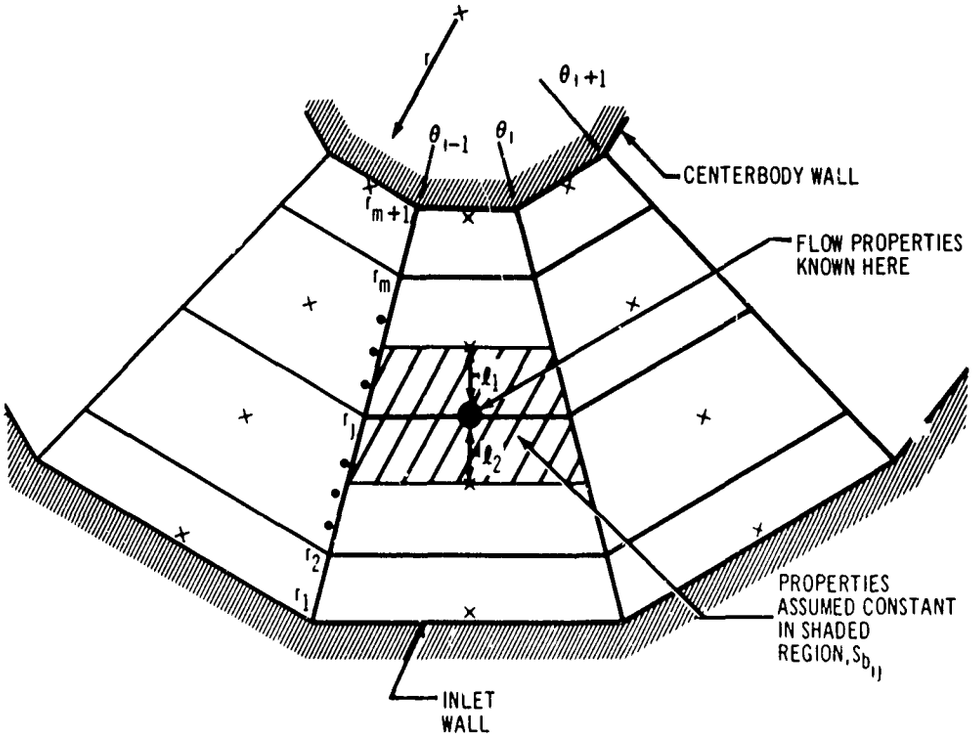

Figure 12. Force Computation on Fan

The ℓ_i's are the distances between the adjacent boundary points and the midpoint of the circumferential segments and are calculated in the program from the definition of the barrier vortices and boundary points. The r_i's and θ_i's, however, are provided by a separate input array. Normally these will correspond to the values used to define the barrier vortex network.

The fan force and moment are obtained by summing the contribution from each of these regions. The individual terms in Equations (26) and (27) are summed separately to provide separate results for the pressure and momentum terms. In this manner, the pressure forces acting on the fan face contribute

$$\tilde{C}_{F_{\substack{\text{fan face}\\ \text{pressure}}}} = -\frac{1}{S_r}\left[\sum S_b C_p \tilde{n}_b\right]_{\text{fan area}}$$

$$\tilde{C}_{m_{\substack{\text{fan face}\\ \text{pressure}}}} = -\frac{1}{S_r L_r}\left[\sum S_b C_p (\tilde{r} \times \tilde{n}_b)\right]_{\text{fan area}} \tag{54}$$

where C_p = pressure coefficient at the midpoint of the circumferential vortex segment in S_b

$\tilde{r}$ = vector from the moment center to the vortex segment midpoint

S_b = barrier area (Figure 12)

The fan exit pressure, C_{p_e}, which is input to the program, gives

$$\tilde{C}_{F_{\substack{\text{fan exit}\\ \text{pressure}}}} = \frac{C_{p_e}\tilde{n}_b}{S_r}\left[\sum S_b\right]_{\text{fan area}}$$

$$\tilde{C}_{m_{\substack{\text{fan exit}\\ \text{pressure}}}} = \frac{C_{p_e}(\tilde{r}_c \times \tilde{n}_b)}{S_r L_r}\left[\sum S_b\right]_{\text{fan area}} \tag{55}$$

where $\tilde{r}_c$ is the vector from the moment center to the center of the fan exit.

The momentum into the fan face gives the following terms:

$$\vec{C}_{F_{\substack{\text{inflow}\\\text{momentum}}}} = \frac{-2}{S_r}\left[\sum(\vec{V}_b \cdot \vec{n}_b)\,\vec{V}_b\,S_b\right]_{\text{fan area}}$$

$$\vec{C}_{m_{\substack{\text{inflow}\\\text{momentum}}}} = \frac{-2}{S_r L_r}\left[\sum(\vec{r}\times\vec{V}_b)(\vec{V}_b \cdot \vec{n}_b)\,S_b\right]_{\text{fan area}} \qquad (56)$$

where $\vec{V}_b$ is velocity computed at the midpoints of the circumferential vortex segments.

The momentum leaving the fan exit gives

$$\vec{C}_{F_{\substack{\text{exit}\\\text{momentum}}}} = \frac{2}{S_r}\left[\sum\frac{(\vec{V}_b \cdot \vec{n}_b)^2\,\vec{n}_e\,S_b}{\vec{t}\cdot\vec{n}_b}\right]_{\text{fan area}}$$

(57)

$$\vec{C}_{m_{\substack{\text{exit}\\\text{momentum}}}} = \frac{2}{S_r L_r}\left[\sum\frac{(\vec{V}_b \cdot \vec{n}_b)^2}{\vec{t}\cdot\vec{n}_b}\,((\vec{r} - h\vec{n}_b)\times\vec{t})\,S_b\right]_{\substack{\text{fan}\\\text{area}}}$$

where h is the distance between the fan face and the exit plane and $\vec{t}$ is the unit vector in the fan efflux direction.

Finally, the force and moment on the centerbody base are computed assuming that the centerbody base is in the fan exit plane.

$$\vec{C}_{F_{\substack{\text{centerbody}\\\text{base}}}} = \frac{\pi d_c^2}{4S_r} C_{p_c}\,\vec{n}_b$$

(58)

$$\vec{C}_{m_{\substack{\text{centerbody}\\\text{base}}}} = \frac{\pi d_c^2}{4 S_r L_r} C_{p_c}\,(\vec{r}_c \times \vec{n}_b)$$

The centerbody base pressure C_{p_c} and diameter d_c are inputs.

The three components of the moment vector parallel to the coordinate axis are printed out as C_{mx}, C_{my}, C_{mz}, the rolling, pitching, and yawing moments, respectively. The force coefficients are given both as C_{fx}, C_{fy}, C_{fz}, the

components parallel to the coordinate axis and as C_L, C_D, and C_S. The drag coefficient C_D is defined conventionally as the force component parallel to the free stream. C_L is defined as the component perpendicular to C_D and lying in the plane formed by the free-stream vector and the z axis. The side force coefficient C_S is the component perpendicular to the lift and drag directions and positive when directed in the positive y direction.

The force and moment on the configuration are defined conventionally in terms of the corresponding coefficients as

$$\vec{F} = \frac{1}{2} \rho_\infty U_\infty^2 S_r \vec{C}_F$$

$$\vec{M} = \frac{1}{2} \rho_\infty U_\infty^2 S_r L_r \vec{C}_m \qquad (59)$$

The moment reference length L_r is submitted individually for each of the moment components. When the free-stream velocity is zero, the substitution of U_R for U_∞ in these equations will produce the correct force and moment.

3.4 SURFACE STREAMLINES

Streamlines on the surface are computed by approximating the streamline direction on each surface source panel as a straight line, parallel to the boundary-point velocity vector. They are traced in the reverse-flow direction, beginning at an initial point along an edge of a specified source panel.

Starting at this initial point, a line parallel to the boundary-point velocity vector is constructed across the source panel in the negative velocity direction. The intersection of this line with one of the other panel edges defines the point where the streamline leaves the panel. If this line does not enter the initial panel from the chosen point (i.e., the negative velocity vector does not cross some portion of the panel), the streamline will terminate (see Figure 13). Thus, the user must have an a priori knowledge of the direction of the flow on the initial panel to be assured that the streamline will proceed. In practice, this presents little difficulty, because the general direction of the flow is usually known. If there is any doubt, two streamlines can be requested on adjacent panels, but with their starting points lying at the same point on the common panel edge. Then, one of these will terminate immediately and the other will proceed.

Within a source-panel network the streamline must transfer from one panel to another. Because each panel is planar, edges of adjacent panels on a compound curved surface may not exactly coincide. The transfer across adjacent panel edges is performed by requiring the streamline to enter the new panel and leave the old one at the same fractional distance along the adjacent panel edges. If, as rarely happens, a streamline proceeds directly to a panel corner, the program arbitrarily selects one of the two sides at the corner and proceeds as though the streamline had intersected that side. If a streamline attempts to enter a panel in which the negative velocity vector does not point into the panel, two things may happen (such an eventuality is shown in Figure 14): If the angle between the velocity vector on either panel and the common edge exceeds

20 degrees, the streamline will terminate. If both these angles are less than, or equal to, 20 degrees, the streamline will proceed into the next panel to a point along one edge, as shown. This procedure applies only across internal edges of a source-panel network.

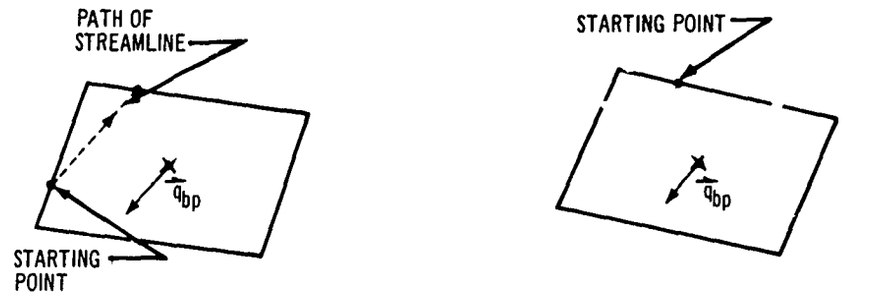

(a) STREAMLINE PROCEEDS. (b) STREAMLINE TERMINATES.

Figure 13. Initial Streamline Construction.

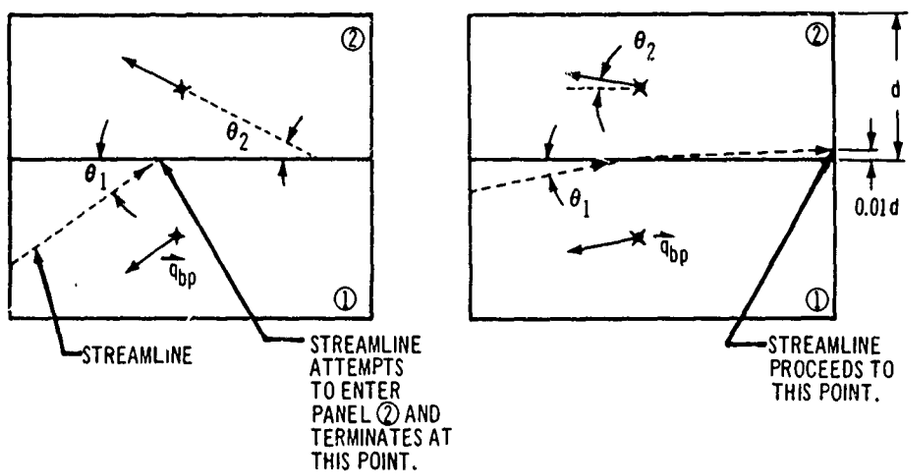

(a) θ_1 OR θ_2 > 20 DEGREES (b) θ_1 AND $\theta_2 \leq$ 20 DEGREES

Figure 14. Streamline Behavior Across Panel Edges.

When a streamline reaches the periphery of a source panel network, a search is made for an adjacent panel, which may lie along the periphery of any network

in the problem. Consider Figure 15. A streamline has progressed to point p on the periphery of a network and seeks to proceed into a panel of another network. A candidate must pass the following tests in order to be selected as the panel adjacent to point p:

1. The x and y distances from p to the panel boundary point must both be less than 80 percent of the length of the maximum panel diagonal occurring anywhere in the problem.

2. The distances d_1, d_2, d_3, shown in Figure 15, must obey the relations

$$d_2 + d_3 < 1.01\, d_1$$

$$d_2 < d_1$$

$$d_3 < d_1 \qquad (60)$$

The first panel along the periphery of a network that passes these tests is selected as the adjacent panel. If no adjacent panel can be found, the streamline terminates. The point at which the streamline enters the new network is found as a fractional distance, $d_2/(d_2 + d_3)$, along the new panel edge. If the negative velocity vector points into the new panel, the streamline will proceed into the new network; otherwise, the streamline will terminate. No special procedure, such as that described for interior panel edge crossings, is used when the negative velocity vector does not enter the new panel.

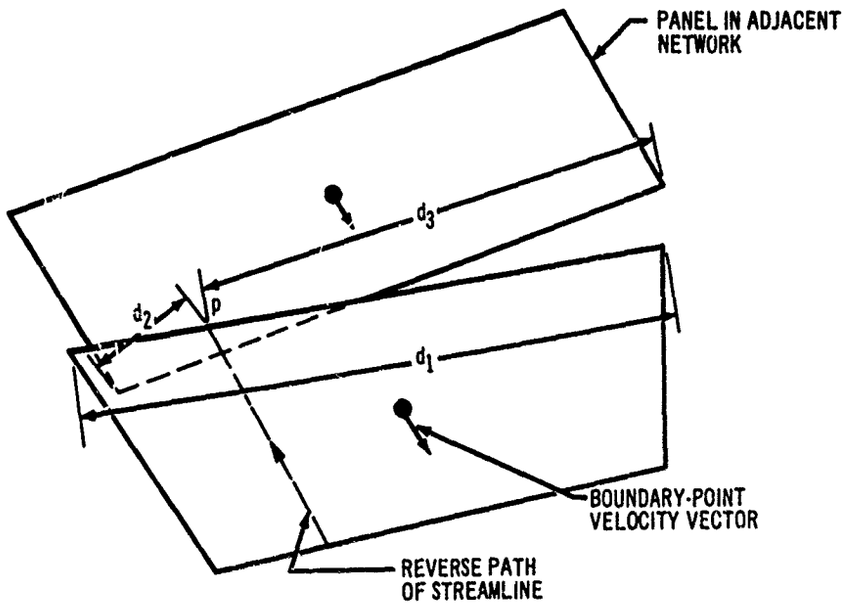

Figure 15. Search for Adjacent Panel.

Each streamline is defined in the output as a series of point coordinates. These are the midpoints of the streamline segments crossing each panel, as shown in Figure 16. The initial and termination points at panel edges are not given. The length Δs_i of each streamline segment across a panel is given, and the distance of each point along the streamline, measured from the initial starting point, is computed as

$$s_i = \sum_{j=1}^{i-1} \Delta s_j + \frac{\Delta s_j}{2} \tag{61}$$

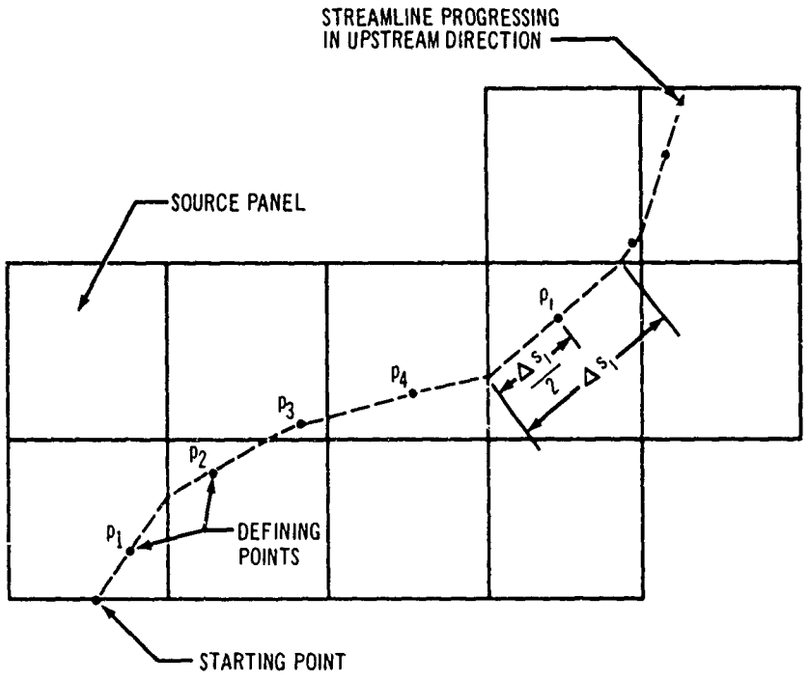

Figure 16. Points Defining Streamline.

The velocity and the velocity derivative normal to the streamline in the plane of the panel are furnished at each output point. These are computed at the panel boundary point containing the output point. The velocity derivative is calculated by finite difference, by constructing a unit vector $\vec{b}$ normal to the velocity vector at the boundary point and calculating the velocity $\vec{V}_{bo}$ at a point along $\vec{b}$ a small distance ϵ_{10} from the boundary point. The derivative is obtained as $(\vec{V}_{bo} \cdot \vec{b})/\epsilon_{10}$. As mentioned in Section 6.1, this value is not an accurate value of the desired velocity derivative, but is only indicative of the general magnitude

and sign of this quantity. An approximate value for the streamline divergence factor K_1, used by the boundary-layer program, is given by

$$K_1 = -\frac{1}{V}\frac{\vec{V}_{bo} \cdot \vec{b}}{\epsilon_{10}} \tag{62}$$

It is computed in the boundary-layer program from the information furnished along streamlines.

The option of eliminating the calculation of $\vec{V}_{bo} \cdot \vec{b}/\epsilon_{10}$ along streamlines is available in the potential-flow program. If only streamlines and velocities along streamlines are desired, it is recommended that this option be used, because the velocity derivative calculation is the most time-consuming operation in the streamline computations.

3.5 BOUNDARY LAYER

This section describes the numerical aspects of the boundary-layer program that integrate the system of boundary-layer equations. The input data, which are described in detail in Section 5.3, consist of certain constants and control numbers as well as a table of streamwise velocity and normal velocity derivatives at discrete distances s along a streamline. This table, obtained from the potential-flow program, is in the inverse order to that required in the calculations of the boundary-layer program. The potential-flow analysis begins at the fan inlet and proceeds toward the origin of the streamline at stagnation, whereas the boundary-layer analysis progresses in the opposite direction. The table inserted as data in the boundary-layer program is in the same order as the output from the potential-flow program, and is inverted within the boundary-layer program.

In addition to inverting the table, the boundary-layer program smoothes the values of velocity and normal velocity derivative using the subroutine MEAN, described in Volume II (Reference 4). A modified second-order Lagrangian interpolation routine is used to determine the values of velocity and normal velocity derivative between the tabular points. The streamwise velocity derivative dV/ds is determined by differentiation within the interpolation routine, and the divergence K_1 is calculated by dividing the normal velocity derivative by the streamwise velocity.

Initial values of momentum thickness and shape factor are required to begin the integration of the boundary-layer equations. Depending on the value of the control number FLAG on the first data card, the program either takes the initial momentum thickness directly from the input data or calculates it from constants on the first data card, as described in Section 5.3. The initial shape factor is set equal to 1.5.

Numerical integration of the simultaneous system of Equations (29), (33), and (34) is accomplished using an Addams-Molton variable step-size, predictor-corrector routine. The solution, together with other parameters, is printed out according to the instruction of another control number on the first data card. Thus, results may appear at the end of every integration step in the Addams-Molton routine, or at equal increments in s. If the latter output occurs, solutions at values of s between the integration steps are obtained by using the Lagrangian interpolation method.

4. GEOMETRY

This section describes the geometry program, which is used to prepare input for the potential-flow program. Basically this input consists of the (x, y, z) panel corner point coordinates arranged in rectangular network form. All of the surfaces represented by source panels, quadrilaterals, and multihorseshoe vortices are input in this form and must be prepared either using the geometry program or by hand. The types of surfaces that can be represented are:

- A wing
- An internal lifting system for the wing
- A fan-in-wing inlet region
- A jet efflux tube
- Axisymmetric or pseudoaxisymmetric surfaces.

4.1 WING GEOMETRY

The WING subroutine is used to develop an array of (x, y, z) coordinates on a wing surface that define the corner points of the surface source paneling. Subroutine WING deals only with parts of a wing not containing a fan. A minimum of input information describing the wing geometry and paneling arrangement is required. The source-panel corner-point coordinate output is punched on cards in the format required by the potential-flow program.

Wing location and orientation. — Location and orientation of the wing in the reference coordinate system must be established first. The angles of attack and yaw are defined in the potential-flow program in terms of the direction of the free stream with respect to the reference coordinate system (pp. 112). Consequently, it is most convenient to orient the wing in the reference coordinate system so that these angles have their usual meaning with respect to the wing. The orientation is shown in Figure 17 with the x axis in the chordwise direction, the y axis in the spanwise direction of the right half of the wing, and the z axis upward. The origin of the (x, y, z) reference coordinate system is usually taken in the wing plane of symmetry at a convenient chordwise reference point.

The location and orientation of the wing in the reference coordinate system should take advantage of any symmetry properties of wing and flow. The plane of symmetry is the x-z plane. If a wing has this symmetry and if a symmetric solution (no yaw) is desired, only the right half of the wing geometry must be generated.

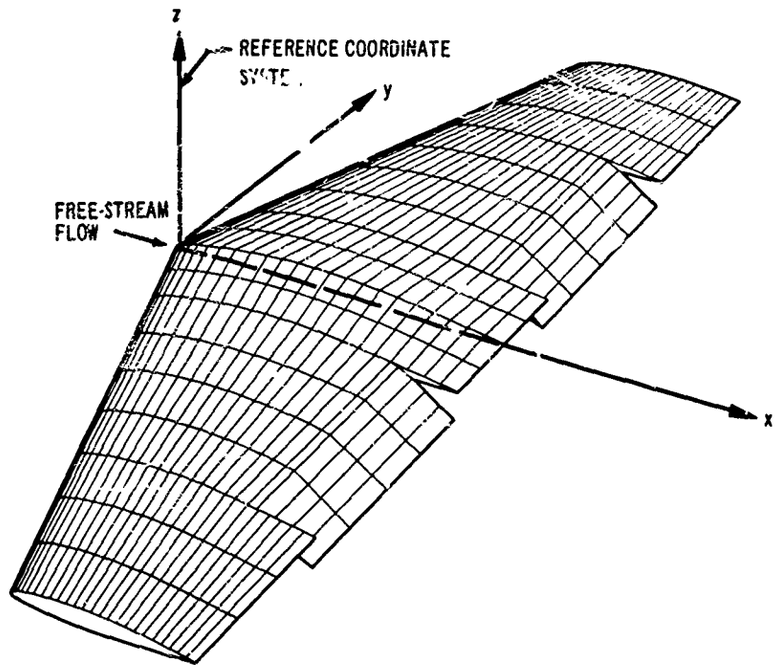

Figure 17. Paneled Wing in Reference Coordinate System.

Wing definition.—In the present method, a wing or part of a wing is defined by linear spanwise generators between two defining airfoil sections. Hence, a complete wing must often be divided into PARTS, each defined by linear spanwise generators, in order to provide an adequate definition. For example, the right half wing shown in Figure 17 can be prepared in three PARTS. The first PART would be the inboard unflapped section of the wing, the second PART would be the flapped section, and the third PART would be the outboard unflapped section. The definition and paneling of each PART is performed separately.

The inboard and outboard airfoil sections of a PART are defined by arrays of airfoil coordinates, input in a two-dimensional $(x/c,\ z/c)$ coordinate system made nondimensional with respect to the local chord. Figure 18 displays a typical airfoil section and shows the sequential order of the defining coordinates $(x/c,\ z/c)_i$ for use in the program. There are ORD_I of these $(x/c,\ z/c)_i$ pairs for the inboard section and ORD_O for the outboard section.

$$\left\{\left|(x/c)_1,\ (z/c)_1\right|,\ \left|(x/c)_2,\ (z/c)_2\right|,\ \ldots\ \left|(x/c)_{ORD_I},\ (z/c)_{ORD_I}\right|\right\} \tag{63}$$

$$\left\{\left|(x/c)_1,\ (z/c)_1\right|,\ \left|(x/c)_2,\ (z/c)_2\right|,\ \ldots\ \left|(x/c)_{ORD_O},\ (z/c)_{ORD_O}\right|\right\} \tag{64}$$

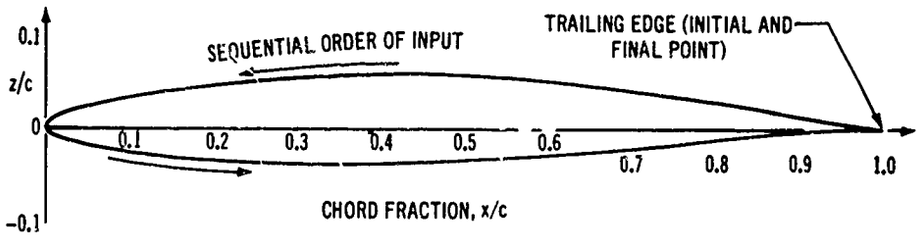

x/c	z/c
1.000000	0.000000
0.987500	0.001500
0.975000	0.002900
0.950140	0.006220
0.900280	0.013270
0.850380	0.020570
0.800420	0.027830
0.750450	0.034790
0.700430	0.041280
0.650360	0.047120
0.600270	0.052170
0.550140	0.056250
0.500000	0.059150
0.449840	0.060580
0.399680	0.060670
0.349510	0.059540
0.299360	0.057320
0.249210	0.053970
0.199090	0.049380
0.148990	0.043380
0.098940	0.035550
0.073940	0.030690
0.048980	0.024910
0.024080	0.017570
0.011690	0.012730
0.006780	0.009990
0.004350	0.008190
0.002500	0.006430
0.001250	0.004770
0.000500	0.003240
0.000050	0.001490

TRAILING EDGE

UPPER SURFACE

x/c	z/c
0.000000	0.000000
0.000230	-0.001250
0.001000	-0.003020
0.002250	-0.004760
0.003750	-0.006240
0.005690	-0.007760
0.008270	-0.009250
0.013370	-0.011410
0.025980	-0.014980
0.051100	-0.020140
0.076140	-0.024310
0.104170	-0.028120
0.138890	-0.031940
0.173610	-0.034860
0.208330	-0.037080
0.277780	-0.038680
0.347220	-0.039100
0.416670	-0.039240
0.486110	-0.038610
0.555560	-0.036180
0.625000	-0.031460
0.659720	-0.028060
0.699540	-0.024040
0.749520	-0.018670
0.799530	-0.013250
0.849590	-0.008030
0.899700	-0.003440
0.949850	0.000080
0.975000	0.000600
0.987500	0.000600
1.000000	0.000000

LEADING EDGE

LOWER SURFACE

TRAILING EDGE

Figure 18. Typical Airfoil Definition.

The location of these sections with respect to the reference coordinate system is fixed by specifying the reference coordinates of the leading-edge and trailing-edge points (x/c = 0, z/c = 0; x/c = 1.0, z/c = 0) of the inboard and outboard sections, denoted as

$$(XLE_I, YLE_I, ZLE_I) \quad (XTE_I, YTE_I, ZTE_I)$$
$$(XLE_O, YLE_O, ZLE_O) \quad (XTE_O, YTE_O, ZTE_O) \tag{65}$$

These coordinates are shown in Figure 19.

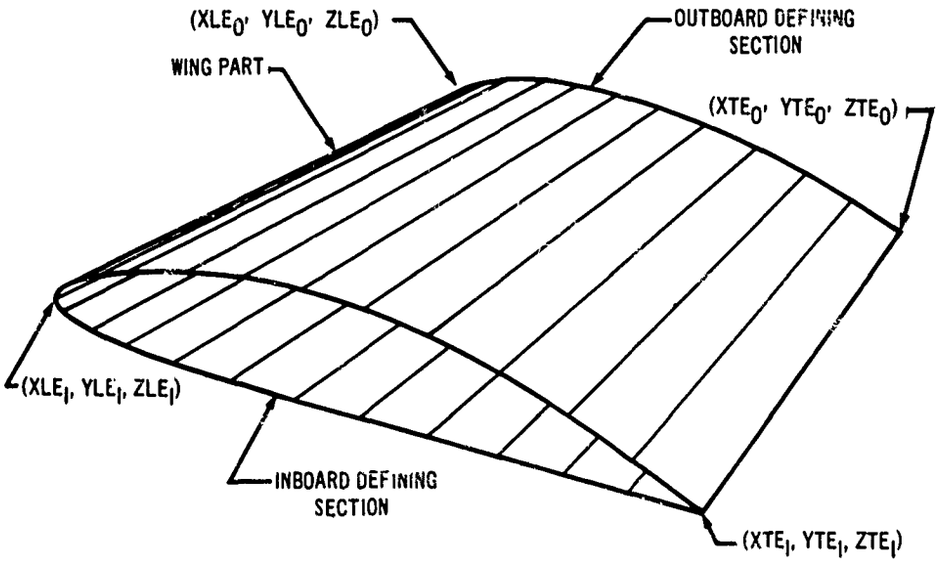

Figure 19. Definition of Wing PART.

The defining sections may be oriented at any angle with respect to the wing; the program constructs the defining sections perpendicular to the x-y plane of the reference coordinate system.

If the airfoil section leading and trailing edges are at (x/c = 0, z/c = 0; x/c = 1.0, z/c = 0) in the airfoil coordinate system, then the input coordinates of Equation (65) are the actual location of the four planform corner points. If the airfoil leading and trailing edge are not at (x/c = 0, z/c = 0; x/c = 1.0, z/c = 0) respectively, as is frequently the case for the trailing edge of a flapped airfoil, then the input coordinates of Equation (65) may not physically coincide with the actual wing trailing edge.

The pointwise definition of the inboard and outboard airfoil sections, together with their leading-edge and trailing-edge coordinates in the reference coordinate system, furnish the basic geometric definition of a wing PART.

The user has the option of two different wing surface definitions between the inboard and outboard airfoil sections. In the first case, the wing surface is defined by spanwise generators connecting corresponding input coordinates on the inboard and outboard airfoils. The number of input coordinates in the inboard and outboard definition tables must then be equal; that is, ORD_I must equal ORD_O. The $(x/c)_i$ locations in the two tables need not coincide. This type of definition must be used to panel wing PARTS where the spanwise generators connect points of unequal percent chord. The flapped section of the wing shown on Figure 17 was prepared using this first option.

In the second case, the wing surface is defined by spanwise generators connecting points of equal percent chord. A curve-fitting procedure is used to establish the defining airfoil ordinates at the desired percent chord locations from the basic pointwise airfoil definition. The number of defining coordinates ORD_I and ORD_O may be different. This second option is normally used for simple unflapped wings.

Wing paneling. — Figure 20 displays an example of a paneled wing PART. Panel corner points are defined by the intersection of spanwise generators with a plane parallel to the x-z plane. Thus, chordwise panel edges are restricted to being in a plane parallel to the x-z plane. A series of these planes is specified by a table of y_k values input to the geometry program. There are COL of these y_k values input in order of increasing y.

$$\left(y_1, y_2, \ldots y_k, \ldots y_{COL}\right) \tag{66}$$

There are two types of surface paneling corresponding to the two types of wing surface definition. In the first case, the spanwise generators connect corresponding coordinates in the inboard and outboard airfoil coordinate tables, which are, perhaps, at different $(x/c)_i$ locations. In the second case, the spanwise generators connect lines of constant percent chord, and an independent table of $(x/c)_i$ panel locations is input to the program. There are ROW of these $(x/c)_i$ values for each wing PART.

$$\left[(x/c)_1, (x/c)_2 \ldots (x/c)_{ROW}\right] \tag{67}$$

The order of input of the paneling $(x/c)_i$ table is the same as for the defining airfoil section; that is, from the trailing edge along the upper surface to the leading edge and back along the lower surface to the trailing edge.

Curve-fitting and paneling details. — If the latter definition involving constant percent chord spanwise generators is desired, airfoil ordinates at the desired chordwide positions are obtained from a curve fitted to adjacent airfoil ordinates. The program takes each (x/c) panel location input and searches for neighboring $(x/c)_i$ values in the inboard and outboard defining $(x/c, z/c)_i$ tables. The search is begun at the airfoil trailing edge and proceeds forward

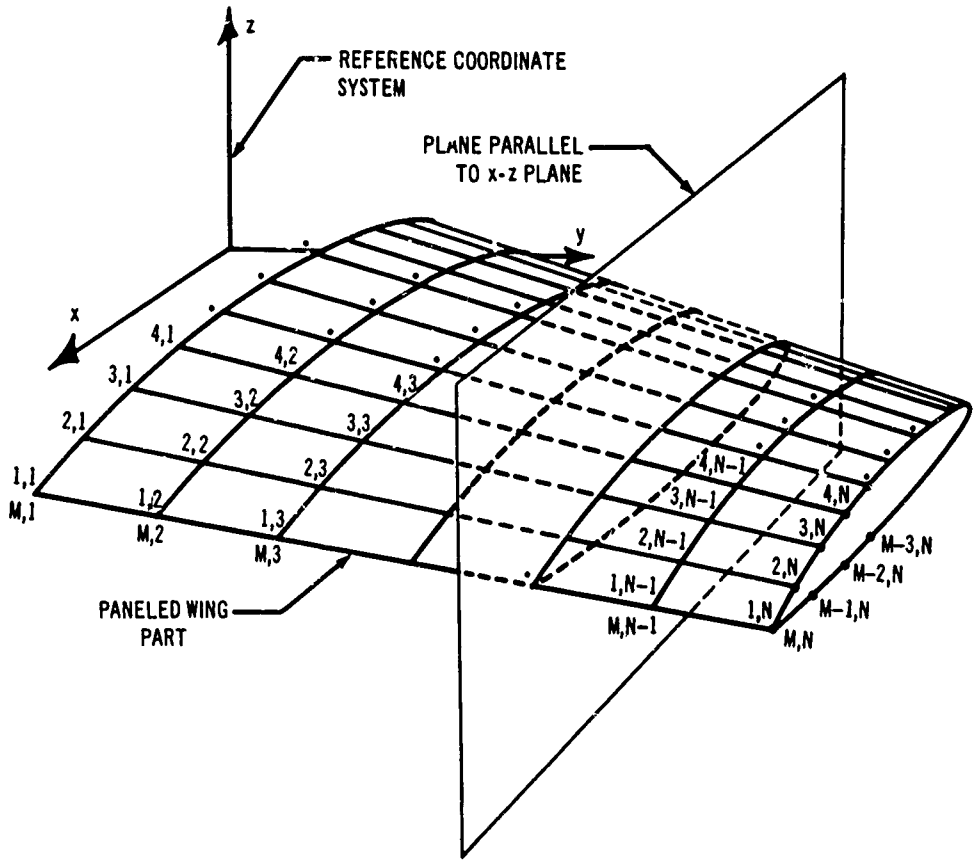

Figure 20. Example of Paneled Wing PART.

over the upper surface to the leading edge and along the lower surface back to the trailing edge. It is extremely important that the definition and paneling tables be correctly input. The $(x/c)_i$ values in each table must continuously decrease to a minimum value, usually zero at the leading edge, and then increase continuously. The object of the search is to find for each input (x/c) panel location four points bracketing the desired (x/c) panel point between the second and third point. The result of this search procedure is four pairs of $(x/c,\ z/c)_i$ points from the defining airfoil section table.

$$\begin{aligned} &(x/c)_1,\ (z/c)_1 \\ &(x/c)_2,\ (z/c)_2 \\ &(x/c)_3,\ (z/c)_3 \\ &(x/c)_4,\ (z/c)_4 \end{aligned} \tag{68}$$

The program next constructs a local x'-z' coordinate system on the airfoil surface, as shown in Figure 21. The origin is at the point $(x/c)_1$, $(z/c)_1$ and the x' axis passes through the point $(x/c)_4$, $(z/c)_4$. The above coordinates of Equation (68) are then transformed into this new coordinate system, as shown in Figure 22.

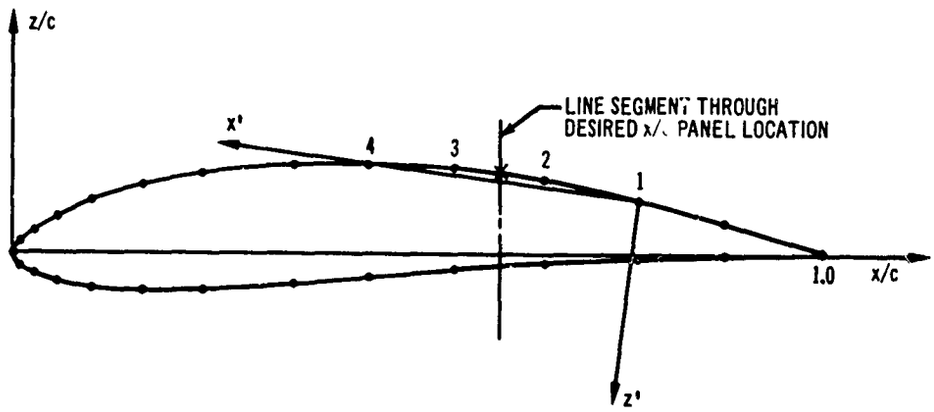

Figure 21. Four Points Needed for Curve Fitting.

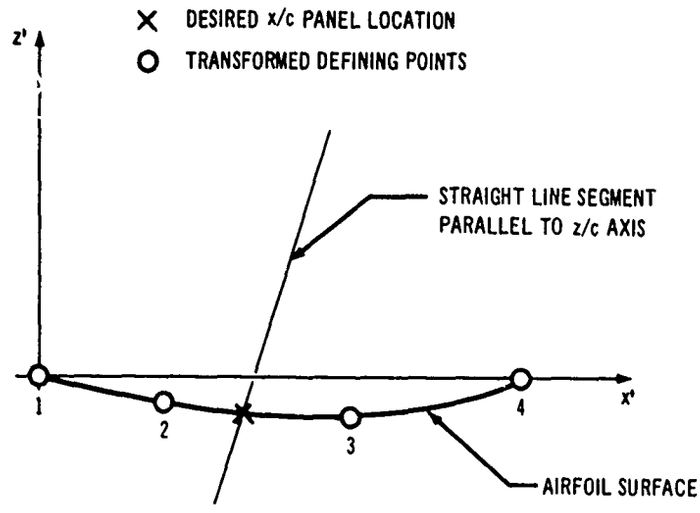

Figure 22. Airfoil Surface Local Coordinate System.

The definition of a line segment at the desired (x/c) panel location and parallel to the z axis is also transformed into the x'-z' coordinate system. This will intersect the airfoil surface in the interval between points 2 and 3, except, perhaps, for the trailing-edge panels. To find this intersection, the airfoil section surface is fitted with a biquadratic curve between points 1 and 4. A quadratic $Q_1(x')$ is first found that passes through points 1, 2, and 3. Then a second quadratic $Q_2(x')$ is found that passes between the points 2, 3, and 4. Figure 23 illustrates the curves under discussion.

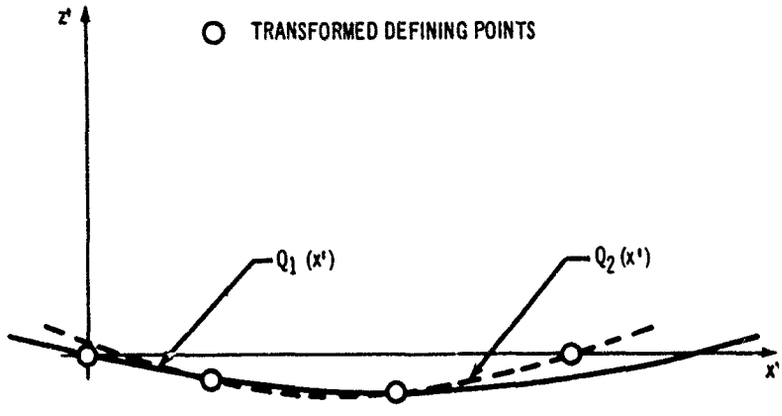

Figure 23. Biquadratic Curve-Fitting Procedure.

Between points 2 and 3 a curve is constructed that is weighted between the two curves $Q_1(x')$ and $Q_2(x')$ on the basis of x'.

$$C(x') = \frac{(x_3' - x')\, Q_1(x') + (x' - x_2')\, Q_2(x')}{x_3' - x_2'} \tag{69}$$

The cubic C(x') always lies between $Q_1(x')$ and $Q_2(x')$.

The program finds the intersection of the straight line segment and the cubic curve by an iterative technique. When the intersection is in the interval between points 2 and 3, this cubic curve is used. If the desired (x/c) panel point is too near the trailing edge, the search procedure may not bracket the desired point in the interval 2-3. The desired point then falls in the interval 1-2 or the interval 3-4, and the appropriate quadratic equation is employed. The panel corner point found by this curve intersection procedure is transformed back into the (x/c, z/c) coordinate system.

The described curve-fitting procedure is used to determine the (z/c) coordinate for each desired (x/c) panel location in both the inboard and outboard airfoil planes. The two defining $(x/c, z/c)_i$ tables are then replaced by these tables of panel corner point coordinates. The resulting $(x/c, z/c)_i$ panel tables are then scaled to the local chord length and placed on the planform in the correct position as determined by the coordinates in Equation (65). The result is two sets

of (x, y, z) panel edge coordinates, one on the inboard section and the other on the outboard section. If the first method is used, these two sets of (x, y, z) coordinates come directly from the input airfoil tables with no curve fitting. The resultant two tables are subsequently handled in the same fashion, regardless of the manner in which they were constructed.

The actual paneling procedure is straightforward. Corresponding points on the two defining airfoil sections are connected by straight lines, and intermediate panel corner points are given by the intersection of these lines with the planes defined by Equation (66). The final output is a network of ($x_{i,k}$, $y_{i,k}$, $z_{i,k}$) panel corner point coordinates, with the subscript i increasing chordwise (from 1 to M = ROW) and the subscript k increasing spanwise (from 1 to N = COL). (A paneled wing PART and the network numbering was shown in Figure 20.)

As an example of an application of subroutine WING, consider the flapped section of the NASA wing shown in Figure 17. The constant chord flap of this wing dictated that a spanwise panel line be parallel to the flap knee line. As a result, the spanwise panel lines connect lines of unequal percent chord. The procedure for preparing the wing panel geometry was to first construct large drawings of the planform and airfoil sections at each end of the flapped section. Different panel arrangements were then layed out on these drawings until a good design was reached. The panel (x/c)'s determined from this procedure did not coincide with the defining (x/c)'s for the airfoil so a preliminary computer run was made with the standard airfoil definition and the selected $(x/c)_i$ paneling table. A fictitious planform with a chord of unity was used for this preliminary computer run. The results then gave the two $(x/c,\ z/c)_i$ tables used to define and panel the flapped section in a second computer run.

4.2 LIFTING SYSTEM GEOMETRY

The present method employs an internal lifting system of multihorseshoe vortices that emanate from the wing trailing edge to form a trailing vortex sheet. Subroutine LIFT in the geometry program prepares the vortex network (x, y, z) coordinates, the positions of the Kutta condition boundary points and the boundary-point normal vectors (n_x, n_y, n_z) from a simplified lifting system definition. The output is punched on cards in the format required by the potential-flow program.

The internal lifting system for a complete configuration is divided into PARTS, in a manner analogous to the surface source panel arrangement, with each PART treated independently. The lifting system for the NASA fan-in-wing model (shown in Figures 81, 82, and 83) is composed of five separate PARTS. Three of these emanate from the wing trailing edge to form the trailing vortex sheet (Figure 81). The fourth lifting system network is in the inlet region and connects to the barrier network in the fan face (Figure 82). The fifth lifting system network geometrically coincides with the fourth one except at the inner boundary, where it connects to the jet efflux tube (Figure 83).

Subroutine LIFT was designed primarily to provide a convenient geometric definition of those PARTS not adjacent to the fan. The arrangement in the

vicinity of the fan is partly handled by subroutine INLET (Section 4.3). However, in many cases it is necessary to prepare portions of the internal systems near the fan by hand, due to individual tailoring requirements. In the example referred to above, the lifting systems for those wing sections inboard and outboard of the flapped section were prepared using subroutine LIFT. The lifting system routed behind the fan in the flapped section, and the two systems associated with the barrier and efflux tube were prepared by hand, with the aid of information obtained from the surface source panel geometry. The interior network coordinates were found by averaging the corresponding upper and lower surface source network coordinates.

Interior lifting system definition.—A multihorseshoe lifting system is composed of an interior portion, consisting of chordwise and spanwise vortex segments, and a trailing portion external to the wing, as shown in Figure 24. The interior portion is constructed in a manner analogous to that for the surface source panels. Inboard and outboard defining stations are introduced, with spanwise generators formed by connecting corresponding points at the two defining stations. The corner point coordinates defining the interior multihorseshoe network are found at the intersection of these spanwise generators with specified planes parallel to the x-z plane.

The positions of the spanwise segments at the inboard and outboard defining stations are input as arrays of coordinates in a two-dimensional (x/c, z/c) coordinate system.

$$\left\{\left[(x/c)_1,\ (z/c)_1\right],\ \left[(x/c)_2,\ (z/c)_2\right],\ \ldots\ \left[(x/c)_{ROWI_I},\ (z/c)_{ROWI_I}\right]\right\} \tag{70}$$

$$\left\{\left[(x/c)_1,\ (z/c)_1\right],\ \left[(x/c)_2,\ (z/c)_2\right],\ \ldots\ \left[(x/c)_{ROWI_O},\ (z/c)_{ROWI_O}\right]\right\} \tag{71}$$

The $(x/c,\ z/c)_i$ coordinates begin with the point nearest the leading edge and proceed aft to the trailing edge, as shown in Figure 24. Corresponding inboard and outboard points are connected to form the spanwise vortex segments, so the number of coordinates for the inboard and outboard tables must be equal; that is, $ROWI_I$ must equal $ROWI_O$. No curve-fitting option, such as is used to provide intermediate points in the surface panel definition, is provided here. The number of $(x/c,\ z/c)_i$ coordinates may be greater than the number of bound vortices desired to provide for bends in the chordwise segments. The last $(x/c,\ z/c)_i$ coordinate is usually placed at the trailing edge. It is the point to which the trailing vortices are attached, and defines the boundary between the interior and exterior portions of the multihorseshoe network.

The position and orientation of the defining stations are given by the following input quantities:

$$(XLE_I,\ YLE_I,\ ZLE_I) \qquad (XTE_I,\ YTE_I,\ ZTE_I) \tag{72}$$

$$(XLE_O,\ YLE_O,\ ZLE_O) \qquad (XTE_O,\ YTE_O,\ ZTE_O) \tag{73}$$

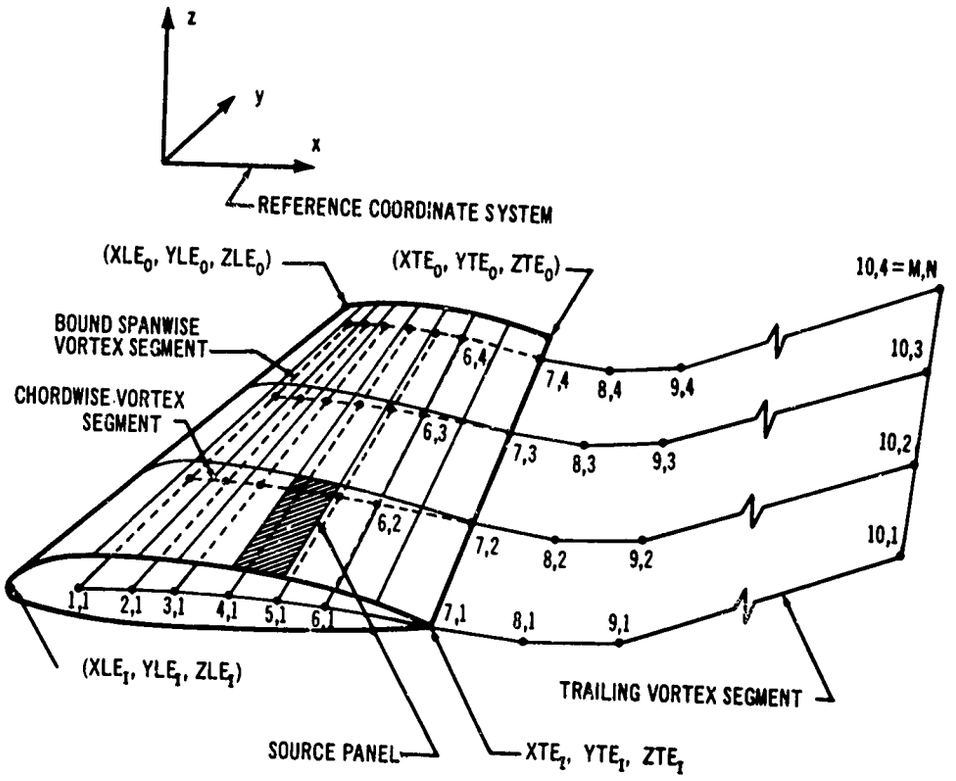

Figure 24. Wing and Lifting System.

These (x,y,z) coordinates of the four lifting system corner points are located in the reference coordinate system. Subroutine LIFT scales the nondimensional coordinates of Equations (70) and (71) so that the coordinates (x/c = 0, z/c = 0, x/c = 1.0, z/c = 0) are placed on the leading-edge and trailing-edge points, respectively, of Equations (72) and (73). The lifting system can be prepared independently of the wing surface geometry. However, because the internal vortices are usually aligned with source panel edges, it is usually most practical to consider the lifting system as embedded in a corresponding wing PART so that the four planform corner points of the wing PART and lifting system PART coincide. The x/c and z/c axes also coincide for the airfoil section and the lifting system definition in these cases.

The corner-point coordinates defining the interior multihorseshoe network are found as the intersection of the spanwise generators connecting corresponding points in the two $(x/c,\ z/c)_i$ tables with planes parallel to the x-z plane of the reference coordinate system. The location of these planes is given by a table of y_k values, input in the order of increasing y.

$$y_1,\ y_2,\ \ldots\ y_k,\ \ldots\ y_{COL} \qquad (74)$$

Trailing vortex definition. — The trailing vortices attach to the points defined by the intersections of the straight line connecting the last pair of $(x/c, z/c)_i$ points with the y_k planes, as is evident in Figure 24. The inboard and outboard trailing vortices are defined by tables of segment lengths and direction cosines of each segment, input in increasing order in the downstream direction.

$$\left(L_1, L_2, \ldots L_{ROWT_I}\right) \tag{75}$$

$$\left\{\left[a_x, a_y, a_z\right]_1, \left[a_x, a_y, a_z\right]_2, \ldots . \left[a_x, a_y, a_z\right|_{ROWT_I}\right\} \tag{76}$$

Similarly, there are $ROWT_O$ values for the outboard trailing vortex, which are not shown here. The number of values in the inboard tables must match the number in the outboard tables; that is, $ROWT_I$ must equal $ROWT_O$.

The inboard and outboard vortices are constructed by placing the segment lengths end to end, each segment aligned according to its direction cosines. The desired (x, y, z) coordinates at the end points of adjacent segments are obtained from equations of the form

$$\begin{aligned} x_{i+1} &= x_i + L_i a_{x_i} \\ y_{i+1} &= y_i + L_i a_{y_i} \\ z_{i+1} &= z_i + L_i a_{z_i} \end{aligned} \tag{77}$$

The points defining the intermediate trailing vortices are obtained by linear interpolation between the inboard and outboard vortices, and are given by the equations

$$\begin{aligned} x_{i,k} &= x_{i,1} + \left(x_{i,NY} - x_{i,1}\right)\left(\frac{y_k - y_1}{y_{NY} - y_1}\right) \\ y_{i,k} &= y_{i,1} + \left(y_{i,NY} - y_{i,1}\right)\left(\frac{y_k - y_1}{y_{NY} - y_1}\right) \\ z_{i,k} &= z_{i,1} + \left(z_{i,NY} - z_{i,1}\right)\left(\frac{y_k - y_1}{y_{NY} - y_1}\right) \end{aligned} \tag{78}$$

where NY is the total number of trailing vortices.

Boundary-point definition. — Subroutine LIFT also computes the Kutta condition boundary-point coordinates (x, y, z) and direction cosines (n_x, n_y, n_z) of unit normals constructed perpendicular to the local trailing-edge bisector, as required by the potential-flow program.

Two options are available to determine the spanwise or y values of the boundary points. In the first method, the boundary points are located at y_k values input by the user. (These are different from the y_k values defining the vortex corner points.) The second method was designed to locate the boundary points directly behind (the same y value) the most rearward source-panel boundary points on the wing upper surface. With this option, subroutine LIFT requires as input the y_k locations of the source-panel edges on the exterior wing surface.

For both cases, the eight $(x/c,\ z/c)_i$ points shown in Figure 25 must be input. In the latter case, these points, together with y_k locations of the source-panel edges, define a row of panels on the upper surface, which will be the same as the surface source panels provided that the input points correspond to those used to define the surface source panels. Subroutine LIFT computes the y location of the centroids of the upper surface panels thus defined, and assigns these same values to the y coordinates of the Kutta condition boundary points. It is not necessary that the eight $(x/c,\ z/c)_i$ points be coincident with the surface source-panel definition. The only effect will be that the Kutta condition boundary points would then not be exactly behind the source-panel boundary points, which in most cases is not significant. It is imperative, however, that the eight input points are situated such as to adequately define the trailing-edge angle at both ends of the PART, for they are used to define the trailing-edge bisector, as explained below.

The direction of the trailing-edge bisector for each boundary point is calculated in the plane parallel to the x-z plane at the boundary-point y location. The intersection of the upper and lower surface panels (Figure 25) with this plane defines two lines in the plane. The bisector of these two lines is defined as the trailing-edge bisector.

The average trailing edge is defined as the line midway between the upper and lower surface trailing edges (Figure 25). For the usual case of a closed airfoil, these are coincident.

The x and z coordinates of each boundary point are obtained along the trailing-edge bisector aft of the average trailing edge. Two options are available for setting the distance aft of the trailing edge. In both cases, the length of the upper surface panel at each boundary-point y location is calculated as the distance between the points of intersection of the line connecting $(x/c,\ z/c)_2$ and $(x/c,\ z/c)_6$, and the line connecting $(x/c,\ z/c)_1$ and $(x/c,\ z/c)_5$, with the plane parallel to the x-z plane passing through the boundary point. With the first option, the boundary point is placed a standard distance off the trailing edge $\epsilon_{bp} = 0.01$ times the length of the upper surface panel. The second option is to input an arbitrary value of ϵ_{bp}, which is the ratio of the offset distance to the upper surface panel length.

The direction cosines of the normal vector are found in two different ways. In the first method where the y_k of the boundary points are input directly, subroutine LIFT computes the boundary-point vector by forming the vector product of the vector bisecting the trailing edge and a vector parallel to the average trailing edge. In the second method where the y_k of the panel edges are input, subroutine LIFT computes the unit vectors normal to the upper and lower surface

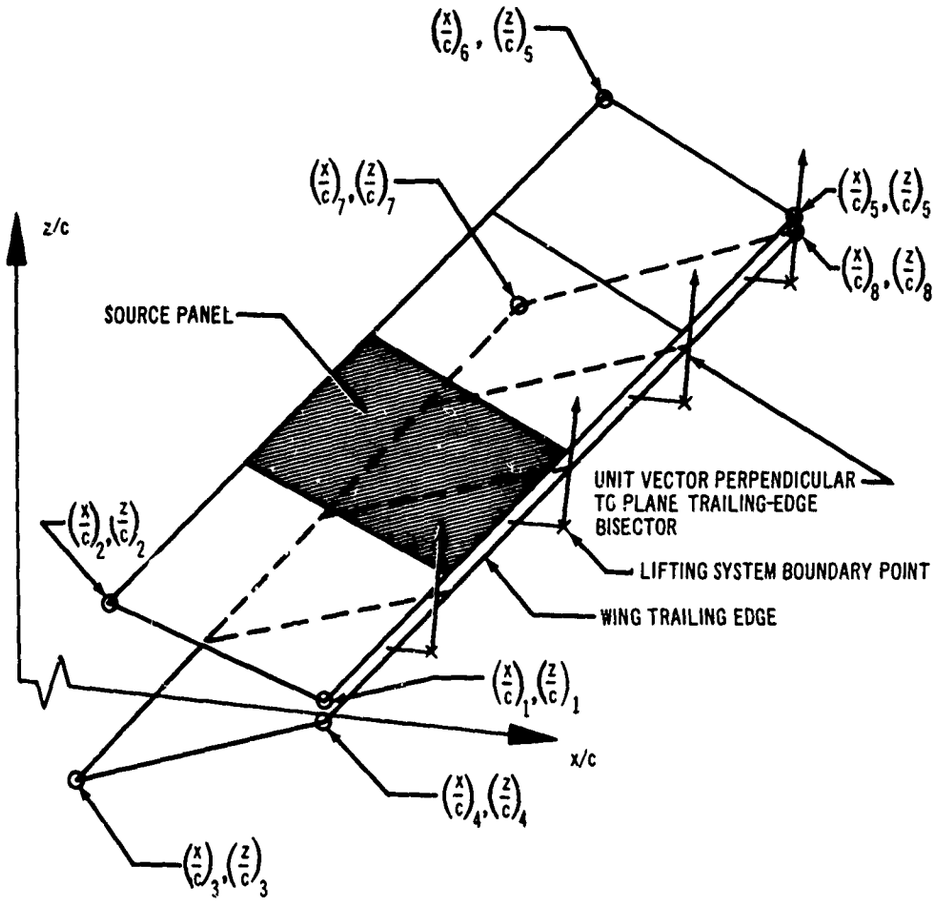

Figure 25. Lifting System Boundary-Point Placement.

panels by forming the vector product of vectors joining opposite corners of the quadrilateral panels. The boundary-point vector is then found by normalizing the x, y, and z components of the difference between the upper and lower surface normal vector components.

4.3 INLET GEOMETRY

The paneling layout for a fan-in-wing configuration, such as the NASA model shown in Figure 26, is distinguished by an area of special surface paneling near the fan, shown within the heavy line. This special area, and a similar area on the lower surface, are called collectively the "inlet geometry," and are prepared using subroutine INLET. The wing surface outside the heavy line is prepared in the ordinary manner, using subroutine WING. This section describes the methods employed to panel the inlet geometry on both the upper and lower wing

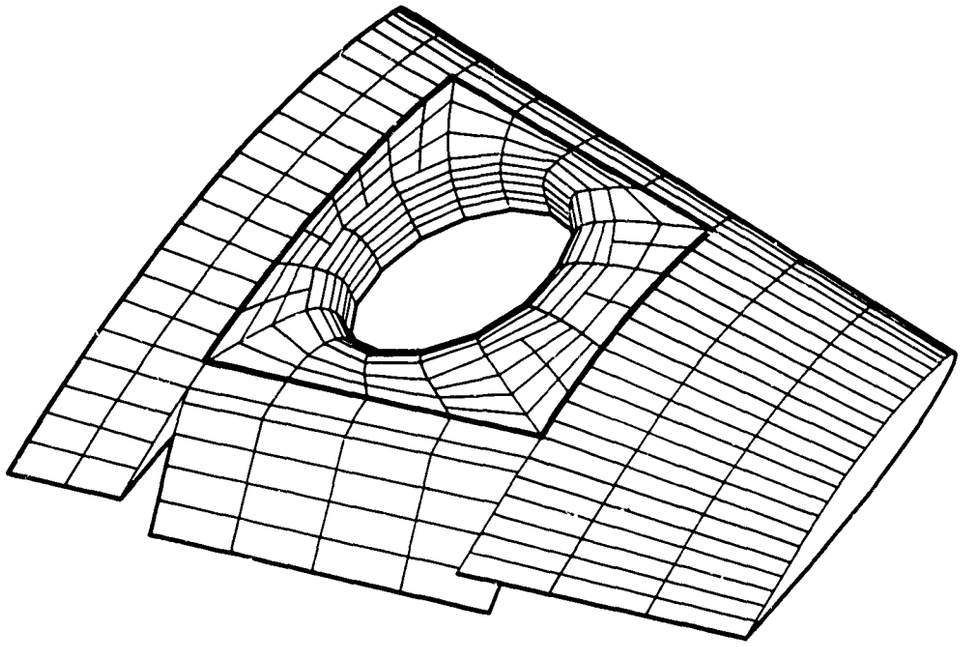

Figure 26. Wing Containing Paneled Inlet.

surfaces, and also to determine the location of the internal lifting systems surrounding the fan. The resulting source panel and internal system corner-point coordinates are punched on cards in the format required by the potential-flow program.

The inlet geometry on the wing upper surface consists of a portion of unmodified wing surface adjacent to the periphery of the inlet geometry, a curved inlet lip contour between the unmodified wing surface and the inlet throat, and a cylindrical inlet throat extending to the wing lower surface. The lower wing surface is generally unmodified between the fan exit and the outer boundary of the inlet geometry. Five different types of paneling definition are used, each adapted to a particular part of the inlet geometry. Figure 27, a cross section of the wing through the fan axis, shows the inlet geometry subdivided into REGIONS that delineate the parts of the inlet containing the five different types of paneling. Correspondingly, subroutine INLET is divided into REGIONS. Each REGION requires its own input and is handled separately. Subroutine INLET also contains a sixth REGION, which is used to furnish a definition of the wing surface in any radial cutting plane but does not actually panel the wing surface or produce punched cards.

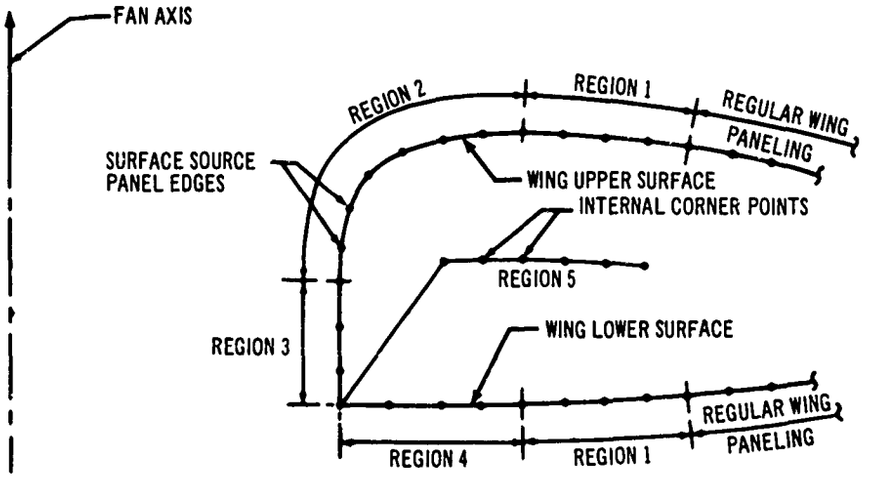

Figure 27. Division of Inlet into Geometric REGIONS.

Both the upper and lower wing surfaces contain a REGION 1. The paneling in REGION 1 provides a transition between the ordinary wing paneling and the paneling on the inlet lip or near the fan exit, which is defined radially. On the upper surface, REGION 1 extends from the outer boundary adjacent to the regular wing paneling to an arbitrary inner boundary circumscribing the inlet lip. This inner boundary can be located at the juncture of the inlet lip with the wing surface, or may be outside of this juncture. In any event, the wing surface in REGION 1 must not contain any part of the inlet lip. The boundaries of REGION 1 on the lower surface are usually chosen to be directly below those on the upper surface, so that the upper and lower surface paneling in this area will be similar.

REGION 2 extends over the inlet lip and down into the inlet to a point at or beyond where the surface contour becomes cylindrical. REGION 3 consists of the lower cylindrical surface of the inlet extending to the wing lower surface. The lower surface adjacent to the fan exit is REGION 4. Panel edges in REGIONS 2, 3, and 4 lie in radial planes through the fan axis. REGION 5 defines the location of the multihorseshoe vortex networks that connect to the fan barrier and the efflux tube.

The paneling in each REGION may be divided into PARTS, if desired, which are treated independently. A PART consists of a single rectangular array of panels. For complex configurations it is often necessary to divide a REGION into several PARTS in order to achieve a satisfactory paneling arrangement.

All of the REGIONS require as input the coordinates of a point on the fan axis and the direction cosines of the fan axis. These serve to define a fan coordinate system aligned with the fan axis. Each REGION, except 5, also requires a basic wing definition similar to that required for subroutine WING. The defining stations should be located at the inboard and outboard boundaries of the inlet geometry. A detailed description of each of the different REGIONS follows.

REGION 1. — REGION 1 lies on the unmodified wing surface and is used as a transition region between the ordinary wing paneling and the near-axisymmetric inlet paneling. A typical panel arrangement for a portion of REGION 1 is shown in Figure 28. Two tables of (x,y) coordinates are input, one defining the panel corners along the outer boundary and the other defining the panel corners on the boundary between REGIONS 1 and 2. These points are denoted in Figure 28 by heavy dots. The z coordinates of the points are computed by the technique explained in Appendix II. These initial defining points must be chosen carefully, so that the paneling blends smoothly into the adjacent REGIONS. Intermediate panel corner points between the two input arrays are found as follows: Corresponding points in the two arrays are connected by straight lines (e.g., the i^{th} point in the first array is connected to the i^{th} point in the second array). Divisions along these lines are specified by an input fraction table. The same set of fractions applies to all connecting lines for a particular PART. The fraction values vary from .0 to 1.0, when .0 signifies an (x,y) value in the first input table and 1.0 indicates an (x,y) value in the second input table. At each fractional value along these lines, another line parallel to the z axis is constructed. The intersection of this line with the wing surface determines the surface z coordinate by the method of Appendix II. Thus, columns of panel corner points lie in planes perpendicular to the x-y plane and pass through corresponding points in the two input arrays. The fractional values used for the network shown in Figure 28 were .0, .5, 1.0. This particular network was selected for the sample case presented in Appendix III.

The following rules should be observed to ensure a right-hand network of surface panels. The first (x,y) table should be for those points that lie on the boundary with the ordinary wing paneling. The second (x,y) table should be for those points closer to the fan axis that lie on the boundary with the radially paneled inlet contour, REGION 2. The order of input for the upper surface should be counterclockwise viewed from above. For the lower surface, the order of input should be clockwise when viewed from above.

REGION 2. — This REGION encompasses the inlet lip and extends from the edge of REGION 1 on the unmodified wing surface to the cylindrical portion of the inlet throat or beyond. In practice, it is usually convenient to extend REGION 2 to the lower edges of the source panels intersected by the fan barrier. The need for paneling in REGION 3 is thus removed, for the inlet is not usually paneled below the barrier. However, care must be taken to ensure that the fan barrier intersects the lower source panels near their centroids.

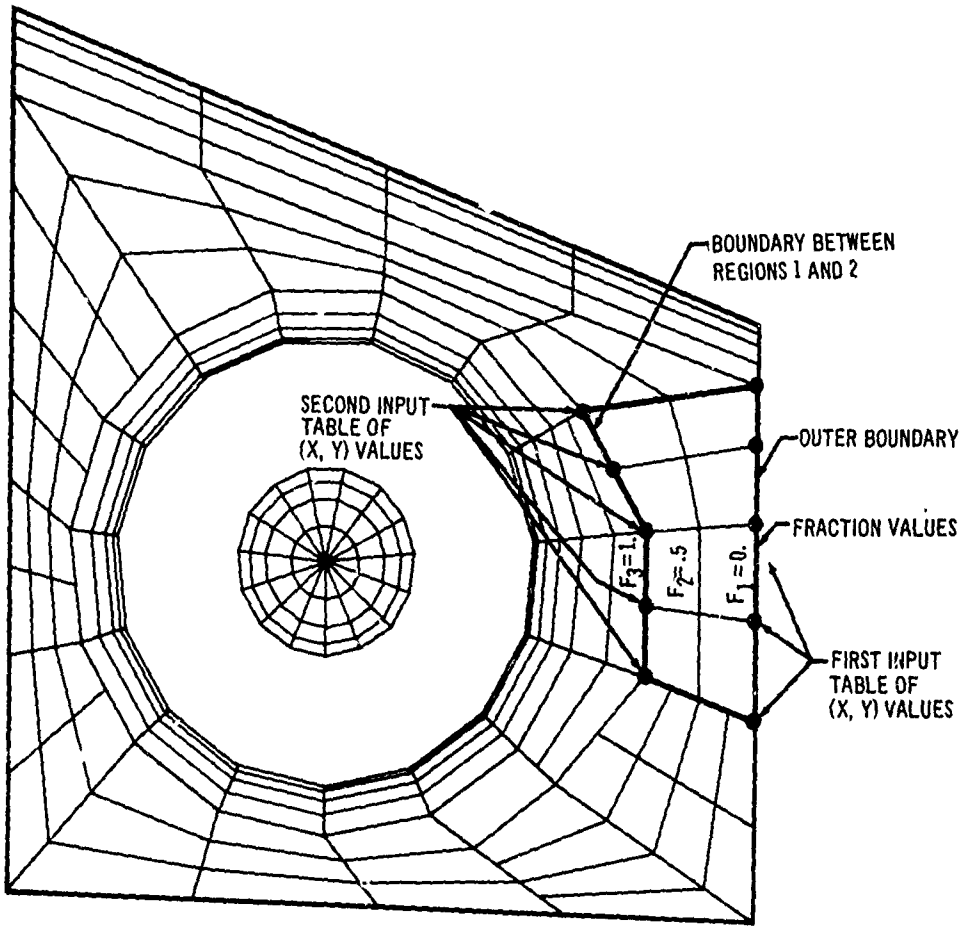

Figure 28. REGION 1 Source-Panel Network.

The paneling in REGION 2 is done in a series of radial planes passing through the fan axis. A typical plane is shown in Figure 29. The angular location θ of these planes is referenced from that plane through the fan axis whose line of intersection with the fan face plane is parallel to the x-z plane. The direction of positive θ is shown in Figure 29. A two-dimensional (R, Z) coordinate system is defined in each radial plane, with the origin located at the input (x_o, y_o, z_o) point on the fan axis and the Z axis aligned with the fan axis.

Panel corner points are input as an (R, Z) table in two radial defining planes, called θ_{D1} and θ_{D2}. There must be the same number of points in these two planes, but their coordinates may be different. Corner points in intermediate planes between these two are then obtained by the program through an interpolation procedure that will be explained later. An input array of θ_P values defines the location of these intermediate paneling planes.

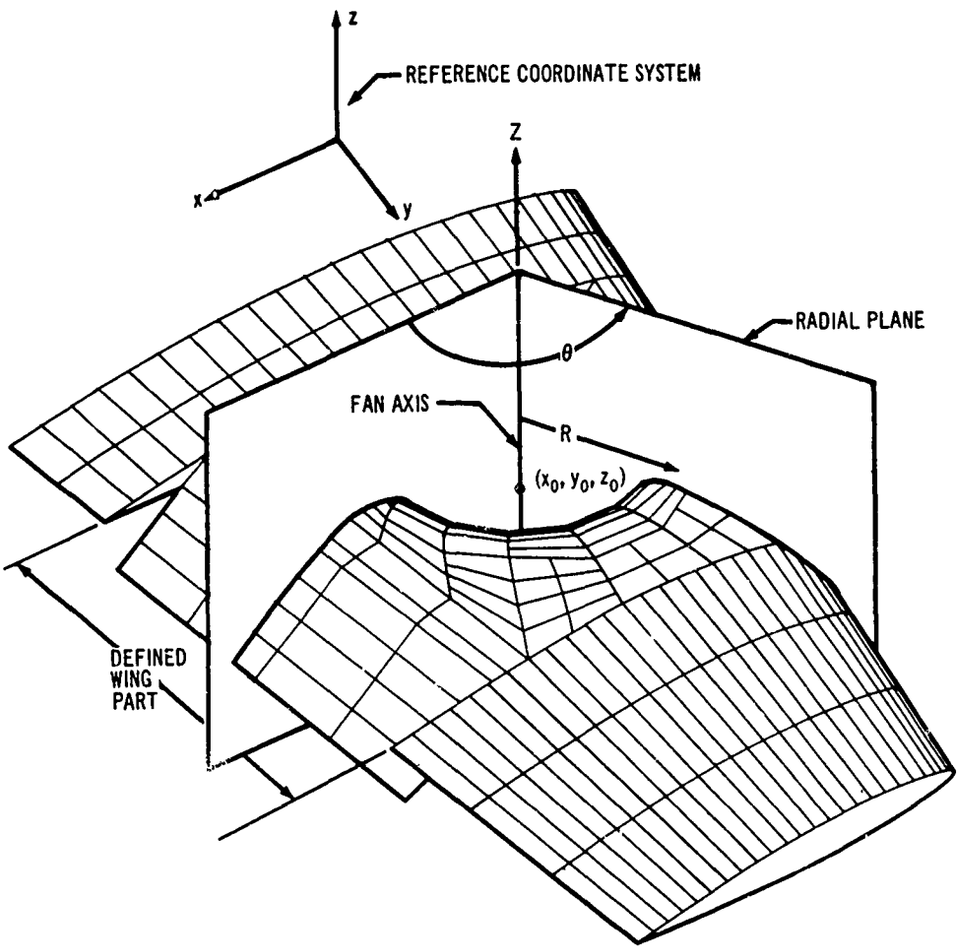

Figure 29. Radial Plane Used for Inlet Definition.

A typical set of panel corner points in a radial plane is shown in Figure 30. The order of input is from the first point on the upper wing surface, called (R_1, Z_1), to the last one, called (R_{ref}, Z_{ref}), on the cylindrical inlet throat. It is necessary that the first point lies on the upper wing surface. If not, the program will shift it to the surface. REGION 6 of subroutine INLET provides the user with a convenient definition of the wing upper surface intersection in arbitrary radial planes, so that the details of the intersection of the inlet lip with the wing surface can be easily examined.

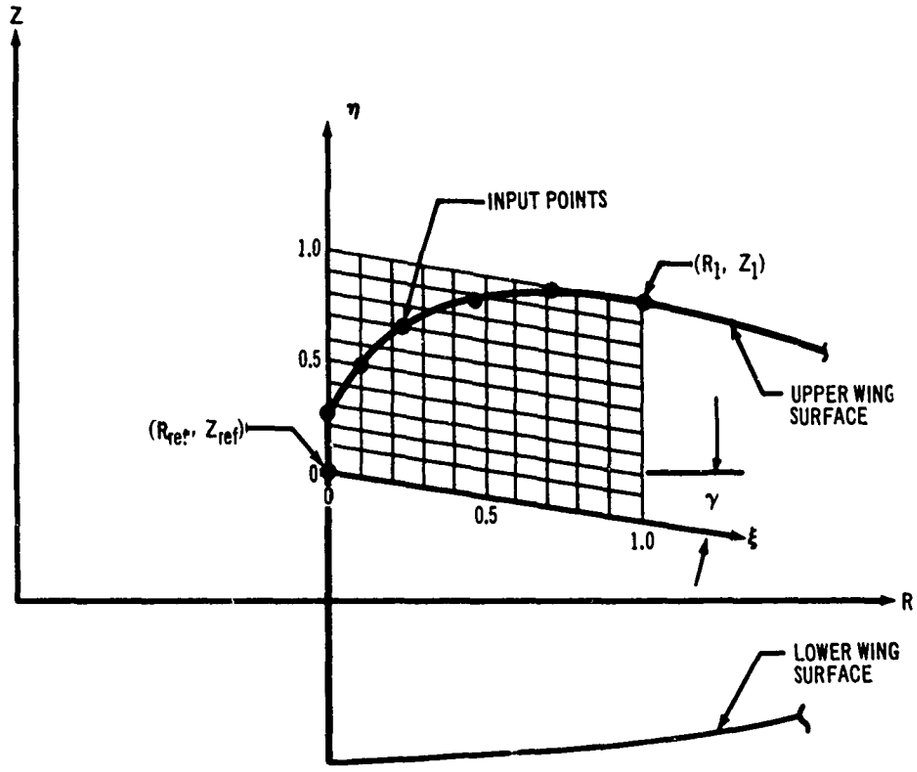

Figure 30. Construction of Sheared Coordinate System.

The interpolation procedure for determining the (R, Z) coordinates of panel corner points in the intermediate planes utilizes a sheared, normalized coordinate system in each radial plane. Figure 30 shows the sheared (ξ,η) system, which in each radial plane is constructed with the origin at (R_{ref}, Z_{ref}). The η axis is parallel to the fan axis, and the ξ axis is parallel to the wing surface tangent at (R_1, Z_1). This tangency condition ensures that no undesired slope discontinuities will appear at the intersection of REGIONS 1 and 2. The system is normalized with the point (R_1, Z_1) having coordinates $\xi = 1$, $\eta = 1$. In order to establish this system in the intermediate planes, values of R_{ref}, Z_{ref}, and R_1 are obtained by linear interpolation in θ from the input values at θ_{D1} and θ_{D2}. The Z_1 coordinate in each plane is placed on the wing upper surface. The program then determines the surface tangent at (R_1, Z_1) by finite difference, thus obtaining sufficient information to establish the sheared coordinate system.

Corner-point coordinates in the intermediate planes are determined as follows: The two input (R, Z) tables at θ_{D1} and θ_{D2} are transformed into the sheared coordinate system by the equations

$$\xi_{i,j} = \frac{R_{i,j} - R_{ref,j}}{R_{1,j} - R_{ref,j}}$$

$$\eta_{i,j} = \frac{(Z_{i,j} - Z_{ref,j}) - (R_{i,j} - R_{ref,j}) \tan\gamma_j}{(Z_{1,j} - Z_{ref,j}) - (R_{1,j} - R_{ref,j}) \tan\gamma_j} \tag{79}$$

where subscript i refers to the particular point in the defining table and subscript j refers to the defining plane. The angle γ is defined in Figure 30. The corner-point coordinates at intermediate θ_{Pj} planes are found by linear interpolation as

$$\xi_{i,j} = \xi_{i,D1} + (\xi_{i,D2} - \xi_{i,D1})\left(\frac{\theta_{Pj} - \theta_{D1}}{\theta_{D2} - \theta_{D1}}\right)$$

$$\eta_{i,j} = \eta_{i,D1} + (\eta_{i,D2} - \eta_{i,D1})\left(\frac{\theta_{Pj} - \theta_{D1}}{\theta_{D2} - \theta_{D1}}\right) \tag{80}$$

The inverse of Equation (79) is used to transform the points back to the (R, Z, θ) system, from which they are finally transformed to the (x, y, z) reference coordinate system.

In summary, a PART in REGION 2 is defined by inputting the panel corner points in two radial planes. Equal numbers of points are input in each plane. Corner points in intermediate planes are generated by interpolation, involving a local sheared coordinate system, between corresponding points in the two defining planes.

REGION 3. — This REGION is in the inlet throat from the boundary with REGION 2 to the lower wing surface, as shown in Figure 27. Ordinarily, source panels are not used below the fan face, so REGION 3 is not used extensively. There are cases, however, such as when the alternate type of barrier (see pp. 173, 176) producing "natural flow" is used, that paneling in REGION 3 is desirable.

This REGION is cylindrical about the fan axis and is paneled in radial planes passing through the fan axis in a manner similar to that in REGION 2. The Z coordinates of the panel corner points change circumferentially to adjust to the wing lower surface, but the R coordinates are constant and equal to the fan radius R_{fan}, which is input. The paneling is defined by sets of Z coordinates in two defining planes θ_{D1} and θ_{D2}, and a list of intermediate planes in which panel corners are desired. The Z values at θ_{D1} and θ_{D2} are input beginning at Z_{ref} and proceeding down to the wing lower surface at a point called Z_b. If this point is not precisely on the surface, the program will shift it there. Angles around the fan axis are measured from the same reference plane used in REGION 2.

However, the angles θ_{D1} and θ_{D2}, and the coordinates of the Z_{ref} points need not be identifical to those used in REGION 2.

The Z coordinates of all panel corner points are subsequently referred to as $Z_{i,j}$, where the subscript i refers to the axial position of the point and the subscript j refers to the radial plane. The intermediate planes containing panel corner points are denoted as θ_{Pj}. The Z_{ref} at an intermediate paneling plane is linearly interpolated as

$$Z_{ref,j} = Z_{ref,\ D1} + (Z_{ref,D2} - Z_{ref,D1})\left(\frac{\theta_{Pj} - \theta_{D1}}{\theta_{D2} - \theta_{D1}}\right) \tag{81}$$

The intersection of the fan cylinder with the lower wing surface in intermediate planes is called $Z_{b,j}$ and is found using the iterative geometric intersection technique of Appendix II.

The panel corner points in intermediate paneling planes are interpolated linearly, based on a normalized distance from $Z_{ref,j}$ to $Z_{b,j}$ and are given by

$$Z_{i,j} = Z_{ref,j} + (Z_{b,j} - Z_{ref,j})\left\{\frac{Z_{i,D1} - Z_{ref,D1}}{Z_{b,D1} - Z_{ref,D1}}\right.$$

$$\left. + \left[\frac{Z_{i,D2} - Z_{ref,D2}}{Z_{b,D2} - Z_{ref,D2}} - \frac{Z_{i,D1} - Z_{ref,D1}}{Z_{b,D1} - Z_{ref,D1}}\right]\left(\frac{\theta_{Pj} - \theta_{D1}}{\theta_{D2} - \theta_{D1}}\right)\right\} \tag{82}$$

The (R, Z, θ) coordinates are finally transformed into the reference coordinate system for output.

REGION 4.—This REGION is on the wing lower surface from the fan exit outward to the boundary of REGION 1, as shown in Figure 27. The REGION is thus directly below REGION 2, which is on the inlet lip. The paneling for REGION 4 is in radial planes passing through the fan axis. The input consists of R tables in two defining planes, θ_{D1} and θ_{D2}, together with a set of intermediate planes that will contain panel corners. The R values are input beginning at the fan radius, R_{fan}, and proceed outward to the boundary with REGION 1. The last R value in many cases will be identical to the first input R value in REGION 2 at the same station. This ensures that the boundary between REGIONS 4 and 1 on the lower surface lies directly below the corresponding boundary on the upper surface.

The R values of panel corners are subsequently referred to as R_{ij}, where the subscript i refers to the radial order of the points, and j refers to the angular location. The radii at intermediate paneling stations are obtained by linear interpolation as

$$R_{i,j} = R_{i,D1} + (R_{i,D2} - R_{i,D1})\left(\frac{\theta_{Pj} - \theta_{D1}}{\theta_{D2} - \theta_{D1}}\right) \tag{83}$$

The iterative geometric intersection technique of Appendix II is used to find the wing lower surface Z coordinates from the (R,θ) definitions. The (R, Z, θ) coordinates are finally transformed into the reference coordinate system for final output.

REGION 5.—This REGION is used to prepare the network coordinates for the multihorseshoe lifting systems, which are interior to the wing and connect to the jet efflux tube and barrier. REGION 5 is restricted, however, to multihorseshoe networks that are quite simple. First, it can only prepare networks that lie in radial planes passing through the fan axis. This restriction precluded using REGION 5 for the NASA fan-in-wing model, since the multihorseshoes were aligned with source-panel edges of REGIONS 1 and 5 that were not radial. The multihorseshoe lifting systems for that model were prepared by hand. As explained in Section 6.4, it is desirable to place the internal vortex filaments near the camber surface and directly below the surface source-panel edges. Thus, the surface source panels govern the placement of the internal vortices.

A second restriction is that this subroutine does not ensure that the vortex network corner points are placed near the camber surface except for simple configurations. The corner-point coordinates in intermediate paneling planes are found by circumferential interpolation, without recourse to the wing definition. Thus, intermediate corner points could conceivably turn out to be too close to one of the wing surfaces. As a consequence of these deficiencies, the network coordinates must often be prepared by hand, by averaging the coordinates of appropriate upper and lower surface source panel corner points.

The input for REGION 5 is identical in form to the input for REGION 2, but the computations are more direct. The geometry input consists of two tables of (R, Z) coordinates at two planes θ_{D1} and θ_{D2} and a series of intermediate θ_{Pj} planes. (R, Z) coordinates in the intermediate planes are obtained directly by linear interpolation, with Equation (83) for R and a similar one for Z. These are then transformed to the (x, y, z) reference coordinate system.

REGION 6.—This REGION is used to find wing surface contours in arbitrary planes passing through the fan axis. It is typically used for determining the intersection of a fan lip with the upper wing surface and is invaluable as an aid in preparing inputs to REGION 2, which include points on the wing surface in radial planes.

The wing surface contour is obtained as a series of equally spaced points between two radii. The input consists of the number of points desired on a wing cut, the minimum and maximum radial distances of the points from the fan axis, and the angles at which the wing cuts are desired (with respect to the angular reference defined for REGION 2). The surface coordinates are found by the geometric surface intersection technique described in Appendix II. Both the (x, y, z) coordinates and the (R, Z, θ) coordinates of points on the upper and lower surfaces are computed. The output points are evenly distributed between the minimum and maximum radius input.

4.4 JET EFFLUX TUBE GEOMETRY

The potential-flow program requires an array of (x, y, z) corner points defining the quadrilateral vortex network on the jet efflux tube surface, as shown in Figure 31. Subroutine TUBE in the geometry program prepares the efflux tube network coordinates from a simplified tube definition. The TUBE subroutine also prepares the boundary points for the multihorseshoe vortex network that extends below the wing and attaches to the tube. Both the position and direction cosines of the normal vector at these boundary points beneath the wing lower surface are provided.

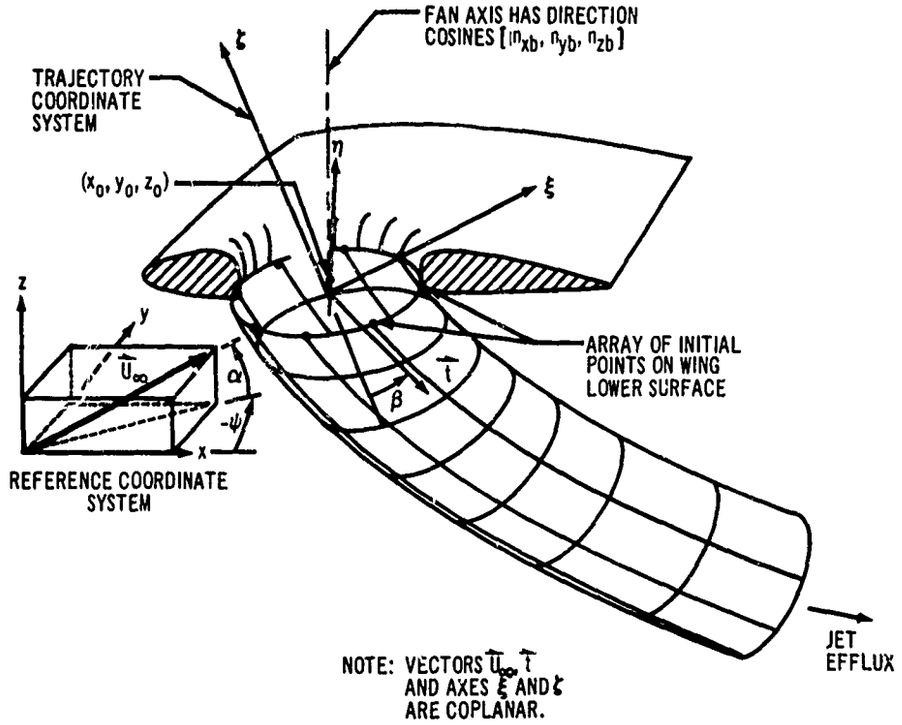

Figure 31. Example of Efflux Tube.

An empirical equation is used to provide the jet core trajectory, which depends upon the fan exit diameter D_{fan}, thrust vector angle β, and the ratio of free stream to jet velocity U_∞/V_j. The empirical equation was obtained from flow visualization studies using a jet containing water vapor exhausting into a wind tunnel (Reference 10).

$$\frac{\xi}{D_{fan}} = -\frac{0.25}{\cos\beta}\left(\frac{U_\infty}{V_j}\right)^2\left(\frac{\zeta}{D_{fan}}\right)^3 - \left(\frac{\zeta}{D_{fan}}\right)\tan\beta \qquad (84)$$

V_j is here defined as the volume flow into the inlet per unit time, divided by the inlet area. With thrust vectoring, the actual cross-sectional area of the jet is less than the inlet area, so the jet velocity, for a constant volume rate of inflow, will increase with increasing thrust vectoring. However, this effect has already been incorporated into the trajectory Equation (84), and the quantity V_j appearing in this equation must be the one defined above.

The (ξ, η, ζ) efflux trajectory coordinate system is shown in Figure 31. The ξ-ζ plane is the plane containing the free-stream velocity vector $\hat{U}_\infty$ and the thrust vector $\hat{t}$ defining the initial jet efflux direction. The ξ axis is parallel to $\hat{U}_\infty$. The angle the jet makes with the negative ζ axis is the thrust vector angle β. The influence of angle of attack α and yaw ψ is included, since they determine the direction from which $\hat{U}_\infty$ acts on the jet. The velocity ratio, angles of attack and yaw, and the fan exit diameter are input to the program. The direction cosines (t_x, t_y, t_z) of the initial efflux direction in the reference coordinate system are also inputs that determine β. The coordinates of a point (x_o, y_o, z_o) on the fan axis and the direction cosines (n_{xb}, n_{yb}, n_{zb}) of the fan axis are also inputs. These input quantities are used to establish the orientation and initial location of the trajectory coordinate system.

The efflux tube is defined by points that lie along longitudinal stringers emanating from an array of input $(x, y, z)_i$ coordinates around the fan exit. These $(x, y, z)_i$ points, shown in Figures 31 and 32, are the points where the internal multi-horseshoe system emerges from the wing. The corner points forming the tube are basically defined by a series of lateral cuts, spaced along the tube axis [given by Equation (84)] at specified intervals, s_k. The angle of these cuts with respect to the centerline varies down the tube in a regular manner to produce a smoothly varying network spacing. Small longitudinal adjustments in the locations of the points near the wing undersurface are provided to fair the network spacing smoothly into the input $(x, y, z)_i$ points, which may not lie in a plane.

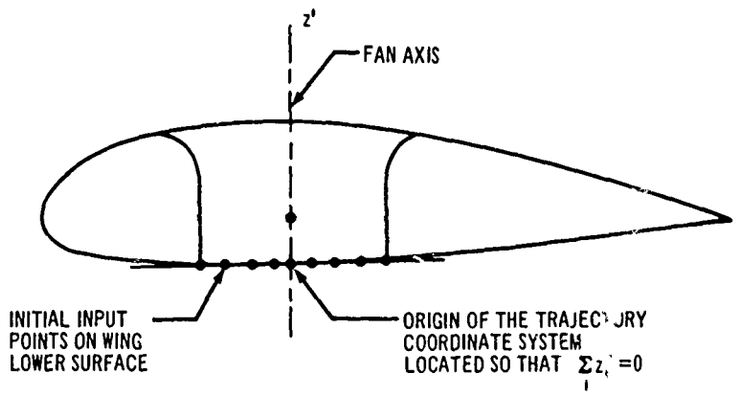

Figure 32. Origin of Trajectory Coordinate System.

The origin of the tube trajectory coordinate system is computed as shown in Figure 32, where the z' axis lies along the fan axis. The origin lies on the fan axis at the average position of the $(x, y, z)_i$ input points. From this origin, the trajectory of the tube centerline is computed from Equation (84).

Each longitudinal stringer originates at an input $(x, y, z)_i$ point at the fan exit and lies in a plane parallel to the ξ-ζ plane. The distance of the stringer from the projection of the tube centerline in this plane, measured perpendicular to the projected centerline, is maintained essentially constant.

The first cut across the tube, a distance s_1 down the centerline, is perpendicular to the fan axis (see Figure 33). Each succeeding cut attempts to become more nearly perpendicular to the tube axis. The rate at which the succeeding cuts approach a perpendicular to the axis is controlled by an input quantity, δ. As shown in Figure 33, δ determines the ratio of segment lengths on opposite sides of the tube. When the cuts finally become perpendicular to the tube axis, they are maintained perpendicular at all stations further down the tube.

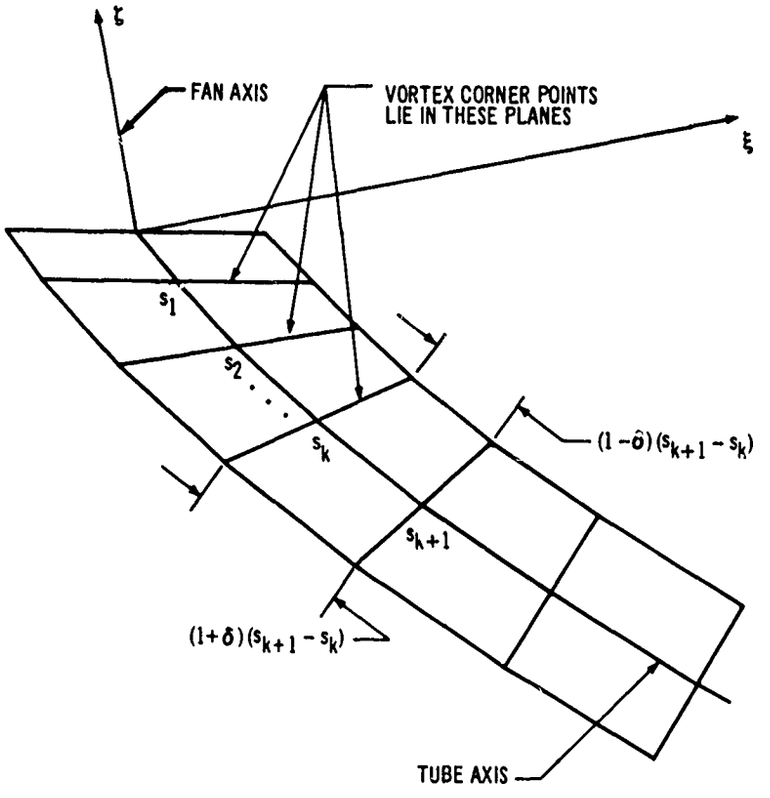

Figure 33. Vortex Spacing Along Tube.

If the input $(x, y, z)_i$ points do not lie in a plane, the segment lengths from these points to the first cut will not necessarily be compatible with the requirement of smoothly varying segment lengths down the tube. This difficulty is alleviated as follows. An input number, N_{TR}, is defined as the number of segment lengths down the tube on which an adjustment is to be made. N_{TR} must be less than or equal to the total number of s_k values. At each cut between the first one and the cut at N_{TR}, the points defined by the intersection of the cuts with the stringers are shifted along the stringers. The points closer to the fan exit are shifted proportionately more, so that the resulting points maintain a smooth spacing variation along each stringer.

The TUBE subroutine also computes the direction cosines and positions of the boundary points located just below the wing lower surface, as shown in Figure 34. The boundary point lies on the line joining the midpoints of the upper and lower line segments. The distance of the boundary point below the wing lower surface is controlled by an input number ϵ_{bp}, the distance from the wing surface to the boundary point divided by the distance from the wing surface to the first row of vortices on the tube. The direction cosines of the normal vector are given by the components of the normalized vector product of the vectors joining opposite corners of the quadrilateral area shown in Figure 34.

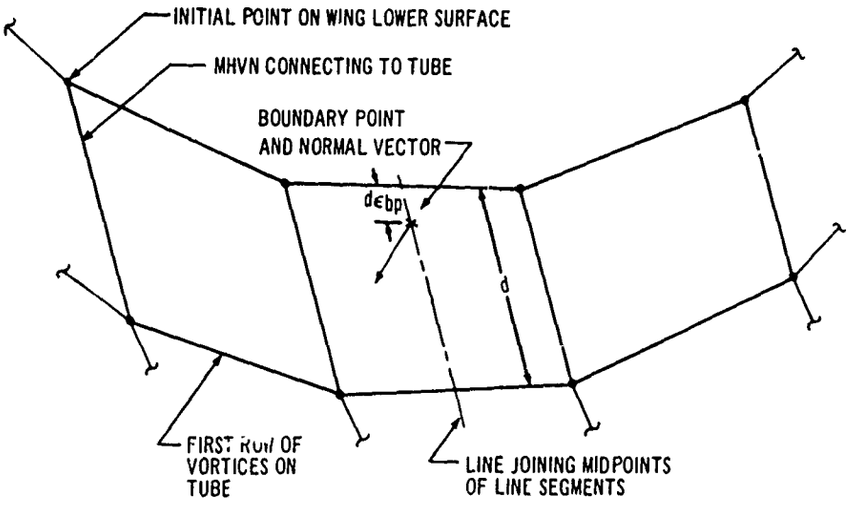

Figure 34. Location of Multihorseshoe Vortex Network Boundary Point Below Wing Lower Surface.

4.5 AXISYMMETRIC SURFACE GEOMETRY

Subroutine AXISYM is included in the geometry program to provide a convenient means of preparing the network coordinate definition of axisymmetric surfaces. It can be used for surfaces represented by source panels or quadrilateral vortices, since both use the same network ordering arrangement. For fan-in-wing configurations, it is ordinarily used to define the inlet centerbody and the fan barrier vortex networks. (These surfaces on the NASA model shown in Figure 80 were generated with this subroutine.) It can also be used for surfaces that are not axisymmetric, but that are nevertheless defined in polar coordinates and paneled in radial cutting planes. In this case, the subroutine serves as a convenient means of transforming polar coordinate input points to the primary (x, y, z) reference coordinate system.

For axisymmetric bodies, a single array of input (r, z) coordinates serves to define the network corner points in all radial planes. A table of θ values, measured from an arbitrary x_1 axis, as shown in Figure 35, are input to define the angular divisions of the desired surface network. For bodies that are not axisymmetric, a separate (r, z) array is input for each value of θ. In both cases the program constructs an ordered array of points to define a surface network between the first and last θ station, with corner points defined by the r, z, and θ values. A means is provided for varying the order of the output point array with a number code, called OUTCODE. If OUTCODE = 0.0, the coordinates will be ordered with θ varying first; if OUTCODE = 1.0, the coordinates will be ordered with (r, z) varying first. This provides the capability of always producing a right-hand surface network, which is essential with a source paneled surface.

The (r, z, θ) coordinates are first transformed from the polar coordinate system to a cartesian system with the relations

$$\begin{aligned} x_1 &= r\cos\theta \\ y_1 &= r\sin\theta \\ z_1 &= z \end{aligned} \tag{85}$$

as shown in Figure 35.

A rotation transformation executed by subroutine AXISYM orients the (x_1, y_1, z_1) axes to a second set of axes (x_2, y_2, z_2) parallel to the reference coordinate system equation

$$\begin{Bmatrix} x_2 \\ y_2 \\ z_2 \end{Bmatrix} = \begin{bmatrix} a_{11} & a_{12} & a_{13} \\ a_{21} & a_{22} & a_{23} \\ a_{31} & a_{32} & a_{33} \end{bmatrix} \begin{Bmatrix} x_1 \\ y_1 \\ z_1 \end{Bmatrix} \tag{86}$$

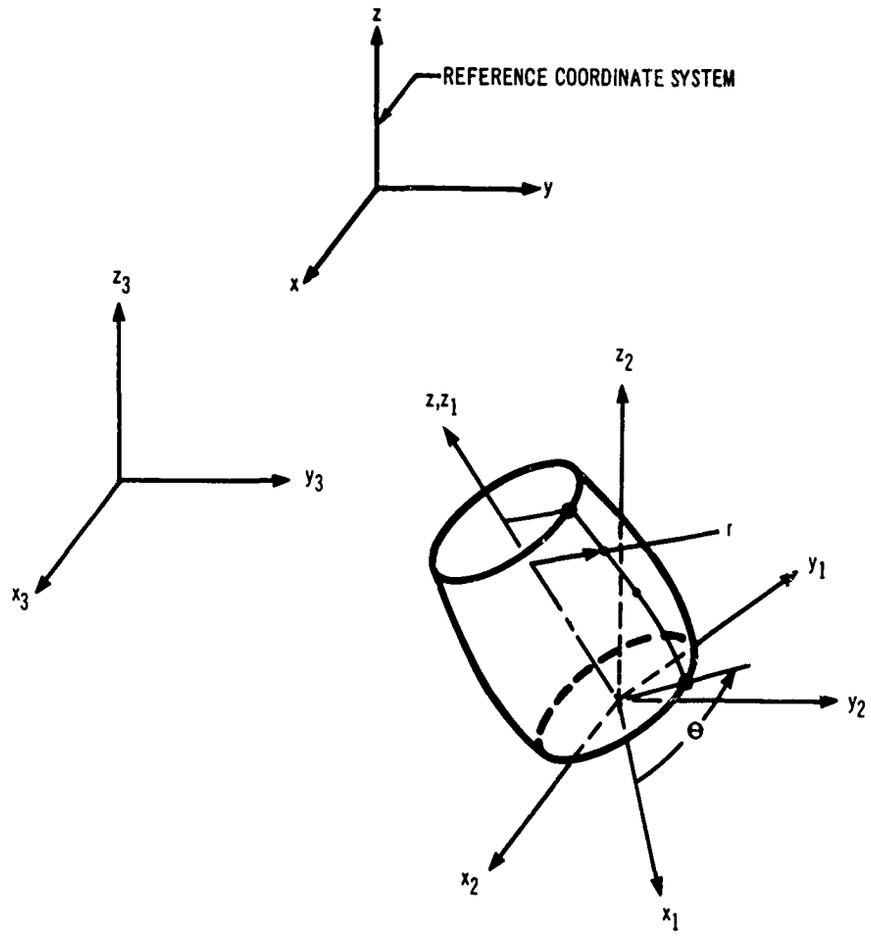

Figure 35. Arbitrary Orientation of Axisymmetric Surface.

The a_{ij}'s are the direction cosines with respect to the (x_1, y_1, z_1) coordinate system and are input to the program.

These (x_2, y_2, z_2) coordinates are then transformed to the (x_3, y_3, z_3) coordinate system by adding a displacement factor according to

$$\begin{Bmatrix} x_3 \\ y_3 \\ z_3 \end{Bmatrix} = \begin{Bmatrix} x_2 \\ y_2 \\ z_2 \end{Bmatrix} + \begin{Bmatrix} x_o \\ y_o \\ z_o \end{Bmatrix} \tag{87}$$

where (x_o, y_o, z_o) is the origin of the (x_2, y_2, z_2) coordinate system with respect to the (x_3, y_3, z_3) coordinate system and is input to the program. Transformation Equations (86) and (87) give the axisymmetric surface any arbitrary orientation with respect to the (x_3, y_3, z_3) coordinate system shown in Figure 35.

Another transformation executed by subroutine AXISYM is a coordinate distortion according to the relations

$$\begin{aligned} x_4 &= k_1 x_3 \\ y_4 &= k_2 y_3 \\ z_4 &= k_3 z_3 \end{aligned} \tag{88}$$

where (k_1, k_2, k_3) are input distortion factors. All of the (x_3, y_3, z_3) coordinates of points on the body are stretched or shrunk by the factors (k_1, k_2, k_3). The last transformation executed by subroutine AXISYM is a translation according to

$$\begin{Bmatrix} x \\ y \\ z \end{Bmatrix} = \begin{Bmatrix} x_4 \\ y_4 \\ z_4 \end{Bmatrix} + \begin{Bmatrix} x_p \\ y_p \\ z_p \end{Bmatrix} \tag{89}$$

where (x_p, y_p, z_p) is the origin of the (x_4, y_4, z_4) coordinate system with respect to the primary (x, y, z) reference coordinate system. The output of subroutine AXISYM is the network of surface coordinates in the (x, y, z) reference coordinate system.

5. COMPUTER PROGRAM USAGE

The present method for solving fan-in-wing problems is contained in three computer programs entitled the geometry program, the potential-flow program, and the boundary-layer program.

For problem-solving, they are normally used in the sequence shown in Figure 36. The geometry program produces a detailed geometric definition of the configuration, which it prepares on input cards for the potential-flow program. The potential-flow program accepts these input cards and gives a potential-flow solution, and, in turn, computes input data for the boundary-layer program. The boundary-layer program produces the boundary-layer characteristics calculated along streamlines. Some user manipulation is necessary in arranging the inputs for each of the programs.

The programs are coded in the FORTRAN IV and ASCENT languages for the Control Data Corporation 6600 (131k) digital computer. Control of the computer is monitored by the SCOPE (Simultaneous Control of Program Execution) Operating System. Because the geometry and potential-flow programs exceed the capacity of a single core load, the segmentation feature of the loader is used, which allows a complete program to be subdivided into several smaller segments. Flow charts and detailed descriptions of the computer programs are presented in Volume II.

The card-deck arrangements for the three programs are shown in Figures 37 and 38. Each consists of monitor control cards, a source deck, and a group of data cards. The monitor control cards are characteristic of the particular computer installation, as discussed in Volume II. The data cards for the particular problem and the first monitor control card, which controls the running time and field length, are inserted into the deck. The other cards normally remain unchanged.

The remainder of this section describes the mechanics of input data preparation. Complete descriptions of the card input to each program are presented. Appendix III contains sample problems to acquaint users with the input card format and printout format for each program. These sample problems are also intended for use in checking out the programs on computer facilities.

5.1 GEOMETRY PROGRAM USAGE

This section describes the use of various capabilities of the geometry program. Complete instructions for preparing the data cards are provided. Sample cases are given in Appendix III.

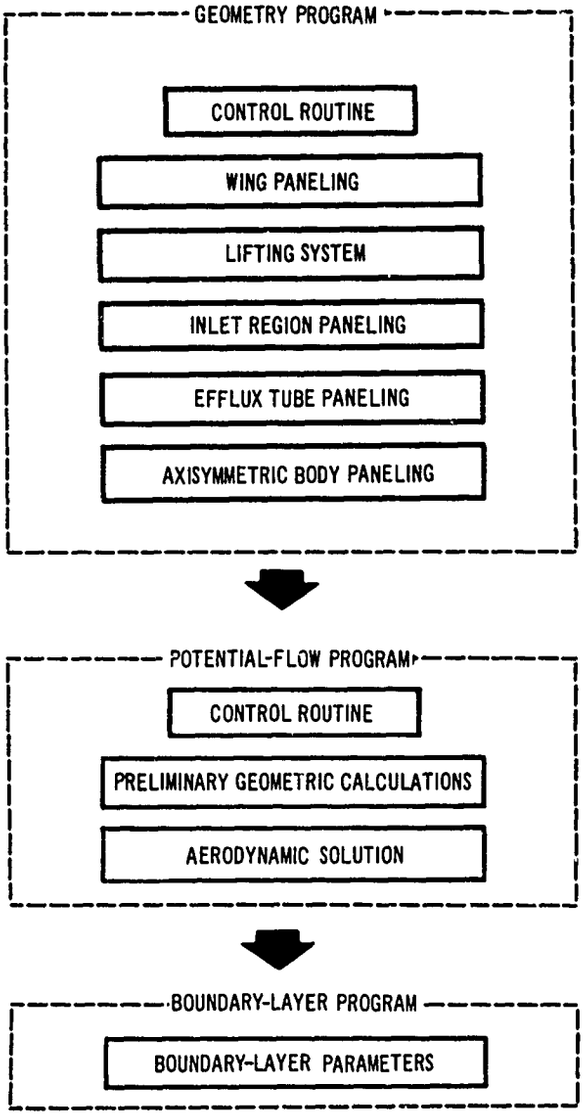

Figure 36. Fan-in-Wing Problem Flow Chart.

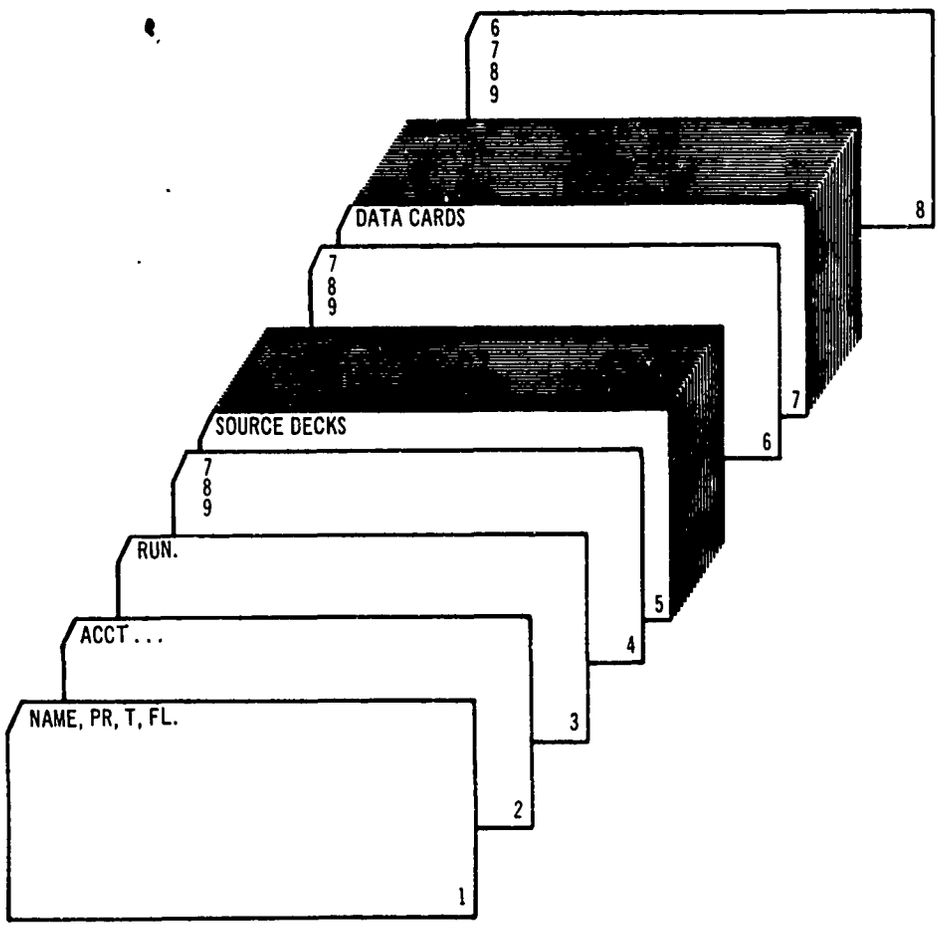

Figure 37. Deck Arrangement for Geometry and Boundary-Layer Programs.

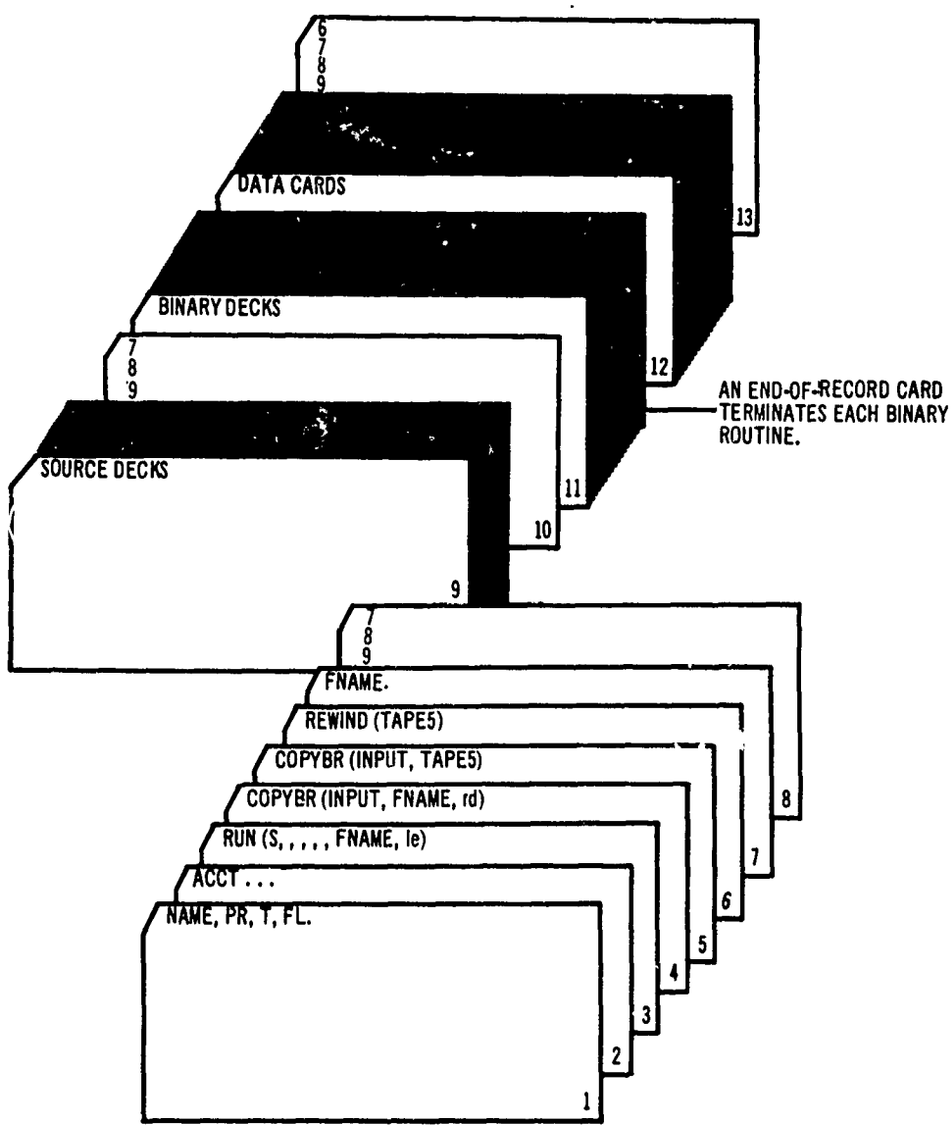

Figure 38. Deck Arrangement for Potential-Flow Program.

This program provides a simple method of obtaining (x, y, z) coordinates of several types of surfaces in punched-card form. The program was written to support the potential-flow program; thus, output is oriented toward that program. The types of surface geometry that can be produced in the reference coordinate system are:

- A wing, page 45
- A lifting system for a wing, page 53
- A fan-in-wing inlet, page 58
- A jet efflux tube, page 68
- Axisymmetric or pseudoaxisymmetric surfaces, page 72

The versatile curve-fitting procedure in subroutine WING makes it easy to tailor the chordwise source panel arrangement independently of the airfoil definition. The curve-fitting feature may also enhance the subroutine's usefulness for other applications where accurate intermediate surface coordinates are needed. Subroutine LIFT is geared closely to the potential-flow program both in input and output. The INLET subroutine is for the most part tied closely to fan-in-wing configurations, but the wing contour capability of REGION 6 makes it potentially useful for other applications where surface intersections are desired. The TUBE subroutine provides the network coordinates for an efflux tube including the influence of velocity ratio, fan diameter, thrust vector angle, angle of attack and yaw. It will adjust the network arrangement so as to fair smoothly to a nonplanar wing lower surface. Subroutine AXISYM will handle any body that can be paneled in radial planes. Taken together, these subroutines provide a powerful capability to prepare surface coordinates for a wide variety of surfaces.

Data input format. —All geometry program data, except title cards and control cards, are punched in number fields ten columns wide, with six fields per card. Decimal points should always be punched for every input number, and, since their omission is not flagged as an error, users must check their data cards carefully before submitting the run.

Input to the geometry program falls into three categories: control cards, title cards, and numeric input. As their name implies, the control cards control the execution of the program. Eight words are used on control cards:

1) CASE
2) CARD
3) WING
4) LIFT
5) INLET
6) TUBE
7) AXISYM
8) EXIT

These control cards must be punched beginning in card column 1 and must not contain any blanks.

The general card-stacking arrangement is shown in Figure 39. If the user does not desire titles on the printed output, he may delete the CASE and two title cards. There are no restrictions as to sequence of the five major geometry subroutines.

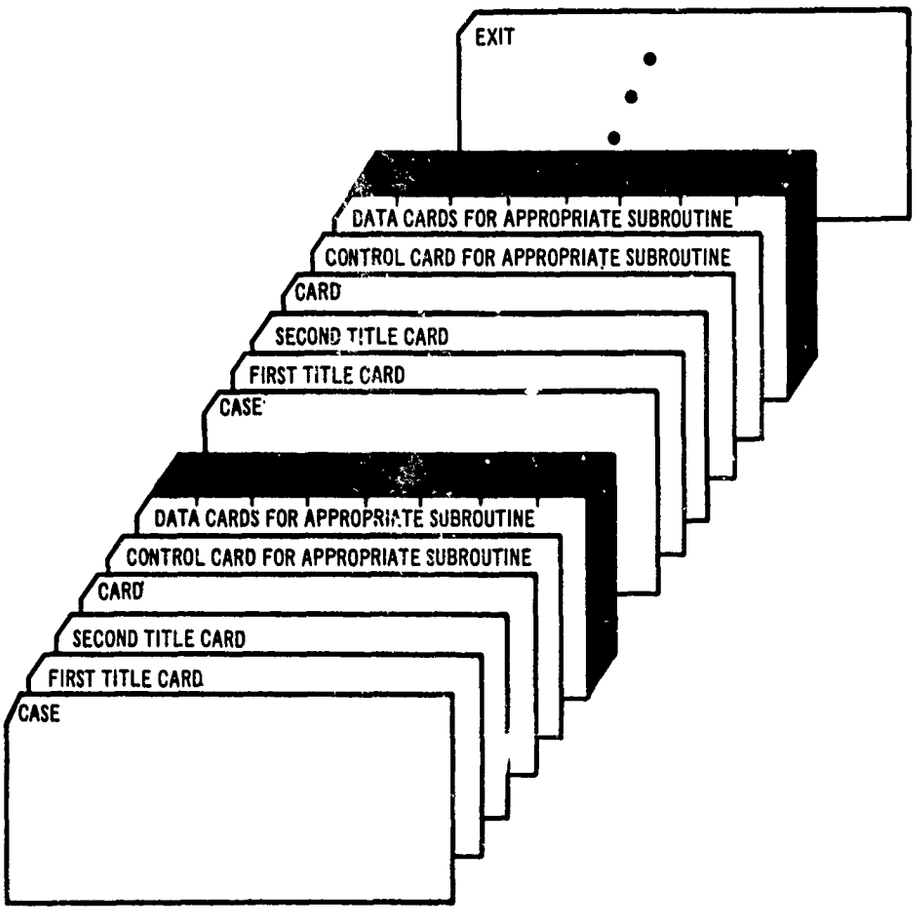

Figure 39. Geometry Program Data Card Arrangement for Several Subroutines.

The functions of the control cards are given below.

Control card CASE: This control card causes execution of two functions: first, an option indicating whether or not card output is desired is set to the no-output condition; second, the program will read the following two cards as title cards, printing columns 1-80 in several places on the output. If the CASE is omitted, no title cards are read, and the title for the previous case is used (blank if this is the first case). The card output option remains as for the

previous case (no card output if this is the first case), unless this option is reset by a CARD control card.

Control card CARD: This word is used when punched-card output is desired. If one of these cards is encountered, card output will be produced for every system (WING, LIFT, INLET, TUBE, AXISYM) following until this option is negated by a CASE control word. A CARD control card is necessary to obtain card output for any system after a CASE control card, regardless of the number of CARD control cards previously used.

The standard format built into the program for card output is the following:

(F10.5, F10.5, F10.5, F10.5, F10.5, F10.5)

Each of the six F10.5's gives the specifications for the corresponding number punched on the output cards. This is, the first F10.5 controls the format of the first number (column 1-10) on the card; the second F10.5 controls the second number (column 11-20) on the card; and so on. Under the F10.5 format, all numbers to be punched on cards must be less than 1,000. If numbers are too large for the specified format, the monitor replaces the numbers with asterisks, making the output cards useless.

An exception is the LIFT subroutine, for which the format has been altered to give numbers up to 10,000 in the first and fourth fields. The modified format is:

(F10.4, F10.5, F10.5, F10.4, F10.5, F10.5)

This alteration was necessary to allow for the large x-values associated with the trailing vortices. The above limitations are built into the program. They can be easily overridden if necessary, but unless such action is taken, these restrictions will be adhered to. It is the responsibility of the user to check that the magnitude of his data is not greater than that allowed.

If a nonstandard format must be used, it is punched in columns 11 through 47 of the pertinent CARD card in exactly the format displayed above (including parentheses and commas, and with no blank spaces). All of the output data to which this CARD card applies will be punched on cards with the nonstandard format. The allowable range for numbers punched under various formats is tabulated here.

Format	Allowable Range
F10.2	a < 1,000,000.
F10.3	a < 100,000.
F10.4	a < 10,000.
F10.5	a < 1,000.
F10.6	a < 100.
F10.7	a < 10.

Note: a is the expected output number.

Control cards WING, LIFT, INLET, TUBE, and AXISYM: These control cards transfer control to the subroutines for the like-named system. Detailed descriptions of the input for each system are found in the section for that system.

Control card EXIT: This control card is used on the last card of the data deck. When this control card is encountered, program execution is terminated.

GEOMETRY PROGRAM CARD INPUT

WING input. —Figure 40 displays the data card arrangement for subroutine WING. A description of the card input to subroutine WING follows.

	Column	Code	Explanation
Card 1	1-4	WING	Control card—contains the word WING.
Card 2	1-10	PARTS	= number of PARTS in this wing. Cards 3 through 12 must be input PARTS times.
Card 3	1-10	XLE_I	coordinates of the leading and trailing edges, respectively, of the inboard defining section for this wing PART
	11-20	YLE_I	
	21-30	ZLE_I	
	31-40	XTE_I	
	41-50	YTE_I	
	51-60	ZTE_I	
Card 4	1-10	XLE_O	coordinates of the leading and trailing edges, respectively, of the outboard defining section for this wing PART
	11-20	YLE_O	
	21-30	ZLE_O	
	31-40	XTE_O	
	41-50	YTE_O	
	51-60	ZTE_O	
Card 5	1-10	ORD_I	= number of pairs of (x/c, z/c) coordinates defining the inboard airfoil section = 0.; coordinates will be used from the outboard section of the previous wing PART. NOTE: ORD_I may not be zero for the first PART, as there is no previous PART from which to obtain coordinates. $0. \leq ORD_I \leq 200.$
Card Set 6	1-10	$(x/c)_1$	coordinates defining the inboard airfoil section, input in the order described on page 46. There must be ORD_I of these pairs, six numbers per card. If ORD_I is zero, delete this card set.
	11-20	$(z/c)_1$	
	21-30	$(x/c)_2$	
	31-40	$(z/c)_2$	
	41-50	$(x/c)_3$	
	51-60	$(z/c)_3$	

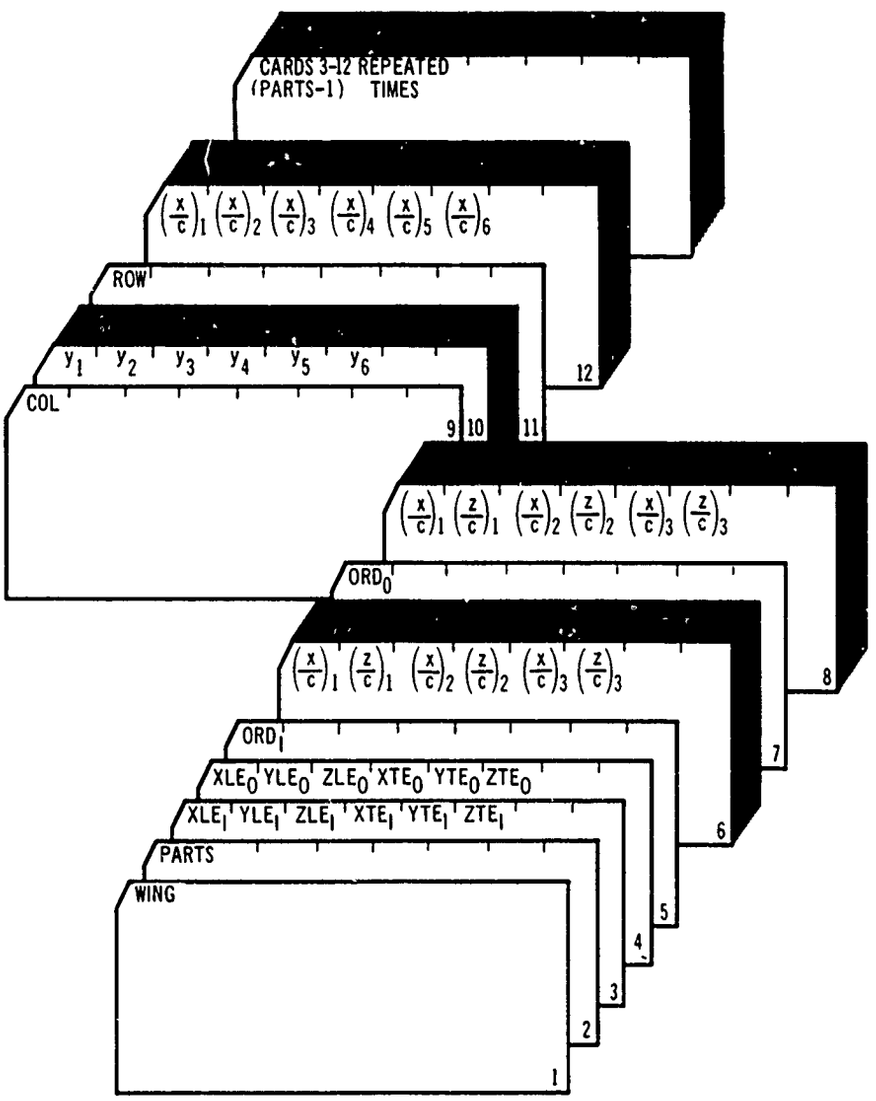

Figure 40. Data Card Arrangement for Subroutine WING.

	Column	Code	Explanation
Card 7	1-10	ORD_O	= number of pairs of (x/c, z/c) coordinates defining the outboard section
			= 0.; coordinates will be used from the inboard section of this wing PART.
			0. ≤ ORD_O ≤ 200.
Card Set 8	1-10	$(x/c)_1$	coordinates defining the outboard airfoil section, input in the order described on page 46. There must be ORD_O of these pairs, six numbers per card. If ORD_O is zero, delete this card set.
	11-20	$(z/c)_1$	
	21-30	$(x/c)_2$	
	31-40	$(z/c)_2$	
	41-50	$(x/c)_3$	
	51-60	$(z/c)_3$	
Card 9	1-10	COL	= number of spanwise panel divisions in this wing PART
			= 0.; the program will output an M x 2 network of corner points consisting of the inboard and outboard panel corner points, scaled and given the correct disposition on the planform
			0. ≤ COL ≤ 200.
Card Set 10	1-10	y_1	spanwise panel divisions, input in order of increasing y_k value. There must be COL of these y_k values, six numbers per card. If COL is zero, delete this card set.
	11-20	y_2	
	21-30	y_3	
	31-40	y_4	
	41-50	y_5	
	51-60	y_6	
Card 11	1-10	ROW	= number of chordwise panel divisions in this wing PART. ROW (x/c)'s are input in card set 12, and a curve-fitting procedure is employed to locate the spanwise generators that form panel edges. In this case, ORD_I need not equal ORD_O.
			= 0.; the program uses the inboard and outboard defining coordinates as spanwise generators to form panel edges. Consequently, ORD_I must equal ORD_O. The zero option for ORD_I and ORD_O may still be used for input.
			0. ≤ ROW ≤ 200.

	Column	Code	Explanation
Card Set 12	1-10	$(x/c)_1$	x/c values of the chordwise panel divisions, input in the order described on page 49. There must be ROW of these values, six numbers per card. If ROW is zero, delete this card set.
	11-20	$(x/c)_2$	
	21-30	$(x/c)_3$	
	31-40	$(x/c)_4$	
	41-50	$(x/c)_5$	
	51-60	$(x/c)_6$	

LIFT input. —Figure 41 displays the data card arrangement for subroutine LIFT. The description of the card input to subroutine LIFT follows.

	Column	Code	Explanation
Card 1	1-4	LIFT	control card—contains the word LIFT.
Card 2	1-10	PARTS	= number of PARTS in this lifting system. Cards 3-21 must be input PARTS times.
Card 3	1-10	XLE_I	coordinates of the leading and trailing edges, respectively, of the inboard defining section for this lifting system PART
	11-20	YLE_I	
	21-30	ZLE_I	
	31-40	XTE_I	
	41-50	YTE_I	
	51-60	ZTE_I	
Card 4	1-10	XLE_O	coordinates of the leading and trailing edges, respectively, of the outboard defining section for this lifting system PART
	11-20	YLE_O	
	21-30	ZLE_O	
	31-40	XTE_O	
	41-50	YTE_O	
	51-60	ZTE_O	
Card 5	1-10	$ROWI_I$	= number of (x/c, z/c) coordinate pairs defining the vortex corner points (including the one at the trailing edge) at the inboard defining station = 0.; coordinates will be used from the outboard section of the previous lifting system PART. NOTE: $ROWI_I$ may not be zero for the first PART, as there is no previous PART from which to obtain coordinates. $0. \leq ROWI_I \leq 50.$
Card Set 6	1-10	$(x/c)_1$	coordinates of the internal vortex corner points at the inboard defining station, input in the order described on page 54. There must be $ROWI_I$ of these pairs, six numbers per card. If $ROWI_I$ is zero, delete this card set.
	11-20	$(z/c)_1$	
	21-30	$(x/c)_2$	
	31-40	$(z/c)_2$	
	41-50	$(x/c)_3$	
	51-60	$(z/c)_3$	

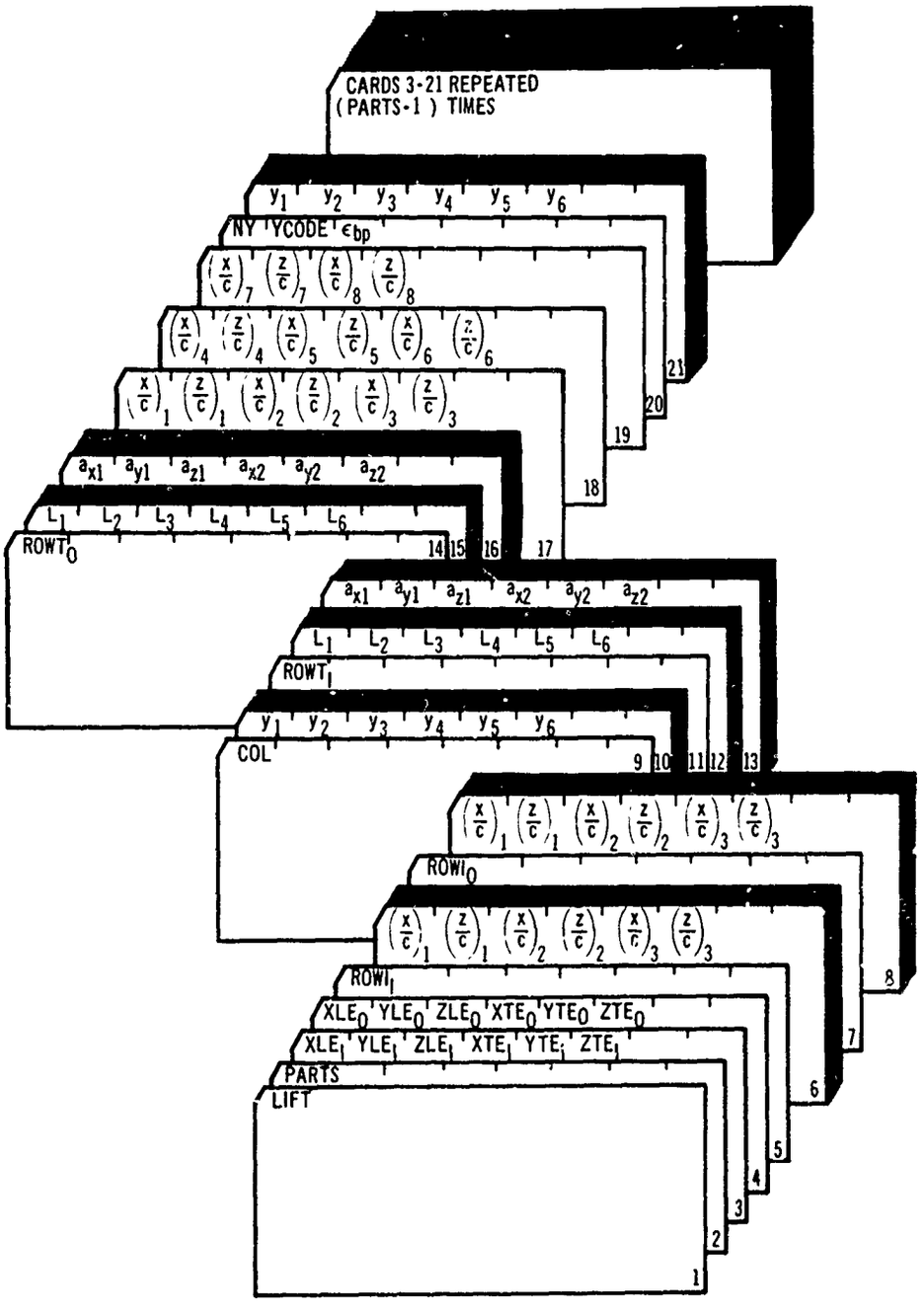

Figure 41. Data Card Arrangement for Subroutine LIFT.

	Column	Code	Explanation
Card 7	1-10	$ROWI_O$	= number of (x/c, z/c) coordinate pairs defining the internal vortex corner points at the outboard defining station. = 0.; coordinates will be used from the inboard section of this lifting system PART. $0. \leq ROWI_O \leq 50.$
Card Set 8	1-10 11-20 21-30 31-40 41-50 51-60	$(x/c)_1$ $(z/c)_1$ $(x/c)_2$ $(z/c)_2$ $(x/c)_3$ $(z/c)_3$	coordinates of the internal vortex corner points at the outboard defining station, input in the order described on page 54. There must be $ROWI_O$ of these pairs, six numbers per card. If $ROWI_O$ is zero, delete this card set.
Card 9	1-10	COL	= number of spanwise divisions (see card set 10) $1. \leq COL \leq 20.$
Card Set 10	1-10 11-20 21-30 31-40 41-50 51-60	y_1 y_2 y_3 y_4 y_5 y_6	spanwise location of the vortex segments that are aligned chordwise, input in order of increasing y_k value. There must be COL of these y_k values, six numbers per card.
Card 11	1-10	$ROWT_I$	= number of trailing segments in the inboard trailing vortex, indicating the number of lengths L_i and direction cosines (a_{xi}, a_{yi}, a_{zi}) that follow on card sets 12 and 13 for the inboard section = 0.; lengths and direction cosines are to be used from the outboard section of the previous lifting system PART. NOTE: $ROWT_I$ may not be zero for the first PART, as there is no previous PART from which to obtain data. $0. \leq ROWT_I \leq 50.$

	Column	Code	Explanation
Card Set 12	1-10	L_1	length of each trailing vortex segment for the inboard section. There must be $ROWT_I$ of these lengths, six numbers per card. If $ROWT_I$ is zero, delete this card set.
	11-20	L_2	
	21-30	L_3	
	31-40	L_4	
	41-50	L_5	
	51-60	L_6	
Card Set 13	1-10	a_{x1}	direction cosines of each trailing vortex segment for the inboard section. There must be $ROWT_I$ of these three numbers, six numbers per card. If $ROWT_I$ is zero, delete this card set.
	11-20	a_{y1}	
	21-30	a_{z1}	
	31-40	a_{x2}	
	41-50	a_{y2}	
	51-60	a_{z2}	
Card 14	1-10	$ROWT_O$	= number of trailing segments in the outboard trailing vortex, indicating the number of lengths L_i and direction cosines (a_{xi}, a_{yi}, a_{zi}) that follow on cards 15 and 16 for the outboard section = 0.; lengths and direction cosines are to be used from the inboard section of this lifting system PART. $0. \leq ROWT_O \leq 50.$
Card Set 15	1-10	L_1	lengths of each trailing vortex segment for the outboard section. There must be $ROWT_O$ of these lengths, six numbers per card. If $ROWT_O$ is zero, delete this card set.
	11-20	L_2	
	21-30	L_3	
	31-40	L_4	
	41-50	L_5	
	51-60	L_6	
Card Set 16	1-10	a_{x1}	direction cosines of each trailing vortex segment for the outboard section. There must be $ROWT_O$ of these three numbers, six numbers per card. If $ROWT_O$ is zero, delete this card set.
	11-20	a_{y1}	
	21-30	a_{x1}	
	31-40	a_{x2}	
	41-50	a_{y2}	
	51-60	a_{z2}	
Card 17	1-10	$(x/c)_1$	Cards 17, 18, and 19 contain eight coordinates used in the computation of the trailing-edge boundary point and the direction cosines of the normal to the boundary point. The first four coordinates are the inboard upper and lower surface trailing-edge panel-edge locations, as described on page 57. The last four coordinates are for the outboard section.
	11-20	$(z/c)_1$	
	21-30	$(x/c)_2$	
	31-40	$(z/c)_2$	
	41-50	$(x/c)_3$	
	51-60	$(z/c)_3$	

	Column	Code	Explanation
Card 18	1-10	$(x/c)_4$	See card 17 explanation.
	11-20	$(z/c)_4$	
	21-30	$(x/c)_5$	
	31-40	$(z/c)_5$	
	41-50	$(x/c)_6$	
	51-60	$(z/c)_6$	
Card 19	1-10	$(x/c)_7$	See card 17 explanation.
	11-20	$(z/c)_7$	
	21-30	$(x/c)_8$	
	31-40	$(z/c)_8$	
Card 20	1-10	NY	= number of y values to follow on card set 21 $1. \leq NY \leq 20.$
	11-20	YCODE	= 0.; the y values on card set 21 are for the panel edges, as explained on page 57.
			= 1.; the y values are for the actual boundary-point locations, as explained on page
	21-30	ϵ_{bp}	= 0.; the standard position of the boundary point aft of the trailing edge is desired. The standard offset spacing is 0.1 times the upper surface panel length.
			= actual value of ϵ_{bp} in terms of a fraction of the upper panel length, if the nonstandard offset spacing is desired
Card Set 21	1-10	y_1	spanwise location of the panel edges or boundary-point locations, depending on YCODE. There must be NY of these y values, six numbers per card.
	11-20	y_2	
	21-30	y_3	
	31-40	y_4	
	41-50	y_5	
	51-60	y_6	

INLET input.—Figures 42 through 48 display the data card arrangement for subroutine INLET. The description of the card input to subroutine INLET follows.

	Column	Code	Explanation
Card 1	1-5	INLET	Control card—contains the word INLET.
Card 2	1-10	XLE_I	coordinates of the leading and trailing edge, respectively, of the inboard defining wing section
	11-20	YLE_I	
	21-30	ZLE_I	
	31-40	XTE_I	
	41-50	YTE_I	
	51-60	ZTE_I	
Card 3	1-10	XLE_O	coordinates of the leading and trailing edge, respectively, of the outboard defining wing section
	11-20	YLE_O	
	21-30	ZLE_O	
	31-40	XTE_O	
	41-50	YTE_O	
	51-60	ZTE_O	
Card 4	1-10	ORD_I	number of pairs of $(x/c, z/c)_i$ coordinates defining the inboard airfoil section $1. \leq ORD_I \leq 200.$
Card Set 5	1-10	$(x/c)_1$	coordinates defining the inboard airfoil section. There must be ORD_I of these pairs, six numbers per card.
	11-20	$(z/c)_1$	
	21-30	$(x/c)_2$	
	31-40	$(z/c)_2$	
	41-50	$(x/c)_3$	
	51-60	$(z/c)_3$	
Card 6	1-10	ORD_O	= number of pairs of $(x/c, z/c)_i$ coordinates defining the outboard airfoil section = 0.; coordinates will be used from the inboard airfoil section. $0. \leq ORD_O \leq 200.$
Card Set 7	1-10	$(x/c)_1$	coordinates defining the outboard airfoil section. There must be ORD_O of these pairs, six numbers per card. If ORD_O is zero, delete this card set.
	11-20	$(z/c)_1$	
	21-30	$(x/c)_2$	
	31-40	$(z/c)_2$	
	41-50	$(x/c)_3$	
	51-60	$(z/c)_3$	

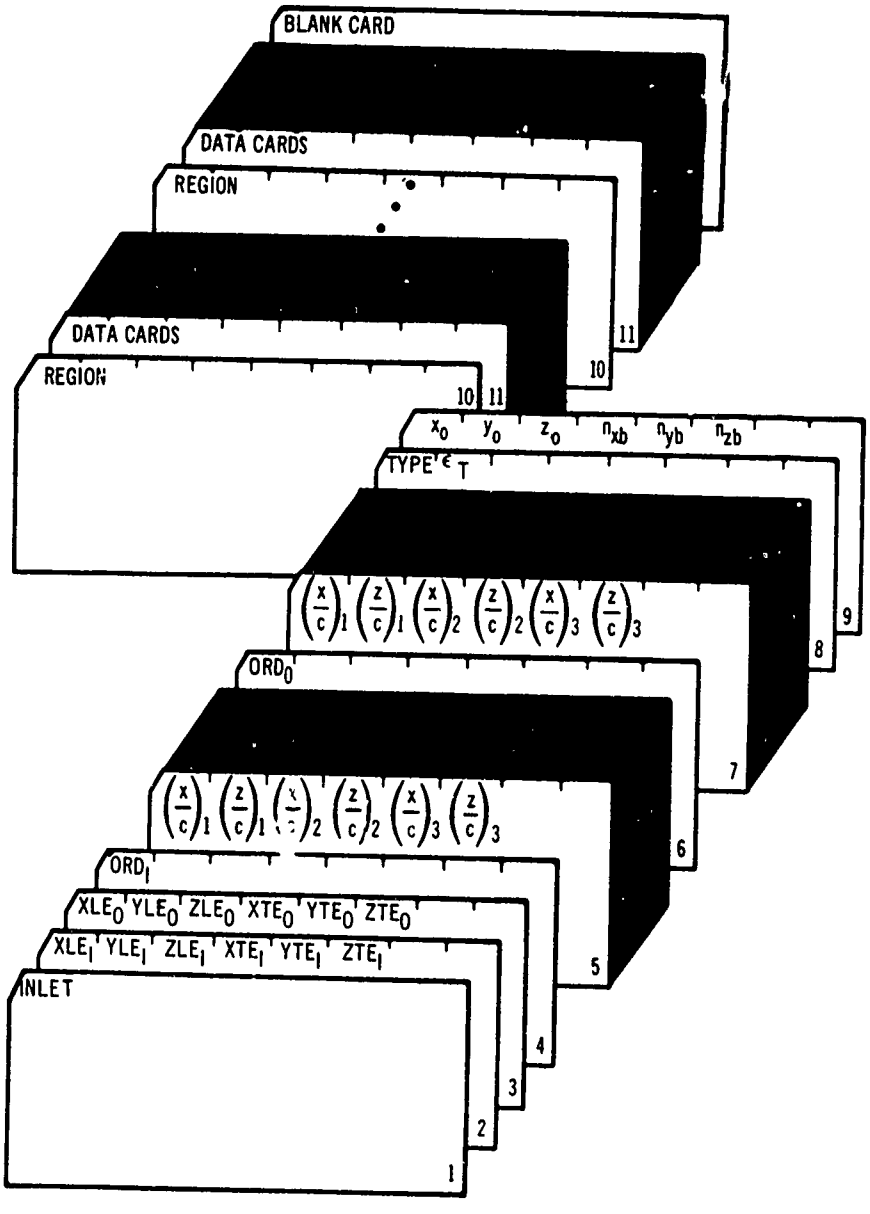

Figure 42. Data Card Arrangement for Subroutine INLET.

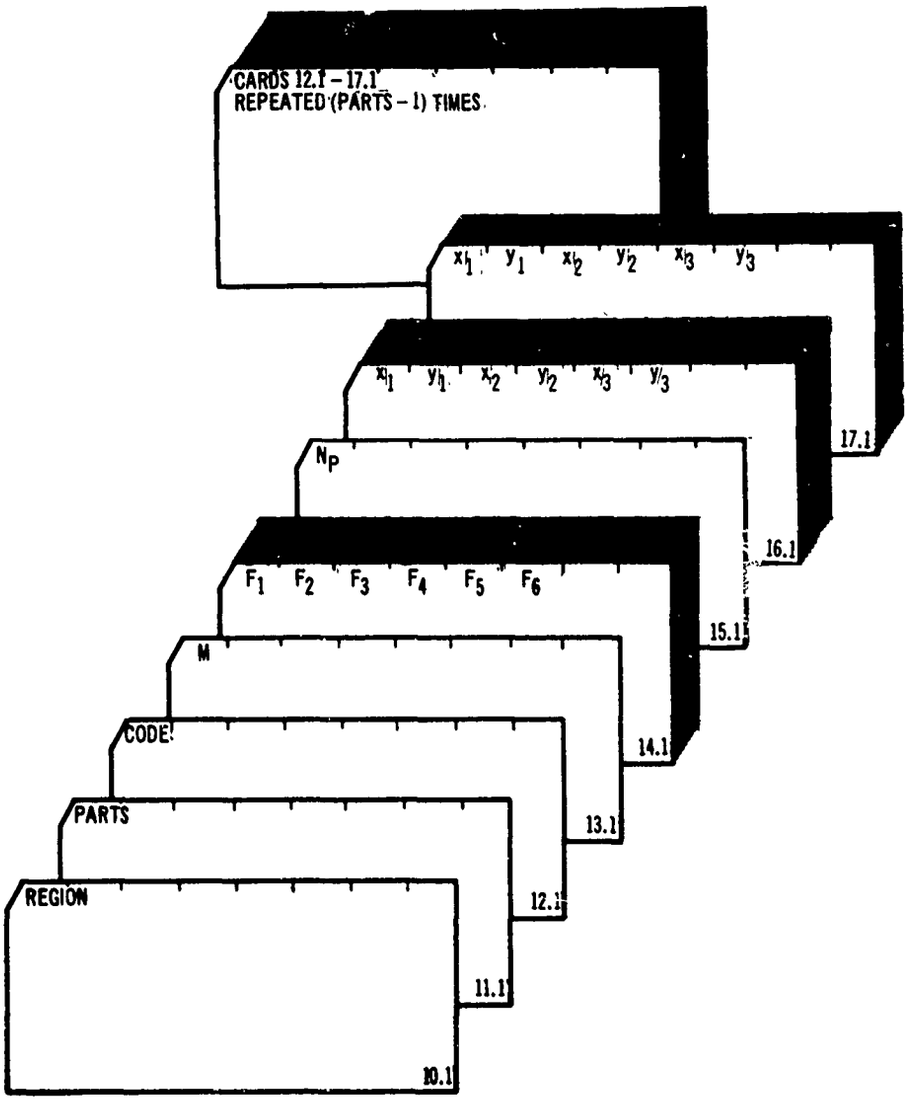

Figure 43. Data Card Arrangement for REGION 1.

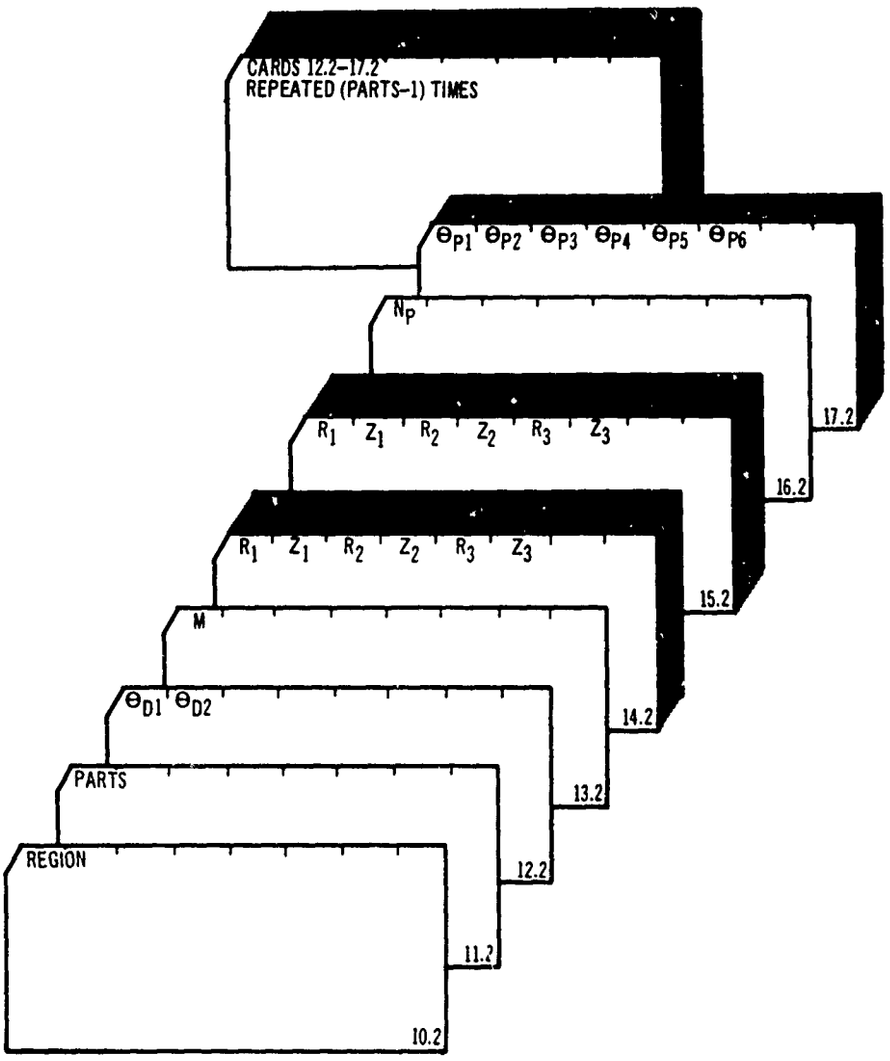

Figure 44. Data Card Arrangement for REGION 2.

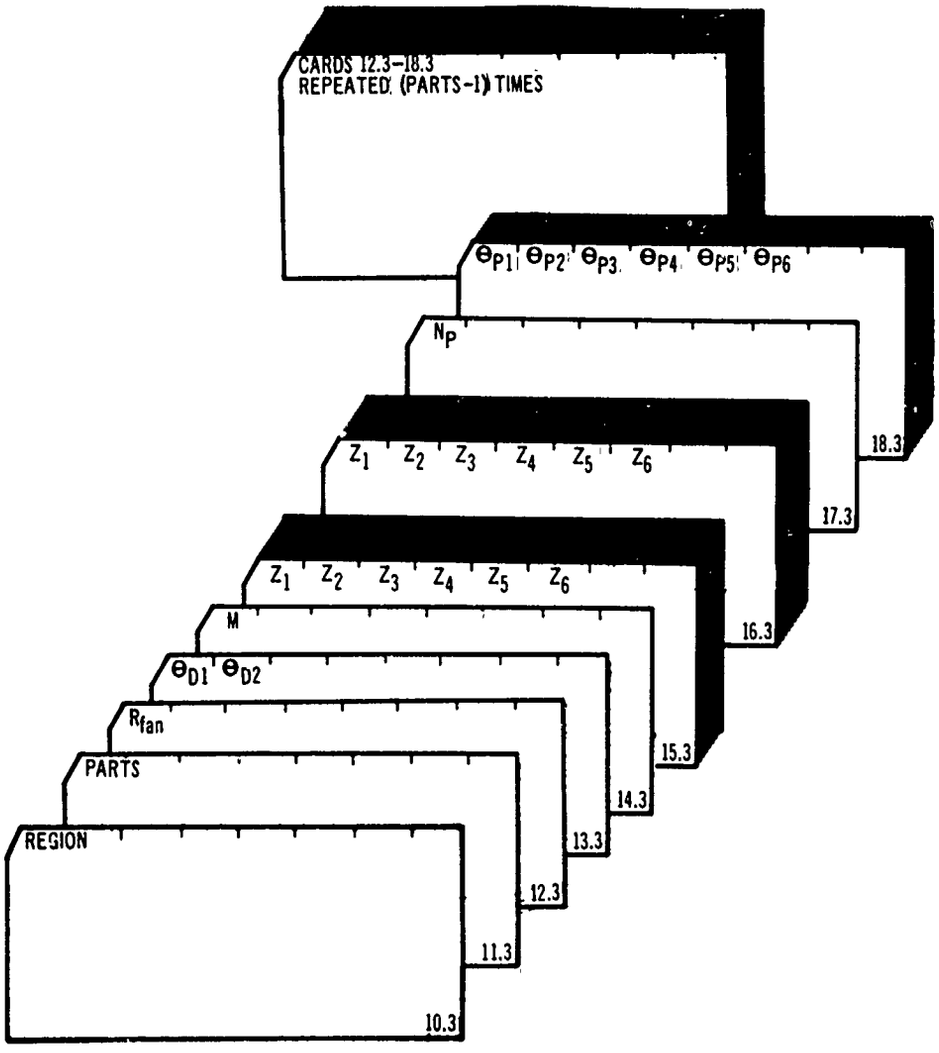

Figure 45. Data Card Arrangement for REGION 3.

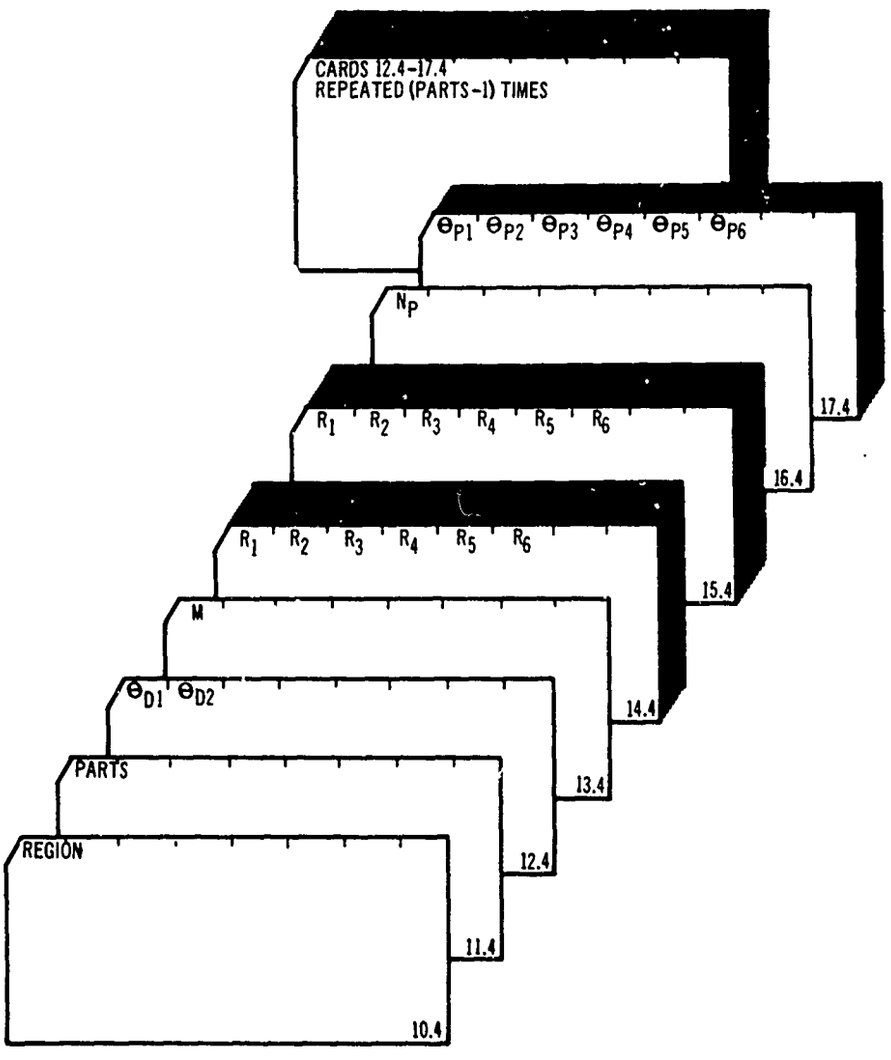

Figure 46. Data Card Arrangement for REGION 4.

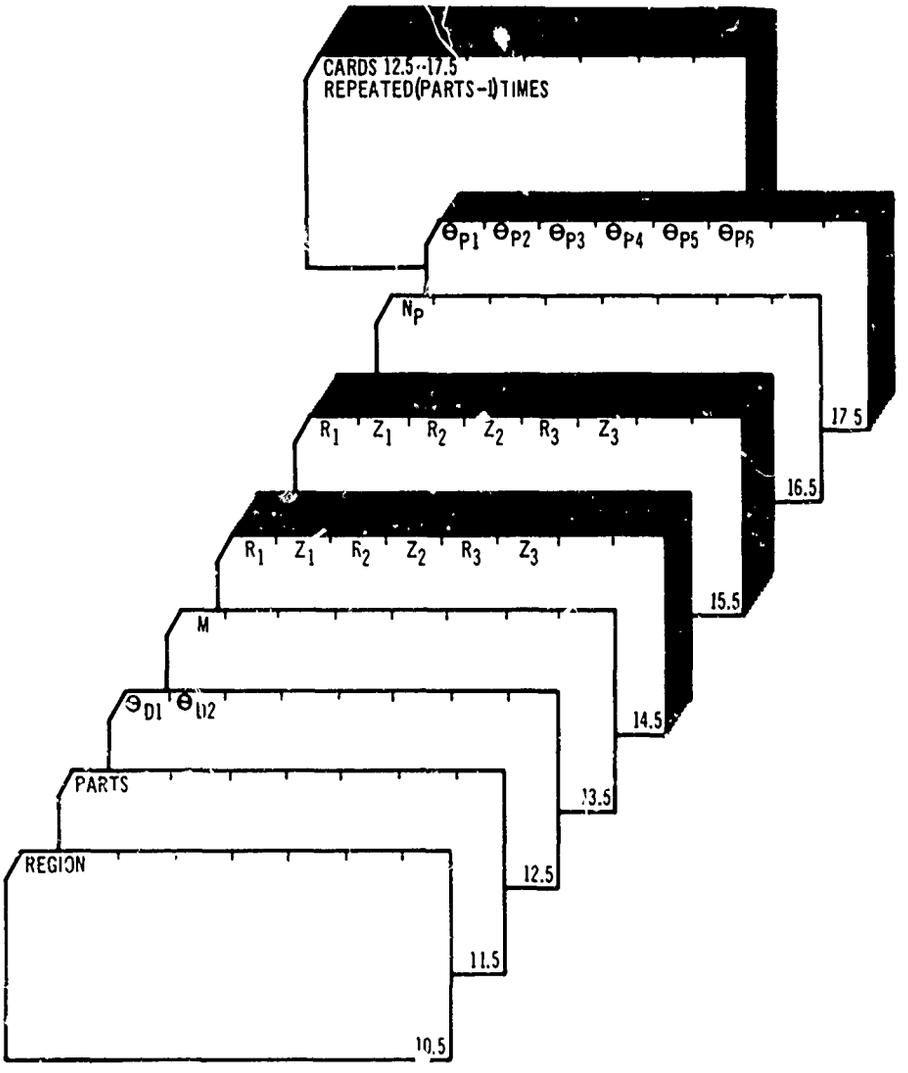

Figure 47. Data Card Arrangement for REGION 5.

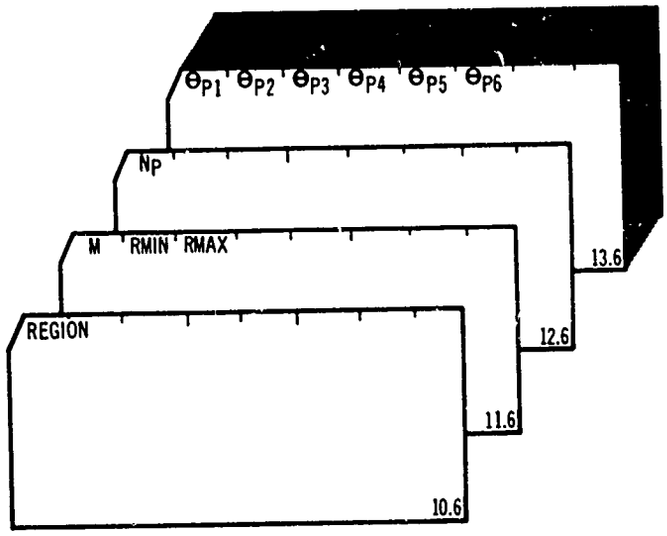

Figure 48. Data Card Arrangement for REGION 6.

	Column	Code	Explanation
Card 8	1-10	TYPE	= 0.; wing is defined by lines connecting ordered points. ORD_O must equal ORD_I or be zero.
			= 1.; wing is defined by lines of constant x/c. ORD_O need not equal ORD_I.
	11-20	ϵ	tolerance used in the iteration scheme to compute points on the wing surface. A recommended value is 10^{-6} times the average wing chord.
Card 9	1-10	x_o	(x_o, y_o, z_o) is the origin of the inlet coordinate system on the fan axis. (n_{xb}, n_{yb}, n_{zb}) are the direction cosines of the fan axis directed upward.
	11-20	y_o	
	21-30	z_o	
	31-40	n_{xb}	
	41-50	n_{yb}	
	51-60	n_{zb}	
Card 10.1	1-10	REGION	= 1.; causes program to perform calculations in REGION 1 of the inlet. Cards 11.1-17.1 that follow are for REGION 1.
Card 11.1	1-10	PARTS	= number of PARTS in REGION 1 of the inlet. Cards 12.1-17.1 that follow must be input PARTS times.
Card 12.1	1-10	CODE	= -1.; upper surface points only are computed.
			= -1.; lower surface points only are computed.
Card 13.1	1-10	M	= number of F_i fraction values to follow on card set 14.1
			$1. \leq M \leq 20.$
Card Set 14.1	1-10	F_1	fraction values that control panel spacing between two input (x, y) points on the wing planform, input in the order of increasing value.
	11-20	F_2	
	21-30	F_3	
	31-40	F_4	
	41-50	F_5	
	51-60	F_6	$0. \leq F_i \leq 1.$
Card 15.1	1-10	N_p	= number of (x, y) pairs to follow on card set 16.1
			$1. \leq N_p \leq 200.$

	Column	Code	Explanation
Card Set 16.1	1-10	x_1	coordinates along the outer boundary of REGION 1; input counterclockwise, viewed from above for the upper surface, and clockwise, viewed from above, for the lower surface. There must be N_P of these (x,y) pairs, six numbers per card.
	11-20	y_1	
	21-30	x_2	
	31-40	y_2	
	41-50	x_3	
	51-60	y_3	
Card Set 17.1	1-10	x_1	coordinates along the inner boundary of REGION 1; input counterclockwise, viewed from above for the upper surface, and clockwise, viewed from above, for the lower surface. There must be N_P of these (x,y) pairs, six numbers per card.
	11-20	y_1	
	21-30	x_2	
	31-40	y_2	
	41-50	x_3	
	51-60	y_3	
Card 10.2	1-10	REGION	= 2.; causes program to perform calculations in REGION 2 of the inlet. Cards 11.2-17.2 that follow are for REGION 2.
Card 11.2	1-10	PARTS	= number of PARTS in REGION 2 of the inlet. Cards 12.2-17.2 must be input PARTS times.
Card 12.2	1-10	θ_{D1}	two defining stations for this inlet PART; input in degrees, counterclockwise when viewed from above
	11-20	θ_{D2}	
			$\theta_{D1} < \theta_{D2}$
Card 13.2	1-10	M	= number of (R,Z) pairs to follow on card sets 14.2 and 15.2
			$1. \leq M \leq 200.$
Card Set 14.2	1-10	R_1	coordinates defining the panel corner points along the inlet contour for the first defining station θ_{D1}; input beginning on the unmodified wing surface and proceeding down into the inlet. There must be M of these (R,Z) pairs, six numbers per card.
	11-20	Z_1	
	21-30	R_2	
	31-40	Z_2	
	41-50	R_3	
	51-60	Z_3	
Card Set 15.2	1-10	R_1	coordinates defining the panel corner points along the inlet contour for the second defining station θ_{D2}; input beginning on the unmodified wing surface and proceeding down into the inlet. There must be M of these (R,Z) pairs, six numbers per card.
	11-20	Z_1	
	21-30	R_2	
	31-40	Z_2	
	41-50	R_3	
	51-60	Z_3	

	Column	Code	Explanation
Card 16.2	1-10	N_P	= number of θ_P paneling stations to follow on card set 17.2
			$1. \leq N_P \leq 20.$
Card Set 17.2	1-10	θ_{P1}	θ_P paneling stations in degrees, input
	11-20	θ_{P2}	counterclockwise viewed from above.
	21-30	θ_{P3}	There must be N_P of these θ_P stations,
	31-40	θ_{P4}	six numbers per card.
	41-50	θ_{P5}	
	51-60	θ_{P6}	$\theta_{D1} \leq \theta_P \leq \theta_{D2}$
Card 10.3	1-10	REGION	= 3.; causes program to perform calculations in REGION 3 of the inlet. Cards 11.3-18.3 that follow are for REGION 3.
Card 11.3	1-10	PARTS	= number of PARTS in REGION 3 of the inlet. Cards 12.3-18.3 must be input PARTS times.
Card 12.3	1-10	R_{fan}	fan radius used to construct panel corner points in REGION 3 of the inlet
Card 13.3	1-10	θ_{D1}	two defining stations for this inlet PART;
	11-20	θ_{D2}	input in degrees, counterclockwise when viewed from above
			$\theta_{D1} < \theta_{D2}$
Card 14.3	1-10	M	= number of Z coordinates to follow on card sets 15.3 and 16.3
			$1. \leq M \leq 200.$
Card Set 15.3	1-10	Z_1	coordinates defining the panel corner
	11-20	Z_2	points along the inlet throat for the first
	21-30	Z_3	defining station θ_{D1}; input beginning at
	31-40	Z_4	Z_{ref} and proceeding downward to the wing
	41-50	Z_5	lower surface Z_b. There must be M
	51-60	Z_6	coordinates, six numbers per card.
Card Set 16.3	1-10	Z_1	coordinates defining the panel corner
	11-20	Z_2	points along the throat for the second
	21-30	Z_3	defining station θ_{D2}; input beginning at
	31-40	Z_4	Z_{ref} and proceeding downward to the wing
	41-50	Z_5	lower surface Z_b. There must be M
	51-60	Z_6	coordinates, six numbers per card.

	Column	Code	Explanation
Card 17.3	1-10	N_P	= number of θ_P paneling stations to follow on card set 18.3
			$1. \leq N_P \leq 20.$
Card Set 18.3	1-10	θ_{P1}	θ_P paneling stations in degrees, input counterclockwise viewed from above. There must be N_P of these θ_P stations, six numbers per card.
	11-20	θ_{P2}	
	21-30	θ_{P3}	
	31-40	θ_{P4}	
	41-50	θ_{P5}	
	51-60	θ_{P6}	$\theta_{D1} \leq \theta_P \leq \theta_{D2}$
Card 10.4	1-10	REGION	= 4.; causes program to perform calculations in REGION 4 of the inlet. Cards 11.4-17.4 that follow are for REGION 4.
Card 11.4	1-10	PARTS	number of PARTS in REGION 4 of the inlet. Cards 12.4-17.4 must be input PARTS times.
Card 12.4	1-10	θ_{D1}	two defining stations for this inlet PART; input in degrees, counterclockwise when viewed from above
	11-20	θ_{D2}	
			$\theta_{D1} < \theta_{D2}$
Card 13.4	1-10	M	= number of R coordinates to follow on card sets 14.4 and 15.4
			$1. \leq M \leq 200.$
Card Set 14.4	1-10	R_1	radius values defining the panel corner points on the lower surface for the first defining station θ_{D1}; input beginning at the edge of the fan exit and proceeding outward. There must be M values, six numbers per card.
	11-20	R_2	
	21-30	R_3	
	31-40	R_4	
	41-50	R_5	
	51-60	R_6	
Card Set 15.4	1-10	R_1	radius values defining the panel corner points on the lower surface for the second defining station θ_{D2}; input beginning at the edge of the fan exit and proceeding outward. There must be M values, six numbers per card.
	11-20	R_2	
	21-30	R_3	
	31-40	R_4	
	41-50	R_5	
	51-60	R_6	

	Column	Code	Explanation
Card 16.4	1-10	N_P	= number of θ_P paneling stations to follow on card set 17.4 $1. \leq N_P \leq 20.$
Card Set 17.4	1-10 11-20 21-30 31-40 41-50 51-60	θ_{P1} θ_{P2} θ_{P3} θ_{P4} θ_{P5} θ_{P6}	θ_P paneling stations in degrees, input counterclockwise viewed from above. There must be N_P of these θ_P stations, six numbers per card. $\theta_{D1} \leq \theta_P \leq \theta_{D2}$
Card 10.5	1-10	REGION	= 5.; causes program to perform calculations in REGION 5 of the inlet. Cards 11.5-17.5 that follow are for REGION 5.
Card 11.5	1-10	PARTS	= number of PARTS in REGION 5 of the inlet. Cards 12.5-17.5 must be input PARTS times.
Card 12.5	1-10 11-20	θ_{D1} θ_{D2}	two defining stations for this inlet PART; input in degrees, counterclockwise when viewed from above. $\theta_{D1} < \theta_{D2}$
Card 13.5	1-10	M	= number of (R, Z) pairs to follow on card sets 14.5 and 15.5 $1. \leq M \leq 200.$
Card 14.5	1-10 11-20 21-30 31-40 41-50 51-60	R_1 Z_1 R_2 Z_2 R_3 Z_3	coordinates defining the interior corner points for the first defining station θ_{D1}. There must be M of these (R, Z) pairs, six numbers per card.
Card Set 15.5	1-10 11-20 21-30 31-40 41-50 51-60	R_1 Z_1 R_2 Z_2 R_3 Z_3	coordinates defining the interior corner points for the second defining station θ_{D2}. There must be M of these (R, Z) pairs, six numbers per card.

	Column	Code	Explanation
Card 16.5	1-10	N_P	= number of θ_P paneling stations to follow on card set 17.5 $1. \leq N_P \leq 20.$
Card Set 17.5	1-10 11-20 21-30 31-40 41-50 51-60	θ_{P1} θ_{P2} θ_{P3} θ_{P4} θ_{P5} θ_{P6}	θ_P paneling stations in degrees, input counterclockwise viewed from above. There must be N_P of these θ_P stations, six numbers per card. $\theta_{D1} \leq \theta_P \leq \theta_{D2}$
Card 10.6	1-10	REGION	= 6.; causes program to perform calculations in REGION 6 of subroutine INLET, which produces wing surface profiles. Cards 11.6-13.6 that follow are for REGION 6.
Card 11.6	1-10	M	= number of points to be computed on the wing surface in each θ_P profile station. These points are computed on both the upper and lower surface and are evenly distributed between RMIN and RMAX.
	11-20	RMIN	minimum radius for which surface points are computed. RMIN may be zero or a negative number, as long as the magnitude does not locate a point off the planform.
	21-30	RMAX	maximum radius for which surface points are computed
Card 12.6	1-10	N_P	= number of θ_P profile stations to follow on card set 13.6 $1. \leq N_P \leq 20.$
Card Set 13.6	1-10 11-20 21-30 31-40 41-50 51-60	θ_{P1} θ_{P2} θ_{P3} θ_{P4} θ_{P5} θ_{P6}	θ_P profile stations in degrees. There must be N_P of these θ_P stations, six numbers per card. $0. \leq \theta_P \leq 360.$
Blank Card			blank card used as the last card in the INLET subroutine data deck, causing the program to exit INLET and to return to the main program

TUBE input. — Figure 49 displays the data card arrangement for subroutine TUBE. The description of the card input to subroutine TUBE follows.

	Column	Code	Explanation
Card 1	1-4	TUBE	Control card—contains the word TUBE.
Card 2	1-10	x_o	(x_o, y_o, z_o) is a point on the fan axis and
	11-20	y_o	(n_{xb}, n_{yb}, n_{zb}) are the direction cosines of
	21-30	z_o	the fan axis directed upward.
	31-40	n_{xb}	
	41-50	n_{yb}	
	51-60	n_{zb}	
Card 3	1-10	t_x	direction cosines of the initial jet efflux
	11-20	t_y	direction
	21-30	t_z	
Card 4	1-10	U_∞/V_j	ratio of free stream to jet velocity
	11-20	α	angle of attack, in degrees
	21-30	ψ	angle of yaw, in degrees
	31-40	D_{fan}	fan exit diameter
Card 5	1-10	M	= number of initial points on the wing lower surface to follow on card set 6 $1. \leq M \leq 50.$
Card Set 6	1-10	x_1	coordinates of the initial points on the wing
	11-20	y_1	lower surface to which the tube is attached;
	21-30	z_1	input counterclockwise viewed from above
	31-40	x_2	beginning at any convenient point. If a
	41-50	y_2	plane through the fan axis is used as a plane
	51-60	z_2	of symmetry for the geometry and flow, only half of the tube needs to be input; otherwise, the entire tube must be input. For the latter case, the first and last points coincide. There must be M of these initial points, six coordinates per card.
Card 7	1-10	N	= number of arc lengths to follow on card set 8 $1. \leq N \leq 50.$

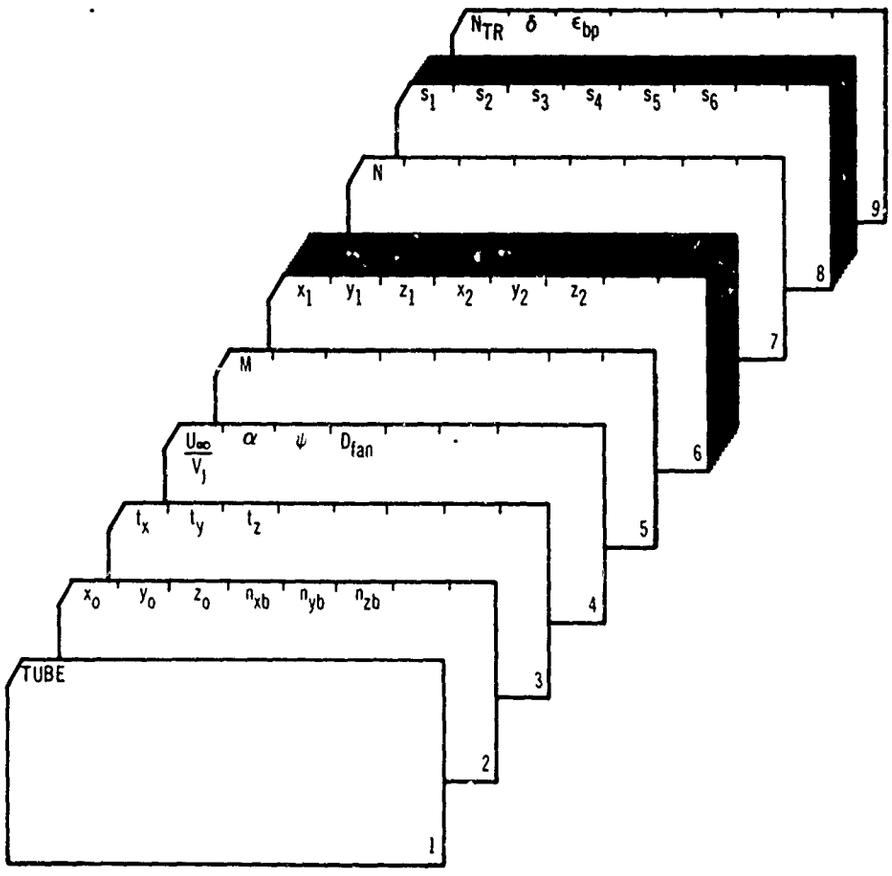

Figure 49. Data Card Arrangement for Subroutine TUBE.

	Column	Code	Explanation
Card Set 8	1-10	s_1	arc lengths measured positive downstream along the jet core trajectory. These define the vortex spacing down the tube.
	11-20	s_2	
	21-30	s_3	
	31-40	s_4	
	41-50	s_5	
	51-60	s_6	
Card 9	1-10	N_{TR}	= number of s_k arc lengths over which the tube geometry is to be adjusted to the shape of the wing lower surface
	11-20	δ	small number ($-1. \ll \delta \ll 1.$) defining the maximum deviation of the vortex spacing on opposite sides of the tube axis and controlling the rate at which cross sections become perpendicular to the tube axis, as shown in Figure 33
	21-30	ϵ_{bp}	small positive number (0.005-0.01) controlling the distance of the boundary point below the wing surface. ϵ_{bp} is the ratio of the distance from the wing surface to the boundary point over the distance from the wing surface to the first row of vortices on the tube, as shown in Figure 34.

When variable spacing is used for the quadrilateral vortices and boundary-point locations on the tube, as described in Section 6.4, the TUBE subroutine is used to generate the positions of the tube boundary points, as well as the vortices. This is an optional feature of the potential-flow program; ordinarily it computes the position of the boundary point for the quadrilateral vortices on the tube, but this feature should not be used with variable tube spacing. The procedure for generating the vortex boundary points with subroutine TUBE is:

First, a new s_k table for the boundary-point locations is input to subroutine TUBE. Second, a new array of $(x, y, z)_1$ initial points for input to subroutine TUBE is prepared by averaging adjacent x, y, and z values of the original initial points on the wing lower surface. Since for a tube there are M x N panel corner points, there are (M-1) x (N-1) boundary points. For the tube boundary-point case, there is one less arc length and initial point than for the original tube geometry.

The third step is the card output procedure. A nonstandard print format is used by punching (3F10.5) in card columns 11-18 of the CARD control card preceding the tube data cards. The boundary points are thus punched out three per card rather than the normal six per card, and will be in the format required by the potential-flow program.

AXISYM input. —Figure 50 shows the data card arrangement for subroutine AXISYM. The description of the card input to subroutine AXISYM follows.

	Column	Code	Explanation
Card 1	1-6	AXISYM	Control card—contains the word AXISYM.
Card 2	1-10	M	= number of pairs of (r, z) coordinates that follow on card set 3.
			1. ≤ M ≤ 50.
	11-20	N_1	= 1.; one (r, z) card set follows that is used for all θ stations input in card set 5.
			= N_2; a separate (r, z) card set is input for each θ station, for a total of N_2 (r, z) card sets.
			NOTE: 1.0 and N_2 are the only permissible values of N_1.
Card Set 3	1-10	r_1	(r, z) coordinates defining the contour of an axisymmetric or pseudoaxisymmetric body in a radial cutting plane. There must be M of these pairs, six numbers per card. If N_1 = 1.0, one (r, z) card set is input. If $N_1 = N_2$, N_2 (r, z) card sets must be input. This is the only permissible number of (r, z) card sets.
	11-20	z_1	
	21-30	r_2	
	31-40	z_2	
	41-50	r_3	
	51-60	z_3	
Card 4	1-10	N_2	= number of radial planes that follow on cards 5
			1. ≤ N_2 ≤ 50.
Card Set 5	1-10	θ_1	θ values of the radial planes that are used to find panel corner points in these planes. There must be N_2 of these values, six numbers per card.
	11-20	θ_2	
	21-30	θ_3	
	31-40	θ_4	
	41-50	θ_5	
	51-60	θ_6	

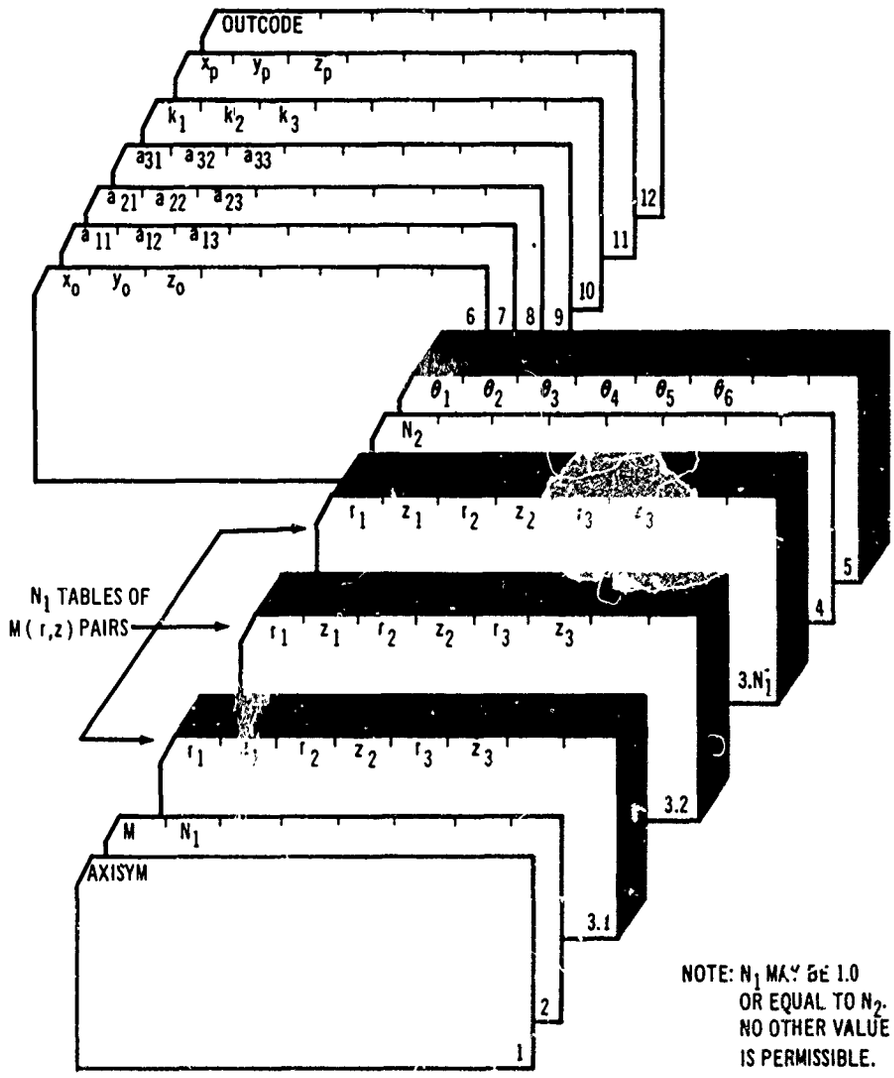

Figure 50. Data Card Arrangement for Subroutine AXISYM.

	Column	Code	Explanation
Card 6	1-10	x_o	coordinates of the origin of the (x_2, y_2, z_2)
	11-20	y_o	coordinate system with respect to the
	21-30	z_o	(x_3, y_3, z_3) coordinate system
Card 7	1-10	a_{11}	direction cosines of x_2 with respect to the
	11-20	a_{12}	(x_1, y_1, z_1) coordinate system
	21-30	a_{13}	
Card 8	1-10	a_{21}	direction cosines of y_2 with respect to
	11-20	a_{22}	the (x_1, y_1, z_1) coordinate system
	21-30	a_{23}	
Card 9	1-10	a_{31}	direction cosines of z_2 with respect to the
	11-20	a_{32}	(x_1, y_1, z_1) coordinate system
	21-30	a_{33}	
Card 10	1-10	k_1	distortion factors that multiply respectively
	11-20	k_2	the (x_3, y_3, z_3) panel corner-point coordi-
	21-30	k_3	nates. The coordinates are distorted after they have been transformed into the (x_3, y_3, z_3) coordinate system.
Card 11	1-10	x_p	displacement factors that are added
	11-20	y_p	respectively to the (x_4, y_4, z_4) panel
	21-30	z_p	corner-point coordinates that have been previously distorted by (k_1, k_2, k_3)
Card 12	1-10	OUTCODE	= 0.; the network of panel corner-points will be output with θ varying first.
			= 1.; the network of panel corner points will be output with (r, z) varying first.
			NOTE: It is important to determine beforehand which OUTCODE is desired, since this determines whether the coordinate output defines a left-hand or a right-hand network, as explained on page 72.

Computer printout and timing. —The sample cases in Appendix III show the computer printout for the five geometry-program subroutines. The format is similar for each subroutine. Titles (if used) and the date are printed in various places on the output. Diagnostics are printed stating whether cards are to be punched, which subroutine has control, and whether curve-fitting is desired (for the WING subroutine). Other diagnostics appear describing or interpreting the input for all the subroutines. The computer printout is

intended to be self-explanatory, and the symbols are all nearly identical to those used for the card input formats (pages 83 to 111). The output for each case consists of the (x, y, z) coordinates on the surface. Some of the inlet REGIONS also have the output in the (R, Z, θ) inlet coordinate system.

The lines of output to be expected for the geometry program are nearly always less than 2,000. The five sample problems in Appendix III produced 1,200 lines of output. The exact number of lines depends on the number of cases and the size of each case, and is approximately six times the number of panels.

The central processor time for the geometry program on the CDC 6600 computer is a matter of seconds. The TUBE subroutine is by far the longest running of the five geometry-program subroutines, taking from 10 to 30 seconds for an average efflux tube. Only if a large number of cases are stacked together does the central processor time exceed 1 minute.

5.2 POTENTIAL-FLOW PROGRAM USAGE

This section describes the usage of the potential-flow program. The first part provides background information and introduces the nomenclature used in the preparation of input data. The second part is a detailed description of the card input format. The third part describes the output.

5.2.1 Background Information

Reference coordinate system. —All geometric inputs must be in the x, y, z reference coordinate system. They can be given in any convenient length dimension. The location and the size of the configuration in this coordinate system is arbitrary except when the symmetry option is used. The angles of attack and yaw define the free-stream direction (see Figure 31) with respect to the reference coordinate axes. For $\alpha = \psi = 0°$ the free-stream velocity is directed along the positive x axis of the reference coordinate system.

Velocities. —All velocities used in the program are nondimensionalized with respect to the free-stream velocity, except for the special case of zero free-stream velocity. In particular, specified normal velocities appearing in the boundary conditions must be nondimensional with respect to the free-stream velocity. For the special case of zero free-stream velocity, the boundary conditions must include nonzero specified velocities, or the solution will be trivial. For this case all the velocities should be considered as velocities nondimensionalized with respect to a reference velocity U_R (see page 32). If necessary, the resultant velocity components can be made dimensional by multiplying them by the free-stream velocity or reference velocity for the respective cases.

Symmetric and unsymmetric flow. —The potential-flow program handles two types of flow: symmetric and unsymmetric. For symmetric flow, the plane of symmetry is the x-z plane and inputs are required only for $y \geq 0$. The angle of yaw must be zero. With symmetry the singularity strengths are symmetric about the x-z plane, and the program combines the influence of the reflected

side ($y \leq 0$) with the influence of the basic side. The obvious advantage of a symmetric flow problem is that the number of singularities is only half of those required for an unsymmetric flow problem, for which the entire body must be defined.

Simultaneous solutions. —The aerodynamic section has the capability of producing up to five aerodynamic solutions simultaneously for a given geometric configuration. Variations of α, ψ, specified inflow distributions, and the zero free-stream condition can be run simultaneously with only slightly greater computation time than required for a single case. This economy occurs because the influence coefficient matrix, which depends only on the geometric configuration, is only computed once.

While several solutions can thus be obtained for a single run, the user must be aware of the effect of further approximations in the theoretical model that may be introduced. For example, the placement of the multihorseshoe vortices for a wake or efflux tube is assumed for a given direction of the free stream velocity and inlet velocity ratio. Moderate variations of the free-stream direction and inlet velocity ratio with the wake and efflux tube positions fixed will still yield useful solutions. However, large variations of these quantities may result in a poor representation of the physical problem, that is, large deviations of the wake and efflux tube from their real position in the flow. As another example, flows with zero free-stream velocity should not be run simultaneously with flows having a free stream, for the zero free-stream cases do not have a trailing wake. However, it is advantageous to combine several zero free-stream cases having different fan inflow velocity distributions.

Off-body points. —The velocity components and pressure coefficients can be found at points off the body by specifying their location in the reference coordinate system. The off-body velocity can be calculated everywhere except in the immediate vicinity, within 10^{-5} units, of a source panel or vortex segment. While the above limitations reflect the computer program's ability to compute the velocity, there exist larger regions where the velocity will not be physically correct. As explained in Section 6, velocities calculated near source panel edges or near concentrated vortices will be meaningless.

Source and quadrilateral vortex panels. —To describe a single source panel or a quadrilateral vortex, it is necessary to input four corner points (x_i, y_i, z_i for $i = 1, 2, 3, 4$) in the reference coordinate system. The order of the points is shown in Figure 51(a). The order of points is important; it controls the direction of the unit normal vector computed by the program at the panel boundary point and also dictates on which face of a source panel the boundary condition is satisfied. The unit normal vector for this panel would be generated as $(\vec{23} \times \vec{14})$, where $\vec{23}$ designates the vector from corner (2) to corner (3). It thus points upward when the corner points are ordered as shown. For source panels, the boundary condition is imposed on the face containing the outward-directed normal, so it is necessary that all normals on a source-paneled surface be directed outward.

A group of panels or quadrilateral vortices can be described more conveniently as a panel network, defined by a rectangular array of panel corner points. The ordering of the point array is shown by the parenthetical numbers in Figure 51(b). These points are arranged in N columns, each containing an equal number of points, M. The size of the network is designated as M x N, the total number of points. The total number of panels is (M-1) x (N-1). In the example of Figure 51(b), M = 4, N = 5, the size of the network is M x N = 20, and the number of panels is (M-1) x (N-1) = 12.

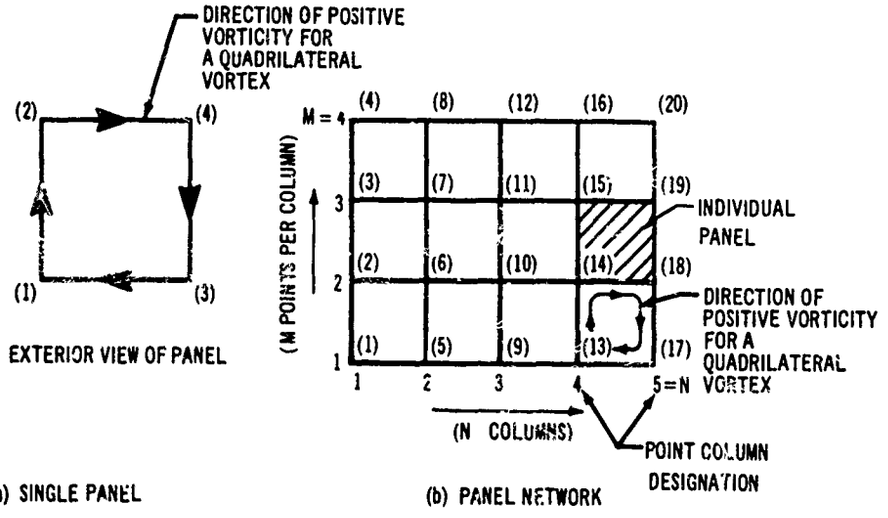

Figure 51. Source and Quadrilateral Vortex Networks.

The terminology used to describe the position of a corner point or singularity panel in a network is shown in Figure 52. Each is denoted in terms of its position in a particular column. A singularity panel in Figure 52 bears the same column designation and position in the column as its lower left corner point. There is one less singularity panel column than point column, and one less singularity per column than point per column. A network arranged on a surface as shown is called a right-hand network because when viewed by an observer standing on the surface exterior and facing in the direction of increasing position in a column, the column number increases to the right. It is necessary that all source panel networks be right-handed, so that the surface normals constructed by the program will be directed outward. For consistency it is helpful but not necessary to input quadrilateral vortex networks in the same manner so that all normals point outward from the surface. The direction of positive vorticity for a single quadrilateral vortex is shown in Figure 51(a). Similarly, each quadrilateral vortex in the network of Figure 51(b) is positive when directed clockwise.

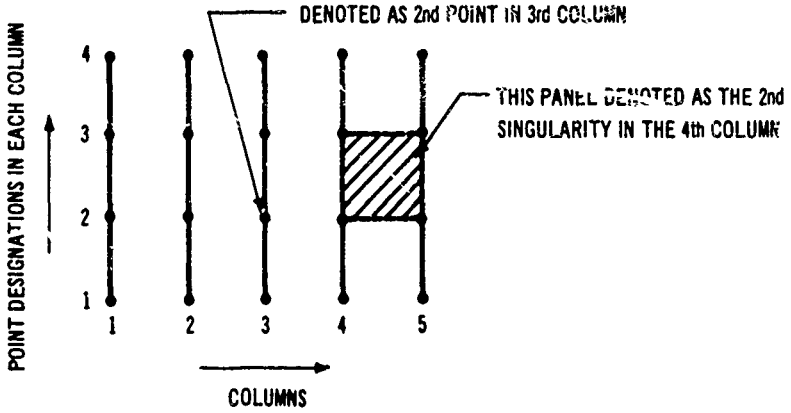

Figure 52. Column Designations.

Multihorseshoe vortex.—The properties of a multihorseshoe vortex are defined in Sections 3 and 6. A single multihorseshoe vortex singularity is input by specifying two columns of points in the reference coordinate system, the number of points in a column (both columns must have the same number of points), the number of bound vortex segments MS, and the weighting W_I ($I = 1, \ldots MS$) of the bound vortex segments. The order of the points for inputing is shown in parenthetical numbers in Figure 53(a). The bound vortex segments are formed by connecting the first MS points in both columns. The direction of positive vorticity for positive weighting is from point column one to point column two.

For a multihorseshoe vortex with trailing legs, such as shown in Figure 53(a), there is no restriction on the choice of weights. The vortex strength of each bound element will be equal to the singularity strength σ multiplied by the weight of the bound element. The vorticity of the trailing elements follows from the continuity of vorticity requirement. It is often convenient to select the weights such that $\Sigma\ W_I = 1.$, so that the total circulation of the multihorseshoe will be equal to σ. It is essential that the points at the ends of the trailing segment (points 7 and 14 in this example) be remote from the wing, since the trailing legs represent vorticity extending to infinity.

The form of multihorseshoe vortex used for the fan and tube internal systems is shown in Figure 53(b). The number of bound elements is equal to the number of points in a column, and there are no trailing legs. To maintain continuity of vorticity it is necessary that $\Sigma\ W_I = 0$. If this requirement is not met, the resulting solution will not satisfy Laplace's equation. An example of the weighting assigned to the multihorseshoe vortex in Figure 53(b) might be $W_1 = -0.4$, $W_2 = -0.3$, $W_3 = -0.3$, $W_4 = +1$. The vorticity on the fourth bound element would then be directed opposite to the other three, with strength equal

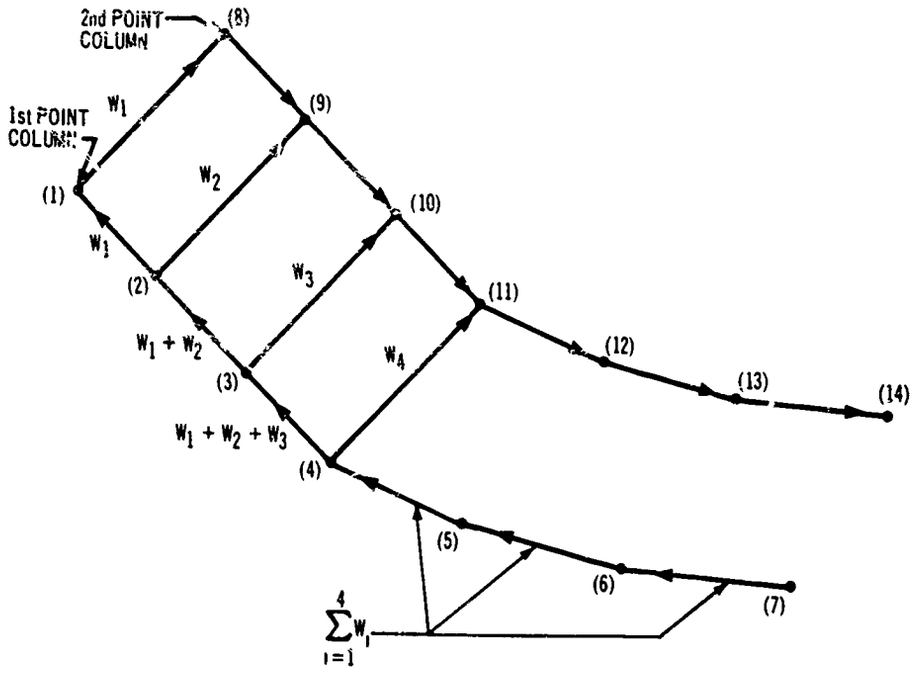

(a) SINGLE MULTIHORSESHOE WITH TRAILING ELEMENTS

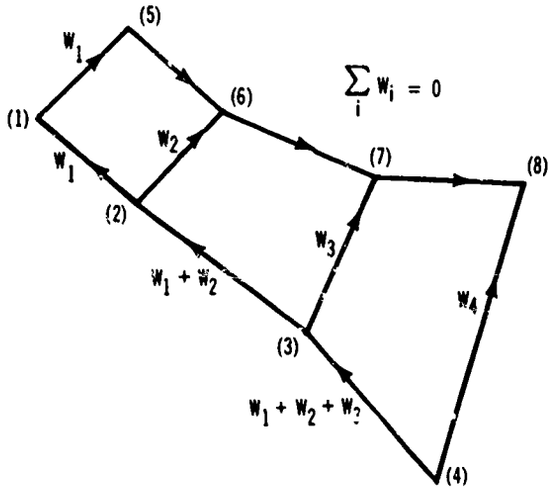

(b) SINGLE MULTIHORSESHOE WITHOUT TRAILING ELEMENTS

Figure 53. Single Multihorseshoe Vortex Arrangements.

to the sum of the other bound vortices. As explained later, the weights applied to the fan and tube internal systems usually are arranged in a similar manner. The one bound element that is exterior to the wing (forming either the first circumferential vortex in the fan face or the first segment of the efflux tube) is assigned a weight of +1, and the sum of the other bound elements interior to the wing must then be -1.

A group of multihorseshoe vortices with common sides are conveniently described by a multihorseshoe vortex network as shown in Figure 54. The parenthetical numbers display the ordering of the input coordinates. The column concept of points is adapted here also, with N denoting the number of columns and M the number of points in each column. A network is described by the numbers M and N, the total number of points M x N, the number of bound segments MS in a column, and the weights W_i (i = 1, . . . MS). One set of weights may be applied throughout a network, or the weighting of each multihorseshoe may be assigned separately. The former option is generally used. For the example in Figure 54, M = 5, N = 6, and MS = 3. The total number of multihorseshoes is N - 1 = 5.

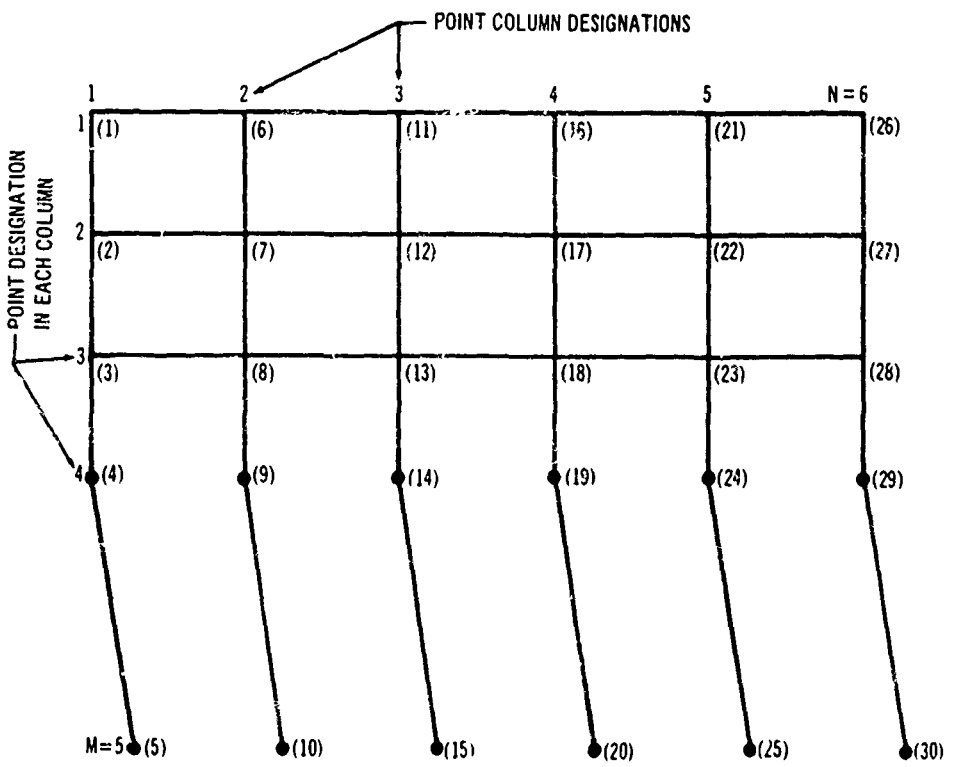

Figure 54. Multihorseshoe Vortex Network Designations.

Boundary-point conditions. —The location (x, y, z) and the unit normal vector (n_x, n_y, n_z) of the boundary points are determined differently for each of the different singularities. For a source panel, the boundary point is fixed by the program at the centroid of the plane panel, with the unit normal vector perpendicular to the panel. The quadrilateral vortex boundary-point location and normal can be computed by the program or input to the program. The computed location of the boundary point is the average of the input points that defines the quadrilateral vortex, and the unit normal vector is directed along the vector product of the diagonals of the quadrilateral vortex. Boundary-point conditions for the multihorseshoe vortex must be input to the program. The various input options for a network are presented in Table I.

TABLE I. BOUNDARY-POINT CONDITIONS

Singularity	Computed by Program	Input to Program
Source Panel	x y z n_x n_y n_z	-
Quadrilateral Vortex	x y z n_x n_y n_z	-
	-	x y z n_x n_y n_z
	n_x n_y n_z	x y z
	x y z	n_x n_y n_z
Multihorseshoe Vortex	-	x y z n_x n_y n_z

The program recognizes two types of boundary conditions at the boundary points. The first boundary condition requires zero normal flow at a boundary point; i.e., the flow must be tangential to the surface. The second condition requires a specified velocity component U_S in the direction of the unit normal vector. If unit normal vectors point outward from a surface, U_S will be negative for flow into a surface.

Forces and moments. —The forces and moment coefficients on both the external wing surface and the lift fans can be calculated as an option in the program. The necessary reference quantities to be input are the coordinates of a point (x_r, y_r, z_r) at the origin of the moment axes, the reference planform area S_r, chord c_r, and span b_r.

Lift fan barrier. —The assembly of singularity networks (multihorseshoe and quadrilateral vortex) representing the fan face and associated internal systems inside the wing and centerbody is termed the barrier assembly. In the framework of the program, each barrier assembly can be represented by up to seven singularity networks. Each of these singularity networks must be identified in the input as belonging to a barrier assembly.

All networks in the barrier assembly must be input in a specific manner if correct fan forces and velocities on the fan face are to be obtained. The point columns of each network must be radially oriented, with the column designation increasing counterclockwise when viewed from above. Each singularity network must evolve completely around the fan axis, 360 degrees, except for a fan with its axis in the plane of symmetry. For the latter case, each network evolves half way around the fan axis. The point columns or radial elements of all singularity networks must line up with one another, and all must begin and end at the same angular position, which is arbitrary. All network corner points not interior to the wing or centerbody must lie in the plane of the fan face. In addition, each network must be input in a manner such that the direction of positive vorticity for each individual singularity (quadrilateral or multihorseshoe) is clockwise when viewed from above. Finally, the individual networks must be assigned a sequence in the order of decreasing distance from the fan axis.

In practice, a barrier is usually represented by a combination of three networks: two quadrilateral and one multihorseshoe. The location of a column of each network with respect to the inlet and centerbody is shown in Figure 55(a). The multihorseshoe network forms the internal lifting system associated with the barrier (see Section 6.4) and extends to the outermost circumferential segment on the barrier. The first quadrilateral network is located entirely on the barrier. The second quadrilateral network extends from the innermost circumferential segment on the barrier to the center of the centerbody. Each network extends entirely around the barrier, 360 degrees. The three networks may be input in any order but must be assigned the following sequence (card 8, page 142). (1) the multihorseshoe, (2) quadrilateral 1, and (3) quadrilateral 2.

The rules for input arrangement laid down above are satisfied when these three networks are input in the following manner: The multihorseshoe network may be input in either of the two ways specified in Figure 55(b) and (c). In either case, the network point columns are radially oriented, with the column designation increasing counterclockwise as viewed from above. In both cases, the weight of the segment on the barrier must be +1. A weight of zero is applied to the point of intersection of the radial vortices with the inlet wall to allow a bend in the vortices at this point. The remainder of the weights of the segments internal to the wing must add up to -1. The number of internal bound elements used is optional. The boundary points for this system are placed adjacent to the source panels on the inlet wall. (See section 6.4.)

The first quadrilateral network on the barrier is input in the order shown in Figure 55(d). The vortex spacing must follow the recommendations given in Section 6.4. If uniform spacing is used radially, the automatic boundary-point placement feature of the quadrilaterals can be used for the boundary-point placement.

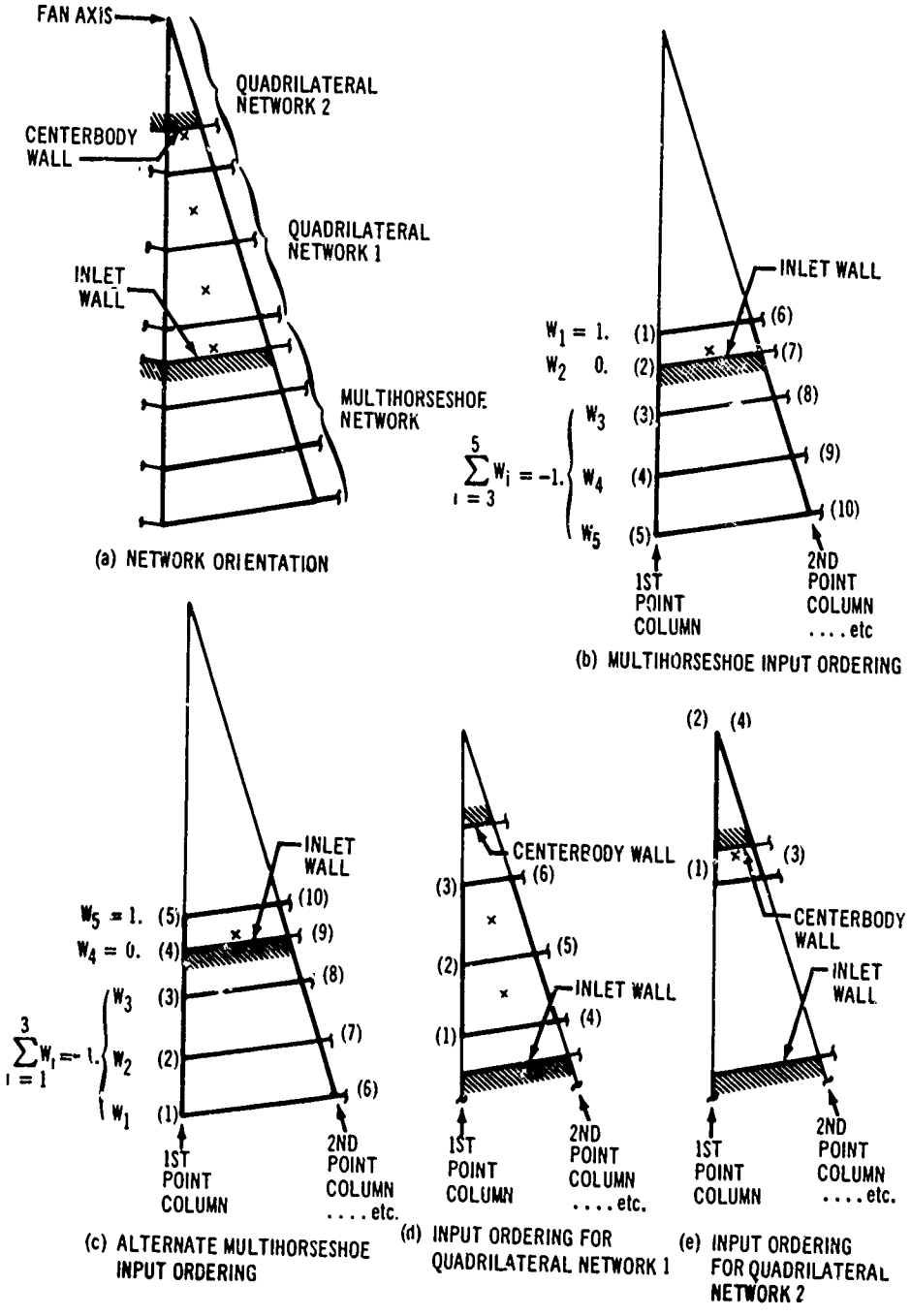

Figure 55. Barrier Networks.

The second quadrilateral network is input as shown in Figure 55(e). The point columns are radial, as before, with the column designation increasing counterclockwise. The boundary-point coordinates for the second quadrilateral must be input.

A systematic specification of the direction of the unit normal vectors at the barrier boundary points should be followed so that the normal velocity is properly directed. If all vectors are directed up, then the specified normal velocity U_S at the barrier boundary points must be negative for flow into the fan. If all vectors are directed down into the fan, the specified normal flow must be positive. Use of the automatic boundary-point placement feature with the first quadrilateral network will produce upward-pointing unit vectors; their direction may be reversed, if desired, by the program option. Some of the above requirements are summarized in Table II.

TABLE II. SUMMARY OF BOUNDARY-POINT PLACEMENT REQUIREMENTS

Vortex Networks	Network Size	Boundary-Point Location	Unit Normal Up*	Unit Normal Down**
Multihorseshoe	$M_1 \times N$	Input	Input	Input
Quadrilateral 1	$M_2 \times N$	Computed (if uniform radial spacing is used)	Computed	Input
Quadrilateral 2	$2 \times N$	Input	Input	Input

*U_S will be negative for flow into the fan.

**U_S will be positive for flow into the fan.

Additional input information must be furnished for the computation of velocities on the barrier, barrier areas, and fan forces (see pages 34-37). These input data consist of the direction cosines (n_{xb}, n_{yb}, n_{zb}) of the fan axis, directed upward, the coordinates (x_b, y_b, z_b) of the point of intersection of the fan axis with the barrier plane, and a table of radii (r_i) and angles (θ_j). The average fan exit pressure coefficient Cp_e, the centerbody base pressure Cp_c, the diameter of the centerbody base d_c, the distance between the barrier and the fan exit plane h, and the direction cosines (t_x, t_y, t_z) of the vectored fan exit flow must also be specified (see Figure 7). The radii and angles to be listed are shown in Figure 12. The radii table is composed of the radial distances from the fan axis to the inlet wall, the singularity corner points, and the centerbody wall. The table of angles θ_j denotes the angular position of the radial barrier vortices; θ is referenced from a radial line in the barrier, parallel to the x-z plane and directed aft from the fan axis. The value of θ is positive in the counterclockwise direction as viewed from above. The program can accept a maximum of ten lift fans for any one configuration.

Streamlines. —Streamlines can be calculated on source panels for any or all of the five solutions that may be run simultaneously. A solution is identified by its order in the input. The starting point for the backward tracking of a streamline is identified by specifying the streamline starting panel and a fractional distance along one of the panel edges where the streamline tracing begins. The initial panel is identified by means of panel column terminology (page 114), specifying its position i in a source-panel column, the column number j, and network k. The particular panel edge e is numbered 1, 2, 3, or 4 according to its position in the network, as shown in Figure 56(a). The position of the starting point along an edge is specified by giving its fractional distance along the edge, measured in the direction of clockwise travel around the panel [Figure 56(b)].

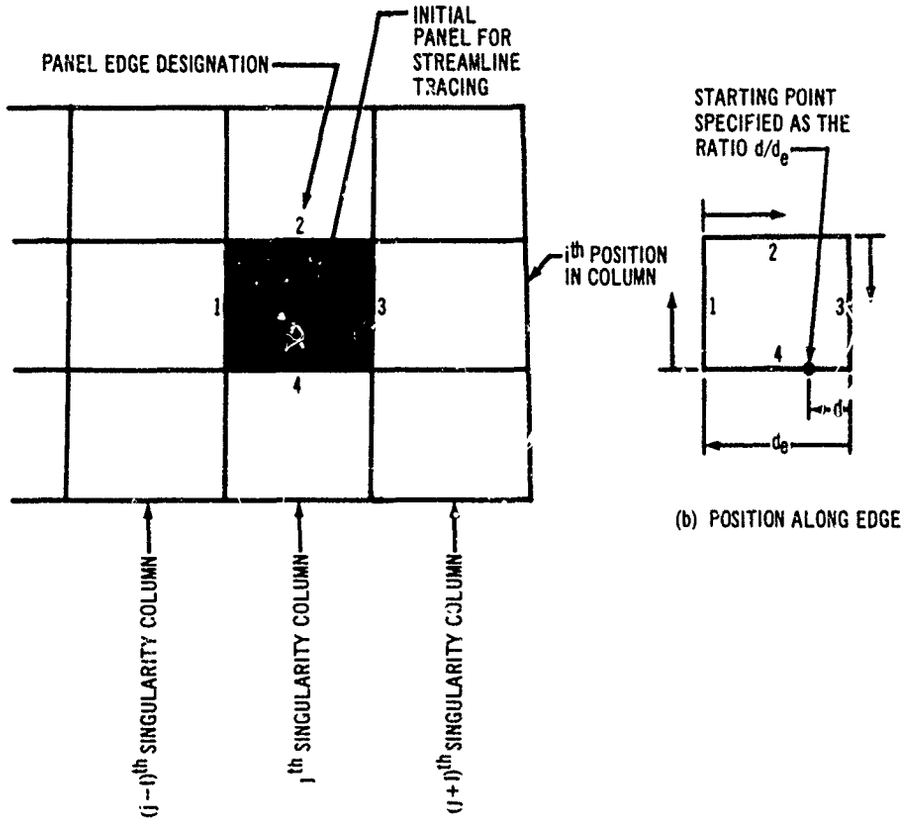

Figure 56. Initial Streamline Data.

The velocity derivative dV_t/ds_t is obtained by finite difference from a velocity calculated at a small offset distance from a source-panel boundary point. This offset distance is formed from an input fraction times the maximum source-panel diagonal of a configuration. Recommended values of the input fraction are between 0.01 and 0.0001.

Checking inputs.—If meaningless results are to be avoided, it is imperative that all geometry be input correctly. For large, complex configurations involving many networks of different singularities, it is not uncommon for errors to occur in the inputs, either through a mispunched data card, or by a simple oversight, or perhaps because of lack of program experience. The program has been designed to furnish aid in checking the inputs by means of the following feature.

The program is divided into several sections, the first one dealing with geometry. This section converts the input coordinate arrays and other information into individual panel coordinates, generates boundary-point coordinates and normals, and in general prepares all geometric information for use by later sections. The program can be set to run through the Geometric Section only and then stop. It can do this extremely rapidly, the time required being approximately 1 percent of the total time required to solve the problem. The output will list the input cards, the boundary-point coordinates and normals, the panel corner points, the area and maximum diagonal of each panel, and other descriptive information listed in Section 5.2.3. Also printed out will be the input for the Aerodynamic Section with the comment INVALID CONTROL CARD. The user can scan these data, looking for irregularities. A mispunched coordinate will usually result in a panel whose area or maximum diagonal is very different from its neighbor's, and it is easily recognized. The displacement distance D that a corner point is moved to produce a planar panel is also printed out, and large values of D are a definite indication that something is wrong. All boundary-point normals should be scanned to ensure that they point outward. A mistake in ordering the network corner points can easily produce this type of error.

It is strongly suggested that this check run and data scanning process be performed before committing a lengthy run to the computer. Because the time required for the check run is negligible, no data-saving feature has been included. After the output has been scanned and errors corrected, the input data must be resubmitted for running through the complete program.

5.2.2 Input Format

This section provides the instructions for assembling a data deck for the potential-flow program. A sample problem is shown in Appendix III.

There are three types of inputs for the potential-flow program: numerical data, title card, and control cards. The numerical data are punched in seven-field, ten-digit format, and all numbers must have a decimal point. The title card will accept any alphanumeric characters. The control cards are identified from the first four columns of a card. The remainder of a control card may contain any alphanumeric symbols but generally contains the words listed on the following page.

The control cards within the data deck are used to:

1) mark the beginning and the end of two blocks of data

GEOMETRIC SECTION
END OF GEOMETRIC SECTION
AERODYNAMIC SECTION
END OF AERODYNAMIC SECTION

2) terminate the computer run after one or more cases

EXIT

3) identify the major divisions of data within the Geometric Section

SOURCE-PANEL GEOMETRY
QUADRILATERAL VORTEX GEOMETRY
MULTIHORSESHOE VORTEX GEOMETRY
OFF-BODY POINTS

If any division of the Geometric Section is not used for a case, the corresponding control card should be omitted. The ordering of these four cards must be maintained.

For submitting a check run through the Geometric Section only, remove the END OF GEOMETRIC SECTION and the AERODYNAMIC SECTION control cards from the data deck. This run will provide a listing of all the input cards plus the output of the Geometric Section (see page 123).

To run multiple cases of either the complete or the check type, stack the cases consecutively as shown in Figure 57.

Program field length, timing, and output estimates. —The maximum field length of the potential-flow program is 240,000 octal words, which is reached when the zero level or the main segment and the level segment containing the streamline subroutines are loaded.

Program timing is divided into central processor timing and peripheral processor timing. Central processor time is the time required to execute and control the program, while peripheral processor time is the time needed to perform all input/output functions required by the program. The central processor timing is largely a function of the number of singularities needed to represent the configuration, although the number of off-body points and the number of streamlines also affect the timing. Figure 58 shows an estimate of the central processor time. The peripheral processor time is generally three to eight times longer than the central processor time, depending on how the computer is loaded with other programs.

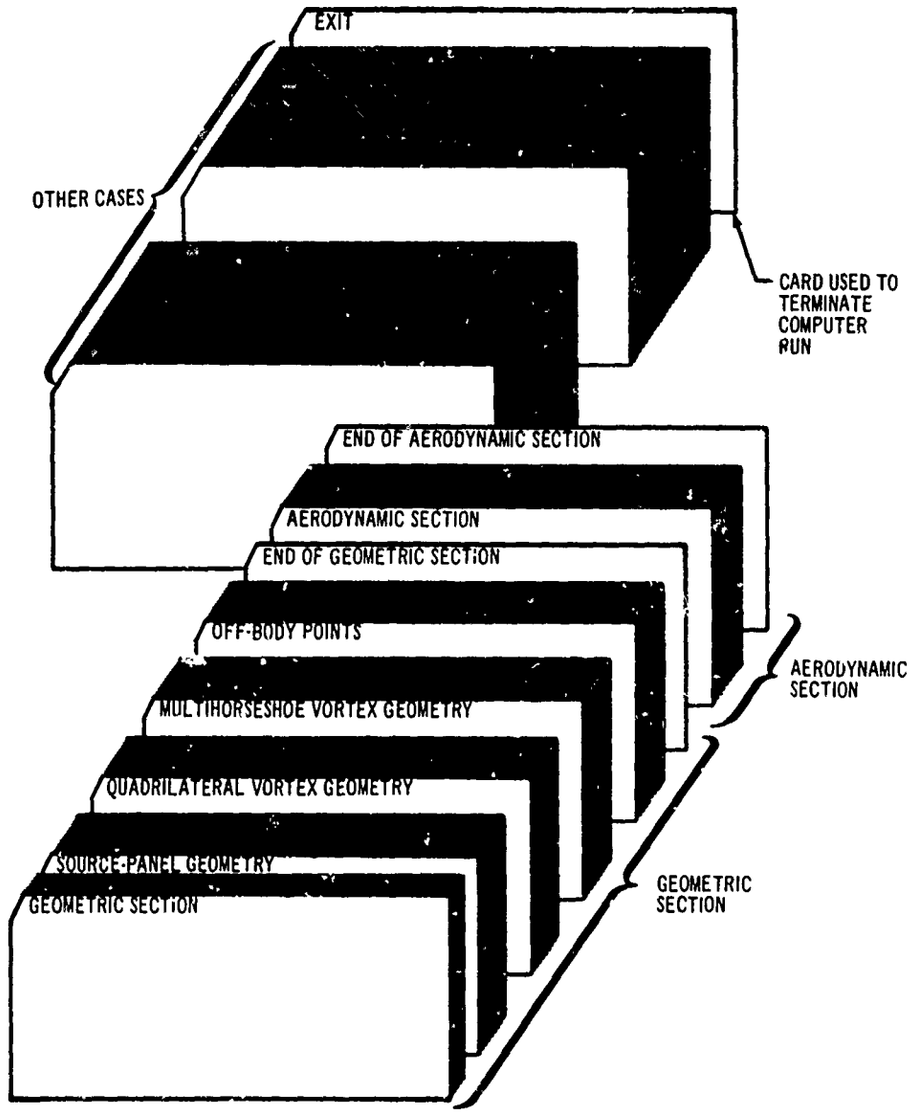

Figure 57. Data Card Arrangement for Potential-Flow Program.

An estimate for the printed output is given by

$$\text{lines} = 5\,\text{NSING} + \text{NOFF} + 1.2\,\text{NSOL}\,(\text{NSING} + \text{NOFF}) + 110\,\text{NSL}$$

where NSING = number of singularities
NOFF = number of off-body points
NSOL = number of solutions desired
NSL = number of streamlines

The maximum number of singularities that can be used depends on the storage capacity of the particular facility. With two disk memory units, the maximum number of singularities is approximately 1200.

The detailed data card input format for the Geometric Section (source-panel geometry, quadrilateral vortex geometry, multihorseshoe vortex geometry, off-body points) and Aerodynamic Section follows.

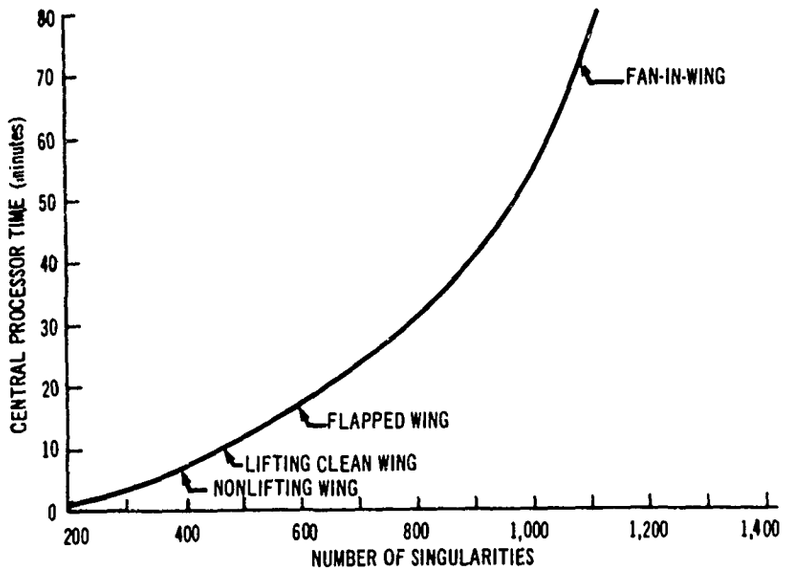

Figure 58. Potential-Flow Program Central Processor Time Estimate.

GEOMETRIC SECTION CARD INPUT

Figure 59 displays the data cards for the Geometric Section of the potential-flow program. All Geometric Section data, except table and control cards, are punched in seven-field, ten-digit format. All geometry is defined in the reference coordinate system. A description of the card input to this section follows:

	Column	Code	Explanation
Card 1	1-4	GEOM	Control card—columns 1-4 contain the word GEOM.
Card 2	1-80	TITLE	any desired title
Card 3	1-10	ICODE	= 1.; symmetric flow = 3.; unsymmetric flow
	11-20	NSING	= number of singularities used to represent the potential-flow model 2. ≤ NSING ≤ 1200.

Source-panel geometry cards
(See page 129.)

Quadrilateral vortex geometry cards
(See page 131.)

Multihorseshoe vortex geometry cards
(See page 134.)

Off-body point cards
(See page 138.)

Card 4	1-4	END	Control card—columns 1-4 contain the word ENDb, where b represents a blank.

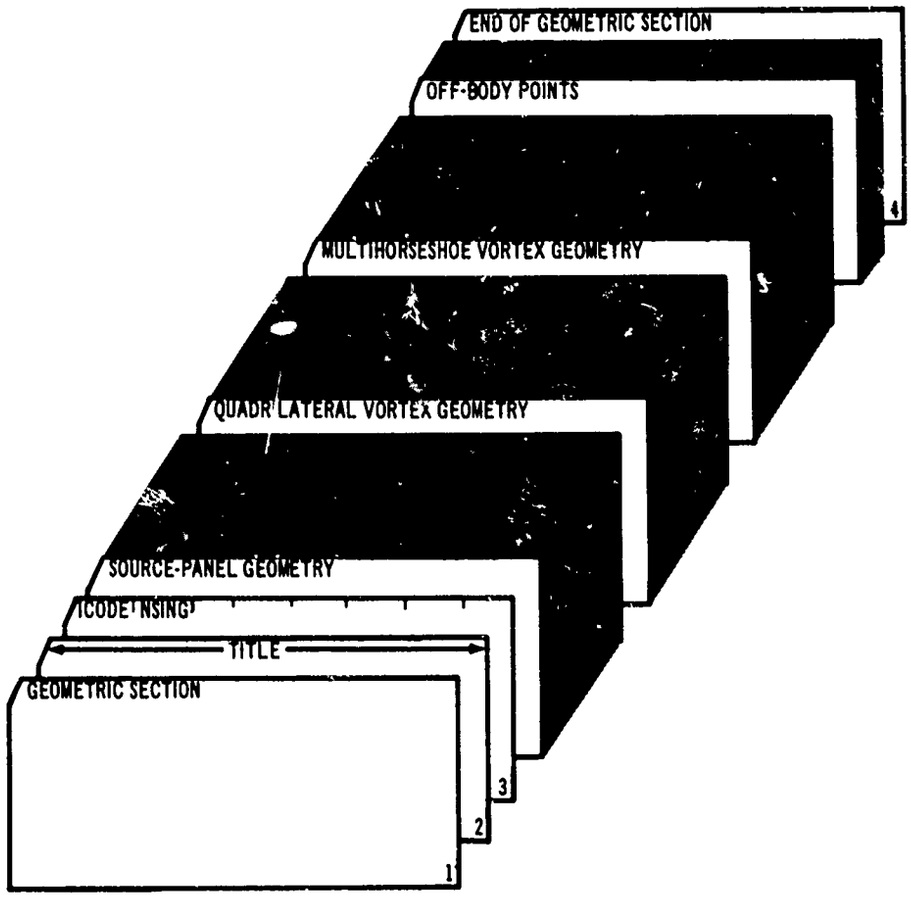

Figure 59. Data Card Arrangement for Geometric Section.

Source-panel geometry.— Figure 60 displays the data cards for the source-panel geometry subdivision of the Geometric Section. These cards are omitted if the potential-flow model does not require the source-panel singularity for its representation.

	Column	Code	Explanation
Card 1	1-4	SOUR	Control card—columns 1-4 contain the word SOUR.
Card 2	1-10	NET	= number of source panel networks
			1. ≤ NET ≤ 200.

Cards 3 through 5 are repeated for each source panel network.

Card 3	1-10	M	= number of points per column
	11-20	N	= number of point columns in the network
			2. ≤ M ≤ 500., 2. ≤ N ≤ 500., and 4. ≤ M x N ≤ 2500. (See Figure 51.)
	21-30		blank
	31-40	OPTUS	= 0.; all normal velocities are zero.
			= 10.; normal velocities specified for each simultaneous solution.
			= 20.; normal velocities specified once and used for all simultaneous solutions.
Card Set 4	1-10	x_1	corner-point coordinates of the source-panel network in the reference coordinate system. The (M x N) corner points are input sequentially, two per card. (See Figure 51.)
	11-20	y_1	
	21-30	z_1	
	31-40	x_2	
	41-50	y_2	
	51-60	z_2	

The next card set is omitted if OPTUS = 0. The card set consists of [(M- . (N-1)] cards, one for each source panel in the network, arranged in the order of increasing position in successive columns (Figure 52).

	Column	Code	Explanation
If OPTUS = 10., the format of the card set is:			
Card Set 5	1-10	U_{s1}	specified normal velocities, one for each simultaneous solution. The first field (columns 1-10) contains the normal velocity for the first solution, etc. The number of fields used equals the number of solutions (maximum of five).
	11-20	U_{s2}	
	21-30	U_{s3}	
	31-40	U_{s4}	
	41-50	U_{s5}	
If OPTUS = 20., the format of the card set is:			
Card Set 5	1-10	U_s	specified normal velocity used for all solutions.

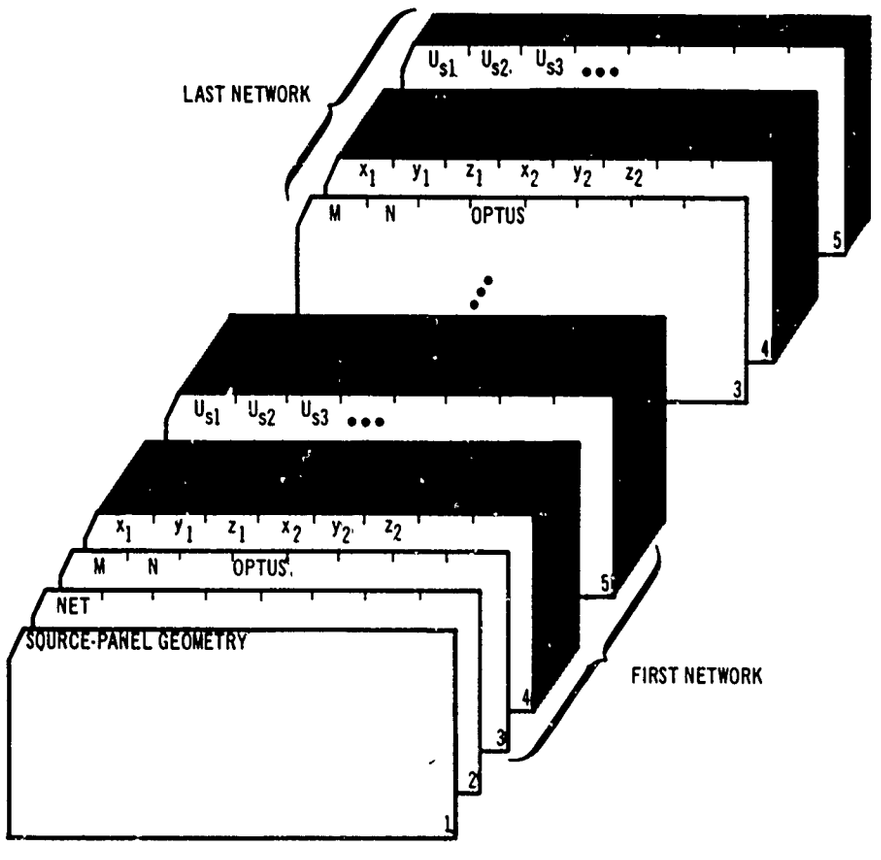

Figure 60. Data Card Arrangement for Source-Panel Geometry.

Quadrilateral vortex geometry. —Figure 61 displays the data cards for the quadrilateral vortex geometry subdivision of the Geometric Section. These cards are omitted if the potential-flow model does not require the quadrilateral vortex singularity for its representation.

	Column	Code	Explanation
Card 1	1-4	QUAD	Control card—columns 1-4 contain the word QUAD.
Card 2	1-10	NET	= number of quadrilateral vortex networks 1. ≤ NET ≤ 200.

Cards 3 through 6 are repeated for each quadrilateral vortex network.

Card 3	1-10	M	= number of points per column
	11-20	N	= number of columns in the network 2. ≤ M ≤ 500., 2. ≤ N ≤ 500., and 4. ≤ M x N ≤ 2500. (See Figure 51.)
	21-30	OPTBP	= 0.; boundary-point coordinates are computed by the program.
			= 10.; boundary-point coordinates (x, y, z) and unit normal vector components (n_x, n_y, n_z) are to be input for all quadrilateral vortices of the network.
			= 20.; only the boundary-point coordinates (x, y, z) are to be input for all quadrilateral vortices of the network (unit normals constructed by the program).
			= 30.; only the boundary-point unit normal vector components (n_x, n_y, n_z) are to be input for all quadrilateral vortices of the network (boundary-point coordinates computed by the program).
	31-40	OPTUS	= 0.; all normal velocities are zero.
			= 10.; normal velocities specified for each simultaneous solution.
			= 20.; normal velocities specified once and used for all simultaneous solutions.

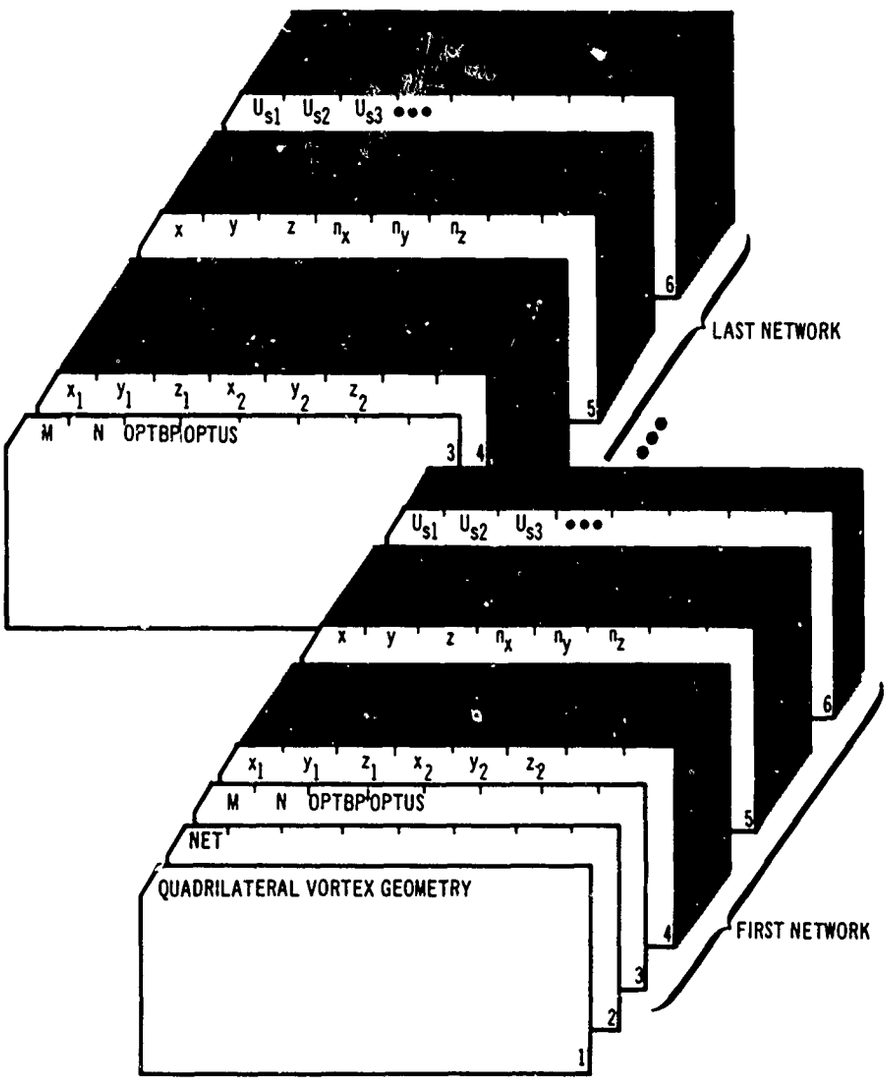

Figure 61. Data Card Arrangement for Quadrilateral Vortex Geometry.

	Column	Code	Explanation
Card Set 4	1-10	x_1	corner-point coordinates of the quadrilateral vortex network in the reference coordinate system. The corner points are input sequentially, two per card. (See Figure 51.)
	11-20	y_1	
	21-30	z_1	
	31-40	x_2	
	41-50	y_2	
	51-60	z_2	

The next card set is omitted if OPTBP = 0. The card set consists of [(M-1) x (N-1)] cards, one for each quadrilateral vortex in the network, arranged in the order of increasing position in successive columns (Figure 52).

If OPTBP = 10., the format of the card set is:

Card Set 5	1-10	x	coordinates of the boundary point
	11-20	y	
	21-30	z	
	31-40	n_x	unit normal vector components at the boundary point
	41-50	n_y	
	51-60	n_z	

If OPTBP = 20., the format of the card set is:

Card Set 5	1-10	x	coordinates of the boundary point
	11-20	y	
	21-30	z	

If OBTBP = 30., the format of the card set is:

Card Set 5	1-30		blank
	31-40	n_x	unit normal vector components at the boundary point
	41-50	n_y	
	51-60	n_z	

The next card set is omitted if OPTUS = 0. The card set consists of [(M-1) x (N-1)] cards, one for each quadrilateral vortex in the network, arranged in the order of increasing position in successive columns (Figure 52).

If OPTUS = 10., the format of the card set is:

Card Set 6	1-10	U_{s1}	array of specified normal velocities, one for each simultaneous solution. The first field (columns 1-10) contains the normal velocity for the first solution, etc. The number of fields used equals the number of solutions (maximum of five).
	11-20	U_{s2}	
	21-30	U_{s3}	
	31-40	U_{s4}	
	41-50	U_{s5}	

If OPTUS = 20., the format of the card set is:

Card Set 6	1-10	U_s	specified normal velocity used for all solutions

Multihorseshoe vortex geometry. —Figure 62 displays the data cards for the multihorseshoe vortex geometry subdivision of the Geometric Section. These cards are omitted if the potential-flow model does not require the multihorseshoe vortex singularity for its representation. A maximum of 110 multihorseshoe vortex singularities may be used.

	Column	Code	Explanation
Card 1	1-4	MULT	Control card—columns 1-4 contain the word MULT.
Card 2	1-10	NET	= number of multihorseshoe vortex networks
			1. ≤ NET ≤ 100.

Cards 3 through 7 are repeated for each multihorseshoe vortex network.

Card 3	1-10	M	= number of points per column
	11-20	N	= number of columns in the network
			2. ≤ M ≤ 50., 2. ≤ N ≤ 100., and 4. ≤ M x N ≤ 2500.
	21-30	MS	= number of weighted segments per multihorseshoe
			0. ≤ MS ≤ 50. (See Figure 53.)
	31-40	OPTWT	= 1.; array of weighting values are specified once, and these values apply to all multihorseshoe vortices of the network.
			= 10.; array of weighting values are specified for each multihorseshoe vortex of the network.
	41-50	OPTBP	= 10.; boundary-point coordinates (x, y, z) and unit normal vector components (n_x, n_y, n_z) are to be input for all multihorseshoe vortices of the network. This option must be used.
	51-60	OPTUS	= 0.; all normal velocities are zero.
			= 10.; normal velocities specified for each simultaneous solution.
			= 20.; normal velocities specified once and used for all simultaneous solutions.

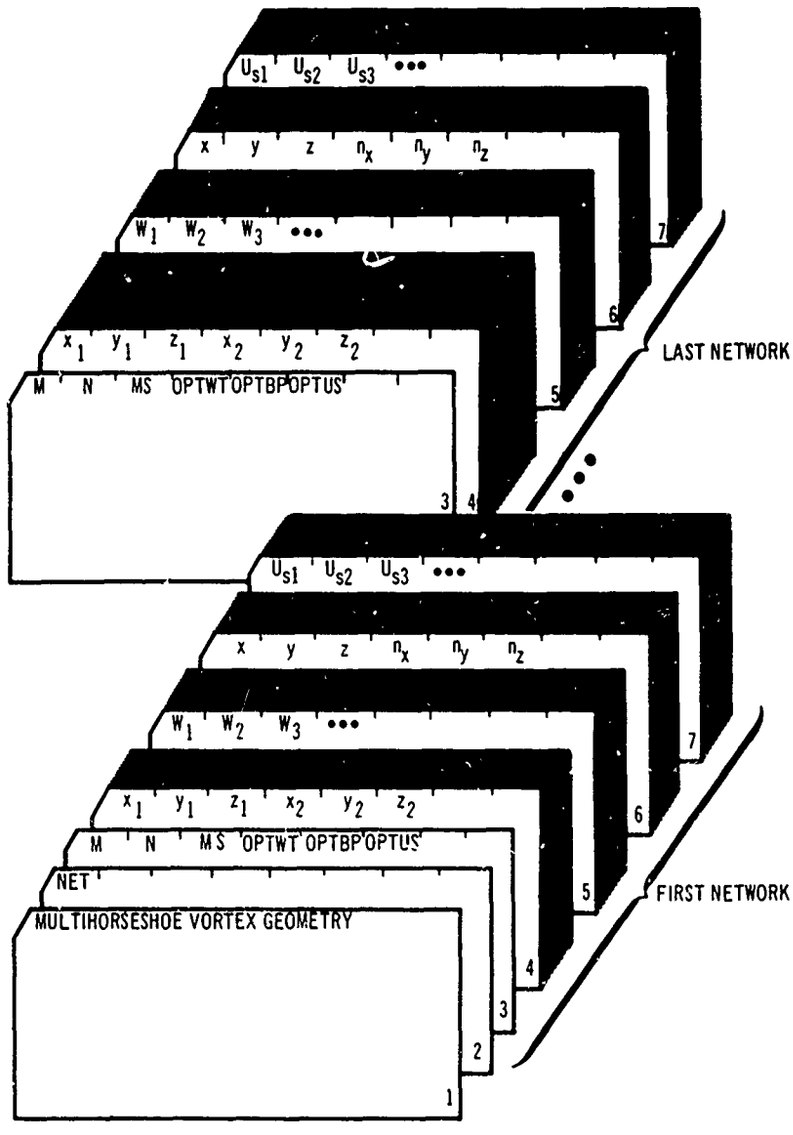

Figure 62. Data Card Arrangement for Multihorseshoe Vortex Geometry.

	Column	Code	Explanation
Card Set 4	1-10	x_1	corner-point coordinates of the multi-horseshoe vortex network in the reference coordinate system. (M x N) corner points are input sequentially, two per card (see Figure 54).
	11-20	y_1	
	21-30	z_1	
	31-40	x_2	
	41-50	y_2	
	51-60	z_2	

The next card set is for the specified weights.

If OPTWT = 1., the format of the card set is:

Card Set 5	1-10	W_1	weighting values for the bound multihorse-shoe vortex segments. MS values are input. These values apply to all multi-horseshoe vortices of the network.
	11-20	W_2	
	21-30	W_3	
	31-40	W_4	
	41-50	W_5	
	51-60	W_6	
	61-70	W_7	

If OPTWT = 10., the format of the card set is:

Card Set 5	1-10	W_1	weighting values for the bound horseshoe vortex segments. (N-1) card sets of MS weighting values are input, one card set for each multihorseshoe vortex.
	11-20	W_2	
	21-30	W_3	
	31-40	W_4	
	41-50	W_5	
	51-60	W_6	
	61-70	W_7	

The next card set consists of (N-1) cards, one for each multihorseshoe vortex in the network.

Card Set 6	1-10	x	coordinates of the boundary point
	11-20	y	
	21-30	z	
	31-40	n_x	unit normal vector components at the boundary point
	41-50	n_y	
	51-60	n_z	

The next card set is omitted if OPTUS = 0. The card set consists of (N-1) cards, one for each multihorseshoe vortex in the network.

If OPTUS = 10., the format of the card set is:

Card Set 7	1-10	U_{s1}	array of specified normal velocities, one for each simultaneous solution. The first field (columns 1-10) contains the normal velocity for the first solution, etc. The number of fields used equals the number of solutions (maximum of five).
	11-20	U_{s2}	
	21-30	U_{s3}	
	31-40	U_{s4}	
	41-50	U_{s5}	

	Column	Code	Explanation
If OPTUS = 20., the format of the card set is:			
Card Set 7	1-10	U_s	specified normal velocity used for all solutions

Off-body point geometry. —Figure 63 displays the data cards for the off-body points. These cards are omitted if the velocity at off-body points is not desired.

	Column	Code	Explanation
Card 1	1-4	OFF	Control card—column 1-4 contains the word OFF- or the word OFFb, where b represents a blank.
Card 2	1-10	NOFF	= number of off-body points 0. ≤ NOFF ≤ 2500.
Card Set 3	1-10	x_1	coordinates of the off-body points. NOFF points are input, two per card.
	11-20	y_1	
	21-30	z_1	
	31-40	x_2	
	41-50	y_2	
	51-60	z_2	

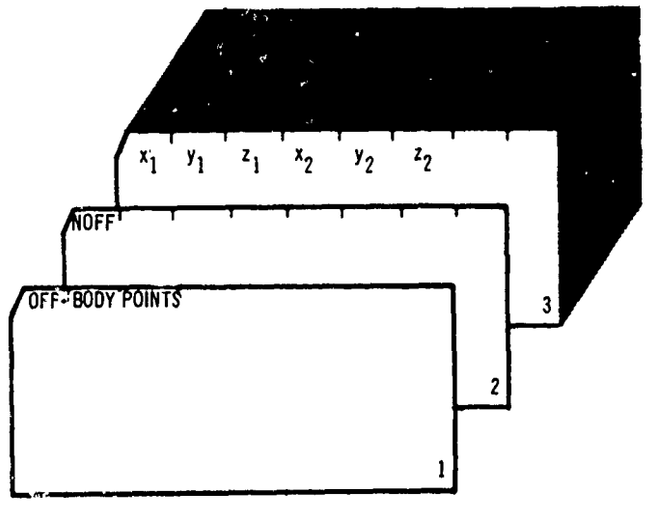

Figure 63. Data Card Arrangement for Off-Body Points.

AERODYNAMIC SECTION CARD INPUT

Figure 64 displays the data cards for the Aerodynamic Section of the potential-flow program.

All Aerodynamic Section data, except control cards, are punched in seven-field, ten-digit format. All input aerodynamic geometry is defined in the reference coordinate system. A description of the card input to this section follows:

	Column	Code	Explanation
Card 1	1-4	AERO	Control card—columns 1-4 contain the word AERO.
Card 2	1-10	NRHS	= number of simultaneous solutions desired
			1. ≤ NRHS ≤ 5.
	11-20	FORCES	force and moment option code
			= 0.; no forces and moments are calculated.
			= 1.; all forces and moments are calculated.
	21-30	PLOT	plotting option code
			= 0.; no plotting desired.
			= 1.; plotting of C_p vs x/c over the source-paneled model is desired (used only if plotting facility is available).
	31-40	NARRAY	= number of lift fans in the model
			0. ≤ NARRAY ≤ 10.
	41-50	NSL	= number of streamlines desired
			0. ≤ NSL ≤ 50.

Card Set 3 consists of one card for each solution.

Card Set 3	1-10	α	angle of attack in degrees
	11-20	ψ	angle of yaw in degrees

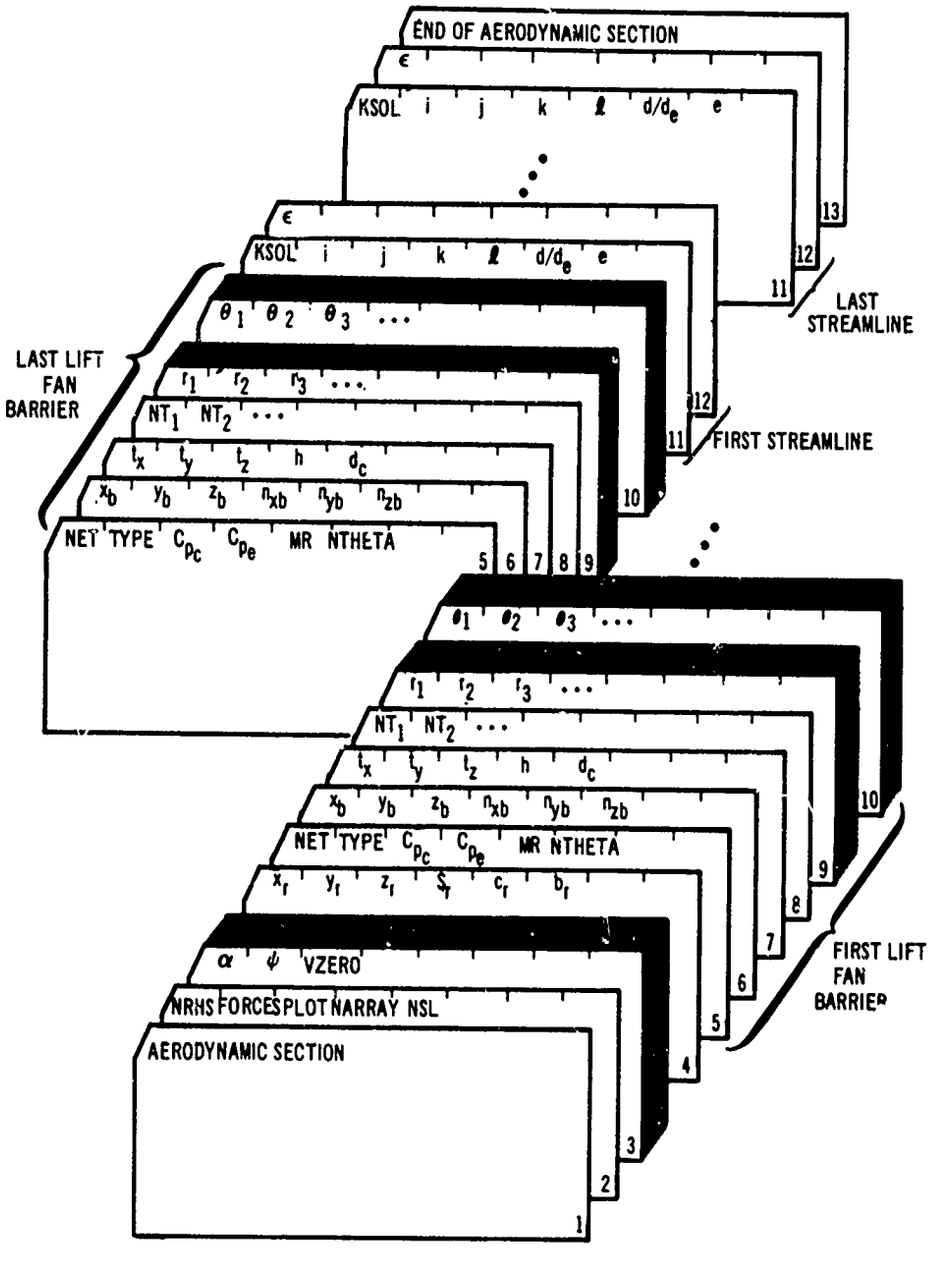

Figure 64. Data Card Arrangement for Aerodynamic Section.

	Column	Code	Explanation
Card Set 3 (Continued)	21-30	VZERO	zero free-stream velocity option
			= 0.; option not exercised. The dimensionless free-stream velocity has a value of unity in a direction specified by the angles of attack and yaw.
			= 1.; zero free-stream velocity condition. The angles of attack and yaw have no meaning.

The following card is omitted unless FORCES = 1.0.

Card 4	1-10	x_r	moment reference coordinates
	11-20	y_r	
	21-30	z_r	
	31-40	S_r	reference planform area
	41-50	c_r	reference chord
	51-60	b_r	reference span

Cards 5 through 10 are repeated for each lift fan in the model. A maximum of ten lift fans can be specified.

Card 5	1-10	NET	= number of quadrilateral and multihorseshoe networks used to form the barrier assembly
			1. ≤ NET ≤ 7.
	11-20	TYPE	= 1.; half fan input. This occurs when the center of the fan is in the plane of symmetry (x-z) and the flow is symmetrical.
			= 2.; complete fan input. This occurs whenever the center of the fan is not in the plane of symmetry (x-z) or when the flow is unsymmetric.
	21-30	C_{p_c}	assumed pressure coefficient at the centerbody base
	31-40	C_{p_e}	assumed pressure coefficient at the exit plane
	41-50	MR	= number of radial points used at each θ location to define the barrier areas
			2. ≤ MR ≤ 20.

	Column	Code	Explanation
Card 5 (Continued)	51-60	NTHETA	= number of angles used to define the barrier areas 2. ≤ NTHETA ≤ 50.
Card 6	1-10	x_b	coordinates of the barrier center
	11-20	y_b	
	21-30	z_b	
	31-40	n_{xb}	unit normal vector components along the fan axis, directed upward
	41-50	n_{yb}	
	51-60	n_{zb}	
Card 7	1-10	t_x	unit vector components in the direction of the flow from the fan exit
	11-20	t_y	
	21-30	t_z	
	31-40	h	average distance between the barrier and the exit plane
	41-50	d_c	diameter of the centerbody base
Card 8	1-10	NT_1	sequential identity of the barrier singularity networks used to form a barrier assembly. They must be ordered from the outside to to the inside of the barrier. The identification number applies to the order in which a network is input. A positive number denotes a quadrilateral vortex network, and a negative number denotes a multihorseshoe vortex network. For example, NT_1 = -3. means that the third multihorseshoe vortex network input is used to represent the first network of the barrier assembly. NET networks are listed, beginning in the first field (columns 1-10).
	11-20	NT_2	
	21-30	NT_3	
	31-40	NT_4	
	41-50	NT_5	
	51-60	NT_6	
	61-70	NT_7	
Card Set 9	1-10	r_1	radial distances used to form barrier areas, in sequential order (see Figure 12). There are MR of these.
	11-20	r_2	
	21-30	r_3	
	31-40	r_4	
	41-50	r_5	
	51-60	r_6	
	61-70	r_7	

	Column	Code	Explanation
Card Set 10	1-10	θ_1	angles used to form barrier areas, in sequential order (see Figure 12). There are NTHETA angles.
	11-20	θ_2	
	21-30	θ_3	
	31-40	θ_4	
	41-50	θ_5	
	51-60	θ_6	
	61-70	θ_7	

Cards 11 and 12 are repeated for each streamline on the model.

Card 11	1-10	KSOL	identifies the particular simultaneous solution for which the streamline is desired, based on the order of input of the simultaneous solutions $1. \leq KSOL \leq 5.$
	11-20	i	position in the panel column of the streamline-starting panel
	21-30	j	panel column of the streamline-starting panel
	31-40	k	source-panel network containing the streamline-starting panel
	41-50	l	maximum length of the streamline
	51-60	d/d_e	fractional distance of the streamline-starting point along edge e
	61-70	e	identifies the streamline-starting edge of the panel (Figure 56)
Card 12	1-10	ϵ	fraction of the maximum source panel diagonal (t_{max}) used to form ϵ_{10}, which is the offset distance used in the calculation of dV_t/ds_t. If $\epsilon = 0.$, the derivative will not be calculated.
Card 13	1-4	END	Control card—columns 1-4 contain the word ENDb, where b represents a blank.

5.2.3 Output

The output of the potential-flow program is divided into three major sections: the program inputs, the Geometric Section, and the Aerodynamic Section. Program inputs are listed in the exact form in which they were submitted. This listing establishes a record of the run and is useful for pinpointing input errors.

The Geometric Section gives the geometry of each singularity and the location of the off-body points. Each singularity has an accumulative number defined by the order of input, a number denoting its position in a column, a column number, and a network number. These numbers aid the user in systematically identifying singularities. If the boundary-point coordinates, normal vectors, or specified normal velocities are input, they will be so labeled in the Geometry Section. All the coordinates are listed in the reference coordinate system.

The source-panel geometry output lists the boundary-point coordinates (x, y, z) and direction cosines of the unit normal vector (n_x, n_y, n_z), the four corner-point coordinates of each planar source panel $(x_i, y_i, z_i, i = 1, \cdots, 4)$, and descriptive quantities useful for checking the geometry. The corner-point printout is ordered in relation to the panel's position in the network, as shown in Figure 65. The descriptive quantities are the maximum panel diagonal t_{max}, the panel area, and the distance D that corner-point 1 of each panel (see Figure 65) was moved from its input value to form a planar panel (D is positive if the point was moved in the direction opposite the panel boundary-point normal). All four corners are moved by the same amount, but adjacent corners move in opposite directions. Summary data of some of the above quantities are provided after each source-panel network and after the last source-panel network.

The quadrilateral vortex geometry output lists the boundary-point coordinates (x, y, z) and normal vector (n_x, n_y, n_z), the specified normal velocity component at each boundary point, and the approximate area and corner points $(x_i, y_i, z_i, i = 1, \cdots, 4)$ of each quadrilateral vortex. These are ordered in the same manner as the source panels. Summary data of some quantities are provided.

The multihorseshoe vortex geometry output lists the defining point coordinates of these singularities and weighting of the bound segments $(W_i, i = 1, \cdots MS)$, the boundary-point coordinates (x, y, z) and normal vectors (n_x, n_y, n_z), and the specified normal velocity component at each boundary point. The corner-point coordinates for each individual multihorseshoe vortex in a network are listed in the order shown in Figure 53.

The Aerodynamic Section printout is subdivided into three parts: flow properties at boundary points and off-body points, forces and moments, and streamlines. At all of the singularity boundary points, the following quantities are listed: the components of velocity (V_x, V_y, V_z), the total velocity V, the pressure coefficient C_p, the singularity strength σ, and the resultant normal velocity component V_{rn}. All the velocities are nondimensionalized with respect to the free-stream velocity or to the reference velocity for a solution with no free stream. For off-body points, the velocity components, the total velocity, and

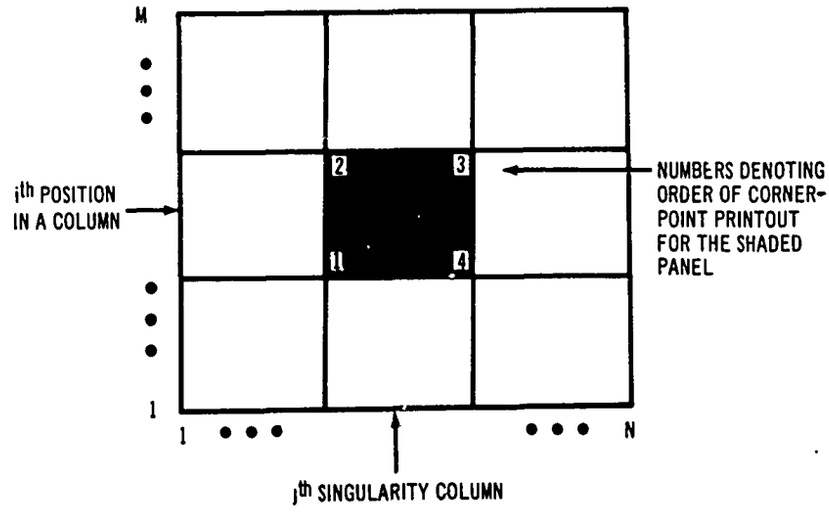

Figure 65. Individual Panel Corner-Point Designation.

the pressure coefficient are output. For a barrier surface, the coordinates of the midpoints of the circumferential vortex segments, the velocity components, the total velocity, and the pressure coefficient computed at the midpoints of the circumferential vortex segments are output (see Section 3.2). The individual areas used in the barrier force calculations (see Figure 12) are also furnished. These are all output in the order of decreasing distance to the fan axis and counterclockwise around the fan.

The force and moment outputs are divided into three parts: forces and moments on the source panels, pressure and momentum effects on the fan control surface and exit plane. and the total force and moment on the complete configuration. The force and moment coefficients on the source panels are printed out as individual sums over each column of panels. The sum of the products of the singularity strengths times their panel areas is also printed out on a per-column basis. Force and moment coefficients on the individual source panels are not furnished. The sums of the force and moment coefficients, singularity strengths, and panel areas for all source panels are printed out before the following fan force coefficients are presented.

The force and moment coefficients on the fan are resolved into the separate contributions of pressure and momentum on the barrier and the fan exit plane. The coefficients are printed out, together with the areas used in the integration, on a per-column basis, one column forming a wedge-shaped portion of the fan. The separate contributions are summed individually and printed out together with the force and moment on the centerbody base.

The total force and moment coefficients on the entire configuration are furnished last, together with the moment reference axes, the reference wing area, span, and chord.

The output for each streamline consists of the starting panel identification (accumulative number, position in a panel column i, column number j, and network number k), the location of the midpoint of the streamline segment over each panel (x_s, y_s, z_s), the velocity components at the source-panel centroid (V_x, V_y, V_z), length of the streamline segment across the panel d_s, numbers denoting (see Figure 56) the panel edges along which the streamline enters and leaves (listed under the headings EE and EX), and the fractional distances along these edges (listed under DDE and DDX). The next section of output consists of the coordinates of the offset point at which the velocity is calculated (x_{bo}, y_{bo}, z_{bo}), the velocity components at point bo, ($V_{x_{bo}}$, $V_{y_{bo}}$, $V_{z_{bo}}$), the scalar product ($\vec{V}_{bo} \cdot \vec{b}$), the derivative for the boundary layer calculation (dV_t/ds_t), and the distance s along the streamline from the starting point. The velocity calculated at point bo does not contain the contribution of the normal velocity component induced by the panel on which the point is located. However, the product $\vec{V}_{bo} \cdot \vec{b}$ is correct because the missing component is perpendicular to the vector $\vec{b}$. If the streamline is terminated near a stagnation region, some quantities from the last streamline panel and the panel it could not enter are listed. The information used by the boundary-layer program is the distance along a streamline s, the velocity at the boundary point (V_x, V_y, V_z), and the derivative term (dV_t/ds_t). These quantities are discussed in Section 3.4.

5.3 BOUNDARY-LAYER PROGRAM USAGE

A description of the input and output formats of the boundary-layer program is given in this section. The majority of the quantities in the data input are obtained from the potential-flow program. Because of the system of panels employed in the potential-flow analysis and because of the method of calculating the streamlines and parameters associated with the streamlines, it is necessary to evaluate and perhaps to interpret the potential flow results before they are used in the boundary-layer program. Such interpretation is discussed in detail in Section 6.5. A sample case is shown in Appendix III.

BOUNDARY-LAYER PROGRAM CARD INPUT

The card input format is illustrated in Figure 66. All cards, except the title card, are punched in a seven-field, ten-digit floating point format. A description of the input data follows.

	Column	Code	Explanation
Card 1	1-72	TITLE	any desired title
Card 2	1-10	A	potential velocity derivative at stagnation, or initial momentum thickness (see FLAG)
	11-20	NX	= number of points along the streamline at which the velocity is specified; i.e., the number of cards in card set 3
	21-30	RINF	R_∞, reference Reynolds number based on the reference velocity
	31-40	STEP	= 0.; the output is printed at each integration step.
			≠ 0.; the output is printed at equally spaced increments equal to STEP along streamline.
	41-50	SL	total length of streamline
	51-60	FLAG	= 0.; initial value of momentum thickness = $\frac{0.2905}{\sqrt{A*RINF}}$
			≠ 0.; initial momentum thickness = A.

The next NX cards specify the streamwise velocity and normal velocity derivative along the streamline. Each card contains the values at one point on the streamline. The points are ordered in sequence proceeding in the upstream direction along a streamline.

Card Set 3	1-10	s	distance from farthest downstream point along the streamline
	11-20	V	potential-flow velocity at the distance s along the streamline
	21-30	dV_t/ds_t	normal velocity derivative at s. The derivative of the component of velocity normal to the streamline along the surface orthogonal trajectory.

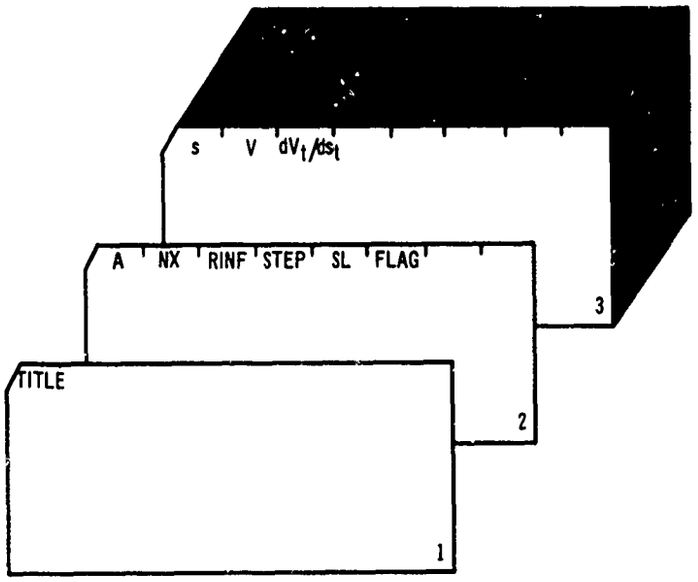

Figure 66. Data Card Arrangement for Boundary-Layer Program.

The output consists of the data as they appear on the input cards, followed by columns of numbers. The column titles and explanation, from left to right, are as follows:

Title	Explanation
S	streamline length, origin at the upstream starting point
CF	local skin friction coefficient
THETA	momentum thickness
H	shape factor
V	potential-flow velocity at S
DV/DS	derivative of V along streamline at S
K_1	divergence term

6. APPLICATION

This section discusses the general nature of the numerical solutions obtained and sets forth guidelines for the arrangement of singularities on various cc :- figurations. Hopefully, it will impart some understanding of solution behavior caused by the inherent approximations of source panels and vortex lattices. Such an understanding is an invaluable a d in the interpretation of results and influences the confidence that may be placed in a particular solution.

6.1 GENERAL CONSIDERATIONS

The potential-flow, boundary-value problem was formulated as an integral equation involving singularity distributions on the wing and efflux-tube surfaces, the wake, and the interior surfaces. The derivation of this integral equation involved no approximations other than those inherent in the development of the theoretical model and, if solved exactly, would produce the exact solution of the prescribed boundary-value problem. In the numerical solution of this integral equation, however, the singularity distributions were approximated in a number of ways. Continuous surface source distributions were approximated by a finite number of planar panels with constant source strength. Doublet distributions were also replaced by vortex lattice arrangements equivalent to a distribution of constant strength doublets arranged in a panel network. The name "quadrilateral vortex network" wa given to the type of vortex lattice used on the efflux tube and fan face surfaces.

Another type of vortex lattice, called the "multihorseshoe" system, was used to represent the internal vortices and the trailing vortex sheets. As the name implies, this type of lattice is related to the well-known horseshoe vortex concept of planar wing theory. The multihorseshoe network is composed of several bound vortices of related strengths together with trailing elements bent in an arbitrary manner to best suit the problem.

The introduction of these singularity distribution approximations is necessary to solve the problem, but it also introduces other considerations. It must be decided how the source panels and vortices should be arranged on any particular configuration and what boundary-condition points on the surface should be chosen. It must be determined where on the surface and in the flow field the correct answer is obtained and where the solution will be meaningless. Also, the numerical results must be interpreted to give the most useful information. Some guidelines are provided below on these subjects to aid in the most efficient use of the program.

Consider first the representation of a smooth, continuous source distribution on a surface by means of planar, constant-strength source panels. It is obvious that the source-panel density required for adequate representation is proportional to the rate of change of the source strength and to the surface curvature. If the source strength varies rapidly over the surface, a large number of constant-strength panels are needed, but if the source strength is nearly constant, a much smaller number may suffice. When the source strength varies rapidly only in a certain direction, then long, narrow panels are suitable, with

the shorter edges parallel to the gradient of the source strength. Such is the case near the wing leading edge, where panels are used whose spanwise dimension is large compared with their chordwise dimension. If the surface is highly curved, then narrow panels must be used, both because large planar panels would deviate grossly from the curved surface and because the source strength changes rapidly on curved surfaces. No adverse effects have been observed from varying source panel sizes. The above criteria usually lead to smoothly varying panel size arrangements over the surface, and it is recommended that such arrangements be adopted wherever possible.

By comparing a source-paneled surface with a smooth, continuous surface source distribution (henceforth denoted as the "exact" representation, since this is the one we are attempting to represent), one can learn something of the nature of the approximations involved and their effect on the solution in various parts of the field. First of all, the approximate solution can be meaningful only if the average source density of the paneled and of the exact representations turns out to be nearly identical. This desired relationship between the panel strengths and the exact source density is established as follows: Consider a panel of arbitrary shape S. The exact source density on this panel can be expanded in a Taylor series about some point p on S as

$$m(S) = m(p) + \nabla m(p) \cdot \vec{r} + \text{higher order terms} \tag{90}$$

where $\vec{r}$ is measured from p. The average source density on the panel is approximately

$$\bar{m} = \frac{1}{S}\iint_S m(S)dS \approx m(p) + \frac{1}{S}\iint_S \nabla m(p) \cdot \vec{r}dS \tag{91}$$

The degree of approximation involved in neglecting higher order terms is dependent on the ratio of panel size to surface curvature and on the smoothness of m(S) as compared with the panel size.

The last term in Equation (91) vanishes if point p is selected to be the panel centroid. Consequently, the source density at the centroid is found to be equal to the average over the panel. Accepting Equation (91) as an adequate approximation, one seeks to achieve a solution wherein the source-panel strengths are equal to the exact source density at the panel centroids.

The source strengths are controlled by Neumann boundary conditions. By comparing the normal velocity components induced at the surface by the two representations, it can be shown that the exact and paneled representations having the desired source density relationship will produce the same normal velocity component only at the panel centroids. If the panel size is small compared with the radii of surface curvature, as supposed, the normal induced velocity at any point on the surface is influenced almost entirely by sources remote from the point of interest and by the local source density at the point. The remote sources of the two representations obviously produce the same velocity, within the order of the stated approximations, everywhere on a panel. However, since the constant source strength on a panel is equal to the exact

source density only at the centroid, the contributions to the normal velocity from the local source densities will be equal only at the centroid. Hence, only at the panel centroids can boundary conditions be applied. Conversely, a numerical solution obtained with source panels satisfying boundary conditions at panel centroids can be expected to produce source strengths within the accuracy of the approximations inherent in Equation (91).

The tangential velocity on the surface determines the surface pressure distribution, forces, and moments. By the same reasoning as above, it is again evident that the influence of remote singularities on the tangential component will be correct. However, those in the near field do not produce the same tangential velocity at a boundary point as an exact surface source distribution. This is easy to see, since the local gradients of source density on the surface, which do influence the local tangential velocity, are different for the paneled and exact representations. The error can be estimated by comparing the induced velocities from these two representations as follows: Consider a series of source panels of strength m_i, as shown in Figure 67. The local flow can be considered two-dimensional without loss of generality. Let the source panels

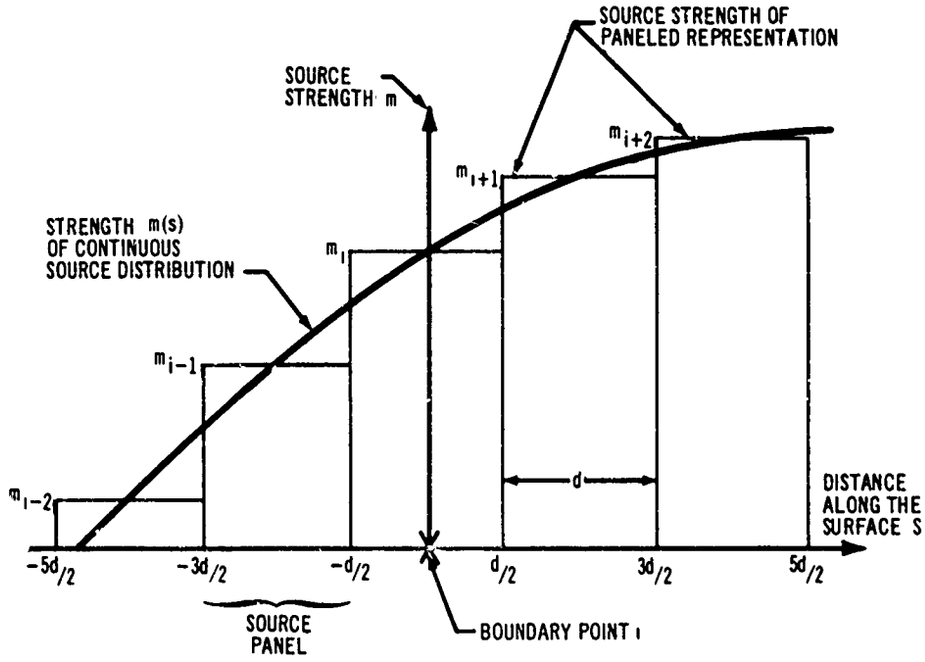

Figure 67. Comparison of Source-Panel and Continuous Source Representations.

be of equal width. The strength of the continuous source distribution can be represented in the neighborhood of the i^{th} boundary point by a Taylor series with the coefficients obtained by finite difference as

$$m(s) = \frac{m_{i-1} + m_{i+1}}{2} + \frac{m_{i+1} - m_{i-1}}{2}\left(\frac{s}{d}\right)$$

$$+ \frac{m_{i-2} - m_{i-1} + m_{i+2} - m_{i+1}}{6}\left(\frac{s}{d}\right)^2 + - - \qquad (92)$$

The error in the tangential velocity component at boundary point i due to the differing source representations over a distance 2d from the boundary point is then

$$u_{exact} - u_{panel} = -\int_{-2d}^{2d} \frac{n_i(s)ds}{s} + \int_{-2d}^{-\frac{3d}{2}} \frac{m_{i-2}}{s}ds + \int_{-\frac{3d}{2}}^{-\frac{d}{2}} \frac{m_{i-1}}{s}ds$$

$$+ \int_{\frac{d}{2}}^{3\frac{d}{2}} \frac{m_{i+1}}{s}ds + \int_{3\frac{d}{2}}^{2d} \frac{m_{i+2}}{s}ds$$

$$= -0.901\,(m_{i+1} - m_{i-1}) + 0.288\,(m_{i+2} - m_{i-2}) \qquad (93)$$

Because the discrepancy is proportional to the difference in source strength of adjacent panels, it can be minimized by using small source panels in regions of rapidly varying source strengths and by arranging the internal vortices to reduce the source gradients on the wing surface. The magnitude of the discrepancy was calculated for several typical source-paneled airfoils, and was found to be inconsequential when the internal vortices were properly arranged. It can, however, appear as local bumps in the surface pressure distribution where strong concentrated vortices lie close to a source-paneled surface, which is an undesirable arrangement that causes rapid changes in the surface source-panel strengths. (The bump appearing in the pressure distribution in Figure 73 at $x/c = 0.8$ was caused by this effect.)

Equation (93), viewed as a small correction factor, was not included in the computer program because its effect, for the type of source and vortex arrangements usually used, is very small. It should also be noted that tangential velocities

calculated on the surface other than at the boundary point will be increasingly erroneous as the panel edge is approached, where the tangential velocity becomes infinite.

The velocity derivatives on a panel, even at the panel boundary point, are not the same as for the real flow over the smooth surface being represented. It is easy to see that the velocity derivatives of higher order must be incorrect when the solution near the surface is considered. The present method produces a velocity field near the surface that is "bumpy," with local regions of high velocity along the panel edges. However, the solution outside the surface is analytic, and can be expressed as a Taylor series about any point. Flow irregularities near panel edges must appear in the coefficients of the higher order terms in the series, which are the velocity derivatives at the point. The order at which difficulties appear in these derivatives is a function of distance from the paneled surface. Errors in the derivatives occur only in the increasingly higher order terms as the point under consideration moves away from the surface. Far from the surface, the first several velocity derivatives in the series will be quite satisfactory. However, near the surface even the first velocity derivatives are inaccurate.

Figure 68 shows the first derivative of the normal velocity component near a sphere as a function of radial distance. The derivatives were calculated by

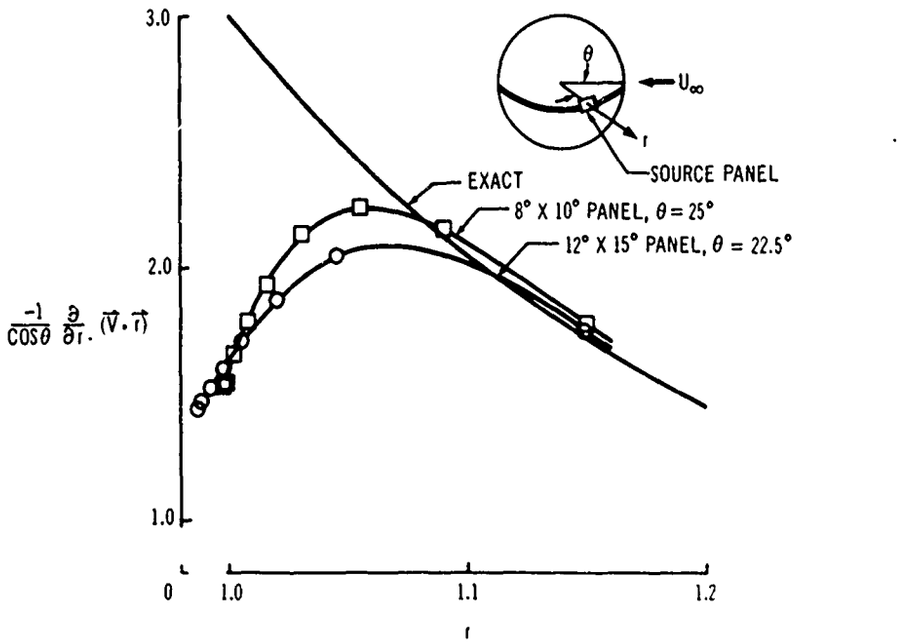

Figure 68. Variation of Normal Velocity Derivative With Distance From Sphere Surface.

finite difference from velocities obtained along a radial line passing through a source-panel boundary point. Results were obtained for two different source-panel sizes, and for both of these the normal derivative at the surface of the sphere (r = 1) is approximately one-half of the exact value. The inner points lie within a unit radius because the source-panel boundary point lies inside of the unit radius sphere due to the planar panel approximation. For both panel sizes, the first derivative reaches the exact value at a distance from the surface nearly equal to half the maximum width of the panel.

It is significant that the derivative on the surface does not improve as panel size decreases. In fact, the second derivative, which is the slope of these curves, deteriorates considerably as panel size decreases. Thus the velocity derivatives at the boundary points apparently do not approach the exact solution as the panel size approaches zero.

Several aspects of the overall behavior of the numerical solution as a function of panel size can perhaps be inferred from the meager evidence available. The velocity distribution on the paneled surface can be likened to an oscillatory function along the surface, with peaks at the panel edges whose amplitude and wavelength decrease as panel size decreases. The velocity magnitude (amplitude) approaches the desired value, but the higher order derivatives diverge as the panel size approaches zero. A simple example of this type of behavior is the sine wave:

$$y(x) = n \sin\left(\frac{x}{n}\right) \to 0 \text{ as } n \to 0$$

$$\frac{dy}{dx} = \cos\left(\frac{x}{n}\right), \text{ which oscillates with increasing frequency as } n \to 0, \text{ but whose magnitude at a given phase remains unchanged}$$

$$\frac{d^2y}{dx^2} = -\frac{1}{n} \sin\left(\frac{x}{n}\right), \text{ which diverges as } n \to 0$$

The distance from the surface over which erroneous derivatives of a given order occur decreases with decreasing panel size, so in this sense it appears likely that the solution at any point a fixed distance away from the surface will approach the exact solution as the panel size diminishes to zero.

The consequences of replacing a continuous doublet distribution with a vortex lattice can also be examined. No fundamental approximation is involved in the use of concentrated vortices inside of the wing (that is, the internal "multi-horseshoe" system), because the surface source distribution always adjusts to counteract the rapidly varying local velocity in the vicinity of internal vortices. Hence, the placement of the internal vortices is not dictated by a spacing requirement if the gradient of the normal velocity component induced at the surface by the internal vortices is small compared to the width of the source panels. However, the latter implies that the internal vortices should be arranged to minimize large local disturbances at the wing surface.

These considerations, together with extensive computational experience, have led to the following general rules for the placement of internal vortices:

- They should be placed near the camber surface to keep them remote from the outer source-paneled surface.
- Several vortices should be used to reduce their individual strengths; their strengths should be weighted along the chord to correspond approximately to the chordwise loading.
- Vortices should be kept about equidistant from the nearest source-panel boundary points, thus placing them nearly in line with source-panel edges.

The approximations inherent in the use of a vortex lattice to represent a continuous surface doublet distribution can be examined like surface source panels. Again, the normal and tangential velocity components are treated separately. It is sufficient to consider a nearly planar, two-dimensional surface of the type sketched in Figure 69, where the concentrated vortices are evenly spaced a distance d apart with boundary points midway between the vortices. A continuous vorticity distribution $\gamma(s)$ is introduced for comparison. The far-field influence of the concentrated vortex representation will be correct if its average vorticity density is the same as $\gamma(s)$; that is,

$$\Gamma_i = \int_{s_i-\frac{d}{2}}^{s_i+\frac{d}{2}} \gamma(s)ds \qquad (94)$$

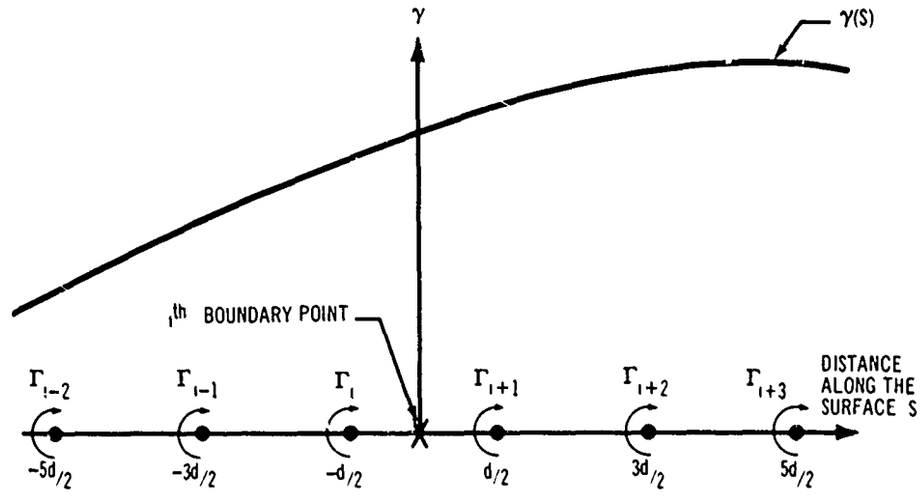

Figure 69. Comparison of Lattice and Continuous Vorticity Representations.

If the normal component of velocity at the boundary points, using this relationship, turns out to be the same with the two representations, then imposition of the boundary conditions will result in a set of Γ_i's satisfying Equation (94).

The influence of the concentrated vortices adjacent to the i^{th} boundary point is

$$w_\Gamma = \frac{\Gamma_{i+1} - \Gamma_i}{2\pi\left(\frac{d}{2}\right)} \tag{95}$$

The corresponding influence of the continuous distribution $\gamma(s)$ between -d and d is obtained by expanding $\gamma(s)$ in a Taylor series with the coefficients determined by finite difference.

$$\gamma(s) = \frac{\Gamma_{i+1} + \Gamma_{i-1}}{2d} + \frac{\Gamma_{i+1} - \Gamma_{i-1}}{d^2}\, s + 0(s^2) \tag{96}$$

The influence of $\gamma(s)$ is then

$$w_\gamma \approx \frac{1}{2\pi}\int_{-d}^{d} \frac{\Gamma_{i+1} + \Gamma_{i-1}}{2d}\frac{ds}{s} + \frac{1}{2\pi}\int_{-d}^{d} \frac{\Gamma_{i+1} - \Gamma_{i-1}}{d^2}\,ds + \int_{-d}^{d} \frac{0(s^2)ds}{s}$$

$$= \frac{\Gamma_{i+1} - \Gamma_{i-1}}{\pi d} \tag{97}$$

Thus, the near-field influence of the two singularity distributions is identical at the boundary point within the quadratic approximation for $\gamma(s)$. Since the influence of more distant portions of $\gamma(s)$ is well represented by concentrated vortices (as can be seen from a multipole expansion of the continuous vorticity integral), the concentrated vorticity representation satisfying Neumann boundary conditions at points midway between the vortices will yield values of Γ_i closely satisfying Equation (94). This in turn implies that a vortex lattice surface representation will produce good results for the flow in the outer field far from the lattice surface.

The tangential velocity component at a boundary point given by the two representations is not the same. The concentrated vortices adjacent to a boundary point produce no tangential component, while the continuous distribution induces a tangential velocity component

$$u(s, \pm 0) = \pm \frac{\gamma(s)}{2} \tag{98}$$

At the i^{th} boundary point this quantity, by finite difference, is

$$u = \pm \frac{\Gamma_{i+1} + \Gamma_i}{4d} \tag{99}$$

Thus, with the concentrated vortex representation, the tangential component at a boundary point can be computed by adding Equation (99) to the velocity induced by the concentrated vortices. The two signs apply to opposite sides of the surface. An example of results obtained by this method is shown in Figure 70. The agreement with the exact solution is extremely good. These basic ideas are readily extended to three-dimensional flow over surfaces represented by a vortex lattice. Reference 2 gives several examples of the use of a vortex lattice to predict the flow properties about thin, nonplanar surfaces.

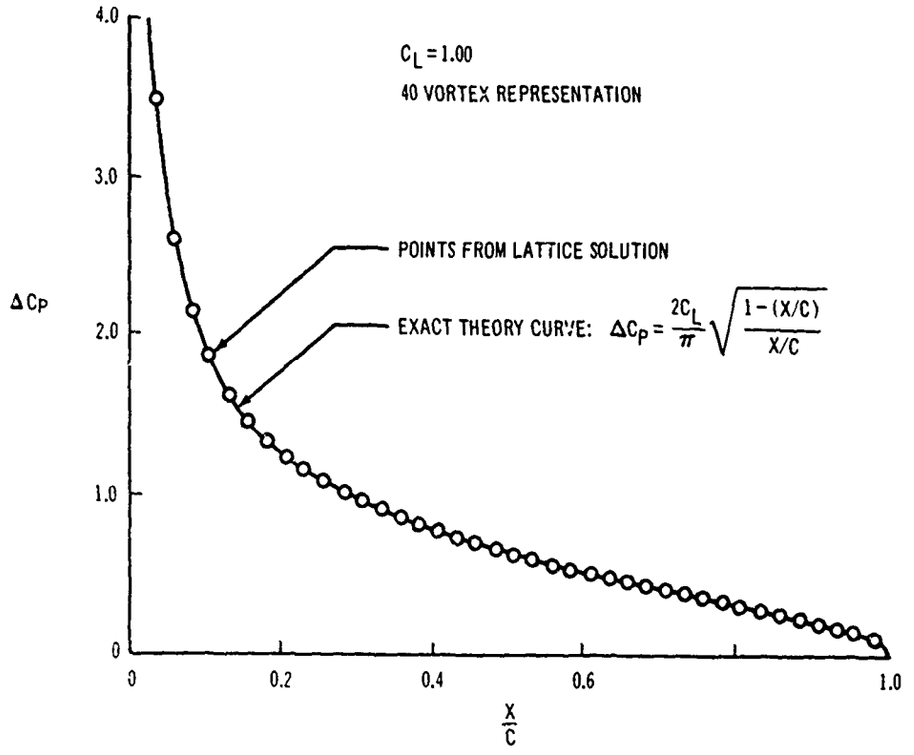

Figure 70. Flat Plate Vorticity Distribution.

It is evident from the preceding discussion that care must be taken in arranging the lattices. Improper spacing of the vortices or positioning of the boundary points can severely compromise the lattice concept. Much experience has led to the general rules for lattice spacing outlined below, which, if followed, will produce reliable results.

The two sets of lattice lines (that is, the longitudinal and lateral concentrated vortices) have independent spacing. Long, narrow lattice elements may be used. As with source panels, the lattice spacing must be kept small in the direction of rapidly changing surface curvature or velocity. The longitudinal and lateral lines need not be perpendicular but may be inclined arbitrarily.

A lattice of uniformly spaced lines, with the boundary points located midway between the lattice lines, will always give good results. However, in many cases uniformity in spacing cannot be accurately maintained because of geometric constraints. It is usually permissible to deviate from the uniform spacing requirement, as long as the deviation is small compared to the dimensions of the lattice elements. This often occurs, for example, with the trailing vortices. The location of flap junctures, wing source paneling, etc., dictates the spanwise spacing of the trailing vortices and can cause the distance between adjacent vortices to vary. When such irregularities occur in a lattice, it is best to maintain the boundary points midway between the lattice lines.

It is also frequently desirable to increase the lattice density in regions of rapidly varying flow velocity or in regions adjacent to source-paneled surfaces. Experience has shown that this can be done by gradually changing the lattice spacing from vortex to vortex, either laterally or longitudinally. The coordinates s_i of successive vortices can be easily computed from a smooth functional relationship, such as $s_i = C_1 + C_2 \cos(i\Delta\theta + C_3)$, $(i = 1, 2, \text{---})$, where C_1, C_2, C_3, and $\Delta\theta$ are constants. The particular function used seems unimportant, as long as it produces a smooth, regular variation. It is of utmost importance, however, that the boundary points can no longer be located midway between successive vortices; instead, they must be spaced relative to the vortices according to the same functional relationship used for the vortex spacing. Thus, if the vortices are spaced according to the above relation, the positions of the boundary points must obey the expression $s_{i_{bp}} = C_1 + C_2 \cos(i\Delta\theta + \Delta\theta/2 + C_3)$.

These restrictions on lattice spacing will ensure reliable results, but only in the far field. Thus, the influence of a vortex lattice efflux tube on the flow about the wing is correctly represented, since the wing is in the far field of the lattice, but any attempt to compute the flow field near the lattice will be meaningless. At the lattice boundary points, of course, the normal velocity component is given correctly, and the correct tangential velocity component can also be obtained with the addition of the local influence, as in Equation (99), from both sets of lattice vortices.

A lattice surface is in many ways analogous to a wavy wall. A wavy wall and a smooth wall are equally effective in controlling overall fluid motion. Far from the wall, the effect of local surface waviness cannot be detected. However, very near the wavy surface the local flow direction and velocity can be quite

different. In general, velocities induced by a lattice at points a distance away equal to the lattice spacing experience a small irregularity, but at greater distances the effect of the lattice approximation is negligible.

6.2 NONLIFTING WINGS

Solutions for nonlifting wings are best obtained by the use of source panels on the exterior surfaces. No other types of singularities are required. The accuracy of the results depends on the number of source panels used. They should be arranged according to the criteria set forth in Section 6.1, which requires the panel density to be greater in regions of large surface curvature and rapidly varying source strength. A typical example of the chordwise panel distribution on a two-dimensional airfoil is shown in Figure 71. Smaller panels are used near the leading edge, where surface curvature and source strength gradients are large. This two-dimensional result was obtained by using source panels of very large span. It is compared with a solution obtained by the method of Reference 11, which produces nearly exact results. Except for a small deviation at the maximum velocity region near the leading edge, the two solutions are almost identical. Increasing the source-panel density in this region would probably eliminate this small difference.

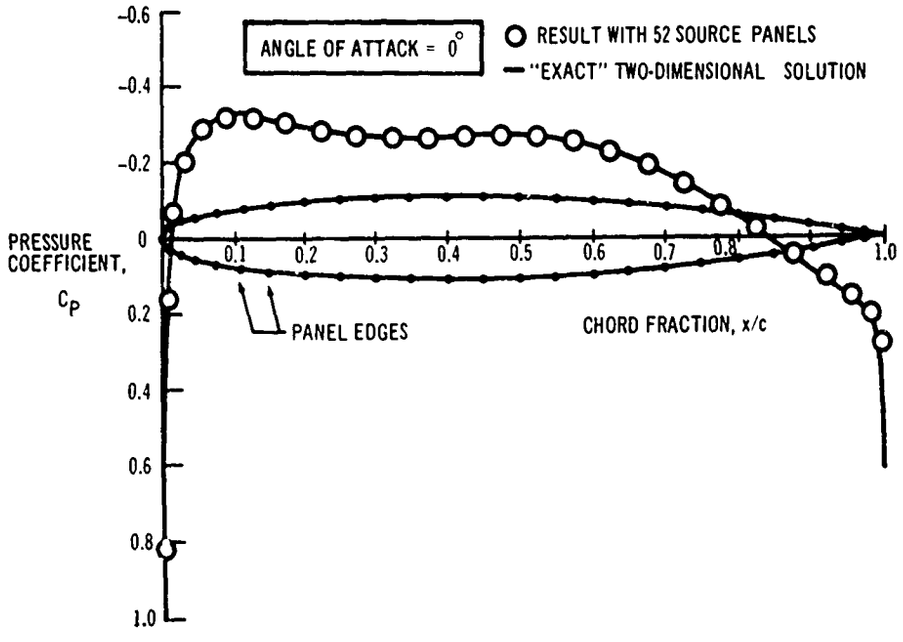

Figure 71. Pressure Distributions on Nonlifting Airfoil.

This same general chordwise paneling arrangement is maintained on three-dimensional wings. A typical arrangement is shown in Figure 72(a). It is not necessary to use panels of equal spanwise dimensions, as shown here, but this practice is often the most convenient. The spanwise dimensions of the panels can be quite large compared to their chordwise size, since the source strength gradient in the spanwise direction is usually quite small. On tapered and swept wings, the spanwise panel edges are often most conveniently placed along constant percent chord lines. The chordwise edges are maintained in the streamwise direction. The geometry program has been written to facilitate the preparation of input data for these types of paneling arrangements.

Wingtips may be paneled in many ways, but it is unnecessary to represent accurately a tip shape unless details of the flow at the tip are desired. Figure 72(a) shows a wingtip, cut off flat and paneled rather crudely. Experience has shown that even this paneling is unnecessary for streamwise tips; it may be omitted without any apparent effect on the solution elsewhere on the wing. It is usually desirable for reasons of economy to leave the tips unpaneled unless details of the flow in the tip region are desired.

Surface pressure distributions at several spanwise stations on this wing are shown in Figure 72(b). The data points shown are at the source-panel boundary points. This wing has the same airfoil section as that shown in Figure 71, and the pressure distribution at the most inboard station is very close to the two-dimensional result. The change in surface pressures toward the tip is qualitatively the same as that predicted by linear theory, with a decrease in the pressure level and a forward movement of the center of pressure.

The present computer program can also be used to predict nonlifting flow over bodies of arbitrary shape. Such use would involve hand preparation of input data consisting mainly of the spatial coordinates of the source-panel corner points. Many examples and results for arbitrary bodies are given by Smith, Hess, and others (References 3 and 12) of the Douglas Aircraft Company, who first applied the source-panel technique to large, three-dimensional, nonlifting problems.

6.3 LIFTING WINGS

Lifting flows are calculated by adding to the surface source-panel representation a system of bound and trailing vortices and incorporating the Kutta condition into the boundary conditions. This "internal lifting system" is composed of a network of multihorseshoe vortices containing both bound and trailing elements, as shown in Figure 10. The total bound strength σ_i at each spanwise station is divided among an arbitrary number MS of bound elements. A system of weights, W_i ($i = 1, \cdots MS$), is assigned to the network to define the relative strengths of bound elements. The vorticity on each segment of the network is completely defined by the values of σ_i ($i = 1, \cdots [N-1]$) and the assigned weights. This system, placed inside the wing with the trailing vortices emanating from the trailing edge, produces lift.

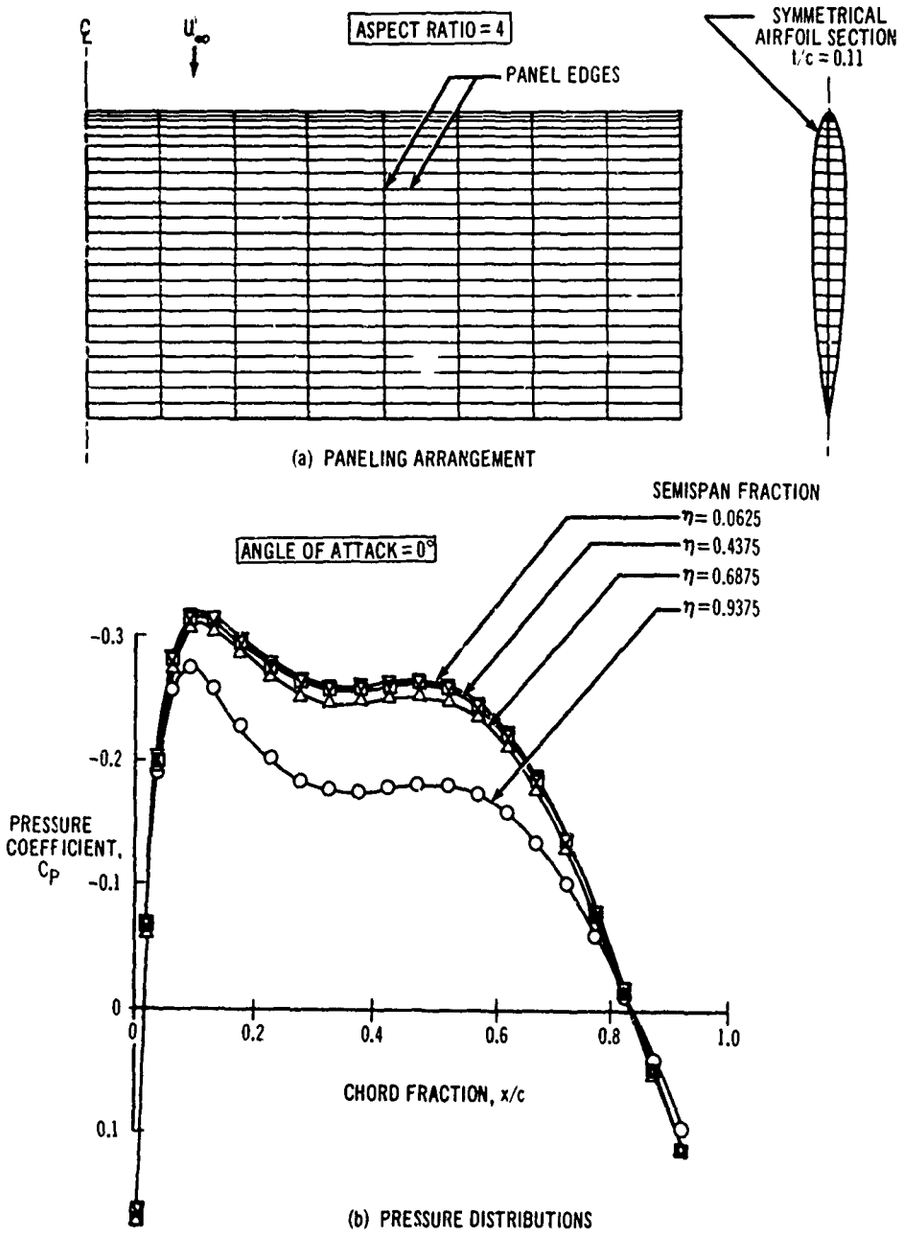

Figure 72. Pressure Distributions on Nonlifting Wing.

To attain maximum numerical accuracy, some care must be taken in placing this system inside the wing. As discussed in Section 6.1, the vortices should be arranged and weighted to minimize the gradient in the normal velocity component induced by them at the wing surface. This can be accomplished by complying with the general rules set forth below, which are the result of extensive operational experience.

The internal vortices should be placed near the mean camber surface to keep them remote from the outer wing surface. The bound vorticity should be distributed among a number of bound elements. These elements are spaced rather uniformly along the camber surface from near the leading edge to some distance ahead of the trailing edge, where the airfoil becomes thin. It has been found desirable to try to keep these bound elements equidistant from the nearest source-panel boundary points. The main requirement in the choice of their weights is to maintain a smooth variation in the vortex strengths. It is usually desirable to decrease the weights slightly toward the leading edge, and to decrease them more strongly near the trailing edge, where the airfoil becomes thin. It is also helpful to weight the vortices to approximate the chordwise load distribution on the airfoil, although this requirement is not absolute. Thus, the vortices closer to the leading edge can be relatively stronger, corresponding to the increased load carried by most airfoils near the leading edge. Similarly, the internal vortices of flapped airfoils should be weighted heavily at the flap hinge line to approximate the loading. The chordwise vortex elements should be aligned with the edges of the surface source panels, except at wingtips and flap junctures, which will be discussed later.

A two-dimensional lifting solution for the airfoil pictured in Figure 71 is shown in Figure 73. Seven bound vortices, all weighted equally and spaced uniformly along the camber line between $x/c = 0.2$ and $x/c = 0.8$, were used. The two solutions shown, differing in the number of surface source panels used, compare favorably with the nearly exact solution obtained by the method of Reference 11, except near $x/c = 0.7$ and 0.8, the locations of the last two internal vortices. The bumps in the surface pressures occurring in these regions are caused by the close proximity of strong internal vortices to the surface. This solution could be improved by following more closely the recommendations outlined above. The weights of the most rearward vortices should be reduced to correspond with the load distribution. More vortices could be added near the front of the airfoil, which would help to reduce the individual vortex strengths. Nevertheless, this solution demonstrates that useful results can be obtained without careful attention to the internal vortex arrangement. The results can be correctly interpreted with the realization that local bumps observed in the surface pressure distribution near concentrated internal vortices are probably caused by the presence of these vortices and will not occur in real flow.

A typical internal lifting system for a rectangular wing is shown in Figure 74(a). The placement of the bound elements was the same as that for the previous two-dimensional airfoil. Note that, except at the tip, the streamwise vortex elements are aligned with source panel edges. Several different arrangements near the wing tip were tried and one that offered the most reasonable solution was chosen. The real lifting flow about a wingtip is complicated by viscous phenomena that produce vortex shedding from the tip.

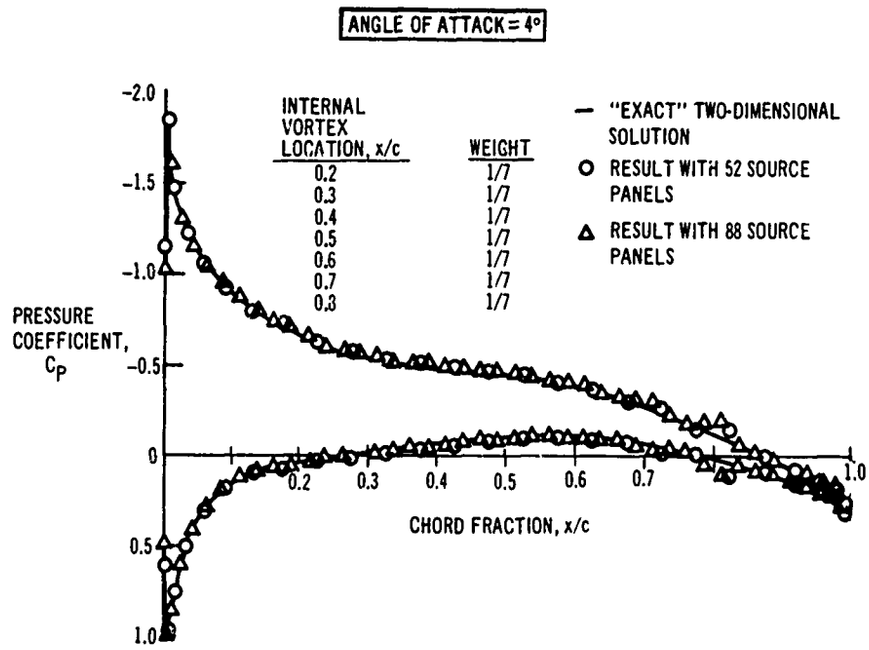

Figure 73. Pressure Distributions on Lifting Airfoil.

This vortex shedding and detailed tip flow cannot be accurately predicted. Hence, the approach was to find a representation that produced what appeared to be the correct overall force and moments, and the surface pressures on the remainder of the wing, without concern about detailed tip flow. The outboard vortex should be inset somewhat from the tip, because it must represent vorticity shed along some finite portion of the trailing edge inboard of the tip, as well as at the tip. It was found that with the outboard vortex inset 10 percent of the distance from the tip to the next inboard trailing vortex, a smooth span loading was achieved that compared well with other lifting surface theories [Figure 74(d)]. Lift, drag, and surface pressures shown in Figure 74(b), (c), and (e) also appear reasonable. The difference in lift coefficient predicted by the present method and by Falkner's lifting-surface theory, which is presumably more accurate than lifting-line theory, is almost exactly the difference observed in two-dimensional flow between this same airfoil and a flat plate. This expected result points out the additional lift caused by the nonlinear influence of thickness on lift, which is not given by linear thin-wing theory. The nonlinear nature of the present lift curve can also be detected.

The induced drag agrees extremely well with lifting-line theory. The minute error at zero lift is caused by the approximate nature of the surface pressure integration. The surface pressure distributions also exhibit the general features given by other theories and by experiment, with both the lifting and thickness pressures decreasing toward the tip. As a final test, the solution was found to be insensitive to the number of spanwise source panels and trailing vortices used,

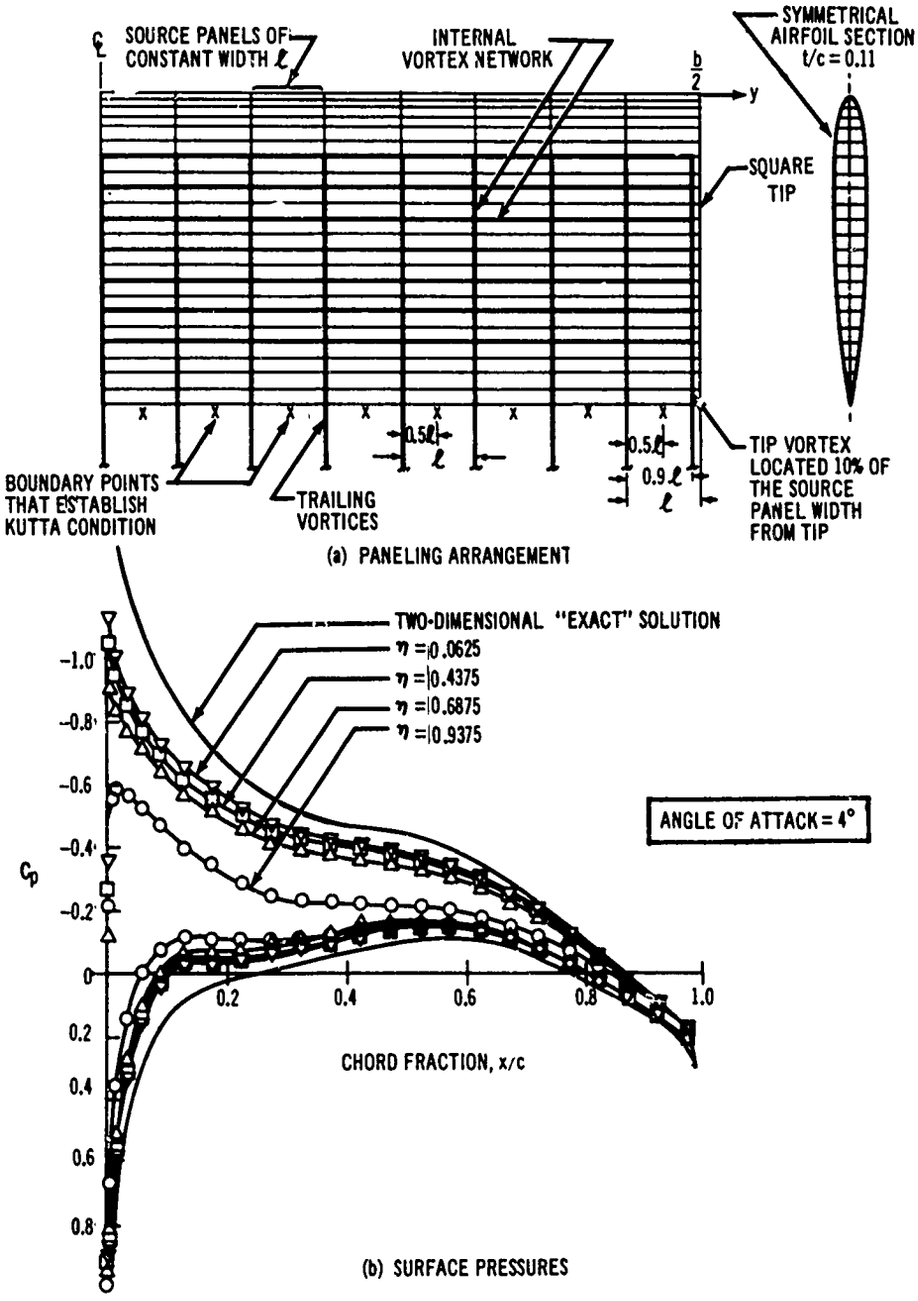

Figure 74. Aerodynamic Characteristics of Aspect Ratio 4 Rectangular Wing.

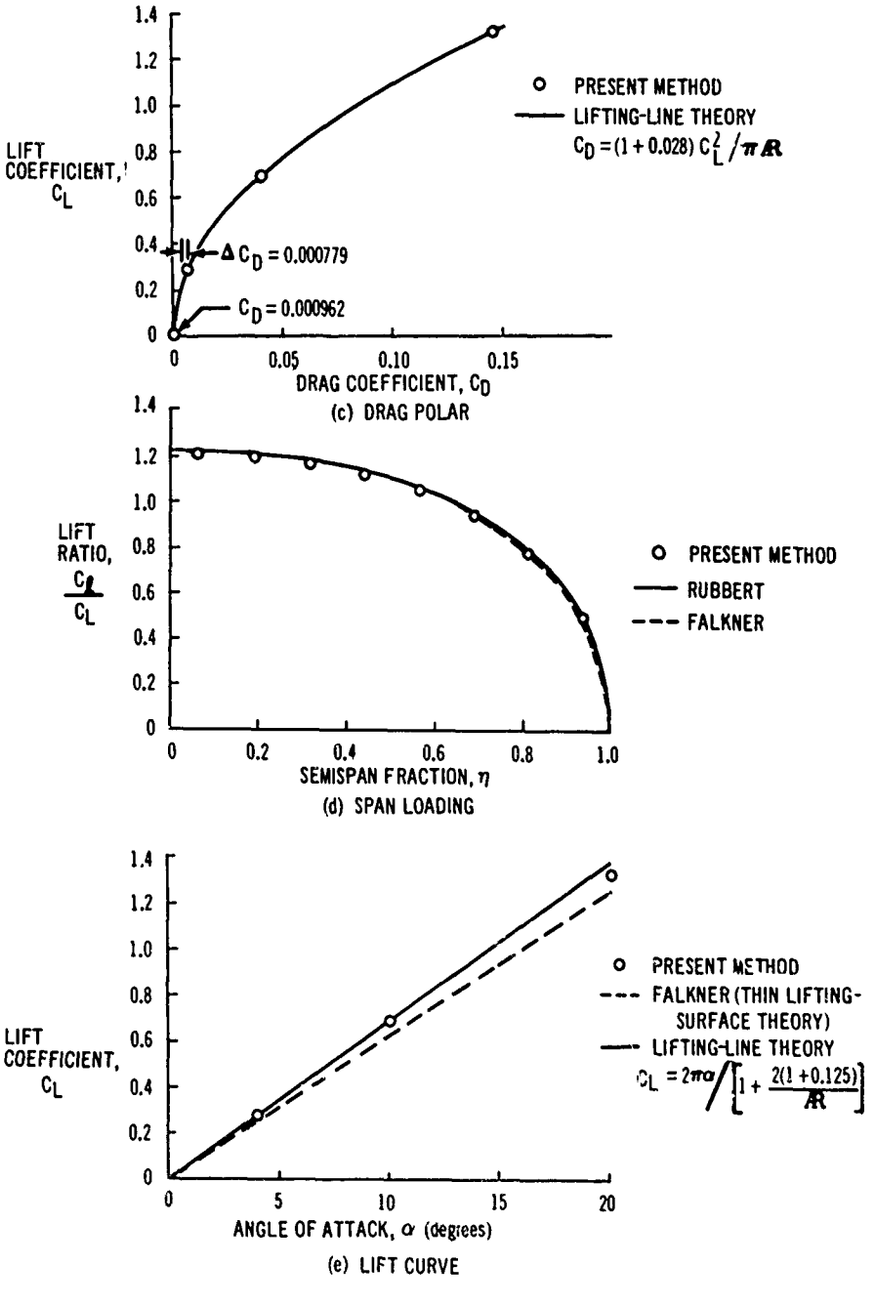

Figure 74. (continued)

which indicated that in the limit of a large number of singularities, the results would be essentially the same. Also, as in the nonlifting case, no appreciable difference could be detected when the tip was left unpaneled; therefore, it is recommended that streamwise tips be left unpaneled to reduce the number of singularities and the computation time required.

Another example of an internal lifting system is shown in Figure 75. This is typical of the arrangement used on tapered wings and has sufficient bound elements to ensure smooth surface pressure distributions. The Kutta condition is established by placing boundary points a short distance aft of the trailing edge and requiring the velocity vector at these points to lie in the plane bisecting the trailing edge. This condition becomes exact in the limit as the boundary point approaches the trailing edge, but for numerical reasons these boundary points must be placed a small distance aft of the trailing edge. Good results have been achieved with the boundary points placed aft a distance approximately 5 percent of the last source-panel chord on the airfoil. These boundary points must be located midway between the trailing-edge source-panel edges, unless a uniform variation in spanwise panel and trailing vortex spacing is used. In that case, the boundary points must be placed relative to the trailing vortices by a scheme such as that given on page 158.

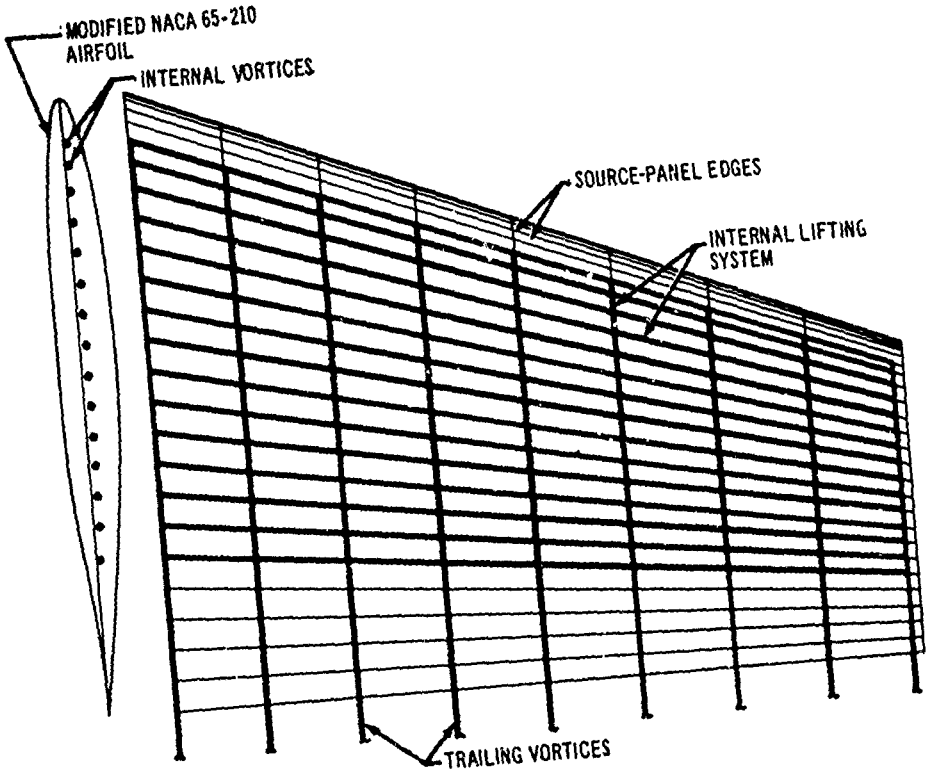

Figure 75. Source-Panel and Internal Vortex Arrangement on NASA Model Wing.

The trailing vortices can be oriented at the discretion of the user; they may be segmented to follow almost any desired path. Experience has shown that, for small angles of attack or flap deflections, the solution is insensitive to vertical orientation between the free-stream direction and the local trailing-edge bisector. For consistency, we have adopted the convention of orienting the vortices straight back from the trailing edge at an angle one-third of the way between the free-stream direction and the local trailing-edge bisector. For large flap deflections ($\delta_F \geq 60°$), it is better to turn the vortices near the trailing edge to follow an assumed local flow direction.

A typical internal lifting system for a flapped wing is shown in Figure 76. It is similar to that for a clean wing except that the streamwise flap edges are treated as wingtips, with the trailing vortex set in from the edge a distance equal to 10 percent of the distance to the adjacent vortex. The vortex inset is normally made near the flap hinge as shown. The span loading and surface

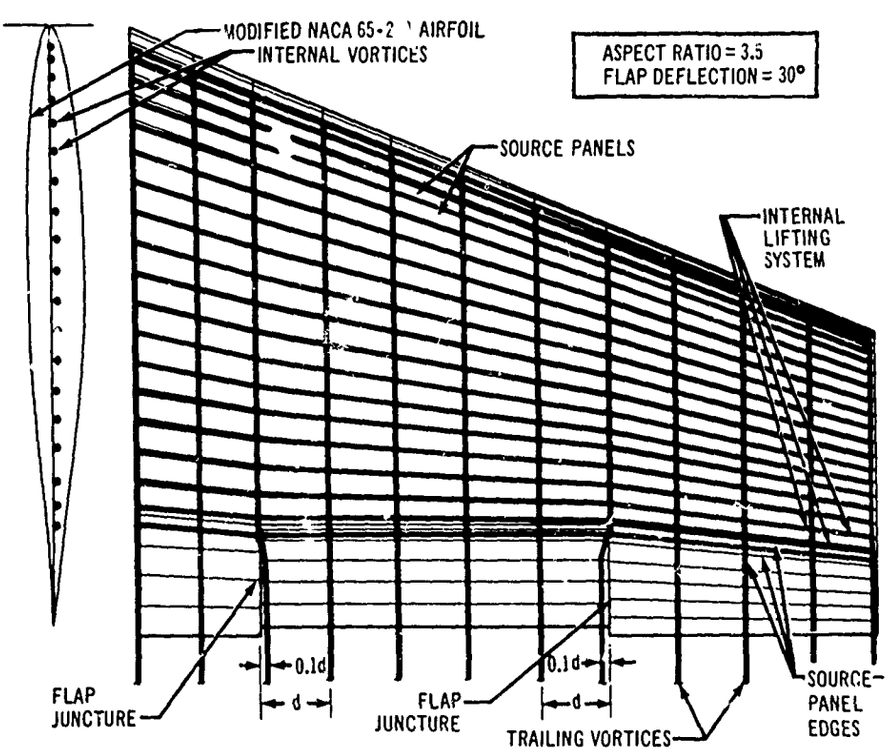

Figure 76. Source-Panel and Internal Vortex Arrangement on NASA Model Wing With Deflected Flap.

pressure distributions for this wing are given in Figures 77 and 78. The lift, drag, pitching moments, and surface pressures are compared with experimental data in Section 7. The solutions appear to be good and exhibit no unusual or suspicious behavior. Unfortunately, a more accurate theoretical solution is not available for comparison, nor do experimental data seem to be available in which boundary-layer control is used to produce data comparable to those for potential flow.

One possible criticism of the internal lifting system concerns the effect of the chordwise internal vortices at the source-panel boundary points. When panels are used whose spanwise dimensions are larger than the airfoil thickness, review of the general considerations concerning source panels and vortices (Section 6.1) seems to indicate that the spanwise velocity component at the source-panel boundary points is incorrect. This is most apparent, for example, near the trailing edge, where a discontinuity in the spanwise velocity component equal to the strength of the trailing vorticity must occur between the upper and lower wing surfaces. No such discontinuity appears in the numerical solution at the Kutta condition boundary point or on the wing surface near the trailing edge. Since the effects of spanwise flow on surface pressures are very small and the discrepancy is pronounced only near the trailing edge where the wing is

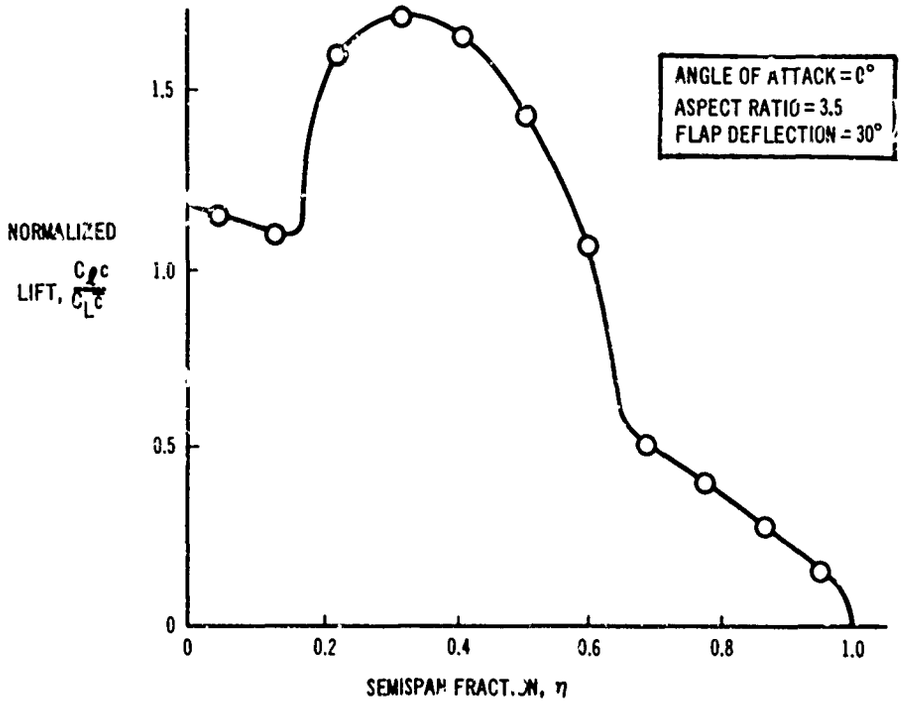

Figure 77. Spanwise Load Distribution on NASA Model Wing With Deflected Flap.

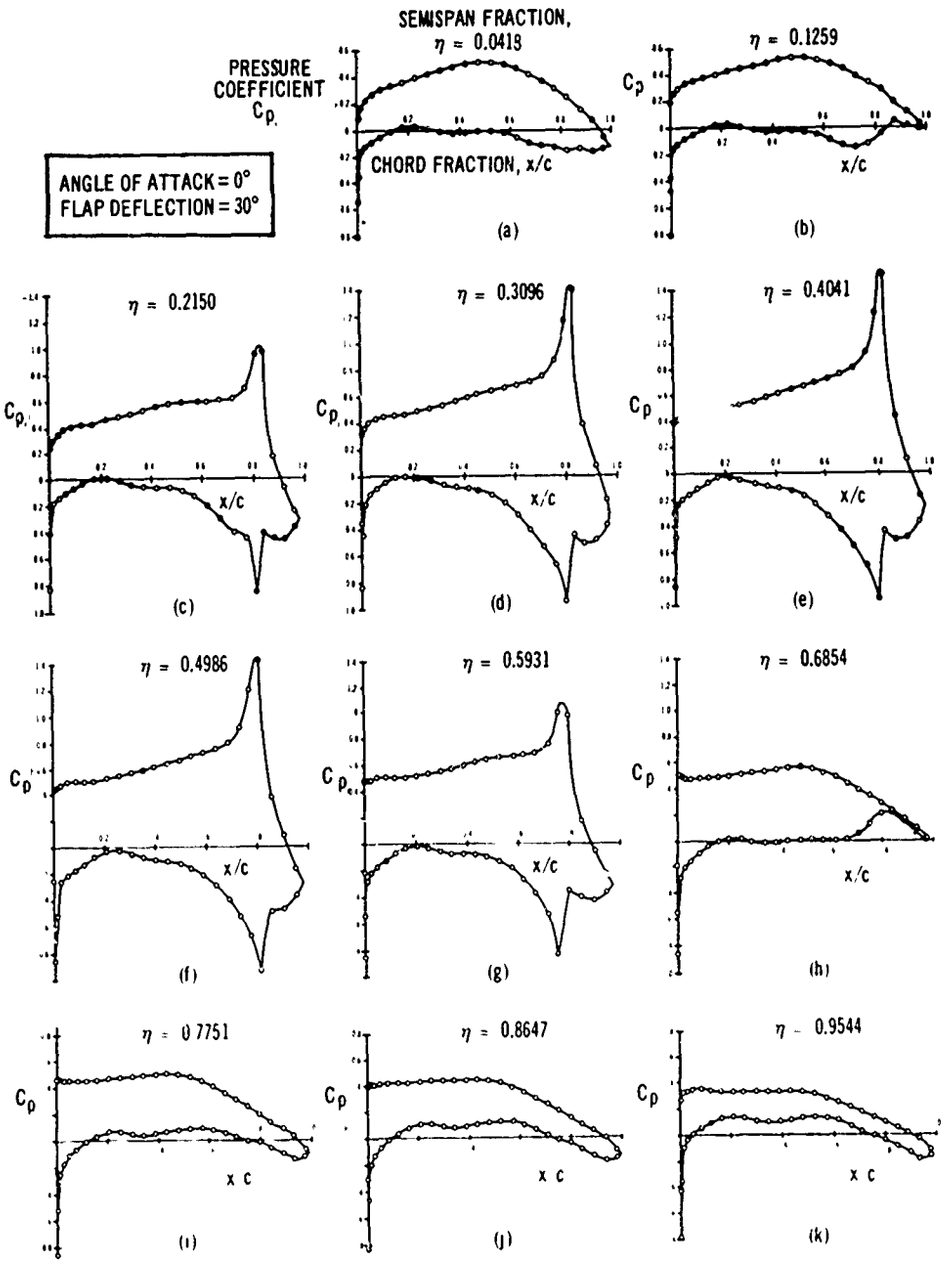

Figure 78. Theoretical Pressure Distributions on NASA Model Wing With Deflected Flap.

thin, this apparently introduces no serious complications. The discrepancy could be reduced by the use of a greater number of panels in the spanwise direction, but the solution improvement would be insignificant.

6.4 FAN-IN-WING CONFIGURATIONS

Fan-in-wing configurations are represented by source panels on the wing and centerbody surface, vortex lattices on the efflux tube and fan control surface, and trailing vortices. Several internal vortex arrangements are also used. Figure 79 shows a simplified view of the external singularity distributions.

The singularity arrangements for this complex problem were developed on the principles outlined in Section 6.1. Experience gained from clean lifting wings was utilized for much of the layout. Details such as the intersection of the fan control surface with the inlet and the efflux tube intersection with the wing were investigated by means of simple two-dimensional and axially symmetric models for which the flow field could be predicted analytically.

The overall layout of both the upper and lower surface source paneling for a fan-in-wing is divided into two distinct regions: one region surrounds the fan, and the other consists of the remaining wing parts. This layout must be tailored to the individual problem because of the variations encountered in wing planform, fan placement, etc. One particular example is shown in Figure 80. In this case, the boundary of the fan region was chosen to be compatible with the partial span trailing-edge flap.

The detailed paneling shown in Figure 80 was developed on the basis of certain guidelines that must be used in the development of paneling for any configuration. These specific guidelines follow directly from the general criteria discussed in Section 6.1. Equal angular divisions should be used around the circumference of the fan so that the lattice spacing on the efflux tube and fan face will be regular. Sufficient panel density must be maintained to ensure a reasonably accurate numerical representation. Fairly long, narrow panels may be used around the inlet lip, since the source strength gradient is mainly in the radial direction. Gross discontinuities in panel size should be avoided. The paneling on the lower surface should correspond closely with that on the upper surface so that the internal vortices can be aligned with panel edges on both surfaces. The centerbody is paneled axisymmetrically with angular increments equal to those used around the inlet. Outside the inlet region, the paneling must follow the recommendations for an ordinary clean wing. The geometry program was developed to have sufficient versatility for a wide choice of panel arrangements.

A cross section of the paneling through the fan centerline is also shown in Figure 80. The important features are the intersection of the fan control surface with the source panels, the efflux tube/lower wing surface intersection, and the absence of source panels in interior regions. Simple test cases demonstrated that good results are obtained when the fan surface intersects the inlet wall and centerbody at the middle of the source panels. The efflux tube is normally attached to the lower wing surface at the edge of the lower surface source panels. The interior walls of the inlet downstream of the fan control surface may be left

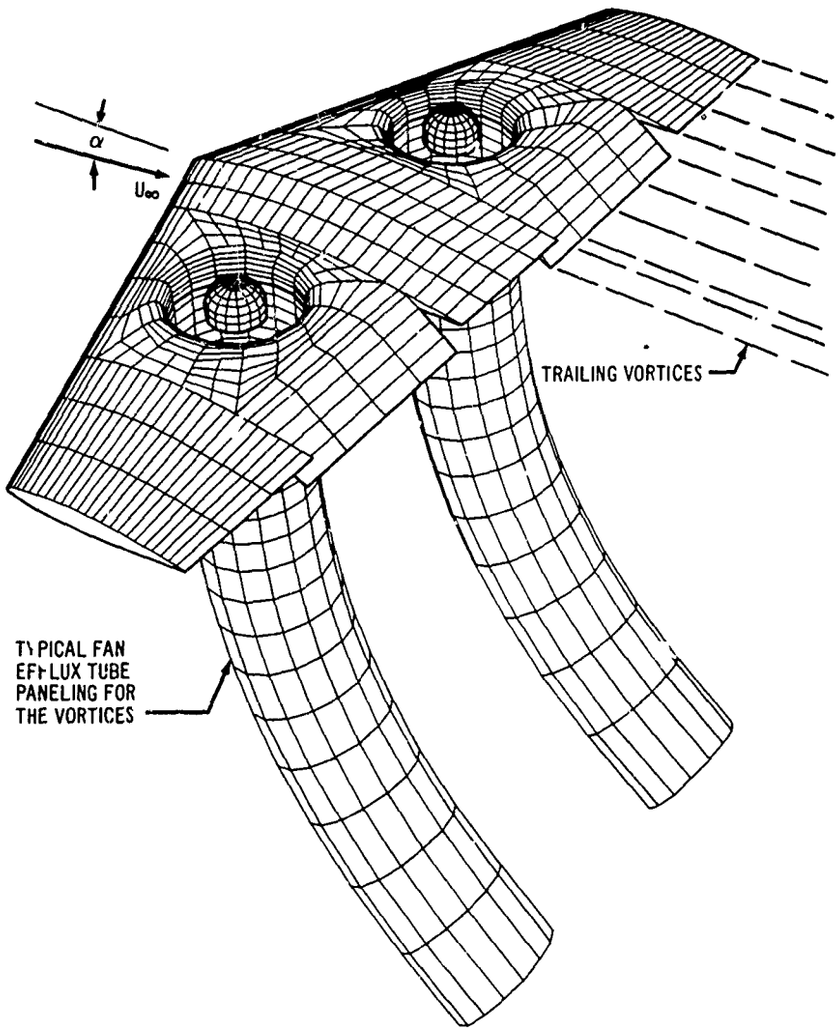

- Arbitrary planform, thickness, camber, inlet geometry, and fan inflow distribution
- Source panels on wing and centerbody surfaces
- Vortices on efflux tube and trailing sheet
- Internal and fan face vortices omitted for clarity

Figure 79. Simplified Singularity Distributions on Fan-in-Wing Configuration.

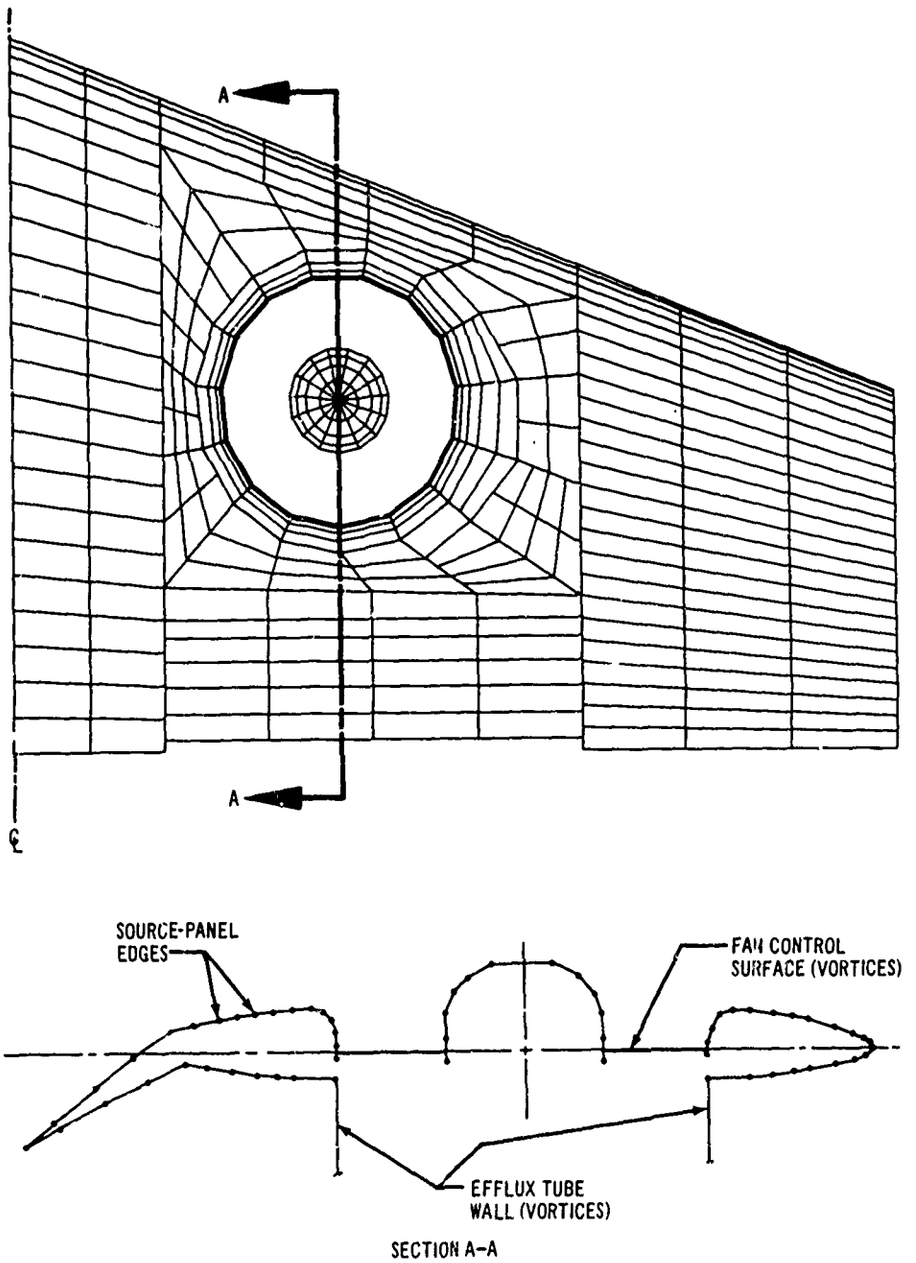

Figure 80. Source-Panel Arrangement on NASA Fan-in-Wing Configuration.

open as well as the lower part of the centerbody, for they cannot affect the exterior solution. It would certainly not be incorrect to panel these surfaces, but this would only increase the computation time without improving the quality of the solution.

A typical multihorseshoe internal system emerging from the trailing edge to form the trailing vortex sheet is shown in Figure 81. For ordinary configurations the arrangement inboard and outboard of the fan region should follow the recommendations for clean wings. The weights of the spanwise segments in these regions are also chosen from the clean-wing criteria.

Aft of the fan the internal system is routed as shown. The vortex segments should be generally aligned with source-panel edges. Several bound segments are used to minimize the strengths of the individual vortices. They are weighted according to the general principles discussed in Section 6.1, keeping the weights small where the wing is thin and the variation smooth. The internal trailing elements near the flap junctures and wingtip should be inset exactly as for ordinary flapped wings. The placement of the boundary points aft of the trailing edge for the Kutta condition is identical to an ordinary lifting wing.

The fan control surface can be represented in two different ways: One representation is used when the inflow distribution is specified; the other representation, which has not been mentioned previously, produces a flow with a constant jump in the velocity potential across the inlet surface, rather than a flow satisfying Neumann boundary conditions. This latter representation is given here as an alternative, since the program is able to produce solutions of this type. However, the geometry definition and fan force calculations have not been adapted to this representation.

A typical vortex arrangement for a fan control surface with specified normal flow, together with the associated internal systems, is shown in Figure 82. It must be positioned vertically to intersect the inlet and centerbody walls at the middle of the surface source panels. The angular divisions around the fan, which should be equal, must correspond to the inlet and centerbody source paneling. The radial vortices on the fan face must intersect the inlet wall and centerbody at the vertical source-panel edges.

The circumferential vortices on the fan face are normally equally spaced, although variable spacing may be used by following the rules outlined in Section 6.1. For equal spacing, the distance from the inlet wall to the nearest circumferential vortex should be one-half of the distance between successive vortices on the fan face, as shown in Figure 82. The arrangement adjacent to the centerbody is similar. The boundary points adjacent to the inlet wall and centerbody should be located away from the surface source panels by a small fraction ($\approx$1 percent) of the distance between successive vortices on the fan face. These boundary points will normally be very close to those at the centroids of the surface source panels.

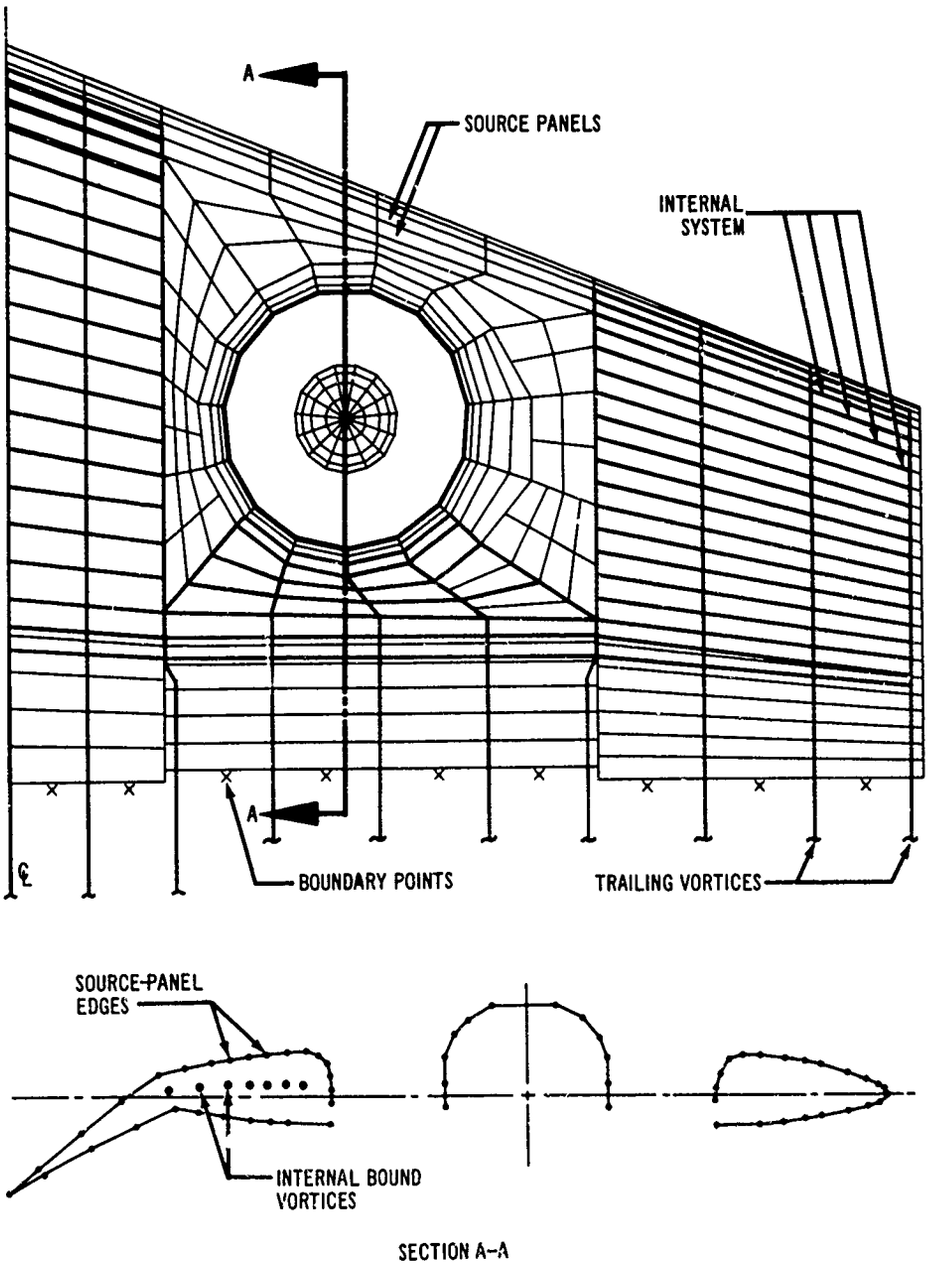

Figure 81. Internal and Wake Multihorseshoe Systems for NASA Fan-in-Wing Configuration.

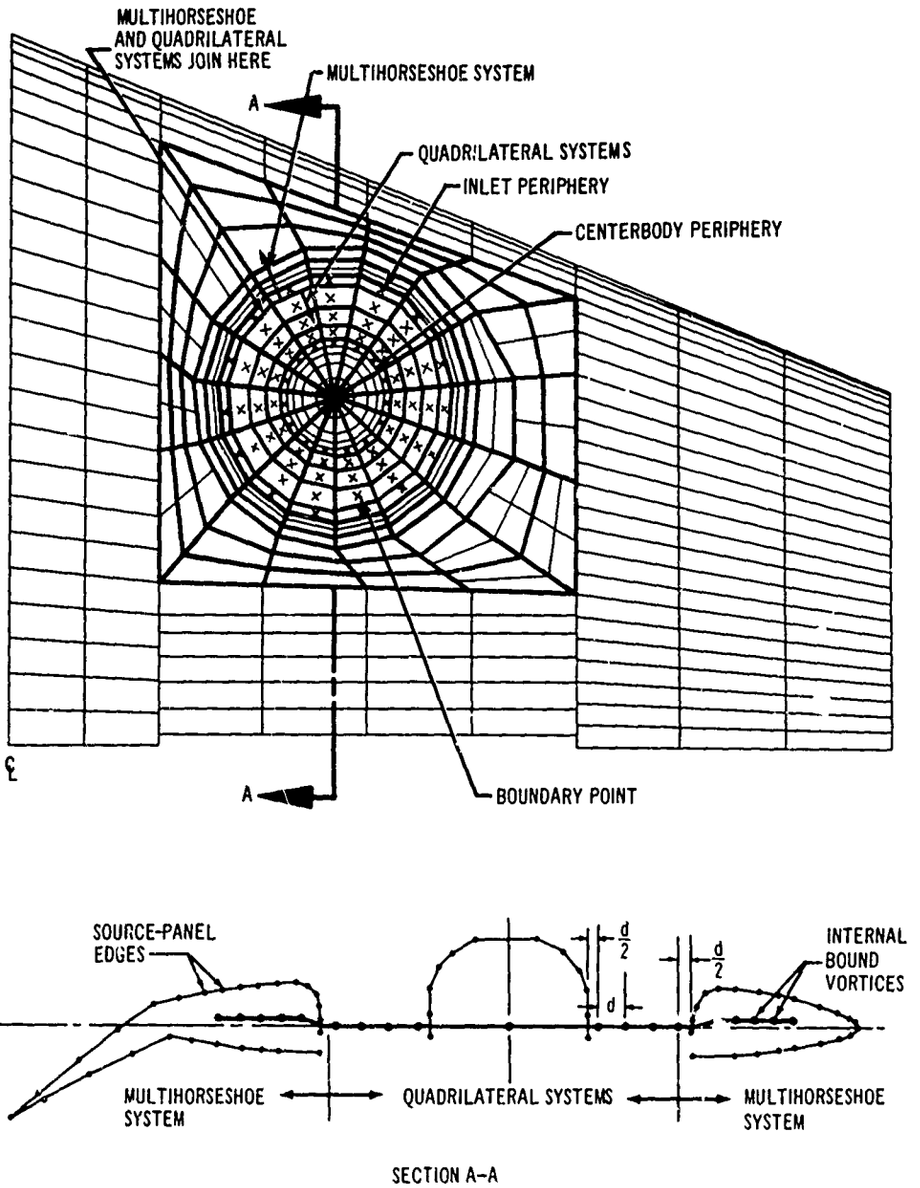

Figure 82. Fan Face Vortex System for NASA Configuration.

Both multihorseshoe and quadrilateral vortex networks are used in a fan face system. The vortices internal to the wing are the multihorseshoe type, having bound elements directed circumferentially. This network extends to the outermost circumferential vortex on the fan face. The boundary points adjacent to the inlet wall belong to this multihorseshoe system. Quadrilateral vortices are used on the remainder of the fan face and in the centerbody.

The internal vortex arrangement must follow previously stated principles. Several bound elements should be used to keep the individual vortex strengths low. They should be aligned with source-panel edges and placed on the camber surface to keep them remote from the surface source panels. It has been found acceptable to weight those in the middle of the array uniformly while reducing the weights of the innermost segment (closest to the inlet wall) and the outermost segment by approximately one-half.

The other type of representation, having a constant potential jump across the fan face, completely eliminates the fan face and associated internal vortices. These are replaced by a single vortex ring around the efflux tube. Its position on the tube is arbitrary but must coincide with the circumferential vortex segments of the tube lattice. Such a ring vortex can be constructed as a weighted multihorseshoe network. The boundary point associated with the ring can be placed anywhere in the inlet or tube with specified velocity to control the amount of inlet flow.

The resulting inlet flow resembles a "natural" flow into a long tube. The most significant solutions with this scheme would be obtained with the inlet surfaces completely paneled with sources. Although the centerbody base can be left open or paneled, smoother inflow velocity distributions will probably be obtained with the centerbody base left open.

Fan force calculations are not provided by the program for this type of representation. They can, however, be easily done by hand if an array of off-body points is placed across the inlet to determine the inflow velocity field. The basic momentum and pressure integrals across the fan can then be computed by quadrature.

Some caution must be used in interpreting the results in the vicinity of the conventional lattice type of fan control surface, because of inherent vortex lattice characteristics. The solution is meaningless within a lattice spacing away from the fan face; consequently, results on the inlet wall can be correctly interpreted only some distance away. Increasing the lattice density on the fan face diminishes the area over which the solution is invalid. The tangential components of velocity furnished by the program at the fan face boundary points are also incorrect, but, as explained in Section 6.1. they may be corrected by including the effect of the local vorticity density. The computer program does compute valid pressures and velocities at the midpoints of the circumferential vortex segments on the fan. These are the quantities to examine when investigating the details of the flow at the fan face.

The program computes total forces by integrating the pressure forces on all exterior surfaces and then adding fan thrust, which is composed of the forces acting on all components downstream of the fan face. This thrust represents the forces on the fan rotor and stator blades, exit guide vanes, inlet and centerbody sidewalls, and centerbody base. Since these thrust forces cannot be derived from a detailed flow field analysis, they are computed from a momentum analysis based on certain assumptions concerning the fan flow (see page 18). The inlet flow is given as part of the aerodynamic solution, but it depends upon the assumed inflow distribution. The exit flow is obtained by assuming an average exit static pressure, a flow direction (the thrust vector direction), and constant stream-tube areas through the fan.

The separate momentum and pressure integrals at the fan face and exit plane, based on these assumptions, are given by the program. This makes it convenient to determine the influence of the various assumptions of the final result. It also allows the fan thrust to be recomputed by hand using different approximations concerning the internal fan flow, if desired, or to be replaced by an experimentally determined value. Unfortunately, most experimental measurements of fan thrust are static; hence, they do not represent forward flight conditions. They also usually include suction forces on a bellmouth or inlet, which in the present scheme are already in the integrated surface pressure forces.

A typical internal vortex system associated with the efflux tube is shown in Figure 83. It is composed of multihorseshoes in exactly the same manner as the internal system connected with the fan face. However, this system emanates from the wing at the source-panel corners on the lower wing surface of the fan exit to form the first segment of the efflux tube. The boundary points for the system are placed a small distance down from the edge of the fan exit, as shown. Good results have been obtained with the boundary points approximately 5 percent of the distance down to the first circumferential tube vortex. The distance of this first vortex from the lower wing surface should be of the same order of magnitude as the width of the wing source panels surrounding the fan exit.

It is important that the interior bound vortices coincide with those of the fan system. Their weights should also be identical. The individual bound strengths of both systems are large in magnitude, but of opposite sign. When properly superimposed, the individual large vortex strengths tend to cancel and leave a combined system that produces a minimum amount of flow irregularity at the outer wing surface.

An efflux tube is composed of quadrilateral vortices. It attaches to the multihorseshoe system at the first segment below the wing, as shown in Figure 84. The vortices should be spaced evenly around the tube, corresponding to the source panel and internal system spacing around the fan. The longitudinal spacing down the tube must follow the recommendations given in Section 6.1. It is usually advantageous to gradually increase the spacing down the tube, as shown, in order to lessen the total number of vortices required. The location of the boundary points on the tube must then also be chosen according to the same relationship as the vortex spacing. The same spacing requirement applies

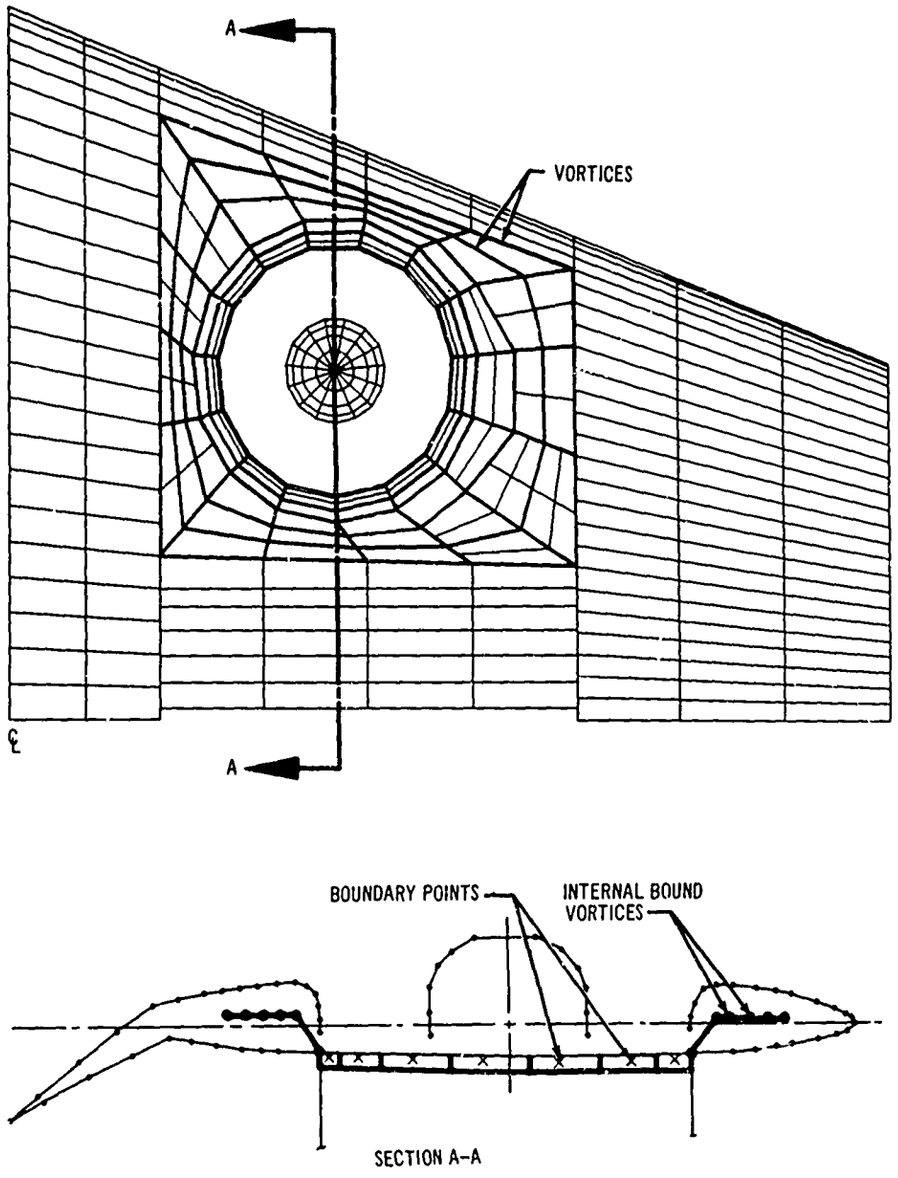

Figure 83. Internal Vortex System Associated With Efflux Tube of NASA Configuration.

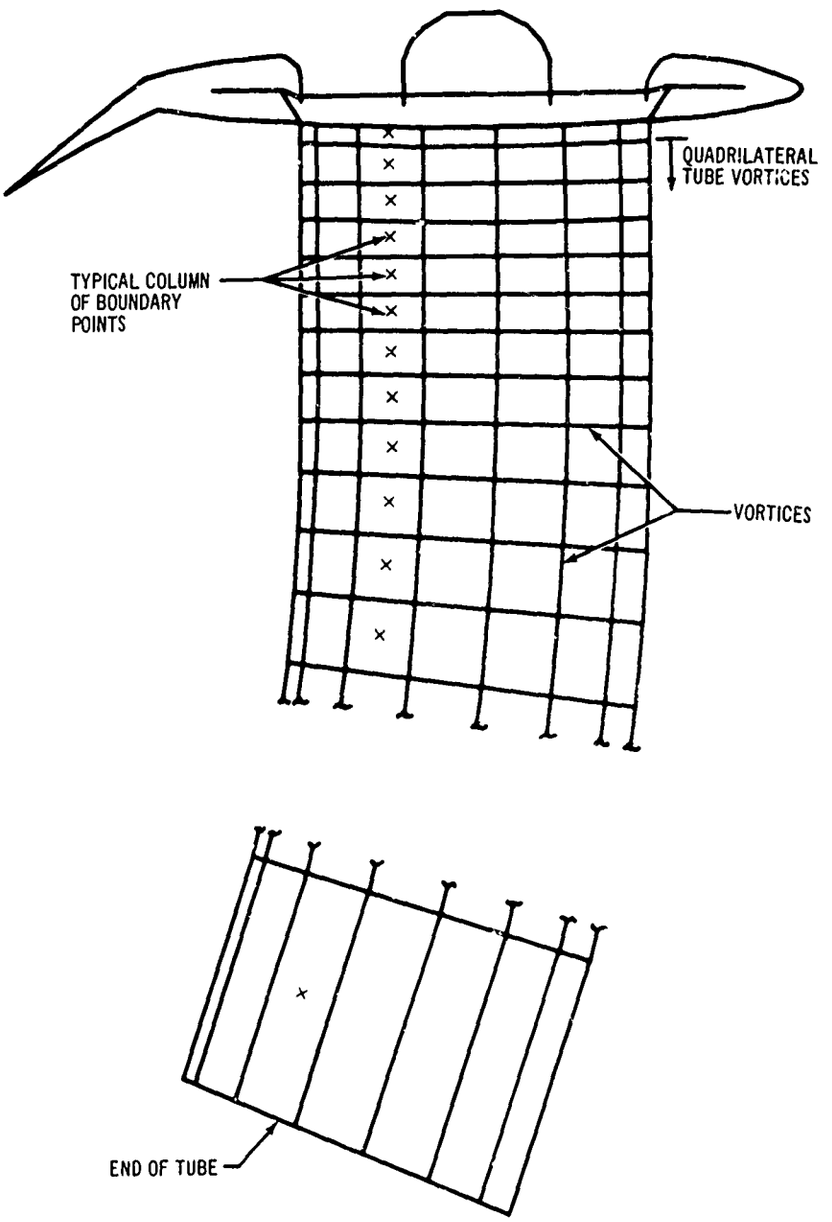

Figure 84. Efflux Tube Quadrilateral Vortex System.

to the first circumferential vortex below the wing, where the efflux tube joins the multihorseshoe system, since it must be consistent with the rest of the tube spacing.

No limit to the maximum longitudinal spacing on the tube has been found. From fundamental considerations it might be expected to be limited to the same order of magnitude as the tube diameter. However, simple axisymmetric tubes have been tested successfully with the vortex and boundary-point spacing gradually increased to a maximum lattice spacing equal to the tube diameter. The spacing law used in these simple test cases, which is a convenient law for most efflux tubes, was

$$\Delta s_{i+1} = (1 + \epsilon)\, \Delta s_i \tag{100}$$

where ϵ = small constant

Δs = distance between a vortex and adjacent boundary point

The acceptability criterion for a simple axisymmetric tube is the resulting average vorticity density. If the strength of each circumferential vortex ring, divided by the distance between the boundary points on either side of the vortex (which gives the average vorticity density at that point on the tube), is invariant along the tube, then the representation is correct (this assumes that the velocity on the exterior surface is constant). The far-field influence will then be that of a tube with impermeable walls. However, if the vorticity density changes down the tube, then the far-field effect will be similar to a "leaky" tube with fluid passing through the tube surface. The amount of fluid flowing in the tube at any section is directly proportional to the vorticity density on the surface except near the ends of the tube.

For reasons of economy, the efflux tube cannot be extended to infinity, but must be terminated some distance away from the wing. It can be shown that the primary effect of tube termination on the flow near the wing is equivalent to a point source located at the end of the tube, with a strength equal to the excess volume of flow leaving the tube. The velocity error induced at the wing can be estimated by assuming that the volume flow through the tube is equal to the specified inlet velocity times the area of the inlet based on the total fan diameter. This is ordinarily a good approximation when the centerbody base and inlet sidewalls are not paneled with source sheets. The resulting velocity induced radially by the source is

$$V_r = \frac{(V_j/U_\infty) - 1}{16\,(r/D_{fan})^2} \tag{101}$$

where r = distance from the end of the efflux tube

D_{fan} = fan diameter

The error is thus proportional to the inlet velocity ratio and dies off as the square of the length of the tube. As a typical example, consider an efflux tube terminated five fan diameters from the wing. The induced velocity at the wing would be approximately $V_r = 0.0025|(V_j/U_\infty) - 1|$. With an inlet velocity ratio of 5, this is 1 percent of the free-stream velocity. For normal tube trajectories, this represents about 0.5 degree in induced angle of attack.

The efflux tube is composed of a vortex lattice; consequently, velocities calculated near the tube surface are meaningless. This is usually noticeable on the lower wing surface close to the efflux tube. The tangential velocity components on the surrounding source panels are not accurate, so the user should expect some output velocities that do not flow smoothly around the tube. Because the affected area is small (it can be made as small as desired by increasing the density of the tube lattice), a negligible error is introduced into the force calculations obtained from integrated wing surface pressures.

6.5 BOUNDARY-LAYER ANALYSIS

This section describes the use of the boundary-layer program, including the modification of the data provided by the potential-flow program, and discusses the physical interpretation of the boundary-layer solutions.

The boundary-layer analysis requires the potential-flow solution to provide the velocity distribution along a surface streamline of the body over which the boundary-layer growth is to be determined. The divergence of the streamlines must also be provided in terms of potential-flow parameters along the streamline.

Additional information required of the potential flow includes the total streamline length and certain properties of the flow at stagnation. This latter information determines the initial values of the boundary-layer solution. Due to the approximate nature of the potential-flow solution, some of the terms provided by the solution for the boundary-layer analysis must be interpreted and modified. A detailed description of the modifications is presented later in this section, after the general procedure for preparing the boundary-layer program input data is described.

The first step in the preparation of the data is to adjust the velocities along a streamline in relation to the streamline path across the panels as determined by the potential-flow program. The velocity on a streamline segment through a given panel is taken as the velocity at the panel centroid, acting at the midpoint of the streamline segment. If the midpoint of a streamline segment is near a panel edge, the velocity should be modified by interpolating between the velocities at the given panel centroid and the closest neighboring panel centroid. A linear interpolation of velocity between panel centroids is usually adequate. (See Figure 85.) Thus,

$$V_{modified} = V_{given} + \left(\frac{\Delta V}{\Delta L}\right) \delta L \qquad (102)$$

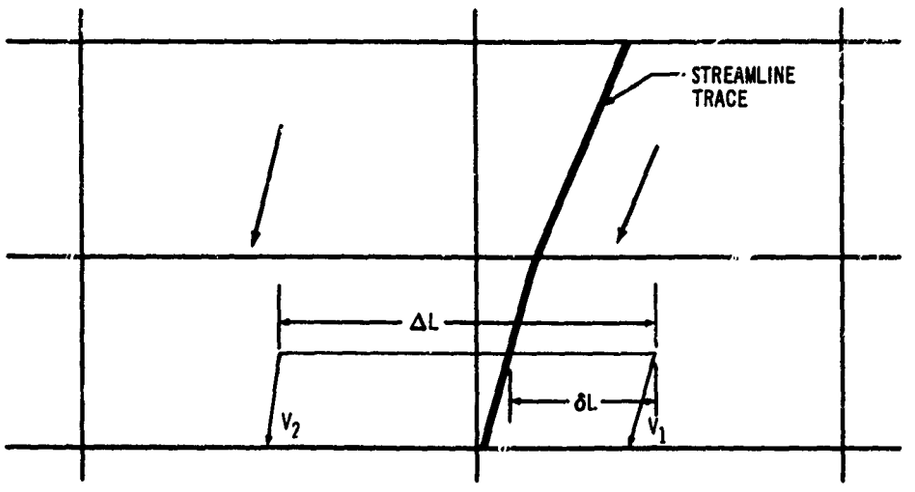

$$V = V_1 + \frac{V_2 - V_1}{\Delta L} \cdot \delta L$$

Figure 85. Interpolation of Streamline Velocity.

where ΔV is the velocity difference between centroids and ΔL is the distance between centroids. The term δL is the distance from the centroid of the panel through which the streamline passes to the streamline, along the line of ΔL.

An initial set of data (s, V, a, and dV_t/ds_t) is required at stagnation if the boundary-layer calculation is to begin there. These data are not given directly by the potential-flow program. For purposes of boundary-layer calculations, the dividing streamline between the flow over the upper and lower wing surfaces is considered to be a stagnation line (see Section 2.3). The location of this dividing streamline is determined by plotting the velocity vectors at the panel centroids near the leading edge. Such diagrams are shown in Section 7. After a curve representing the dividing streamline has been established, the distance along the direction of the streamline over the wing from the termination point of this streamline to the dividing streamline is measured. This distance is then added to the streamline length given by the potential-flow program to provide the total streamline length SL. Next, the velocity V at the dividing streamline must be estimated. There is no definite rule for precisely determining this velocity, but it cannot be set equal to zero. If V = 0 occurs in the boundary-layer program, a program stop due to overflow will occur.

Once a value of s (equal to SL) and a velocity on the pseudostagnation line (dividing streamline) have been derived, the value of dV_t/ds_t remains to be defined. This is obtained as an extrapolation of the distribution of dV_t/ds_t along the streamline to the stagnation point.

The derivative dV/ds along the streamline at stagnation, equal to the parameter a, is best obtained by calculating a second-order curve of the form

$$V = c_1 s^2 + c_2 s + c_3 \tag{103}$$

through the stagnation point and the two points downstream of stagnation. The derivative is then

$$\left.\frac{dV}{ds}\right|_{\text{stagnation}} = a = c_2 \tag{104}$$

A second-order curve fit is used since this is the same procedure used for interpolation in the boundary-layer program.

The use of the reference Reynolds number R_∞ also requires an explanation. In this program, with the velocities nondimensionalized by the free-stream or reference velocity and with lengths retaining a length dimension, R_∞ is the Reynolds number per unit length based on the reference velocity used in the potential-flow program. If all lengths are nondimensionalized by a reference length, R_∞ becomes the Reynolds number on the basis of reference velocity and reference length.

The user is cautioned against a too literal interpretation of the boundary-layer solutions. This analysis is more suitable for comparative studies than for absolute boundary-layer evaluation. In addition, conventional interpretations of the behavior of boundary-layer parameters in two-dimensional flow should not be freely used. For instance, large values of the shape factor H and dH/ds do not necessarily indicate separation of three-dimensional boundary layers. Neither does the disappearance of the streamwise friction coefficient C_f indicate separation, as is usually assumed in two-dimensional flow. In this study, such behavior of boundary-layer parameters probably indicates strong three-dimensional effects, a condition that invalidates the simplified equations used in the analysis.

The interpretation of boundary-layer results must also be tempered by a consideration of the divergence term K_1. This boundary layer analysis has been developed to include the three-dimensional effect associated with streamline divergence in the plane of the wing surface. In order to include this effect, the derivative, normal to a given streamline of the normal component of the potential-flow surface velocity, must be provided. In view of the nature of the numerical potential-flow solution for the derivatives discussed in Section 6.1, however, it is difficult to obtain an accurate value for the desired derivative. To produce an indication of the streamline divergence, the potential-flow program can compute a value for this quantity at source-panel boundary points along a streamline. However, this value, as discussed in Section 6.1, is not correct for flow over a smooth surface, which is represented by the panel approximation. It is included in the program because very limited experience with a sphere and an axially symmetric body has shown that the predicted sign of the derivative correctly indicates streamline convergence or divergence. The magnitude of the divergence factors computed for the sphere and axially symmetric body was approximately half the exact value. Another approach would be to use the method of isoclines,

based on velocities computed at the source-panel boundary points. However, this would require much finer paneling near the inlet than is necessary for good definition of the velocity field, which in most cases would be impractical. A related scheme, namely tracing two adjacent streamlines and computing their divergence graphically, also would not work with current paneling arrangements, because adjacent streamlines often cross the same panel and would thus be locally parallel, due to the approximations inherent in the streamline calculations.

The sample case using the flow about the axisymmetric Rotta body (Reference 13) permits comparison of boundary-layer solutions obtained with the exact and calculated values of divergence K_1. To illustrate the discrepancy between the calculated values of the divergence K_1 and the actual values, Figure 86 shows a comparison between these terms for a variable-radius, axisymmetric Rotta body. The correct K_1 is the value of $-1/r\ dr/ds$ for the body. The calculated K_1 is obtained by the method described in Section 3.2. Generally, K_1 has the same distribution as $-1/r\ dr/ds$, and changes sign at about the same location on the body. However, the magnitude of K_1 is about half the magnitude of $-1/r\ dr/ds$.

Figure 86 compares the calculated values of the boundary-layer parameters θ, H, and C_f using $-1/r\ dr/ds$, $-1/V\ dV_t/ds_t$, and zero for the value of K_1. The case of $K_1 = 0$ corresponds to a two-dimensional solution. With K_1 calculated from $1/V\ dV_t/ds_t$, the values of θ, H, and C_f all lie approximately

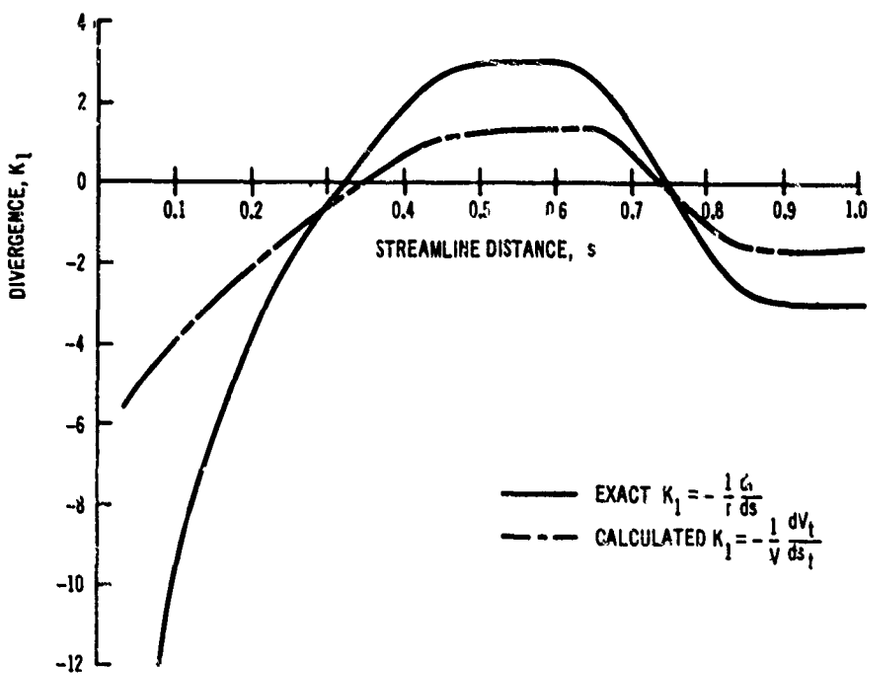

Figure 86. Comparison of Boundary-Layer Results From Various Streamline Divergence Approximations.

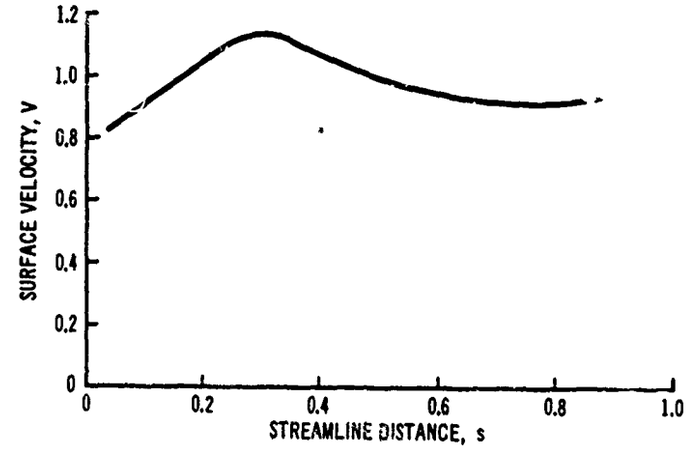

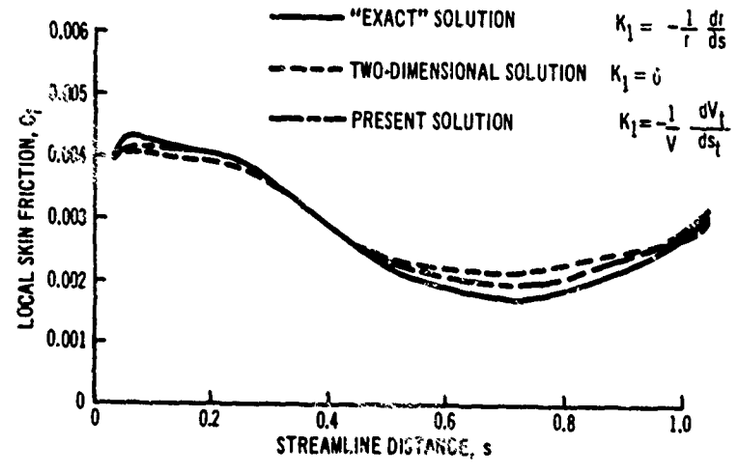

Figure 86. (continued)

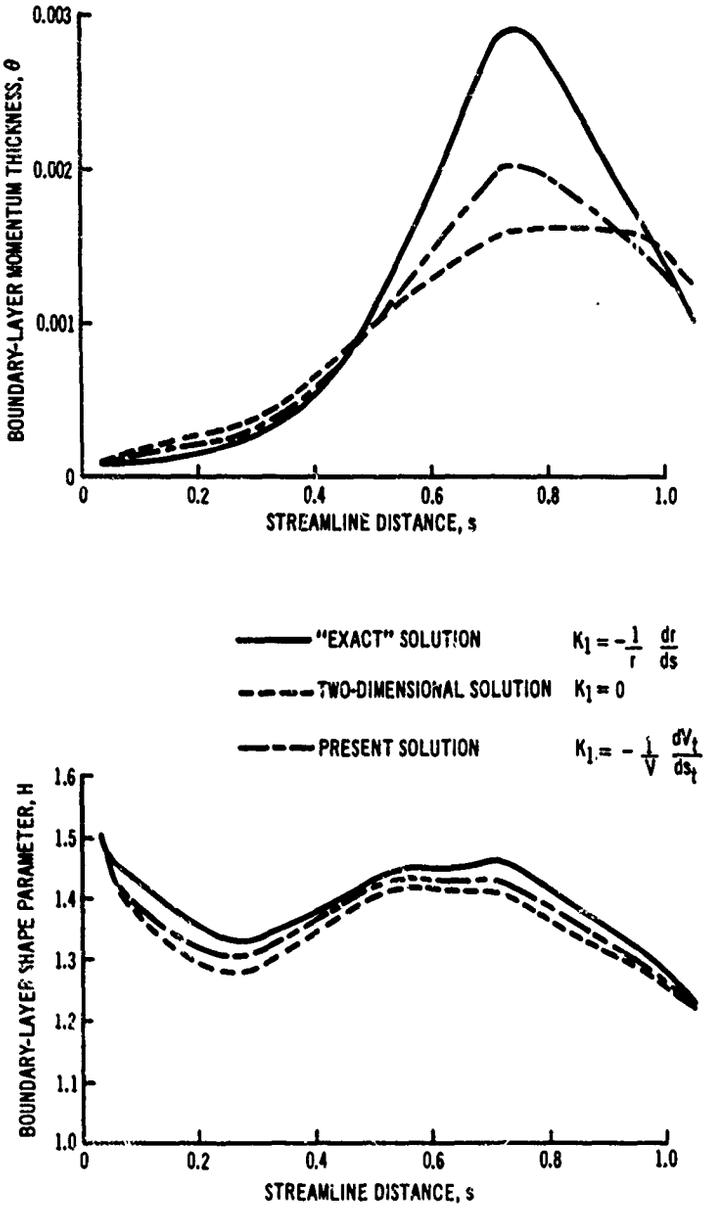

Figure 86. (continued)

halfway between the corresponding values obtained with the correct $K_1 = -1/r dr/ds$ and the values with $K_1 = 0$, the two-dimensional analysis. The ratio of the momentum thickness with the calculated K_1 to the momentum thickness with the exact K_1 varies from a maximum deviation of about 1.5 near the front of the body to a maximum variation of about 0.67 near $s = 0.75$. The shape factor H obtained with the calculated K_1 is approximately 95 percent of the value of H obtained using the exact value of K_1. Thus, the discrepancy in the prediction of the displacement effect of the boundary layer on the potential flow, represented by the quantity $\delta^* = H\theta$, follows the discrepancy of θ. On the axisymmetric body, this program would predict a displacement thickness δ^* about 1.5 times too large near the nose of the body and about one-third too small toward the rear of the body. The local skin friction coefficient C_f is within 95 percent of the value calculated with the correct K_1 in the nose region of the body and is a maximum of about 20 percent too large over the rear portion of the body. The total friction drag coefficient of the body is proportional to the integral with respect to the surface area of the product of the local friction coefficient and the square of the local velocity ratio V/U_∞. It is difficult to estimate the resulting error in total friction drag since the error in C_f varies from negative to positive along the body.

7. EXPERIMENTAL COMPARISON

The fan-in-wing model selected for a comparison of theory and experiment was tested by NASA in the Ames 40-by-80-foot wind tunnel. It is described in NASA TN D-1650 (Reference 14). A sketch of the model giving pertinent dimensions is shown in Figure 87. The wing had an aspect ratio of 3.5, a taper ratio of 0.5, a sweepback of 16 degrees at the quarter-chord line, and a modified 65-210 airfoil section oriented parallel to the plane of symmetry. The wing upper surface was tangent to the fuselage top at its maximum thickness point. The fan was too thick for the tapered wing in the outboard region, so the wing thickness was increased locally to 10.9 percent at 51 percent of the semispan to accommodate the fan. A normal airfoil contour was regained at 57 percent of the semispan. The fan assembly was otherwise completely enclosed by the wing except for the centerbody, which protruded above the wing upper surface. The inlet selected for comparison with theory is shown in Figure 88. The test model had a fixed circular inlet vane and five additional fixed spanwise vanes. None of these inlet vanes were included in the theoretical model.

The configurations and test conditions selected for comparison purposes were the following:

A. Clean wing, flaps up, α = -8, 0, 4, 10, 20 degrees.

B. Flapped wing with 30-degree flap deflection, α = -8, 0, 4, 10, 20 degrees.

C. Fan-in-wing, 30-degree deflected flap, unvectored fan thrust, α = 0, 4, 10 degrees. An inflow velocity ratio of $V_j/U_\infty = 3.636$ was used, which corresponds to the data presented in Reference 14 for U_∞ = 40 knots with a fan tip speed ratio of $\mu = 0.150$. Results were calculated with two different assumed inflow distributions. One was a uniform inflow distribution and the other varied circumferentially as $(1 - \sin\theta)$, where θ is measured in the fan plane from the positive x-axis. The latter inflow distribution produced a maximum inflow on the inboard side of the fan and zero inflow on the outboard side. This nonuniform inflow distribution exhibits the general features observed experimentally, where the retreating blades on the outboard side of the fan were stalled and there was little mass flow through this region. The advancing inboard blades carried most of the mass flow. (Note that this corresponded to the left-wing test conditions only, because the model fans rotated in the same direction.) For the second inflow distribution, only theoretical points for α = 0 and 4 degrees were calculated.

D. Fan-in-wing, 30-degree deflected flap, thrust vectored 20 degrees, α = -4, 0, 8 degrees. An inflow velocity ratio of $V_j/U_\infty = 1.667$ was used, corresponding to the data in Reference 14 for U_∞ = 80 knots and $\mu = 0.300$. Results were calculated with a uniform and a sinusoidally varying inflow distribution and for an inflow distribution that is the average of these two extremes.

The solutions obtained for configurations C and D are summarized in Table III.

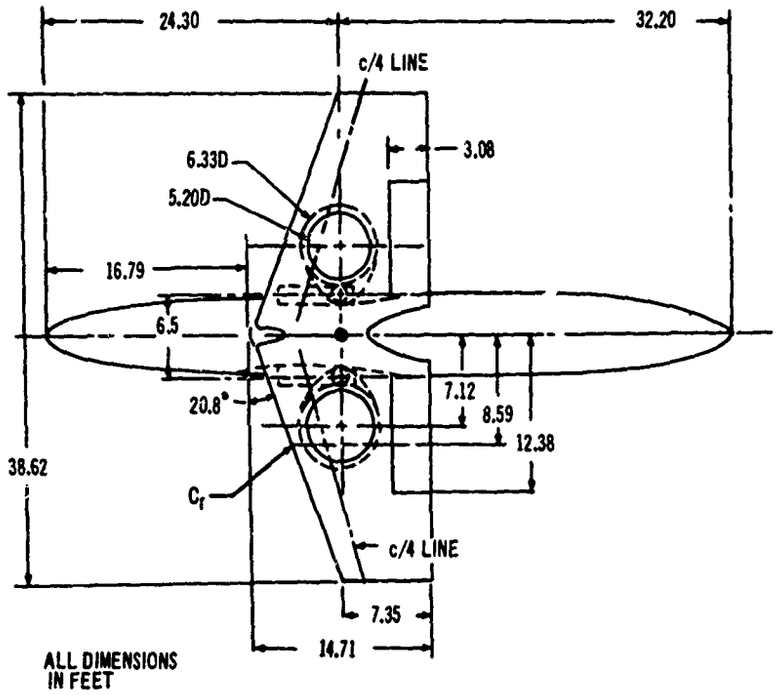

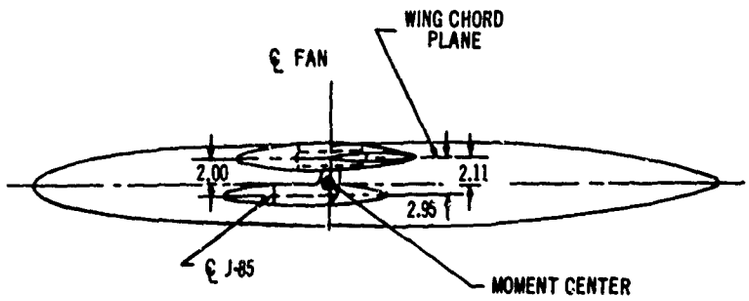

WING CONFIGURATION:

AREA (FT^2)	426.0
ASPECT RATIO	3.5
TAPER RATIO	0.5
AIRFOIL SECTION	65A-210
c_f	11.44

Figure 87. Geometric Details of NASA Fan-in-Wing Model.

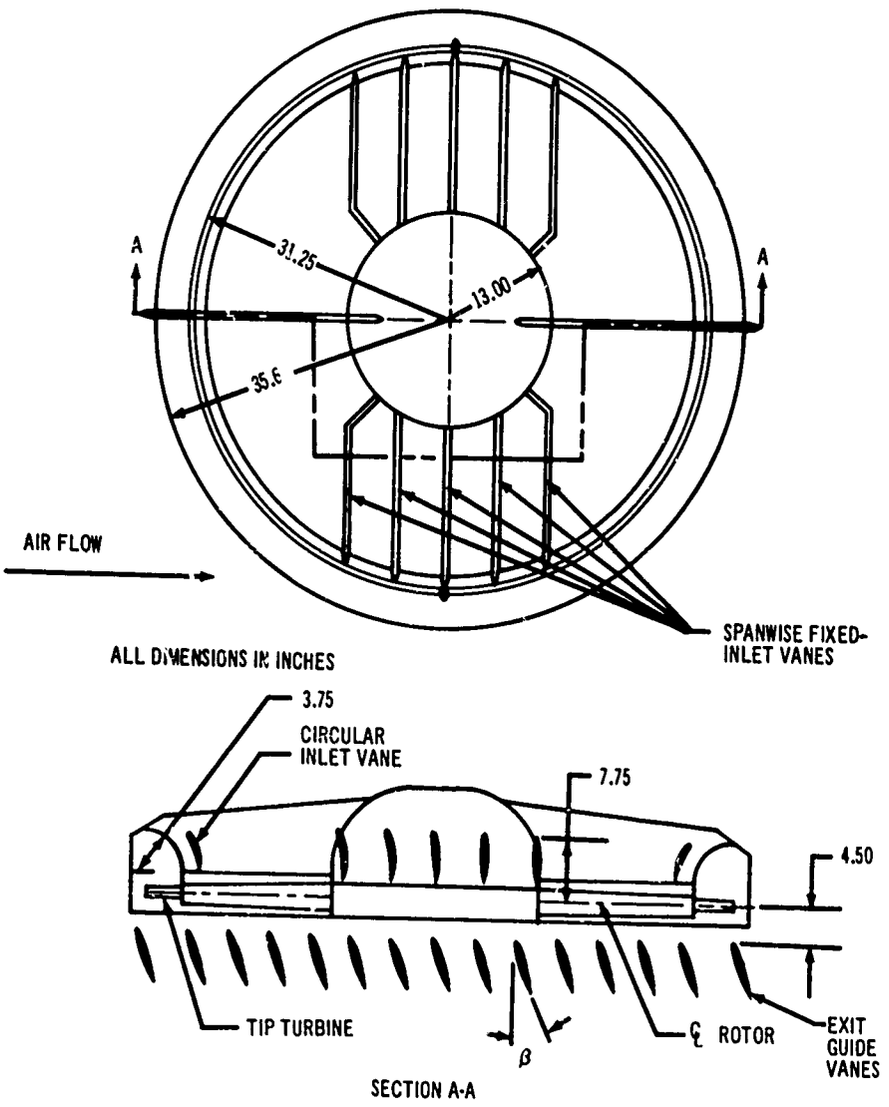

Figure 88. Geometric Details of Model Fan and Inlet.

TABLE III. FAN-IN-WING THEORETICAL SOLUTIONS					
Solution	α (deg)	β (deg)	U_∞ (kn)	μ	$\frac{V_{INFLOW}}{U_\infty}$
1C	0	0	40	0.15	3.636
2C	4	↓	↓	↓	3.636
3C	10	↓	↓	↓	3.636
4C	0	↓	↓	↓	3.636 (1 - sin θ)
5C	4	↓	↓	↓	3.636 (1 - sin θ)
1D	-4	20	80	0.3	1.667 (1 - 1/2 sin θ)
2D	0	↓	↓	↓	1.667 (1 - 1/2 sin θ)
3D	8	↓	↓	↓	1.667 (1 - 1/2 sin θ)
4D	0	↓	↓	↓	1.667
5D	0	↓	↓	↓	1.667 (1 - sin θ)

Configuration A lift, drag, and pitching moment results for the wing are shown in Figure 89(a). These results were achieved with the surface source-panel arrangement shown in Figure 75 using 384 surface source panels and 8 internal vortices. This is half the total number of panels, since the influence of the left wing was computed by symmetry. Also shown in Figure 89(a) for comparison are the experimental data, which include the effects of a fuselage. The lift curves show excellent agreement. The small difference was attributed to viscous and fuselage effects. The theoretical drag polar, which is very close to that for an elliptically loaded wing, lies to the left of experiment, because parasite drag was not included in the theoretical result. If an average parasite drag coefficient of $C_{D_p} = 0.044$ is included as a simple approximation, the theoretical polar agrees very well with the experimental one. The pitching moment curves show a greater variation between theory and experiment. This is mostly attributable to the fuselage moment of the wind-tunnel model, but partly also to the profile drag of the wing, since the point about which moments were taken lies some distance below the wing.

Configuration B results for the flapped wing are shown in Figure 89(b). The source-panel arrangement used on the theoretical model appears in Figure 76; 540 source panels and 11 internal vortices were used on half the wing for this case. The theoretical lift curve is slightly above the experimental one. This, however, was expected, since the effect of boundary-layer thickening or separation on the upper surface of this plain flap would reduce the experimentally

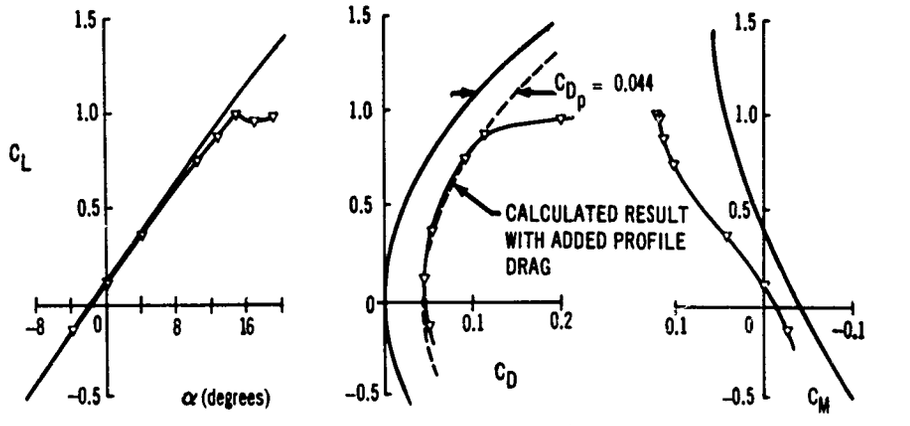

(a) FLAP DEFLECTION = 0°

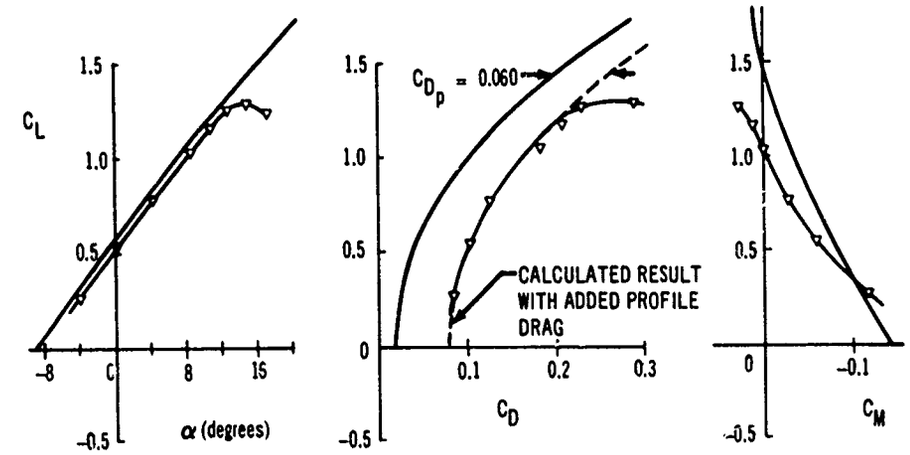

(b) FLAP DEFLECTION = 30°

S_f = 61,400 IN.^{2}

c_f = 137 IN.

MOMENT REF. COORDINATES

x_f = 88.4 IN.

y_f = 0 IN.

z_f = -24 IN.

— CALCULATED RESULTS (WING)

—●— EXPERIMENTAL RESULTS (WING, BODY)

REF. NASA TN D-1650

Figure 89. Comparison of Theoretical Force and Moment Results With Experimental Data: Configurations A and B.

determined lift coefficient. The drag polars again differ by nearly a constant increment in drag, which is somewhat larger than for the unflapped wing case. Note that there is induced drag when the lift is zero, because the outboard wing section carries negative lift while the flapped section carries positive lift. This causes shed vorticity, which results in drag even when the total wing lift is zero.

There is better agreement between the pitching moment curves for the flapped wing, although this is probably fortuitous. Any separated boundary-layer flow on the upper surface of the flap will alter the pitching moment considerably.

The theoretical surface pressure distributions are compared with experimental results for the flapped wing configurations at a 0-degree angle of attack in Figure 90. The symbols used for the upper and lower surface experimental results do not correspond to actual pressure measurement locations, but are points taken from a solid line curve. (The comparisons are for the five spanwise stations shown in Figure 93.) Two distinct differences are noticeable between the theoretical and experimental results at the three inboard stations. First, the experimental pressures on the flap recover to a more negative value than given by theory. This expected behavior is typical of the effect of boundary-layer thickening or separation on the flap. Second, the experimental upper surface pressures are seen to exhibit an unusual increase toward positive values a short distance ahead of the flap hinge. This is undoubtedly caused by the cover doors over the fan inlet, which deviated considerably from the airfoil contour and were not represented theoretically. The potential flow results agree fairly well with the experimental data for the two stations outboard of the flapped section.

It should be mentioned that these theoretical results, for both the flapped and unflapped configurations, were obtained with the assumed position of the trailing vortex sheet held fixed with respect to the wing throughout the angle-of-attack range. The position chosen is most correct for an angle of attack of 4 degrees. At larger angles of attack the trailing sheet is directed downward at a greater angle than would occur in real flow. Experience indicates that this simplification has little effect on lift, but results in a slight decrease in drag at higher angles of attack. Thus the theoretical induced drag values at high lift coefficients should be slightly larger than those shown in the illustrations.

Configuration C surface source-panel and jet efflux tube arrangements are shown in Figure 91(a) and (b). The number of singularities used for half of this configuration was 1093, comprising 679 source panels on the surface of the wing, inlet, and centerbody; 60 quadrilateral vortices on the barrier in the fan plane; 315 quadrilateral vortices on the jet efflux tube; and 39 multihorseshoe vortices for the lifting systems feeding into the fan barrier and efflux tube and trailing from the wing trailing edge.

The theoretical lift, drag, and pitching moment results for configuration C are compared in Figure 92 with the tail-off experimental data from Reference 14. The contribution of the fan thrust is included in both the experimental and theoretical results, which accounts for the much larger lift, drag, and moment

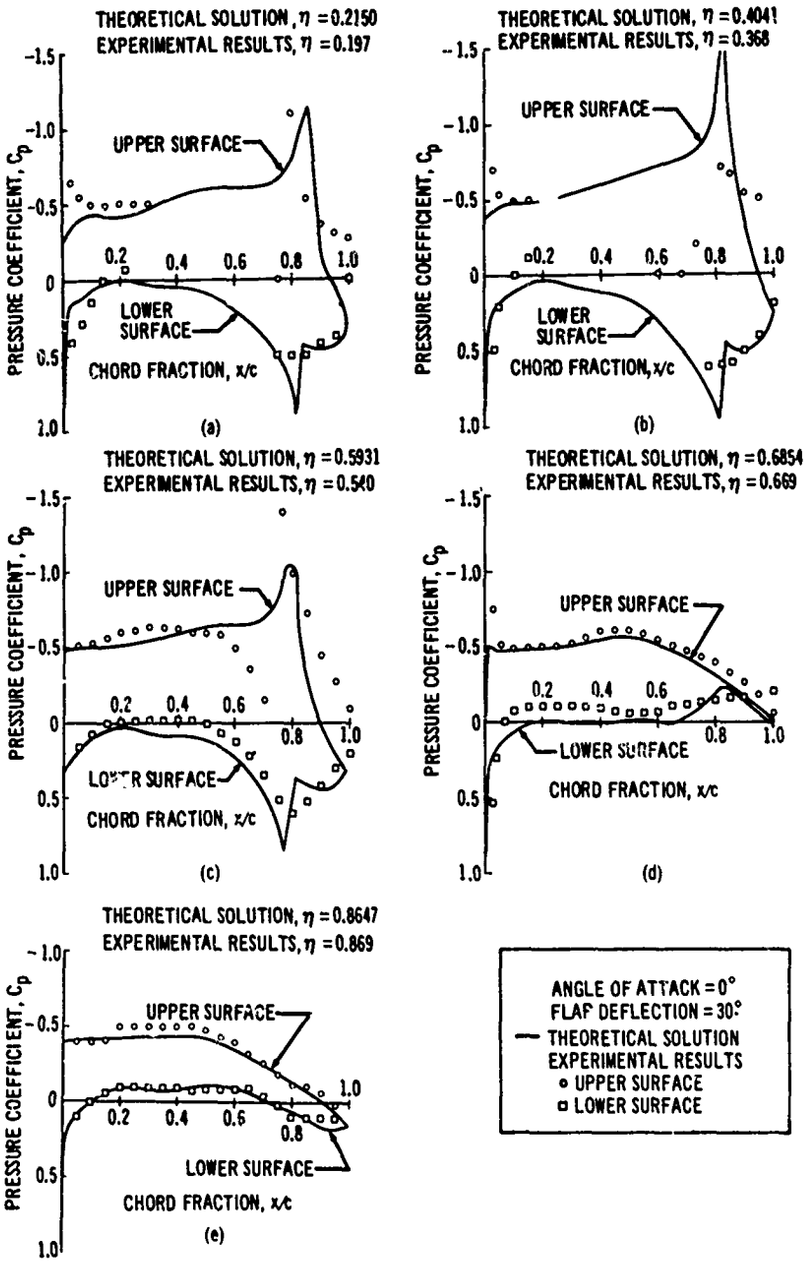

Figure 90. Comparison of Theoretical and Experimental Pressure Distributions on NASA Model Wing With Deflected Flap.

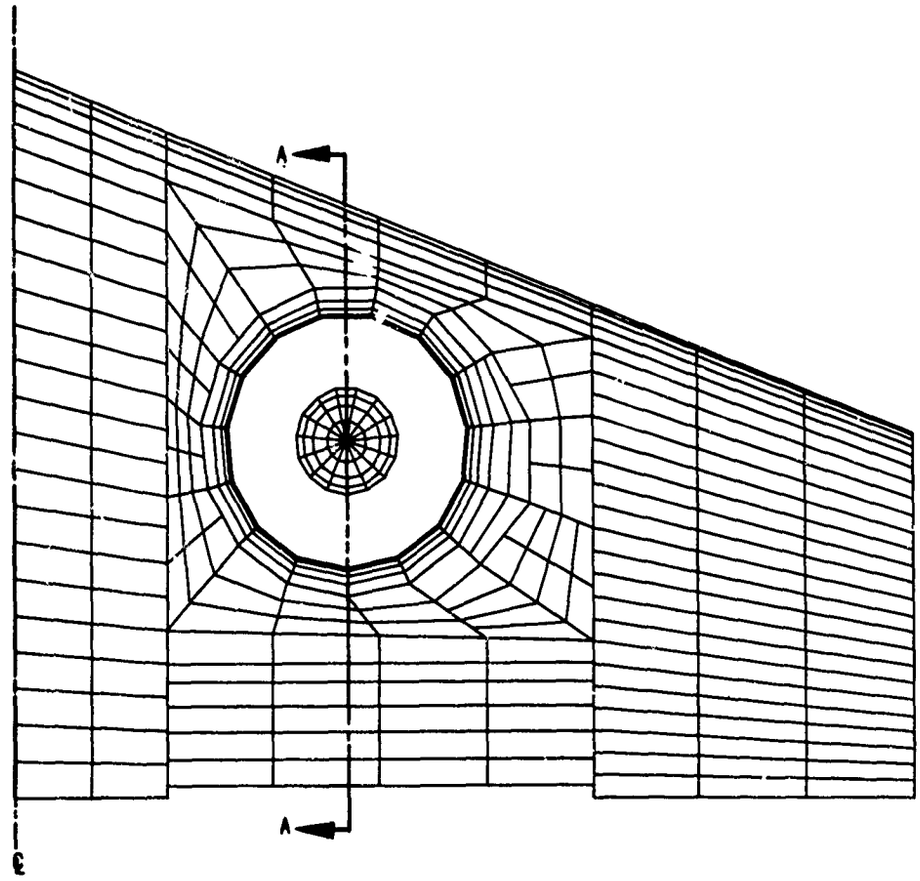

(a) SURFACE SOURCE PANELS

Figure 91. Panel Arrangements for Fan-in-Wing Configurations C and D.

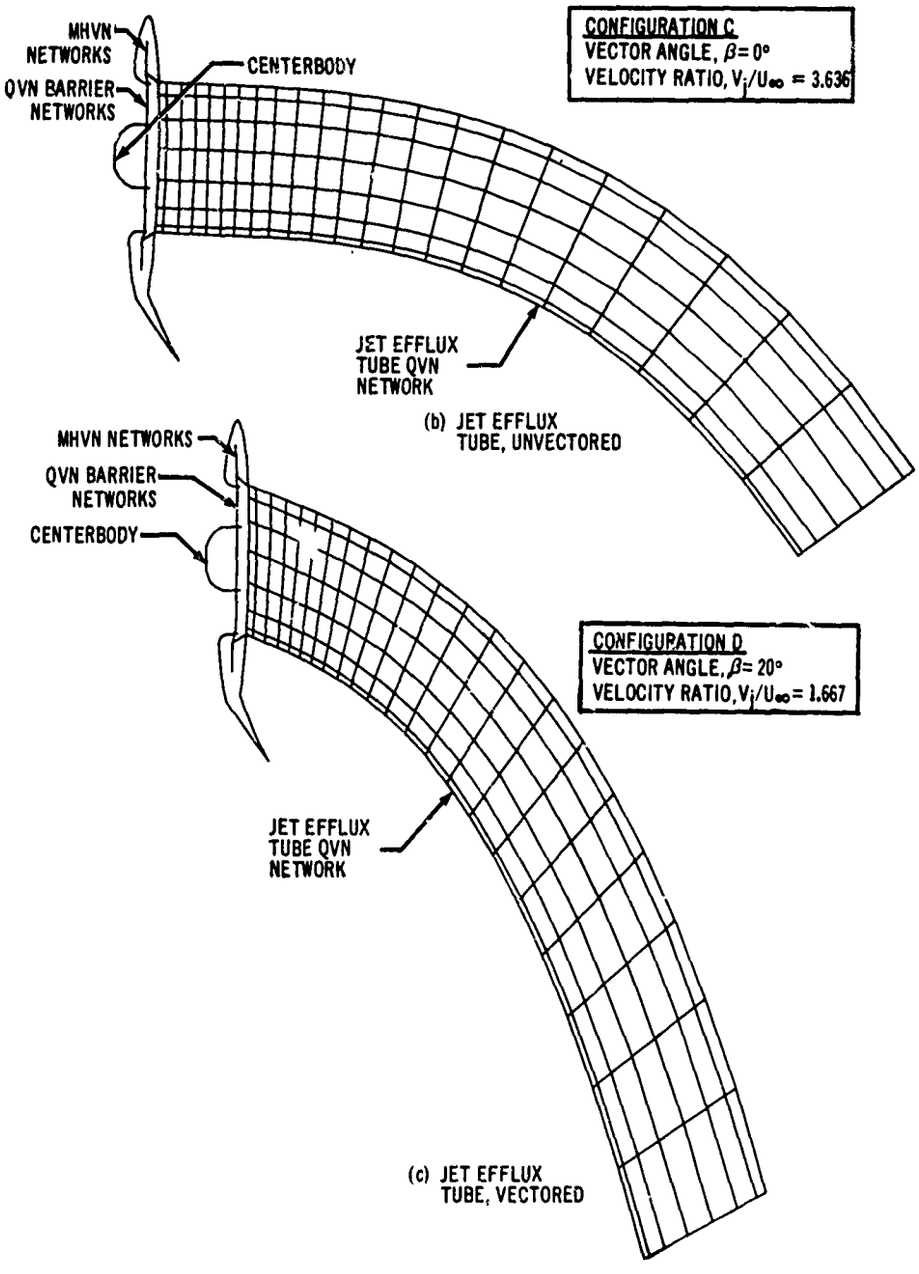

Figure 91. (continued)

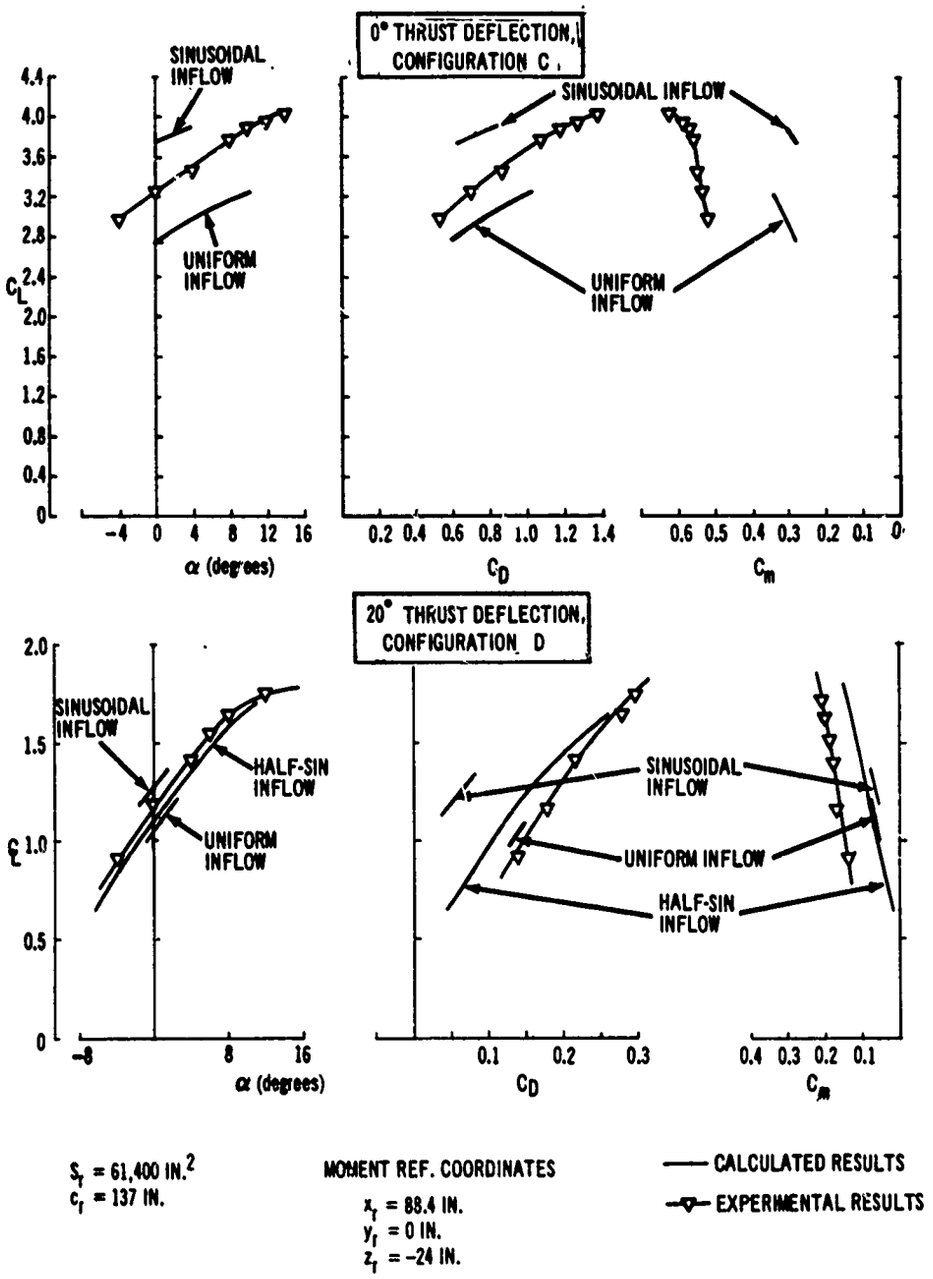

Figure 92. Comparison of Theoretical Force and Moment Results With Experimental Data: Configurations C and D.

coefficients than for the flapped wing data shown in Figure 89. The theoretical lift and drag for the two inflow distributions bracket the experimental results, but the predicted moment coefficients are both less than those measured. The difference between the two theoretical lift curves is due primarily to the difference in the computed pressure increase across the fan, and is indicative of the uncertainty caused by the lack of knowledge of the fan characteristics. There could be several explanations for the differences between theory and experiment. For example, no wind-tunnel wall corrections or drag-tare corrections were made to the experimental fan-in-wing results. Such corrections can be quite large. Viscous and fuselage effects also could cause the differences.

These theoretical results were obtained with the assumed position of the jet efflux tube held fixed with respect to the wing throughout the angle-of-attack range. The position chosen was correct for $\alpha = 0$ degrees. At larger angles of attack the jet efflux tube was directed downward at a greater angle than would occur for real flow. The influence of the erroneous tube location at larger angles of attack on the lift and drag coefficients is believed to be small. These observations also apply to the trailing lifting system, as explained before, which was designed for $\alpha = 4$ degrees.

The theoretical surface pressure distributions are compared with experimental results for solution 1C in Figure 93. The symbols used for the upper and lower surface experimental results do not correspond to actual pressure measurement locations, but are points taken from a solid-line curve. The comparisons are for the five spanwise stations shown. The shape of the theoretical pressure curves in the region of the flap is typical of potential-flow solutions. However, the flap pressures do not agree with the experimental results, which do not close at the trailing edge and do not develop high peaks in the pressure distribution at the flap knee. Boundary-layer thickening and separation on the flap upper surface could account for much of this difference. The theory predicts a low-speed region of positive C_p's on the lower surface behind the fan, while the experimental results show negative C_p's. This may be due to viscous flow entrainment on the lower wing surface, which causes the so-called "suck-down" and is not included in the potential theory. The experimental negative C_p's behind the fan exhaust are probably caused by such viscous entrainment.

The minimum negative C_p for $\eta = 0.197$ in Figure 93 occurs near $x/c = 0.4$ where air is drawn into the side of the fan on the upper surface and is accelerating around the sides of the efflux tube on the lower surface. For $\eta = 0.368$, the C_p reaches a peak as the flow accelerates around the leading edge, decelerates, and then, as the flow approaches the inlet, accelerates again to a peak on the inlet lip. The experimental pressure distribution, however, shows no evidence that the flow reaccelerates on the inlet lip.

There is generally a difference in level between the experimental and theoretical results, which is particularly noticeable at the outboard stations. Little explanation is offered for this other than that wind-tunnel wall interference effects, which are particularly pronounced with fan-in-wing configurations, may be partly responsible. These differences could also be caused by deficiencies in the theoretical model, or in the experimental procedure, or both.

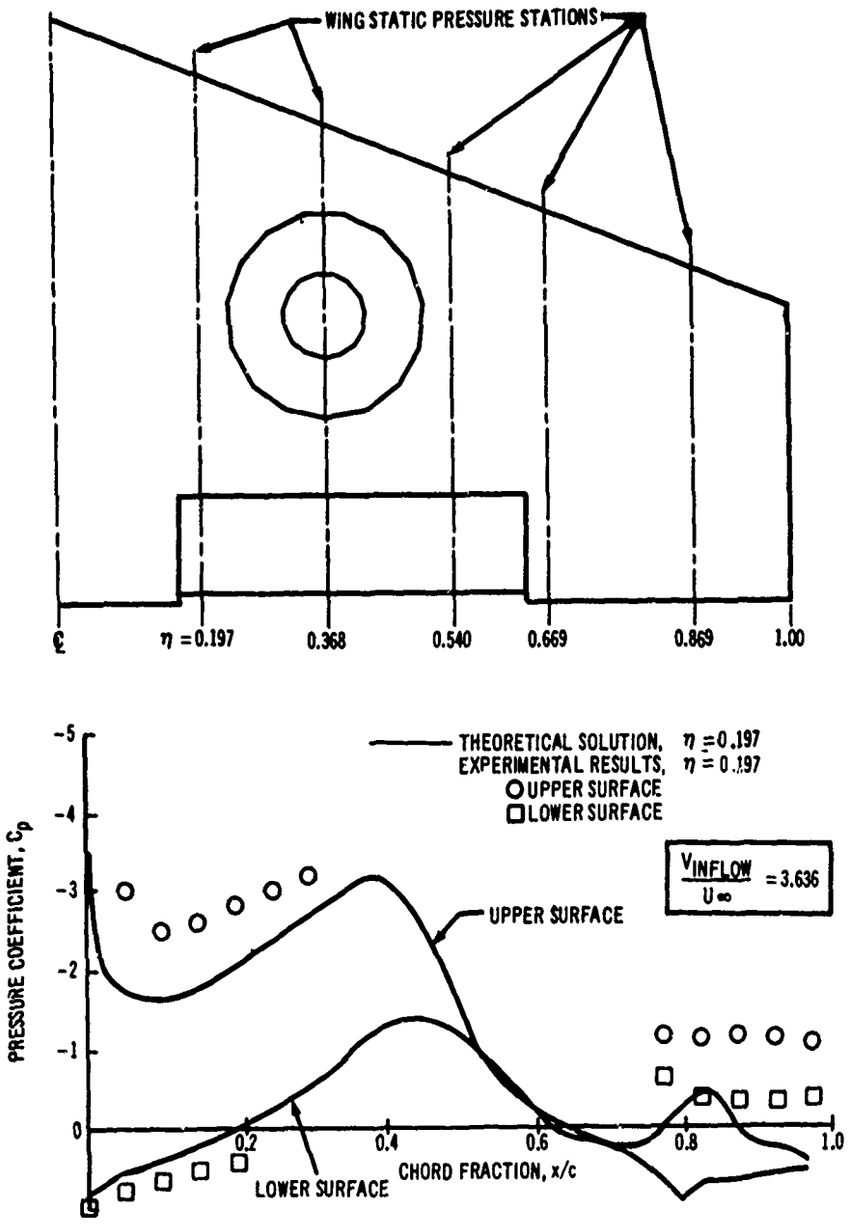

Figure 93. Comparison of Theoretical and Experimental Pressures: Solution 1C.

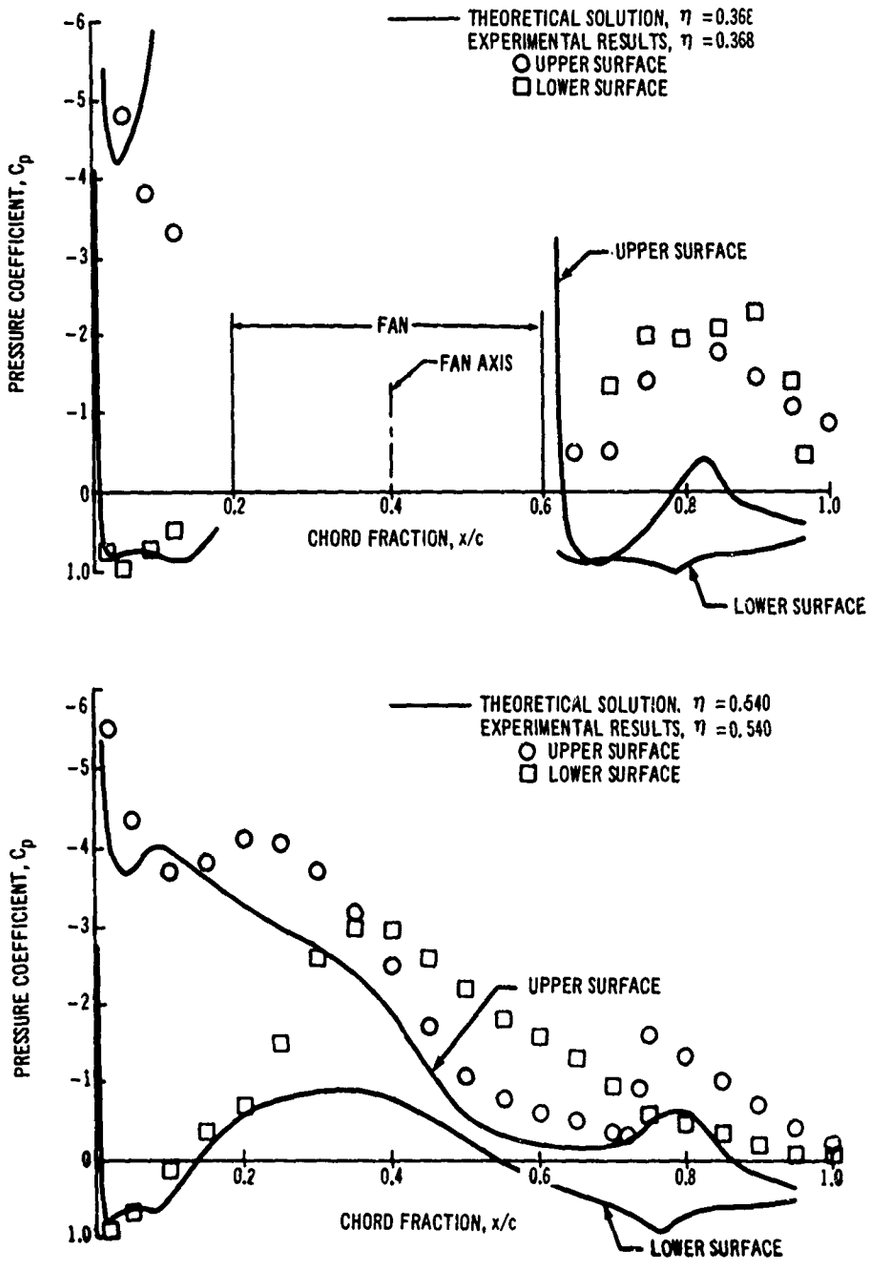

Figure 93. (continued)

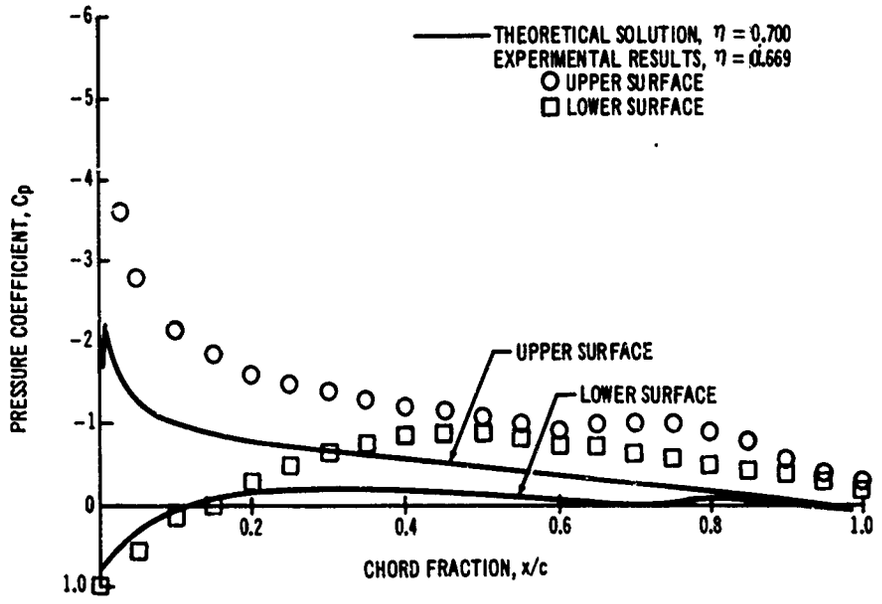

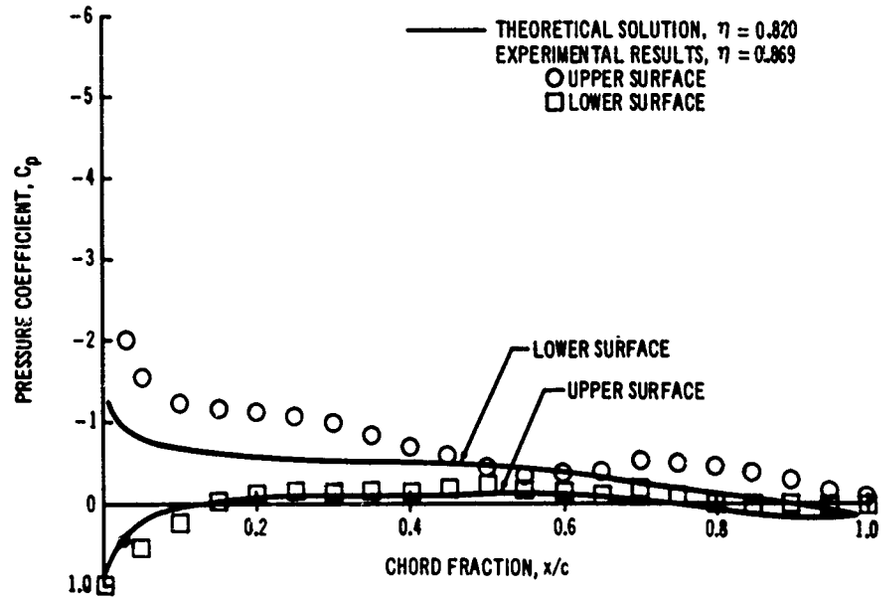

Figure 93. (continued)

The theoretical and experimental pressure coefficients are compared in Figure 94 for solution 4C, which has a nonuniform inflow distribution. The pressure coefficient levels on the upper surface, compared to solution 1C, are most affected for $\eta = 0.197$ and $\eta = 0.540$. Inboard of the fan ($\eta = 0.197$), the pressure level is increased due to the increased inflow to the left side of the fan. Outboard of the fan ($\eta = 0.540$), the pressure level is decreased because of the reduced flow into the right side of the fan. As expected, the lower surface pressure levels are relatively unaffected by the change in inflow distribution. The pressure distributions at the two outboard stations are also relatively unaffected.

The flow pattern on the upper surface near the inlet is shown in Figure 95(a) for solution 1C. The vectors show the local direction of the surface streamlines; the corresponding numbers indicate the magnitude of the velocity ratio V/U_∞. A strong inflow into the inlet is clearly evident, even on the downstream side. On the front part of the inlet the flow accelerates to a velocity of approximately $V/U_\infty = 7.25$, whereas on the rear part the maximum surface velocity reaches 3.60. A dividing streamline occurs between the rear of the inlet and the trailing edge, with the flow ahead of this streamline turning into the inlet and the flow behind going off the trailing edge.

The corresponding flow pattern on the lower wing surface is shown in Figure 95(b). The velocity is much lower on this surface, with a dividing streamline appearing a short distance aft of the leading edge. The flow, as expected, is directed around the efflux tube much like two-dimensional potential flow around a cylinder. The real flow pattern on the lower surface probably appears somewhat different because of viscous entrainment. Some complete flow reversal behind the efflux tube probably occurs instead of the near-stagnation potential-flow velocities.

The flow pattern on the upper surface for the nonuniform inflow solution 4C is shown in Figure 96(a). A peak velocity of $V/U_\infty = 8.97$ is reached on the front left side of the inlet; on the rear right side, velocity reaches only 1.742. The dividing streamline for flow going into the right side of the inlet is shifted closer to the inlet lip. The velocity diagrams and the pressure coefficient curves both indicate that most of the flow is drawn from the left into the fan for the nonuniform inflow, whereas the flow is drawn from directly ahead into the fan for the uniform inflow solution.

The flow pattern on the lower wing surface is shown in Figure 96(b) for the nonuniform inflow solution. For the uniform case, the flow is directed around the efflux tube much like a two-dimensional flow around a cylinder.

Configuration D surface source panel and jet efflux tube arrangements are shown in Figure 91(a) and (c). The number of singularities used for half the configuration was the same as for configuration C. The only geometry difference was the efflux tube, which was designed for a vector angle of 20 degrees and an inflow velocity ratio of $V_j/U_\infty = 1.667$. The aerodynamic operating conditions for which solutions were obtained are summarized in Table III.

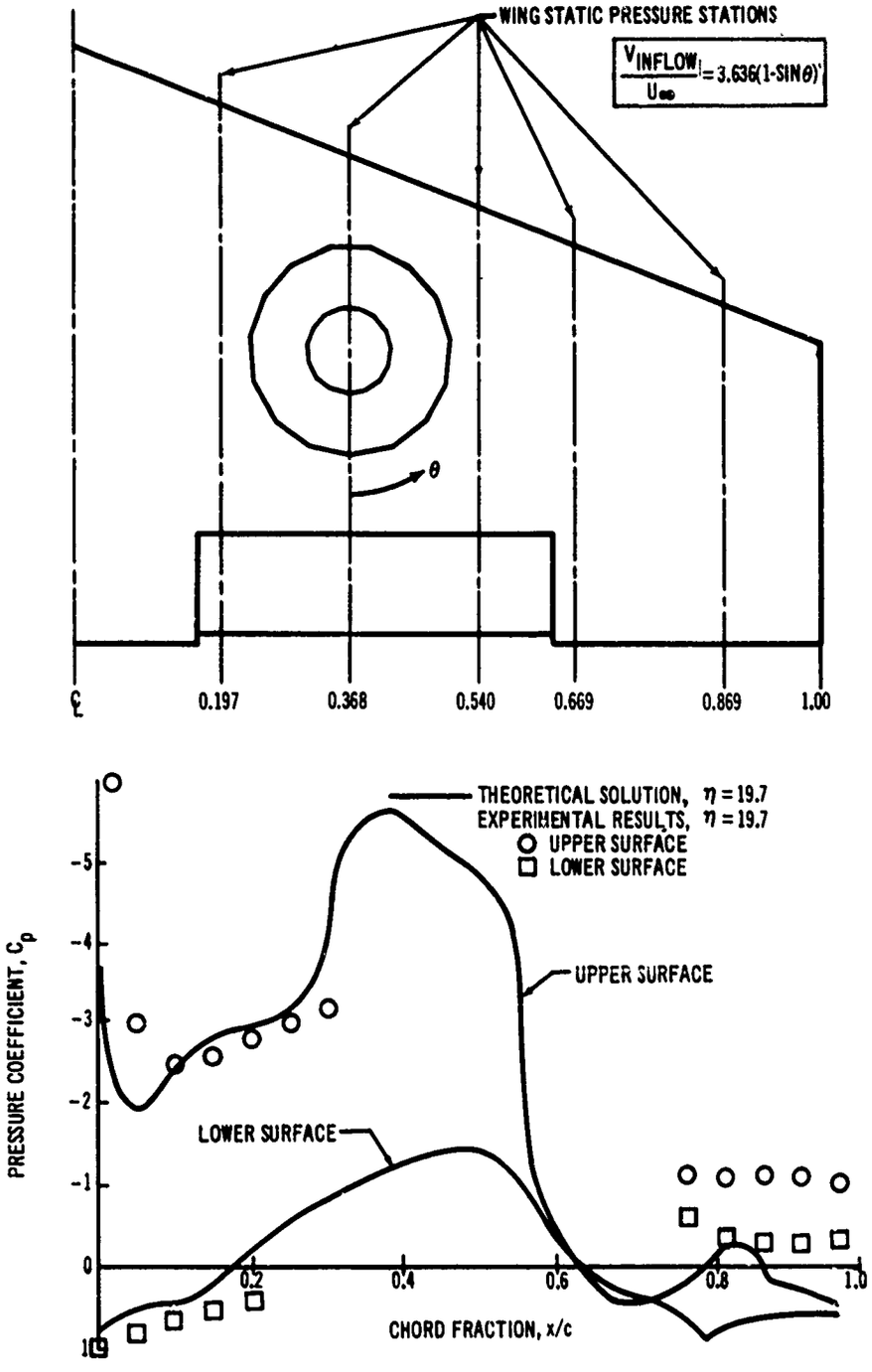

Figure 94. Comparison of Theoretical and Experimental Pressures: Solution 4C.

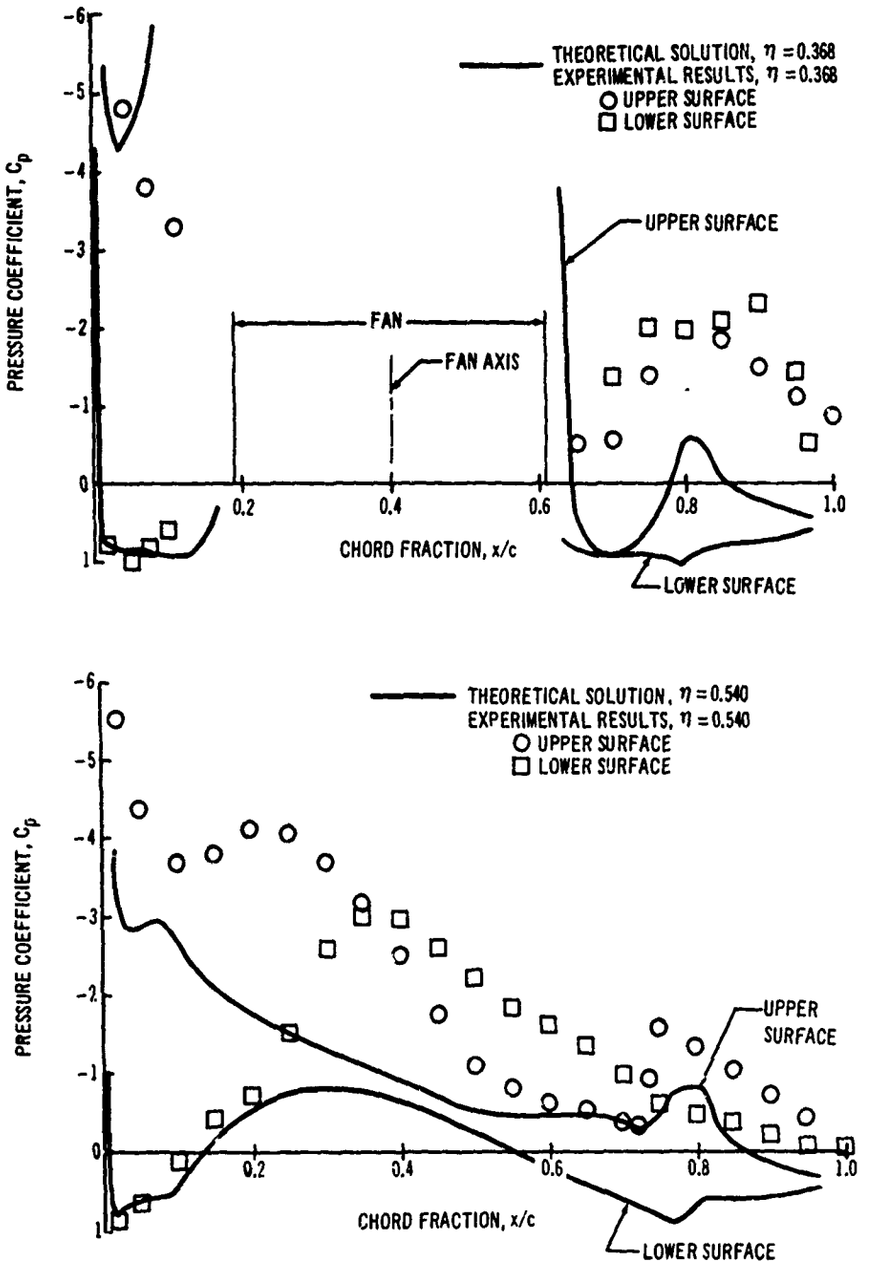

Figure 94. (continued)

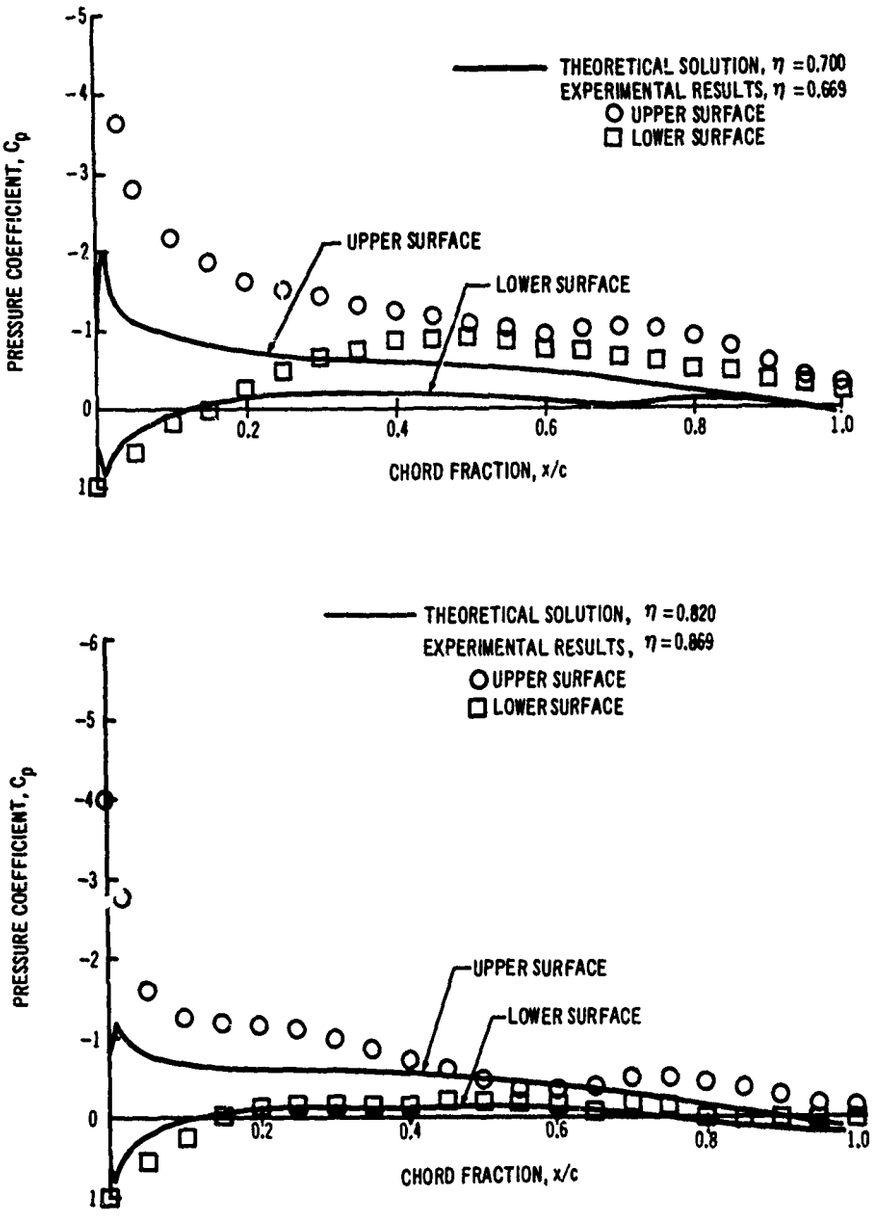

Figure 94. (continued)

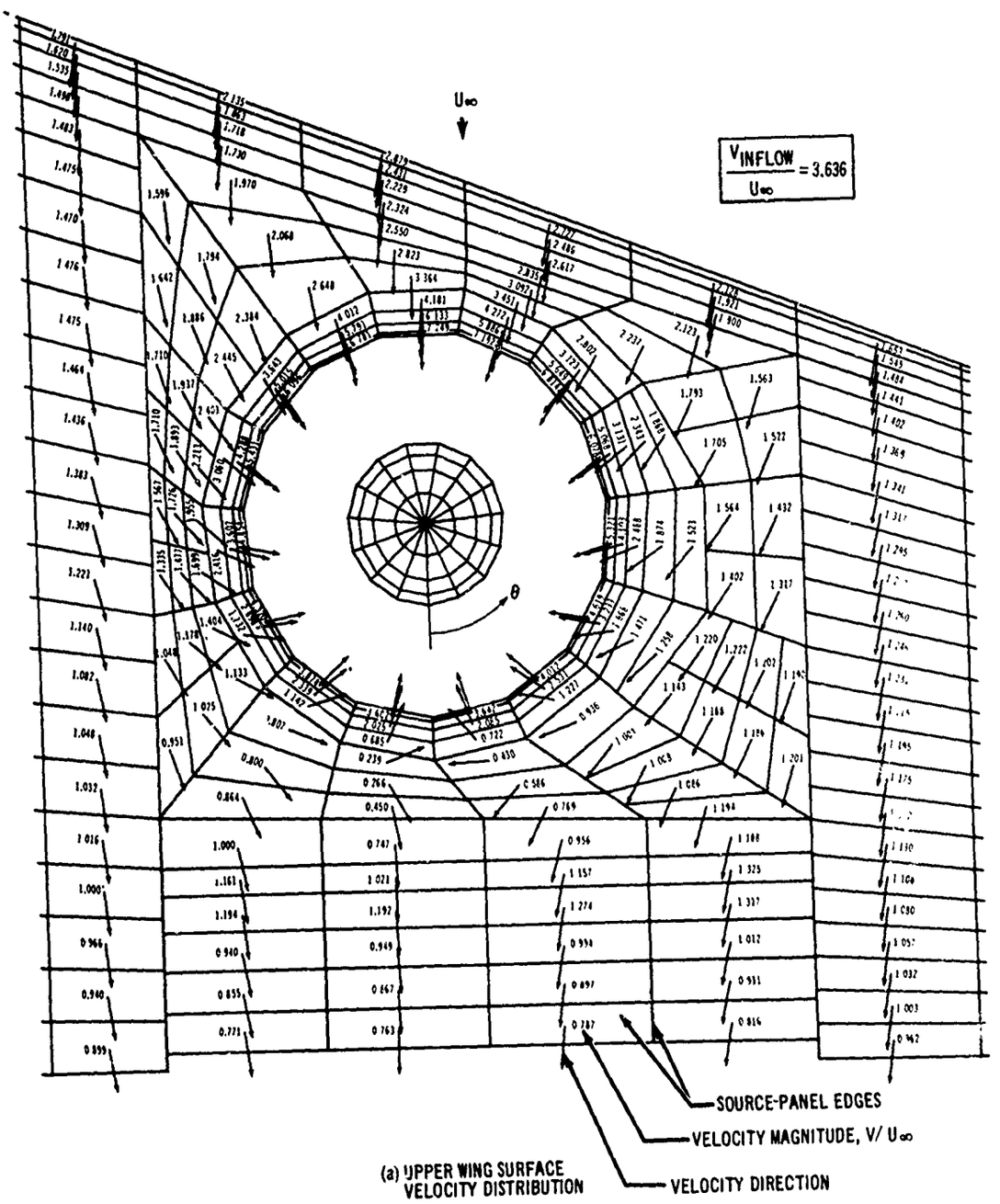

Figure 95. Surface Flow Patterns: Solution 1C.

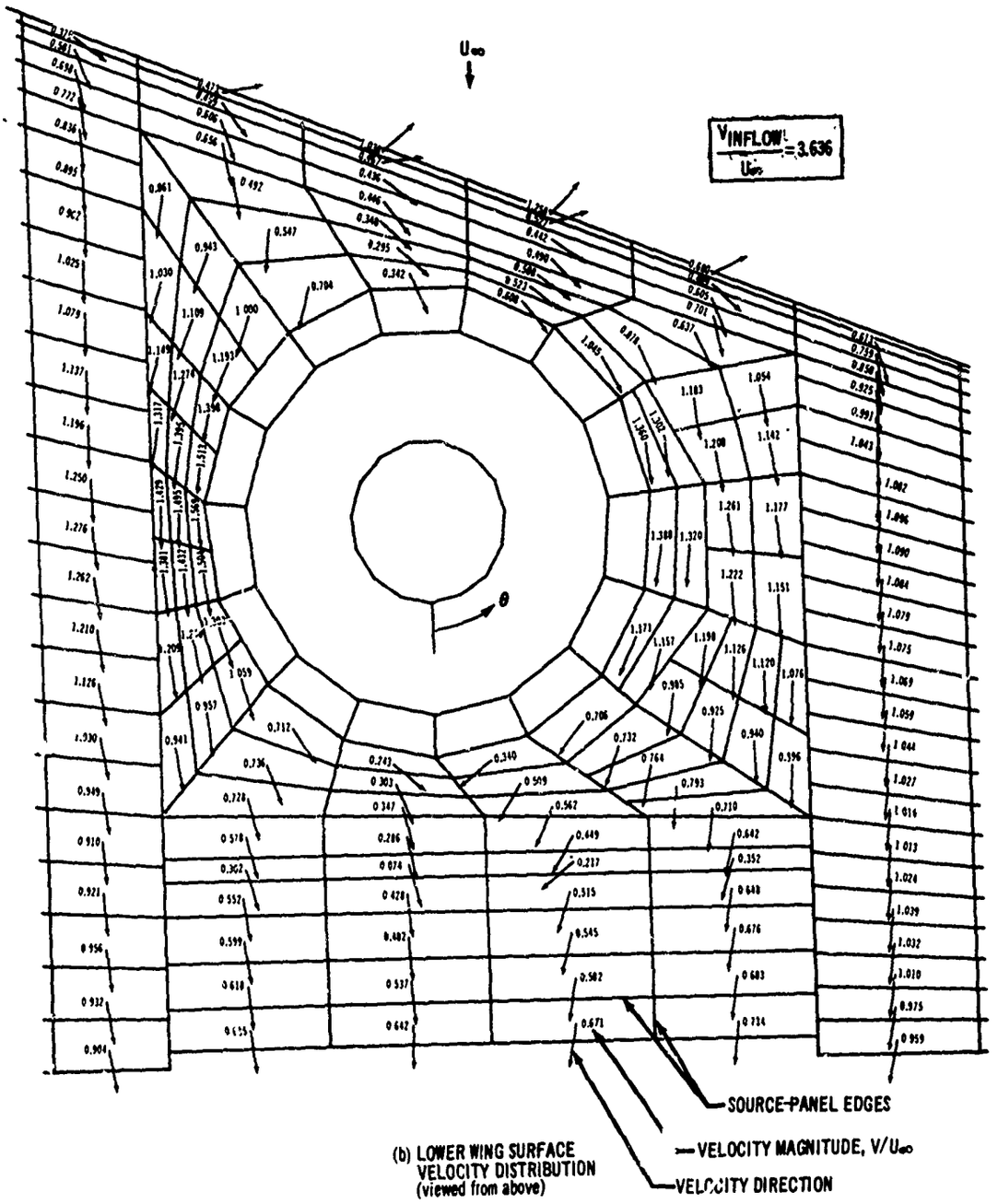

(b) LOWER WING SURFACE VELOCITY DISTRIBUTION (viewed from above)

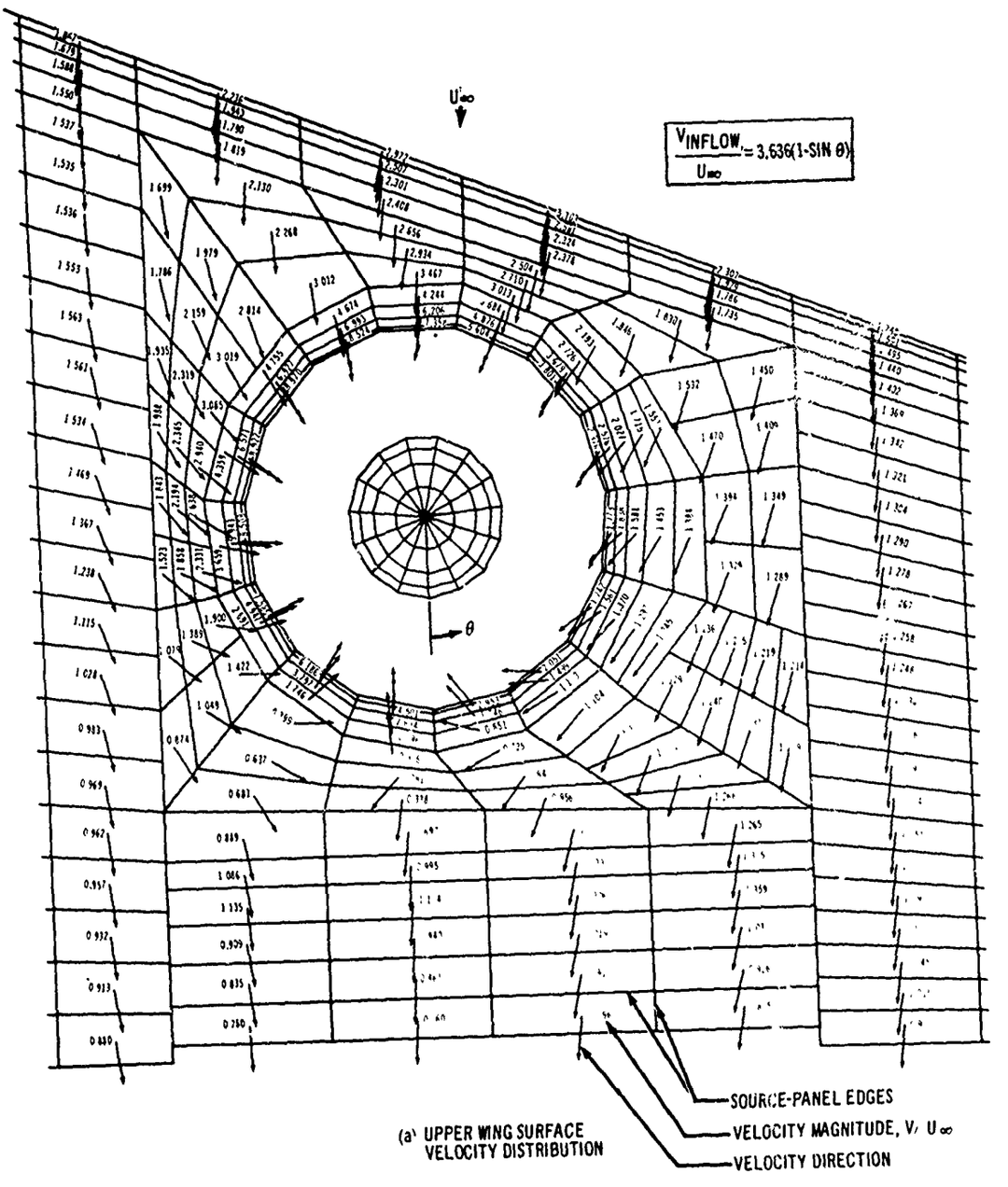

Figure 96. Surface Flow Patterns: Solution 4C.

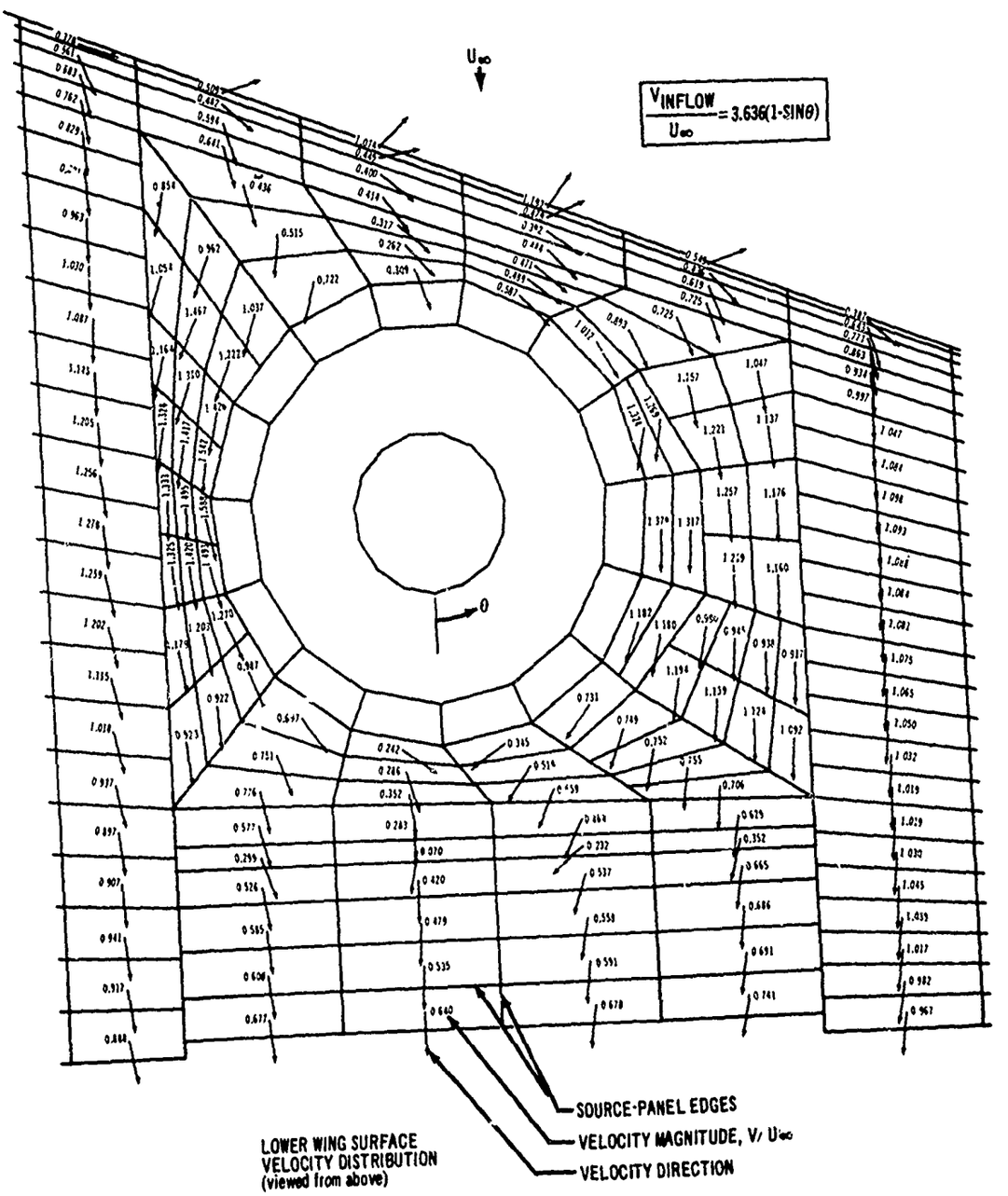

LOWER WING SURFACE
VELOCITY DISTRIBUTION
(viewed from above)

The theoretical lift, drag and pitching moment results for configuration D are compared in Figure 92(b) with the tail-off experimental data. The lift obtained with the three types of inflow distribution again bracket the experimental data. The theoretical lift curve slope also shows good agreement. The effects of the inflow produce significant differences in the drag polar, probably due to differing fan inflow and exit momentum. Again, the predicted moments are less than the experimental results. These theoretical results were obtained with the jet efflux tube positioned for $\alpha = 0$ degrees and the trailing vortex system designed for $\alpha = 4$ degrees.

The theoretical surface pressure distributions at five spanwise stations are compared with experimental results for solution 2D in Figure 97. These curves show the same potential-flow characteristics as for the previous solution. The pressure coefficient levels are of course reduced from configuration C because of the reduced velocity ratio and mass flow. Note that for $\eta = 0.368$, stagnation occurs on the upper surface much nearer the aft inlet lip than for configuration C. The most apparent discrepancy between the theory and the experiment is again in the region behind the efflux tube on the wing lower surface. Elsewhere there is generally better agreement than in the previous example.

The flow pattern on the upper surface near the inlet for the half-sine inflow solution 2D is shown in Figure 98(a). The peak velocity $V/U_\infty = 4.33$ is reached on the front part of the inlet; on the rear right side the inflow velocity reaches only 0.69. Since a smaller velocity ratio is specified for configuration D, the mass flow and hence the area of the entering streamtube are reduced from configuration C. The flow pattern diagram shows that the dividing streamline has moved much nearer the inlet. The corresponding flow pattern on the lower wing surface is shown in Figure 98(b). The flow pattern again resembles that for a two-dimensional flow around a cylinder.

Figure 99 shows the streamlines on the wing that go into the inlet. These streamlines, computed by the potential-flow program, were traced backward from starting points in the inlet and were terminated when they reached a region of dividing streamlines. Those streamlines entering the front and sides of the inlet terminate at the stagnation line on the wing lower surface near the leading edge. Those streamlines entering the rear of the inlet terminate in the near-stagnation region behind the inlet.

The accuracy of a theory such as this cannot be determined absolutely because of the absence of any exact solutions for comparisons. However, in consideration of the overall features of the flow and the experimental comparisons, it appears that the present theory produces the desired flow field within the limitations of the theoretical model.

The boundary-layer velocity distributions along two streamlines, A and B, shown entering the inlet in Figure 99, are given in Figure 100(a). The highest peak velocity along both streamlines occurs on the fan inlet lip.

Figure 100(b) shows the distribution of the calculated divergence K_1. The general trend of K_1 appears to correspond to the streamline pattern across the wing.

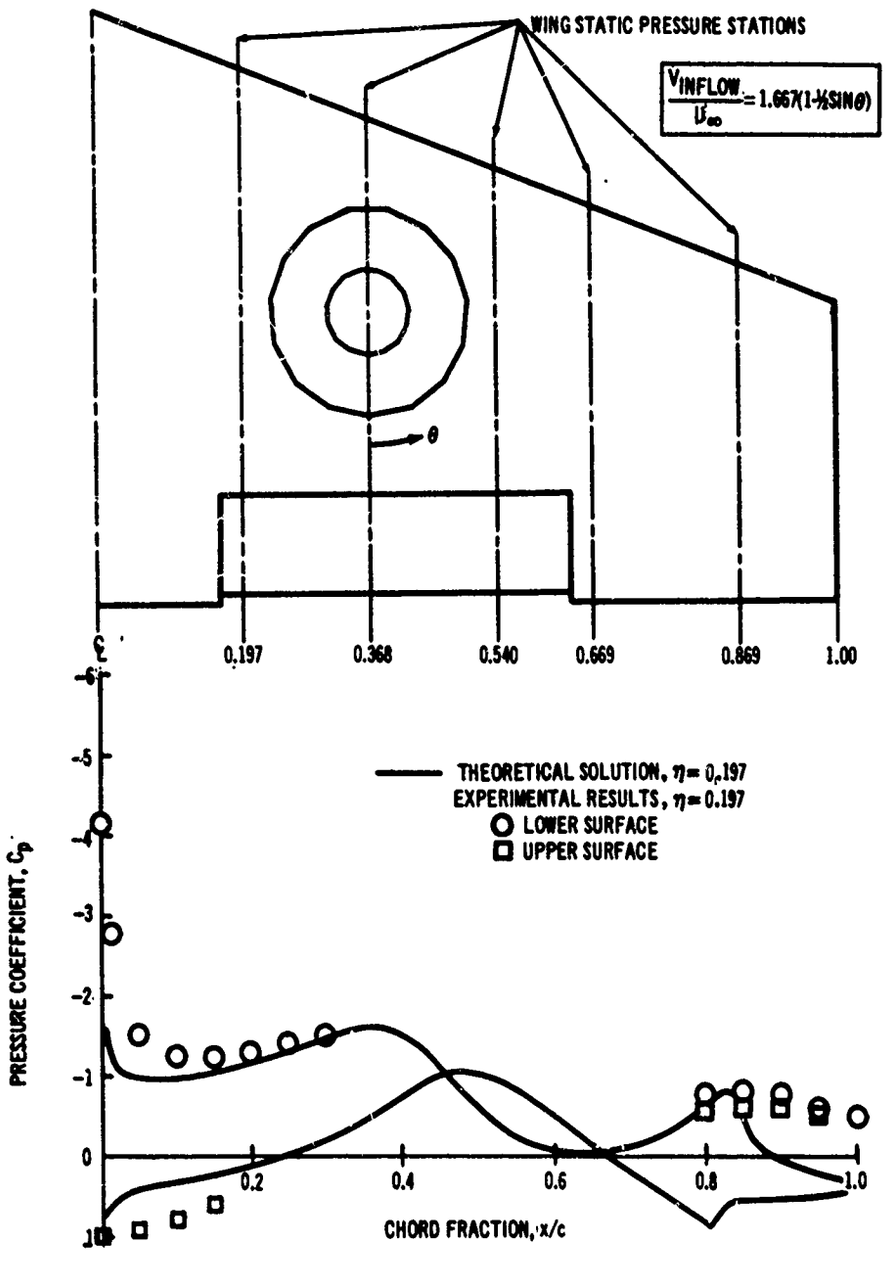

Figure 97. Comparison of Theoretical and Experimental Pressures: Solution 2D.

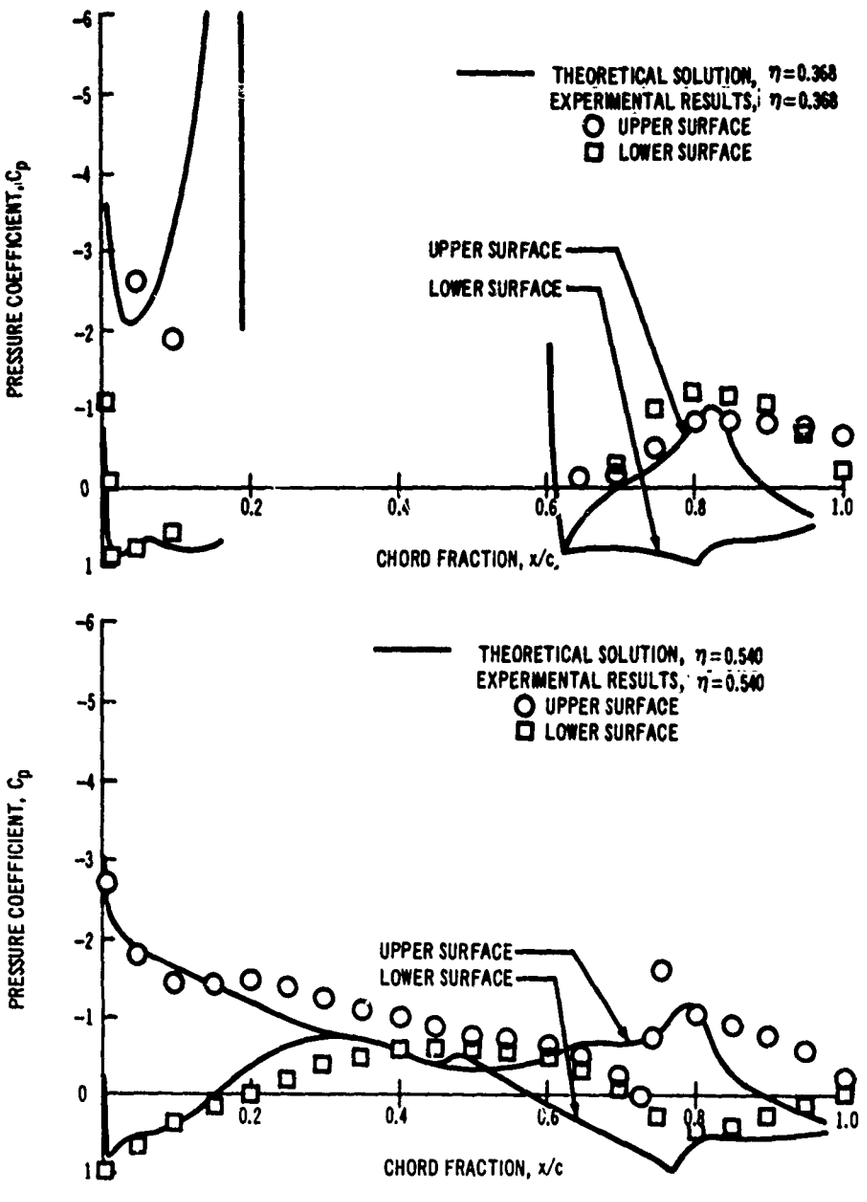

Figure 97. (continued)

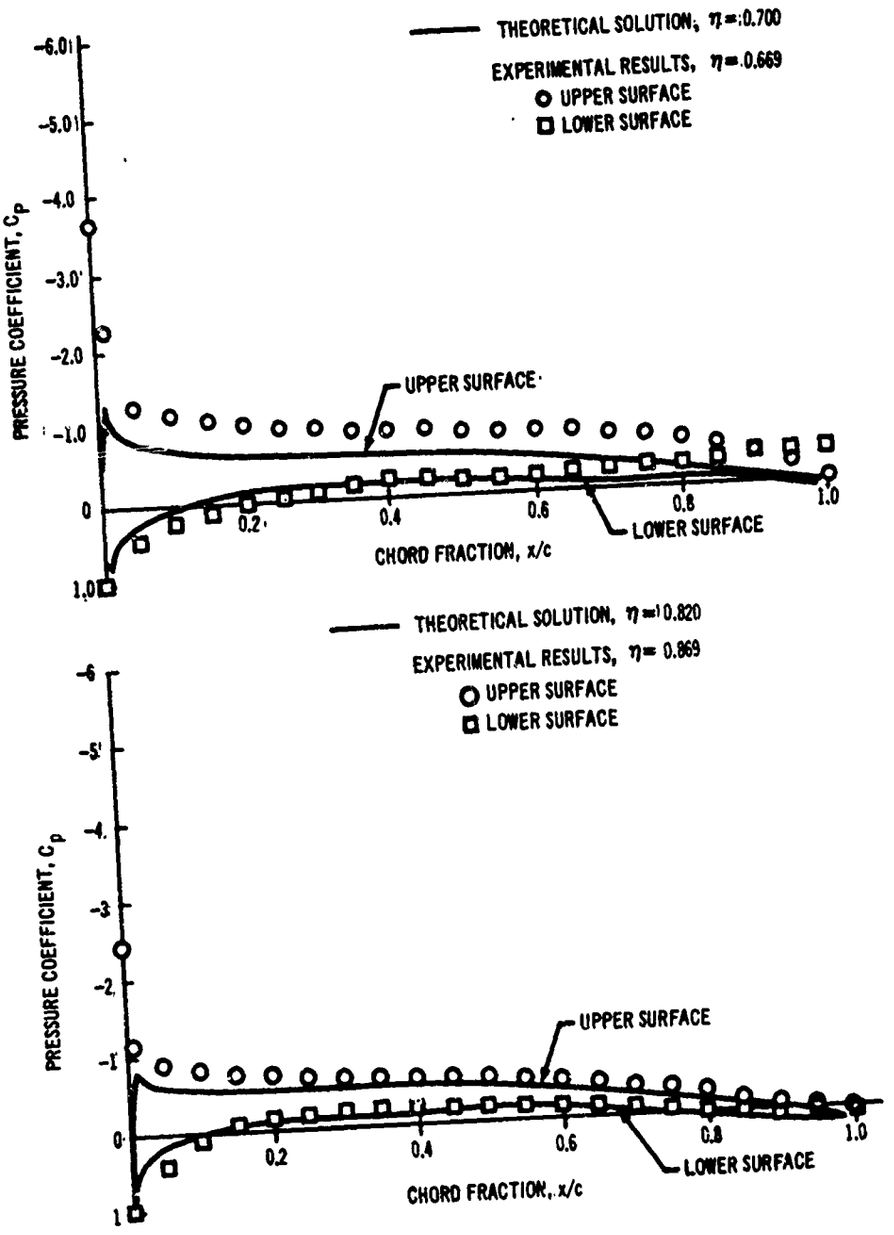

Figure 97. (continued)

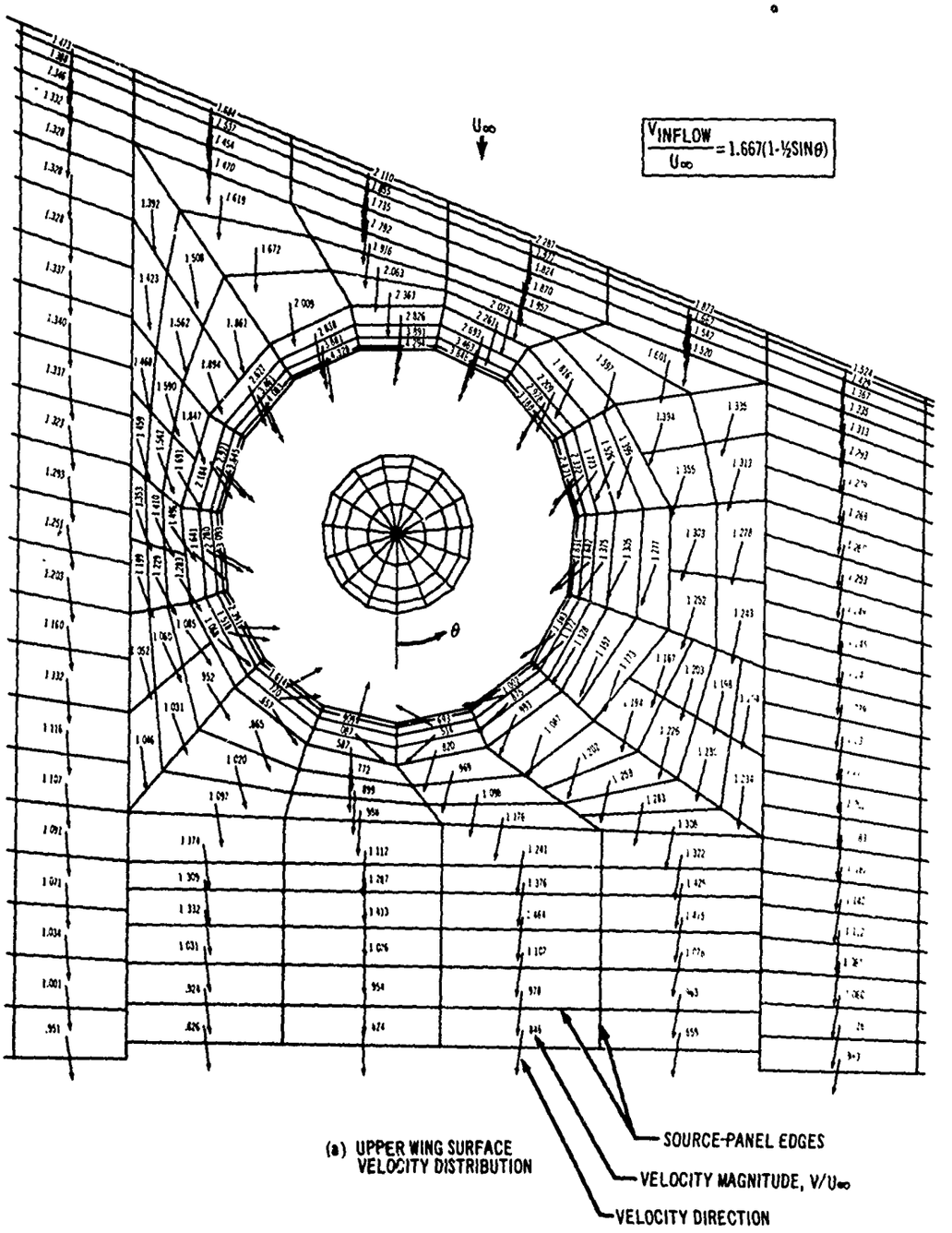

Figure 98. Surface Flow Patterns: Solution 2D.

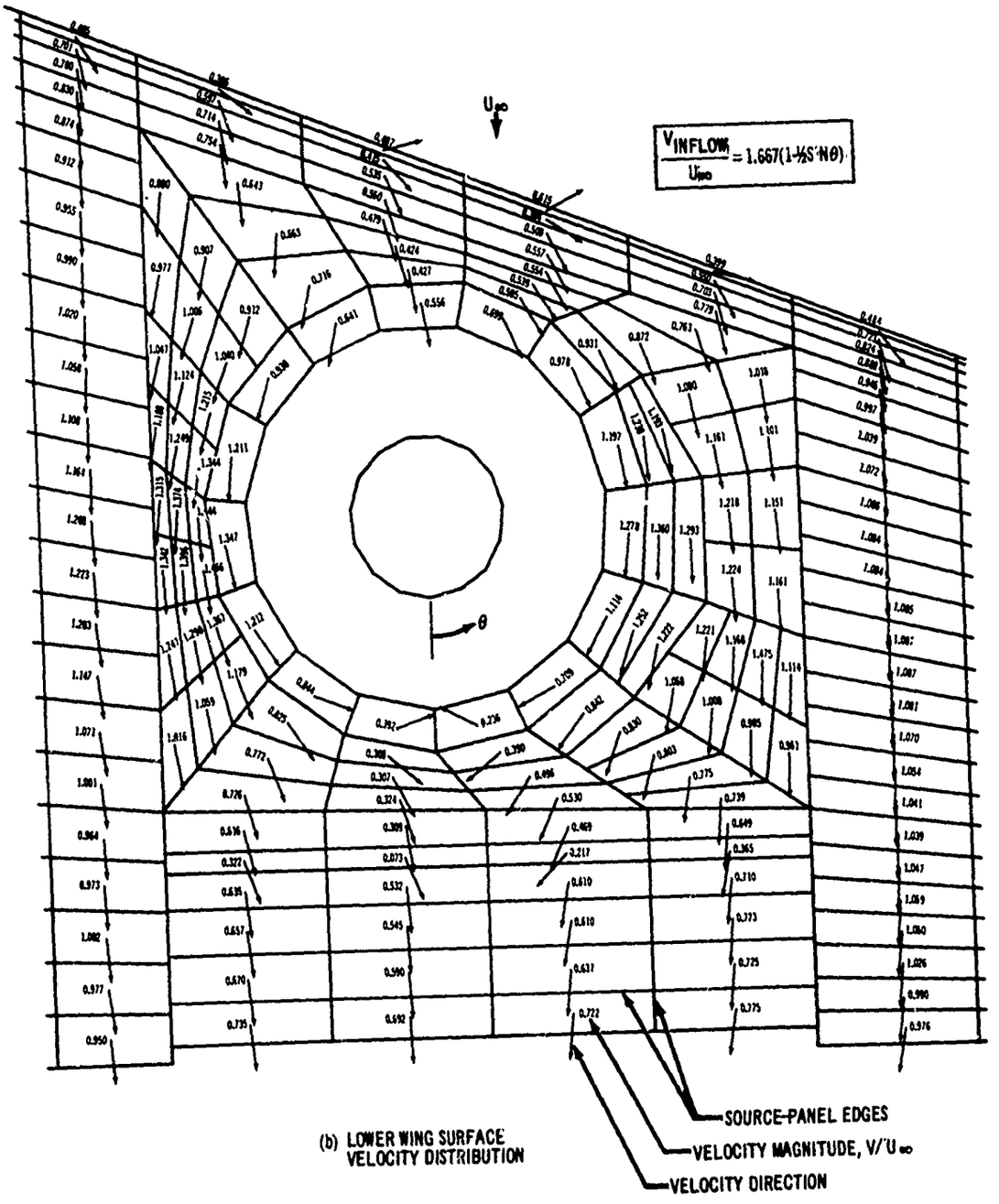

(b) LOWER WING SURFACE VELOCITY DISTRIBUTION

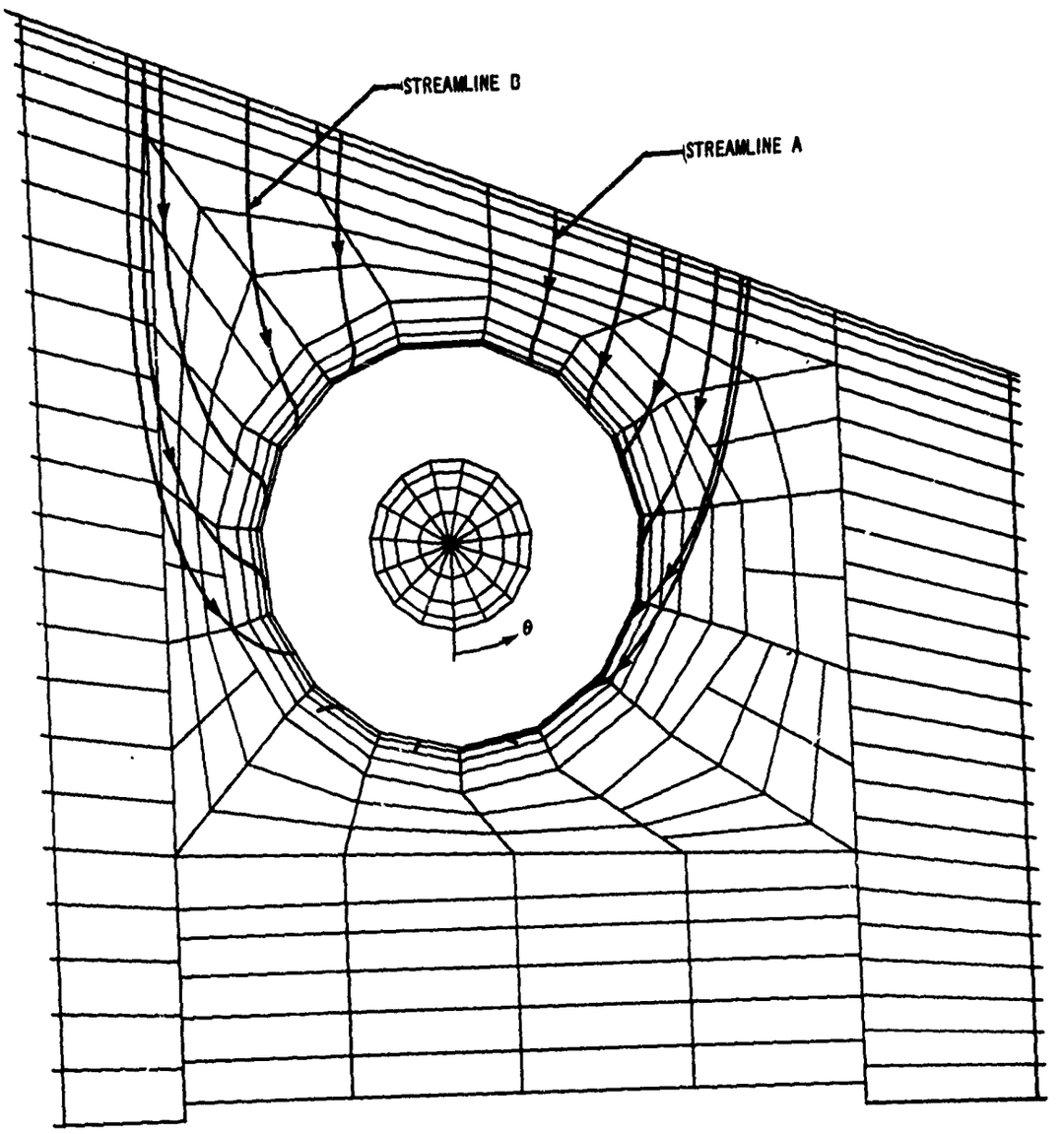

Figure 99. Upper Surface Streamlines: Solution 2D.

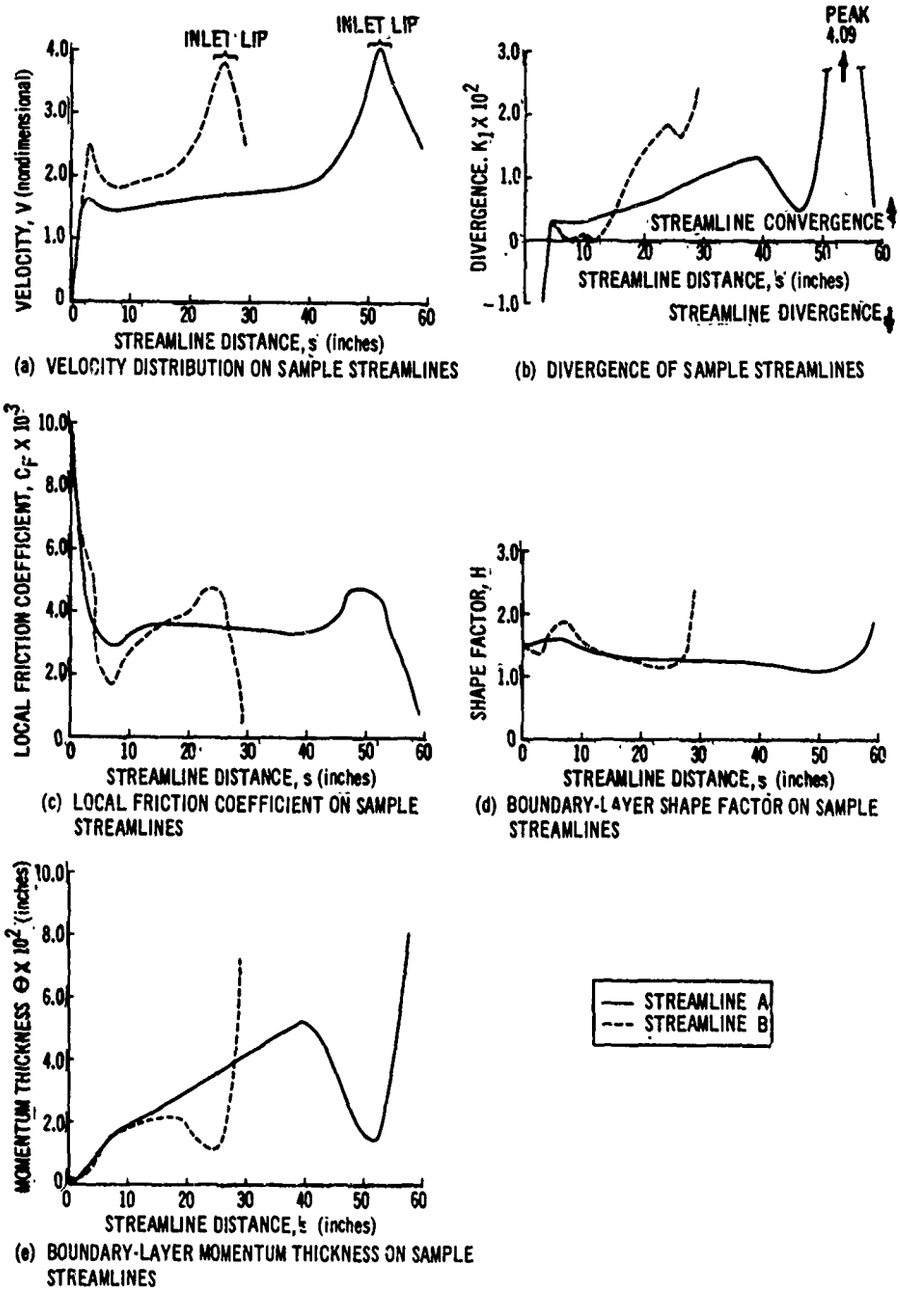

Figure 100. Boundary-Layer Results for Inlet Region: Solution 2D.

The variation of the local friction coefficient, indicated in Figure 100(c), shows typical behavior. The initial rapid decrease in C_f is a Reynolds number effect, accompanied by a large increase in both velocity and momentum thickness. The increase in C_f from s = 40 to s = 50 on streamline A, and from s = 20 to s = 24 on streamline B is a pressure gradient effect, the favorable gradient ($dV/ds > 0$) at the fan inlet lip thinning the boundary layer and causing a greater shearing stress at the wall.

The rapid initial decrease in the shape factor H [Figure 100(d)] for streamline B is probably caused by the large initial pressure gradient and by the selection of H = 1.5 as an initial value. The rise in H to a maximum at s = 7 is, undoubtedly, due to the adverse pressure gradient between s = 3 and s = 7. Further downstream, H decreases moderately and then grows very rapidly on the downstream side of the inlet lip. In a two-dimensional analysis, this rapid growth of H, together with the rapid decrease in C_f and increasing momentum thickness [Figure 100(e)], would indicate separation. As discussed previously, such behavior in this analysis is indicative of at least strongly three-dimensional flow phenomena.

Figure 100(e) shows the increase of momentum thickness across the wing under the influence of a slightly favorable pressure gradient ($dV/ds > 0$) and converging streamlines. The strongly favorable pressure gradient near the fan inlet causes θ to decrease despite the increase in surface friction and the convergent nature of the streamlines. Beyond the fan inlet lip, the momentum thickness and H both increase rapidly as the boundary layer encounters a strong adverse pressure gradient.

The user is cautioned that the predicted behavior of the boundary-layer parameters at and immediately after the fan inlet lip are subject to question. The geometry of the inlet lip is a radical departure from the assumption of a planar surface inherent in this analysis. The effect of centrifugal force normal to the wing surface (that is, streamline curvature in the plane normal to the surface) has not been included in the analysis, and in this region it is certainly of appreciable size. The effect of this force on the boundary layer would be disruptive rather than restorative and may lead to earlier boundary-layer separation on the fan inlet lip.

8. REFERENCES

1. Monical, Richard E., "A Method of Representing Fan-Wing Combinations for Three-Dimensional Potential Flow Solutions," AIAA Paper No. 65-85, January 1965.

2. Rubbert, Paul E., "Theoretical Characteristics of Arbitrary Wings by a Non-Planar Vortex Lattice Method," The Boeing Company, Document D6-9244, Renton, Washington, February 5, 1964.

3. Hess, J. L., and Smith, A. M. O., "Calculation of Non-Lifting Potential Flow about Arbitrary Three-Dimensional Bodies," Douglas Aircraft Company, Report No. E. S. 40622, Long Beach, California, 1962.

4. Hink, G. R., Gilbert R. F., and Sundstrom K. A., "A Method for Determining the Aerodynamic Characteristics of Fan-in-Wing Configurations, Volume II-Computer Program Description," The Boeing Company, USAAVLABS Technical Report 67-61B, U.S. Army Aviation Materiel Laboratories, Fort Eustis, Virginia, 1967.

5. Lamb, H., "Hydrodynamics," Dover Publishing Company, New York, 1945.

6. Ashley, H. and Landahl, M. T., "Aerodynamics of Wings and Bodies," Addison-Wesley Publishing Company, Inc., Reading, Mass., 1965.

7. Cooke, J. C., "An Axially Symmetric Analogue for General Three-Dimensional Boundary Layers," Royal Aeronautical Establishment, Tech. Note, Aero. 2625, Ministry of Supply, London, W. C. 2, June 1959.

8. Granville, P. S., "A Method for the Calculation of the Turbulent Boundary Layer in a Pressure Gradient," David Taylor Model Basin, Report 752, Navy Department, Washington 7, D.C., May 1951.

9. Rosenhead, E. L., "Laminar Boundary Layers," Oxford (Clarendon Press), Amen House, London, E.C. 4, 1963.

10. Heyson, Harry, "Wind-Tunnel Wall Effects at Extreme Force Coefficients," International Congress of Subsonic Aerodynamics, New York, April 3-6, 1967.

11. Davenport, F., "Singularity Solutions to General Potential Flow Airfoil Problems," The Boeing Company, Document D6-7202, Renton, Washington, 1963.

12. Faulkner, S., Hess, J. L., and Geising, J. P., "Comparison of Experimental Pressure Distributions With Those Calculated by the Douglas Neumann Program," Douglas Aircraft Company, Report No. LB31831, Long Beach, California, 1964.

13. Winter, K. G., Smith, K. G., and Rotta, J. C., "Recent Developments in Boundary Layer Research," AGARD Meeting, Naples, Italy, May 10-14, 1965.

14. Hickey, D. H. and Hall, L. P., "Aerodynamic Characteristics of a Large-Scale Model with Two High Disk-Loading Fans Mounted in the Wings," NASA TN D-1650, Ames Research Center, Moffett Field, California, February 1963.

APPENDIX I
INFLUENCE COEFFICIENTS

This appendix presents the method of generating the velocities induced by the three types of singularities used in the numerical solution of the potential-flow problem described in Section 3.1. The perturbation velocity at any point in the field is obtained from integration over the various singularities on the body and trailing system [Equation (16)].

Velocity induced by a planar quadrilateral source sheet. — Consider a planar, quadrilateral source sheet of constant strength, as shown in Figure 101. Define a rectangular coordinate system (ξ, η, ζ) with the panel lying in the ξ, η plane. The origin is at the panel centroid, with the ξ-axis parallel to a panel diagonal. The coordinates of the four panel corner points are subscripted 1 → 4 consecutively around the panel. The velocity induced at an arbitrary point (ξ, η, ζ) by the source panel of constant strength is given by

$$\vec{V}(\xi, \eta, \zeta) = \frac{\vec{q}}{U_\infty} = -\frac{1}{4\pi U_\infty} \nabla \iint_{\text{panel}} \frac{m}{r} dS = \vec{C}\sigma \tag{105}$$

where $\sigma = \dfrac{m}{4\pi U_\infty}$

$$\vec{C} = -\nabla \iint_{\text{panel}} \frac{1}{r}\, dS = \iint_{\text{panel}} \frac{\vec{r}}{r^3}\, dS$$

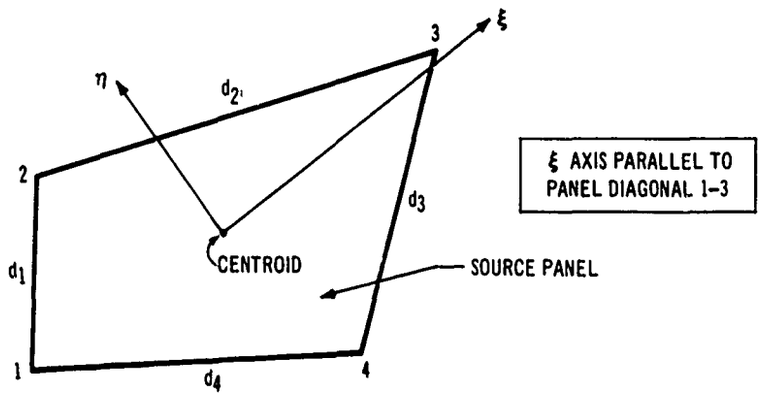

Figure 101. Source-Panel Coordinate System.

The integral for $\widetilde{C}$ is given in Reference 3. The resulting expressions for the components of $\widetilde{C}$ parallel to the ξ, η, ζ axes, which are the velocity components per unit singularity strength σ induced by the source panel, are

$$C_\xi = \frac{V_\xi(\xi,\eta,\zeta)}{\sigma} = \frac{\eta_2-\eta_1}{d_1}\log\left(\frac{r_1+r_2-d_1}{r_1+r_2+d_1}\right)+\frac{\eta_3-\eta_2}{d_2}\log\left(\frac{r_2+r_3-d_2}{r_2+r_3+d_2}\right)$$
$$+\frac{\eta_4-\eta_3}{d_3}\log\left(\frac{r_3+r_4-d_3}{r_3+r_4+d_3}\right)+\frac{\eta_1-\eta_4}{d_4}\log\left(\frac{r_4+r_1-d_4}{r_4+r_1+d_4}\right) \qquad (106)$$

$$C_\eta = \frac{V_\eta(\xi,\eta,\zeta)}{\sigma} = \frac{\xi_1-\xi_2}{d_1}\log\left(\frac{r_1+r_2-d_1}{r_1+r_2+d_1}\right)+\frac{\xi_2-\xi_3}{d_2}\log\left(\frac{r_2+r_3-d_2}{r_2+r_3+d_2}\right)$$
$$+\frac{\xi_3-\xi_4}{d_3}\log\left(\frac{r_3+r_4-d_3}{r_3+r_4+d_3}\right)+\frac{\xi_4-\xi_1}{d_4}\log\left(\frac{r_4+r_1-d_4}{r_4+r_1+d_4}\right) \qquad (107)$$

$$C_\zeta = \frac{V_\zeta(\xi,\eta,\zeta)}{\sigma} = \tan^{-1}\left(\frac{a_1 e_1-b_1}{\zeta r_1}\right)-\tan^{-1}\left(\frac{a_1 e_2-b_2}{\zeta r_2}\right)$$
$$+\tan^{-1}\left(\frac{a_2 e_2-b_2}{\zeta r_2}\right)-\tan^{-1}\left(\frac{a_2 e_3-b_3}{\zeta r_3}\right)$$
$$+\tan^{-1}\left(\frac{a_3 e_3-b_3}{\zeta r_3}\right)-\tan^{-1}\left(\frac{a_3 e_4-b_4}{\zeta r_4}\right)$$
$$+\tan^{-1}\left(\frac{a_4 e_4-b_4}{\zeta r_4}\right)-\tan^{-1}\left(\frac{a_4 e_1-b_1}{\zeta r_1}\right) \qquad (108)$$

where $d_1 = \left[(\xi_2-\xi_1)^2+(\eta_2-\eta_1)^2\right]^{1/2}$

$d_2 = \left[(\xi_3-\xi_2)^2+(\eta_3-\eta_2)^2\right]^{1/2}$

$d_3 = \left[(\xi_4-\xi_3)^2+(\eta_4-\eta_3)^2\right]^{1/2}$

$d_4 = \left[(\xi_1-\xi_4)^2+(\eta_1-\eta_4)^2\right]^{1/2}$

and

$$a_1 = \frac{\eta_2 - \eta_1}{\xi_2 - \xi_1} \qquad a_2 = \frac{\eta_3 - \eta_2}{\xi_3 - \xi_2}$$

$$a_3 = \frac{\eta_4 - \eta_3}{\xi_4 - \xi_3} \qquad a_4 = \frac{\eta_1 - \eta_4}{\xi_1 - \xi_4}$$

and

$$r_k = \left[(\xi - \xi_k)^2 + (\eta - \eta_k)^2 + \zeta^2\right]^{1/2}, \quad k = 1, 2, 3, 4$$

$$e_k = \zeta^2 + (\xi - \xi_k)^2, \quad k = 1, 2, 3, 4$$

$$b_k = (\eta - \eta_k)(\xi - \xi_k), \quad k = 1, 2, 3, 4$$

Various special forms of these equations are used, depending on the relative position of the influence point with respect to the panel. When the ζ coordinate is less than 10^{-5} (the units being those of the input configuration), C_ζ is set equal to zero. This is the proper limit of Equation (108) as $\zeta \to 0$ when ξ, η lie outside of the panel. The normal velocity component at the panel boundary point is obtained by setting C_ζ equal to 2π, the limit of Equation (108) for $\zeta \to 0$ when ξ, η are within the panel.

To reduce computation time, simplified forms of Equations (106), (107), and (108) are used when the distance of the influence point (ξ, η, ζ) from the panel is large compared to the maximum diagonal of the panel. These are obtained by a multipole expansion of the basic integral of Equation (105) about the panel centroid. The details of this expansion and an error analysis for the forms given below are presented in Reference 3. These simplified forms are

When $2.45 \leq r_o/t \leq 4.0$

$$C_\xi = \frac{V_\xi(\xi, \eta, \zeta)}{\sigma} = -\left[A\, w_\xi + \frac{1}{2} I_\eta\, w_{\xi\xi\xi} + I_{\xi\eta}\, w_{\xi\xi\eta} + \frac{1}{2} I_\xi\, w_{\xi\eta\eta}\right] \tag{109}$$

$$C_\eta = \frac{V_\eta(\xi, \eta, \zeta)}{\sigma} = -\left[A\, w_\eta + \frac{1}{2} I_\eta\, w_{\xi\xi\eta} + I_{\xi\eta}\, w_{\xi\eta\eta} + \frac{1}{2} I_\xi\, w_{\eta\eta\eta}\right] \tag{110}$$

$$C_\zeta = \frac{V_\zeta(\xi, \eta, \zeta)}{\sigma} = -\left[A\, w_\zeta + \frac{1}{2} I_\eta\, w_{\xi\xi\zeta} + I_{\xi\eta}\, w_{\xi\eta\zeta} + \frac{1}{2} I_\xi\, w_{\eta\eta\zeta}\right] \tag{111}$$

where $r_o = \left[\xi^2 + \eta^2 + \zeta^2\right]^{1/2}$

t = largest diagonal of the panel

and when $r_o/t > 4.0$

$$C_\xi = \frac{V_\xi\ (\xi, \eta, \zeta)}{\sigma} = -A\, w_\xi \tag{112}$$

$$C_\eta = \frac{V_\eta\ (\xi, \eta, \zeta)}{\sigma} = -A\, w_\eta \tag{113}$$

$$C_\zeta = \frac{V_\zeta\ (\xi, \eta, \zeta)}{\sigma} = -A\, w_\zeta \tag{114}$$

where $w_\xi = -\xi\, r_o^{-3}$

$w_\eta = -\eta\, r_o^{-3}$

$w_\zeta = -\zeta\, r_o^{-3}$

$w_{\xi\xi\xi} = 3\xi\,(3\rho + 10\,\xi^2)\, r_o^{-7}$

$w_{\xi\xi\eta} = 3\eta\rho\, r_o^{-7}$

$w_{\xi\eta\eta} = 3\xi\, q\, r_o^{-7}$

$w_{\eta\eta\eta} = 3\eta\,(3q + 10\,\eta^2)\, r_o^{-7}$

$w_{\xi\xi\zeta} = 3\zeta\rho\, r_o^{-7}$

$w_{\xi\eta\zeta} = -15\,\xi\,\eta\,\zeta\, r_o^{-7}$

$w_{\eta\eta\zeta} = 3\zeta\, q\, r_o^{-7}$

and $\rho = \eta^2 + \zeta^2 - 4\,\xi^2$

$q = \xi^2 + \zeta^2 - 4\,\eta^2$

$A = \iint_{\text{panel}} d\xi\, d\eta \equiv$ panel area

$I_\eta = \iint_{\text{panel}} \xi^2\, d\xi\, d\eta =$ moment of inertia of the panel about the η axis

$I_{\xi\eta} = \iint_{\text{panel}} \xi\,\eta\, d\xi\, d\eta =$ product of inertia

$$I_\xi = \iint_{\text{panel}} \eta^2 \, d\xi \, d\eta = \text{moment of inertia about the } \xi \text{ axis}$$

Velocity induced by a quadrilateral vortex.—Consider a finite line vortex whose length and direction are denoted by $\vec{L}$, as shown in Figure 102. Let the vorticity be positive when directed along $\vec{L}$. The velocity per unit vorticity induced at any point x, y, z is given by the Biot-Savart law as

$$\frac{\vec{V}(x, y, z)}{\sigma} = \frac{1}{4\pi}\int_1^2 \frac{(\vec{R}\times\vec{L})}{|\vec{R}\times\vec{L}|}\frac{\sin\theta}{R^2}\,ds = \frac{L}{4\pi}\frac{(\vec{L}\times\vec{R}_1)}{|\vec{L}\times\vec{R}_1|^2}(\cos\theta_1 - \cos\theta_2) \quad (115)$$

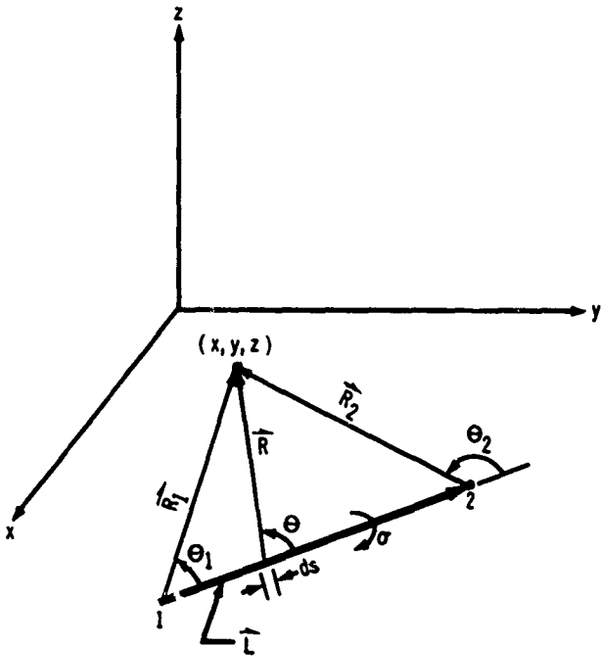

Figure 102. Finite Line Vortex.

A quadrilateral vortex is composed of four equal strength vortex segments, as shown in Figure 103(a). The velocity induced by the quadrilateral is

$$\vec{V}(x, y, z) = \sum_{i=1}^{4} \vec{V}_i \quad (116)$$

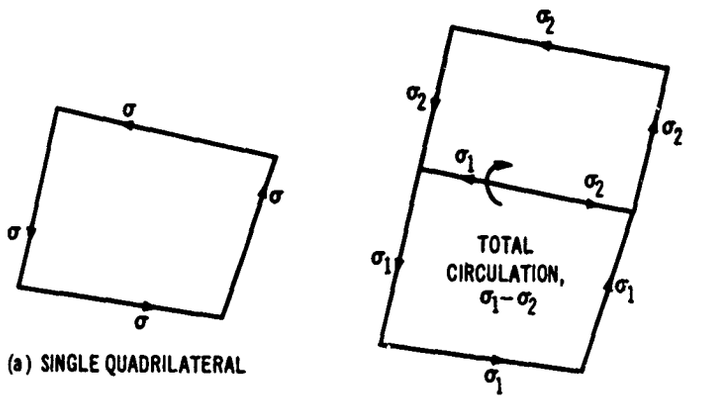

Figure 103. Quadrilateral Vortex.

where $\vec{V}_i$ denotes the velocity induced by the i^{th} segment according to Equation (115). A quadrilateral vortex network consists simply of individual quadrilaterals adjacent to one another, with their common sides superimposed. The total strength of an individual segment is thus the sum of the strengths of the adjoining quadrilaterals, as shown in Figure 103(b).

Velocity induced by a multihorseshoe vortex.—Consider a single multihorseshoe of strength σ, as shown in Figure 104. It is composed of vortex segments whose individual strengths are as shown. The velocity induced by the multihorseshoe is obtained as the sum of the individual contributions of all the segments. Each individual segment contributes a velocity given by Equation (115).

A multihorseshoe network containing several different σ's (see Figure 10) consists simply of a series of single multihorseshoes placed side by side, with adjacent trailing elements superimposed. The net strength of the trailing elements is the sum (with the proper attention to sign) of the adjoining individual trailing elements.

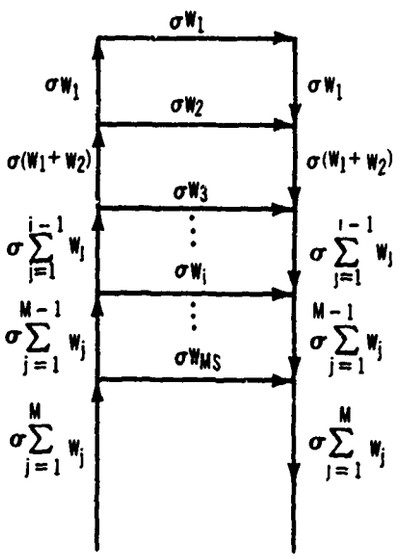

Figure 104. Multihorseshoe Vortex Strengths.

APPENDIX II
ITERATIVE GEOMETRIC INTERSECTION TECHNIQUE

A general iterative technique is described for finding the intersection of an oblique straight line with the surface of a defined wing PART. Figure 105 shows a wing PART, the origin of the inlet coordinate system, the fan axis, and a line parallel to the fan axis intersecting the upper and lower surfaces of the wing PART. Subroutine INLET employs subroutine OBLIQ, which finds both the upper and lower surface intersections. The input to subroutine OBLIQ consists of two tables of $(x, y, z)_i$ coordinates for the inboard and outboard defining sections in the reference coordinate system to define the wing. The origin of the inlet coordinate system, the direction cosines of the fan axis, and the tolerance in the iteration scheme are input to OBLIQ. Subroutine INLET also inputs to OBLIQ the direction cosines (r_x, r_y, r_z) and magnitude R of a radius vector $\vec{R}$ drawn from (x_o, y_o, z_o) to the line parallel to the fan axis. The outputs of OBLIQ are the (x, y, z) coordinates of the upper and lower surface intersection points.

The method of finding these intersection points is as follows: the coordinates at the tip of the radius vector $\vec{R}$ are first computed,

$$\begin{aligned} x_{tip} &= x_o + Rr_x \\ y_{tip} &= y_o + Rr_y \\ z_{tip} &= z_o + Rr_z \end{aligned} \tag{117}$$

Using y_{tip}, OBLIQ interpolates between the inboard and outboard $(x, y, z)_i$ tables to find a single $(x, z)_i$ table valid for y_{tip}. OBLIQ then enters this table with x_{tip}, searching and curve-fitting to find the upper surface z coordinate that is on the line passing through $(x_{tip}, y_{tip}, z_{tip})$ and parallel to the z-axis of the reference coordinate system. The lower-surface intersection is done independently after all computations have been completed for the upper surface. The coordinates of the surface point are called (x_s, y_s, z_s). OBLIQ next computes the perpendicular distance d from the surface intersection point (x_s, y_s, z_s) to a point $(\bar{x}_s, \bar{y}_s, \bar{z}_s)$ on the line parallel to the fan axis, as shown in Figure 106. If d is less than the iteration tolerance ϵ_t input to the program, then (x_s, y_s, z_s) is assumed to be the desired intersection point. Otherwise, $(x_{tip}, y_{tip}, z_{tip})$ are replaced by $(\bar{x}_s, \bar{y}_s, \bar{z}_s)$, and the process is repeated. If this process does not converge within 50 iterations, the last point is used as the desired surface point.

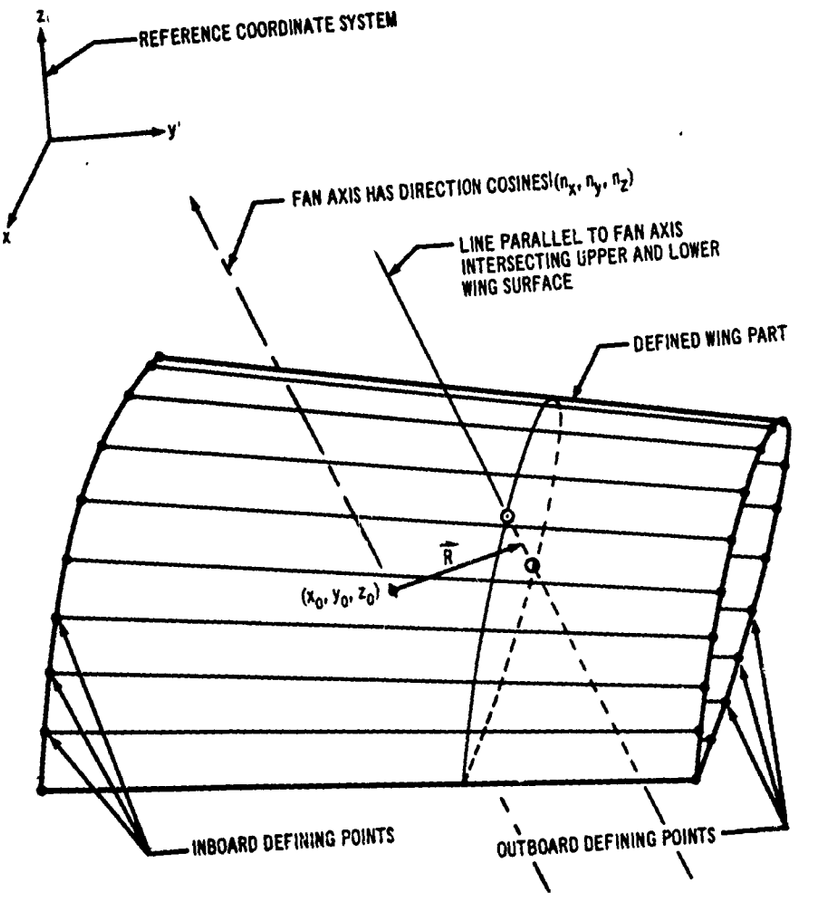

Figure 105. Intersections of Oblique Straight Line With Surface of a Wing PART.

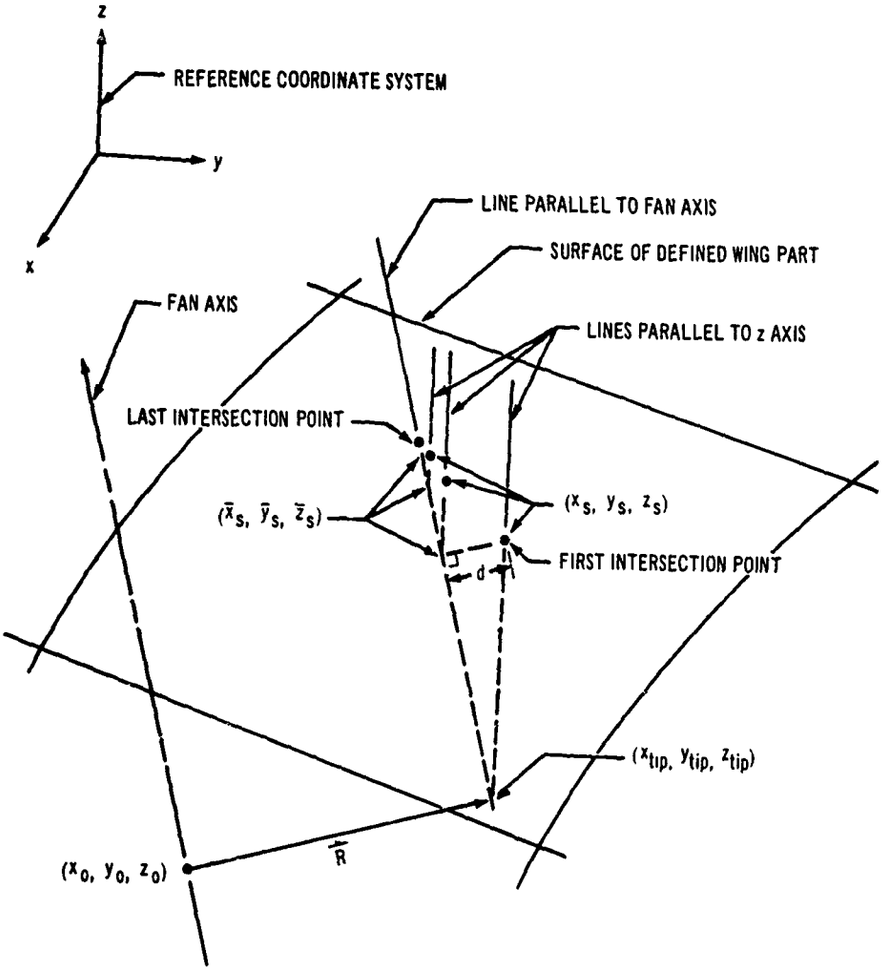

Figure 106. Determination of Surface Intersection Using Iterative Technique.

APPENDIX III
PROGRAM SAMPLE CASES

This appendix contains sample card input formats and computer printouts for sample cases run by the geometry, potential-flow, and boundary-layer programs.

GEOMETRY PROGRAM SAMPLE CASES

The five sample cases run by the geometry program are presented in the following pages.

- A wing; input page 237, printout pages 238-241
- A lifting system; input page 243, printout pages 244, 245
- An inlet network; input page 247, printout pages 248-250
- A jet efflux tube; input page 251, printout pages 252-255
- An axisymmetric centerbody; input page 256, printout pages 257-261

WING input: This sample case is for the wing shown in Figure 107. The wing planform is specified by the four planform corner points input on cards 3 and 4. The inboard airfoil section is defined by card set 6, containing 65 $(x/c, z/c)_i$ coordinates. Since the outboard section is identical, card 7 sets $ORD_O = 0.$ and card set 8 is deleted.

The wing is paneled by the three y_k spanwise dividing planes in card set 10 and the 25 $(x/c)_i$ chordwise divisions in card set 12. Curve-fitting is used for all 25 $(x/c)_i$ panel locations, but only two panel edges near the leading edge are not included in the defining table. The total number of source panels on the right half of the wing is 48.

WING printout: The computer printout lists the input for the wing and the panel coordinate output together with pertinent diagnostic comments as shown on pages 238-241. The panel coordinates were punched on cards that were used in the potential-flow program for the sample case described on page 262.

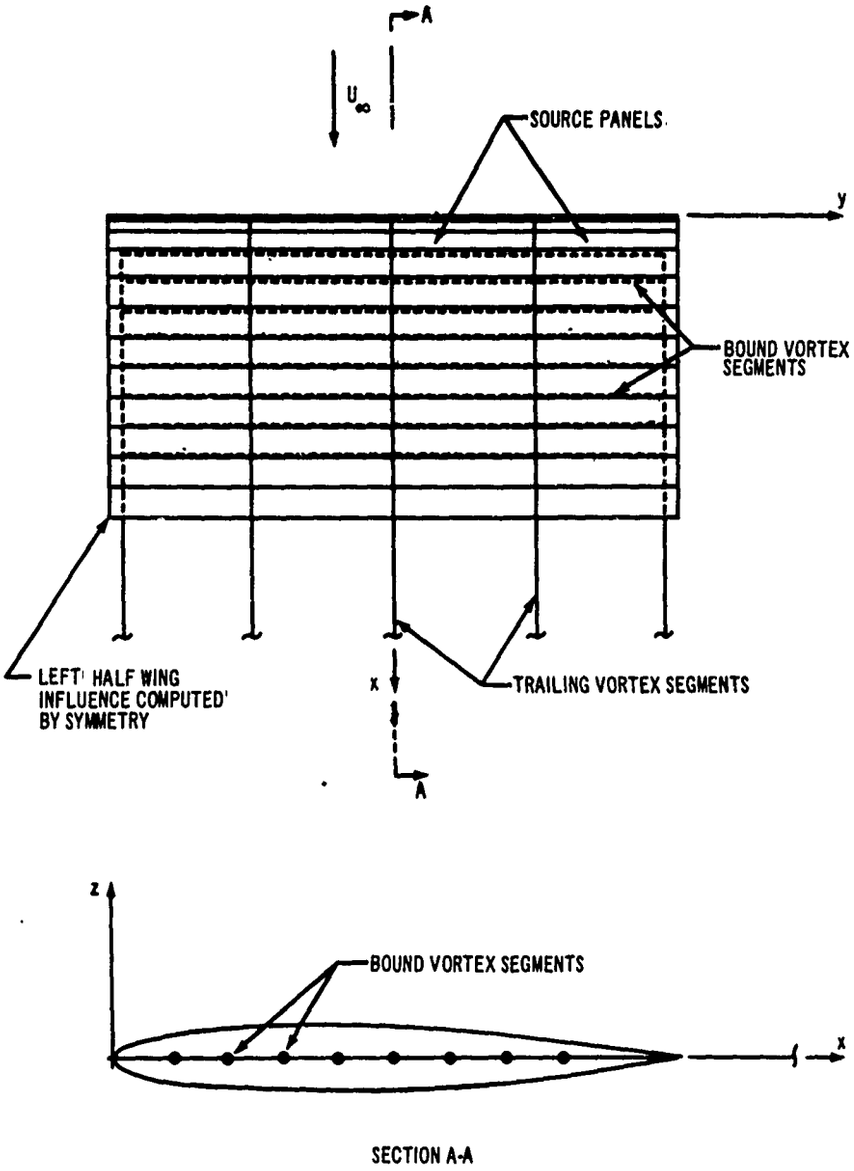

Figure 107. Sample Wing.

SEVEN FIELD, TEN DIGIT CRD FORMAT

1 10	11 20	21 30	31 40	41 50	51 60	61 69/70 71 72	IDENT 80
CASE							
SAMPLE CASE FOR SUBROUTINE WING							TITLE 1
ASPECT RATIO = 2., 48 PANELS RIGHT HALF WING							TITLE 2
CARD							
WING							1
1.							2-PARTS
0.	0.	0.	1.	0.	0.		3
0.	1.	0.	1.	1.	0.		4
65.							5-ORDI
1.	.0	.975	.00301	.95	.00592		6-1
.925	.00914	.9	.01256	.85	.01977		6-2
.8	.02699	.75	.03381	.7	.03992		6-3
.65	.0451	.6	.04923	.55	.05228		6-4
.5	.05429	.45	.05534	.4	.05556		6-5
.35	.05507	.3	.05396	.25	.05222		6-6
.2	.04969	.175	.04799	.15	.04589		6-7
.125	.04325	.1	.03986	.08	.03644		6-8
.06	.03216	.04	.02667	.025	.02135		6-9
.015	.01679	.01	.01392	.006	.01103		6-10
.003	.00806	.0015	.00585	.0	.0		6-11
.0015	-.00585	.003	-.00806	.006	-.01103		6-12
.01	-.01392	.015	-.01679	.025	-.02135		6-13
.04	-.02667	.06	-.03216	.08	-.03644		6-14
.1	-.03986	.125	-.04325	.15	-.04589		6-15
.175	-.04799	.2	-.04969	.25	-.05222		6-16
.3	-.05396	.35	-.05507	.4	-.05556		6-17
.45	-.05534	.5	-.05429	.55	-.05228		6-18
.6	-.04923	.65	-.0451	.7	-.03992		6-19
.75	-.03381	.8	-.02699	.85	-.01977		6-20
.9	-.01256	.925	-.00914	.95	-.00592		6-21
.975	-.00301	1.	.0				6-22
0.							7-ORDO
3.							9-COL
0.	.5	1.					10-1
25.							11-ROW
1.	.9	.8	.7	.6	.5		12-1
.4	.3	.2	.108	.046	.01		12-2
.0	.01	.046	.108	.2	.3		12-3
.4	.5	.6	.7	.8	.9		12-4
1.							12-5
TITLE SAMPLE CASE FOR SUBROUTINE WING			NAME		DATE		PAGE OF

CASE CARD READ. STARTING CASE NUMBER 1

SAMPLE CASE FOR SUBROUTINE WING TITLE1 JUL 07, 1967
ASPECT RATIO = 2.. 48 PANELS RIGHT HALF WING TITLE2

CARD OUTPUT WILL BE OBTAINED FOR THIS CASE.
WING HAS CONTROL.

* * * * * * * * * * * * * * * * INPUT DATA FOR WING * * * * * * * * * * * * * * * *

PARTS = 1.0

* *

THE FOLLOWING DATA REFERS TO PART 1 OF 1 PARTS.

	XLE	YLE	ZLE	XTE	YTE	ZTE
INBOARD =	0.	0.	0.	1.00	0.	0.
OUTBOARD=	0.	1.00	0.	1.00	1.00	0.

ORD = 65.0. INDICATING THAT NEW X/C Z/C COORDS ARE TO BE READ IN.

I	X/C	Z/C	I	X/C	Z/C
1	1.000000	0.	33	0.	0.
2	.975000	.003010	34	.001500	-.005850
3	.950000	.005920	35	.003000	-.008060
4	.925000	.009140	36	.006000	-.011030
5	.900000	.012560	37	.010000	-.013920
6	.850000	.019770	38	.015000	-.016790
7	.800000	.026990	39	.025000	-.021350
8	.750000	.033810	40	.040000	-.026670
9	.700000	.039920	41	.060000	-.032160
10	.650000	.045100	42	.080000	-.036440
11	.600000	.049230	43	.100000	-.039860
12	.550000	.052280	44	.125000	-.043250
13	.500000	.054290	45	.150000	-.045890
14	.450000	.055340	46	.175000	-.047990
15	.400000	.055560	47	.200000	-.049690
16	.350000	.055070	48	.250000	-.052220
17	.300000	.053960	49	.300000	-.053960
18	.250000	.052220	50	.350000	-.055070
19	.200000	.049690	51	.400000	-.055560
20	.175000	.047990	52	.450000	-.055340
21	.150000	.045890	53	.500000	-.054290
22	.125000	.043250	54	.550000	-.052280
23	.100000	.039860	55	.600000	-.049230
24	.080000	.036440	56	.650000	-.045100
25	.060000	.032160	57	.700000	-.039920
26	.040000	.026670	58	.750000	-.033810
27	.025000	.021350	59	.800000	-.026990
28	.015000	.016790	60	.850000	-.019770
29	.010000	.013920	61	.900000	-.012560
30	.006000	.011030	62	.925000	-.009140
31	.003000	.008060	63	.950000	-.005920
32	.001500	.005850	64	.975000	-.003010
			65	1.000000	0.

ORD = 0. . INDICATING THAT OLD X/C-Z/C COORDS ARE TO BE USED.

COL = 3.0

I	Y
1	0.
2	.50
3	1.00

ROW = 25.0. INDICATING THAT CURVE FITTING FOR PANEL COORDS IS DESIRED.

I	X/C	I	X/C	I	X/C
1	1.000000	9	.200000	17	.200000
2	.900000	10	.100000	18	.300000
3	.800000	11	.046000	19	.400000
4	.700000	12	.010000	20	.500000
5	.600000	13	0.	21	.600000
6	.500000	14	.010000	22	.700000
7	.400000	15	.046000	23	.800000
8	.300000	16	.100000	24	.900000
				25	1.000000

COORDINATE OUTPUT. PART 1 OF 1

NETWORK	COLUMN	ROW	X	Y	Z
1	1	1	1.000000	0.	.000000
1	1	2	.900000	0.	.012560
1	1	3	.800000	0.	.026990
1	1	4	.700000	0.	.039920
1	1	5	.600000	0.	.049230
1	1	6	.500000	0.	.054290
1	1	7	.400000	0.	.055560
1	1	8	.300000	0.	.053960
1	1	9	.200000	0.	.049690
1	1	0	.108000	0.	.041043
1	1	11	.046000	0.	.028487
1	1	12	.010000	0.	.013920
1	1	13	0.	0.	-.000000
1	1	14	.010000	0.	-.013920
1	1	15	.046000	0.	-.028487
1	1	16	.108000	0.	-.041043
1	1	17	.200000	0.	-.049690
1	1	18	.300000	0.	-.053960
1	1	19	.400000	0.	-.055560
1	1	20	.500000	0.	-.054290
1	1	21	.600000	0.	-.049230
1	1	22	.700000	0.	-.039920
1	1	23	.800000	0.	-.026990
1	1	24	.900000	0.	-.012560
1	1	25	1.000000	0.	-.000000
1	2	1	1.000000	.500000	.000000
1	2	2	.900000	.500000	.012560
1	2	3	.800000	.500000	.026990
1	2	4	.700000	.500000	.039920
1	2	5	.600000	.500000	.049230
1	2	6	.500000	.500000	.054290
1	2	7	.400000	.500000	.055560
1	2	8	.300000	.500000	.053960
1	2	9	.200000	.500000	.049690
1	2	10	.108000	.500000	.041043
1	2	11	.046000	.500000	.028487
1	2	12	.010000	.500000	.013920
1	2	13	0.	.500000	-.000000
1	2	14	.010000	.500000	-.013920
1	2	15	.046000	.500000	-.028487
1	2	16	.108000	.500000	-.041043
1	2	17	.200000	.500000	-.049690
1	2	18	.300000	.500000	-.053960
1	2	19	.400000	.500000	-.055560
1	2	20	.500000	.500000	-.054290
1	2	21	.600000	.500000	-.049230
1	2	22	.700000	.500000	-.039920
1	2	23	.800000	.500000	-.026990
1	2	24	.900000	.500000	-.012560
1	2	25	1.000000	.500000	-.000000
1	3	1	1.000000	1.000000	.000000
1	3	2	.900000	1.000000	.012560

1	3	3	.800000	1.000000	.026990
1	3	4	.700000	1.000000	.039920
1	3	5	.600000	1.000000	.049230
1	3	6	.500000	1.000000	.054290
1	3	7	.400000	1.000000	.055560
1	3	8	.300000	1.000000	.053960
1	3	9	.200000	1.000000	.049690
1	3	10	.100000	1.000000	.041043
1	3	11	.044000	1.000000	.028487
1	3	12	.010000	1.000000	.013920
1	3	13	0.	1.000000	-.000000
1	3	14	.010000	1.000000	-.013920
1	3	15	.044000	1.000000	-.028487
1	3	16	.100000	1.000000	-.041043
1	3	17	.200000	1.000000	-.049690
1	3	18	.300000	1.000000	-.053960
1	3	19	.400000	1.000000	-.055560
1	3	20	.500000	1.000000	-.054290
1	3	21	.600000	1.000000	-.049230
1	3	22	.700000	1.000000	-.039920
1	3	23	.800000	1.000000	-.026990
1	3	24	.900000	1.000000	-.012560
1	3	25	1.000000	1.000000	-.000000

WING RELINQUISHING CONTROL.

SAMPLE CASE FOR SUBROUTINE WING
ASPECT RATIO = 2., 48 PANELS RIGHT HALF WING

TITLE1 JUL 07, 1967
TITLE2

LIFT input: The input for the lifting system for the wing shown in Figure 107 is shown on page 243. The position of the lifting system is defined by cards 3 and 4, which are identical to those for the corresponding wing PART. The descriptive coordinates of the nine bound vortices are given in card set 6. The $(z/c)_i$ values have been located so that the bound vortices are approximately equidistant from the two nearest source-panel boundary points. Since the outboard coordinates are identical, card 7 sets $ROWI_O = 0.$ and card set 8 is deleted. The three y_k values are given in card set 10.

For the trailing sheet, one vortex segment is used (card 11) whose length is 3999 (card set 12) and whose direction cosines are given in card set 13. Because the outboard trailing segment is identical, card 14 sets $ROWT_O = 0.$ and card sets 15 and 16 are deleted. The $(x/c, z/c)_i$ coordinates of the eight trailing-edge points (see Figure 25) needed for determination of the multi-horseshoe boundary point are input on cards 17, 18, and 19. The three y_k values input on card 21 define the streamwise source-panel edges, rather than the actual location of the boundary point. The boundary point is placed off the wing trailing edge a distance 0.05 times at the upper surface source-panel length.

LIFT printout: The printout for the lifting system, shown on pages 244 through 245, includes a listing of the input with appropriate diagnostic comments, the (x,y,z) coordinate output of the internal lifting system and trailing vortex sheet, the positions of the boundary points, and the direction cosines of their normal vectors. The output was also punched on cards that were transferred to the potential-flow program and used for the sample case described on page 262.

SEVEN FIELD, TEN DIGIT CRD FORMAT

1 10	11 20	21 30	31 40	41 50	51 60	61 69	70 71	72	IDENT 80
CASE									
SAMPLE CASE FOR SUBROUTINE LIFT									TITLE 1
LIFTING SYSTEM FOR ASPECT RATIO 2 WING									TITLE 2
CARD									
LIFT									1
1.									2-PARTS
0.	0.	0.	1.	0.	0.				3
0.	1.	0.	1.	1.	0.				4
9.									5-ROWII
.1208	.0	.205	.0	.3012	.0				6-1
.4	.0	.498	.0	.5967	.0				6-2
.6953	.0	.7963	.0	1.	.0				6-3
0.									7-ROWIO
3.									9-COL
0.	.5	.95							10-1
1.									11-ROWTI
3999.									12-1
1.	0.	0.							13-1
0.									14-ROWTO
1.	.0	.9	.01256	.9	-.01256				17
1.	.0	1.	.0	.9	.01256				18
.9	-.01256	1.	.0						19
3.	0.	.05							20-NY
.0	.5	1.							21
TITLE SAMPLE CASE FOR SUBROUTINE LIFT				NAME		DATE			PAGE 1 OF 1

```
                    CASE CARD READ.  STARTING CASE NUMBER  2
                    SAMPLE  CASE  FOR  SUBROUTINE  LIFT                                  TITLE1    JUN 09, 1967
                    LIFTING  SYSTEM  FOR  ASPECT  RATIO  2  WING                         TITLE2
CARD OUTPUT WILL BE OBTAINED FOR THIS CASE.
LIFT HAS CONTROL.

* * * * * * * * * * * * * * *    I N P U T    D A T A    F O R    L I F T    * * * * * * * * * * * * * * *
                                              PARTS =  1.0
* * * * * * * * * * * * * * * * * * * * * * * * * * * * * * * * * * * * * * * * * * * * * * * * * * * * *

                    THE FOLLOWING DATA REFERS TO PART  1 OF  1 PARTS.

                          XLE        YLE        ZLE        XTE        YTE        ZTE
             INBOARD =    0.         0.         0.         1.00       0.         0.
             OUTBOARD=    0.         1.00       0.         1.00       1.00       0.

      ROW  INTERNAL  (INBOARD) =  9.0 INDICATING THAT NEW X/C-Z/C COORDINATES ARE TO BE READ IN.

             I      X/C          Z/C                     I      X/C          Z/C
             1     .120800      0.                       5     .498000      0.
             2     .205000      0.                       6     .596700      0.
             3     .301200      0.                       7     .695300      0.
             4     .400000      0.                       8     .796300      0.
                                                         9    1.000000      0.

      ROW  INTERNAL (OUTBOARD) =  0.  INDICATING THAT OLD X/C-Z/C COORDINATES ARE TO BE USED.

                                     COL =   3.0

                                     I        Y
                                     1       0.
                                     2        .50
                                     3        .95

      ROW  TRAILING  (INBOARD) =  1.0, INDICATING THAT NEW LENGTHS AND COSINES ARE TO BE READ IN.

             I       L                  I       L                  I       L
                                                                   1   3999.000000

             I           X-COSINE             Y-COSINE             Z-COSINE
             1           1.000000             0.                   0.

      ROW  TRAILING (OUTBOARD) =  0. , INDICATING THAT OLD LENGTHS AND COSINES ARE TO BE USED.
                                       TRAILING EDGE COORDINATES
                                  POINT 1      POINT 2      POINT 3      POINT 4
            INBOARD     X/C      1.000000      .900000      .900000     1.000000
                        Z/C      0.            .012560     -.012560     0.
```

OUTBOARD	X/C	1.000000	.900000	.900000	1.000000
	Z/C	0.	.012560	-.012560	0.

NY = 3.0
YCODE = 0.
EBP = .05000000

I	Y
1	0.
2	.50
3	1.00

C O O R D I N A T E O U T P U T , P A R T 1 O F 1

INTERNAL LIFTING SYSTEM

NETWORK	COLUMN	ROW	X	Y	Z
1	1	1	.120800	0.	0.
1	1	2	.205000	0.	0.
1	1	3	.301200	0.	0.
1	1	4	.400000	0.	0.
1	1	5	.498000	0.	0.
1	1	6	.596700	0.	0.
1	1	7	.695300	0.	0.
1	1	8	.796300	0.	0.
1	1	9	1.000000	0.	0.
1	2	1	.120800	.500000	0.
1	2	2	.205000	.500000	0.
1	2	3	.301200	.500000	0.
1	2	4	.400000	.500000	0.
1	2	5	.498000	.500000	0.
1	2	6	.596700	.500000	0.
1	2	7	.695300	.500000	0.
1	2	8	.796300	.500000	0.
1	2	9	1.000000	.500000	0.
1	3	1	.120800	.950000	0.
1	3	2	.205000	.950000	0.
1	3	3	.301200	.950000	0.
1	3	4	.400000	.950000	0.
1	3	5	.498000	.950000	0.
1	3	6	.596700	.950000	0.
1	3	7	.695300	.950000	0.
1	3	8	.796300	.950000	0.
1	3	9	1.000000	.950000	0.

TRAILING VORTEX SHEET

NETWORK	COLUMN	ROW	X	Y	Z
1	1	10	4000.000000	0.	0.
1	2	10	4000.000000	.500000	0.
1	3	10	4000.000000	.950000	0.

BOUNDARY POINTS

COLUMN	X	Y	Z	DCX	DCY	DCZ
1	1.005039	.250000	0.	0.	0.	1.000000
2	1.005039	.750000	0.	0.	0.	1.000000

LIFT RELINQUISHING CONTROL.

SAMPLE CASE FOR SUBROUTINE LIFT
LIFTING SYSTEM FOR ASPECT RATIO 2 WING

TITLE1 JUN 09, 1967
TITLE2

INLET input: The input shown on page 247 is for an upper and lower surface network of the fan-in-wing configuration shown in Figure 91. The networks are in REGION 1 of the inlet (see Figure 27), the transition region from the regular wing paneling to the pseudoaxisymmetric inlet paneling. The INLET subroutine uses a wing PART for a surface definition. The planform definition for the wing PART is on cards 2 and 3. The inboard section is the modified NACA 65-210 airfoil, whose 62 $(x/c, z/c)_i$ coordinates are input in card set 5. Since the outboard section is identical, card 6 sets $ORD_O = 0.$ and card set 7 is deleted. On card 8, TYPE = 0. indicates that the wing is defined by lines connecting the ordered sets of airfoil coordinates. The iteration tolerance is set equal to a small value. For this orientation of the fan axis (card 9), the iteration will produce the exact surface intersection in the first computer cycle. Cards 2 through 9 complete the definition of the wing and the fan axis. The remaining cards are for REGION 1.

Two PARTS in REGION 1 are prepared, one network on the upper surface and another on the lower surface. Three f_i fraction values and five (x,y) coordinates along the boundary of the network are employed to construct the remaining coordinates. Note that a considerable number of input cards is needed to produce, in this case, a relatively small number of output cards for these two source-panel networks. Over half the input, however, defines the wing geometry, and a comparatively small number of cards is needed to panel the different REGIONS of the inlet.

The last card of the geometry program indicates the end of the inlet geometry. When the program encounters this card, execution is returned to the main program. The program then seeks a new control card (such as WING, CASE, CARD, EXIT, etc.) and continues accordingly.

INLET printout: The printout for the inlet network is shown on pages 248 through 250. The printout includes all the input quantities that define the wing PART and the fan axis for subroutine INLET; the input for the first PART of REGION 1, which is on the upper surface; and the (x,y,z) coordinate output. The last page of the printout lists the input and (x,y,z) coordinate output for the second PART or network, which is on the lower surface. The (x,y,z) coordinates were also punched on cards for input to the potential-flow program.

These two small networks were only a minor part of the inlet geometry for the NASA fan-in-wing configuration (see Figure 27). The other networks were similarly prepared with other REGIONS of the INLET subroutine.

SEVEN FIELD, TEN DIGIT CRD FORMAT

1 10	11 20	21 30	31 40	41 50	51 60	61 69	70 71 72	IDENT 80
CASE								
INLET NETWORK NUMBER	10 FOR NASA FAN - IN - WING							TITLE 1
CARD								
INLET								1
0.	0.	0.	176.52	0.	0.			2
88.32	231.72	0.	176.52	231.72	0.			3
62.								4-ORDI
1.	.0	.9875	.0015	.975	.0029			5-1
.95014	.00622	.90028	.01327	.85038	.02057			5-2
.80044	.02783	.75045	.03479	.70043	.04128			5-3
.65036	.04712	.60027	.05217	.55014	.05625			5-4
.5	.05915	.44984	.06058	.39968	.06067			5-5
.34951	.05954	.29936	.05732	.24921	.05397			5-6
.19909	.04938	.14899	.04338	.09894	.03515			5-7
.07394	.03069	.04898	.02491	.02408	.01757			5-8
.01169	.01273	.00678	.00999	.00435	.00819			5-9
.0025	.00643	.00125	.00477	.0005	.00324			5-10
.00005	.00149	.0	.0	.00023	.00125			5-11
.001	-.00302	.00225	-.00476	.00375	-.00624			5-12
.00569	-.00776	.00827	-.00925	.01337	-.01141			5-13
.02598	-.01498	.0511	-.02014	.07614	-.02431			5-14
.10417	-.02812	.13889	-.03194	.17361	-.03486			5-15
.20833	-.03708	.27778	-.03868	.34722	-.0391			5-16
.41667	-.03924	.48611	-.03861	.55556	-.03618			5-17
.625	-.03146	.65972	-.02806	.69954	-.02404			5-18
.74952	-.01867	.79953	-.01325	.84959	-.00803			5-19
.8997	-.00344	.94985	.00009	.975	.0006			5-20
.9875	.0006	1.	.0					5-21
0.								6-ORDO
0.	.00001							8
90.12	85.44	0.	0.	0.	1.			9
1.								10. 1
2.								11. 1PART
1.								12. 1CODE
3.								13. 1-M
.0	.5	1.						14. 1-1
5.								15. 1-NP
111.35199	148.56	97.66988	148.56	83.98779	148.56			16. 1-1
73.04209	148.56	64.72343	148.56					16. 1-2
105.38559	132.42236	95.28588	132.40185	85.18618	132.38134			17. 1-1
76.87809	127.57362	68.57	122.76589					17. 1-2
-1.								12. 1CODE
3.								13. 1-M
.0	.5	1.						14. 1-1
5.								15. 1-NP
64.72343	148.56	73.04209	148.56	83.98779	148.56			16. 1-1
97.66988	148.56	111.35199	148.56					16. 1-2
68.57	122.76589	76.87809	127.57362	85.18618	132.38134			17. 1-1
95.28588	132.40185	105.38559	132.42236					17. 1-2
0.								
TITLE SAMPLE CASE FOR SUBROUTINE INLET				NAME		DATE		PAGE OF

CASE CARD READ. STARTING CASE NUMBER 3

INLET NETWORK NUMBER 10 FOR
NASA FAN - IN - WING

TITLE1 JUN 09, 1967
TITLE2

CARD OUTPUT WILL BE OBTAINED FOR THIS CASE.
INLET HAS CONTROL.

********** INPUT DATA FOR INLET **********

WING DEFINITION

	XLE	YLE	ZLE	XTE	YTE	ZTE
INBOARD =	0.	0.	0.	176.52	0.	0.
OUTBOARD=	88.32	231.72	0.	176.52	231.72	0.

ORDE(1) = 62

I	X/C	Z/C	I	X/C	Z/C	I	X/C	Z/C	I	X/C	Z/C
1	1.000000	0.	16	.349510	.059540	31	.003050	.001490	46	.208330	-.037090
2	.987500	.001500	17	.299360	.057320	32	0.	0.	47	.277780	-.038680
3	.975000	.002900	18	.249210	.053970	33	.003230	-.001250	48	.347220	-.039100
4	.950160	.006220	19	.199090	.049380	34	.001100	-.003020	49	.416670	-.039240
5	.900240	.013270	20	.148990	.043380	35	.002250	-.004760	50	.486110	-.038610
6	.850290	.020570	21	.099960	.035450	36	.003750	-.006240	51	.555560	-.036180
7	.800440	.027830	22	.073940	.030690	37	.005690	-.007760	52	.625000	-.031460
8	.750490	.034790	23	.048380	.024410	38	.008270	-.009250	53	.694720	-.023060
9	.700430	.041280	24	.024080	.017570	39	.013370	-.011410	54	.699540	-.024040
10	.650360	.047120	25	.011690	.012730	40	.025980	-.014980	55	.749520	-.018670
11	.600270	.052170	26	.006780	.009990	41	.051100	-.020140	56	.799530	-.013250
12	.55. 40	.056250	27	.004350	.008190	42	.076140	-.024310	57	.849590	-.008030
13	.500000	.059150	28	.002500	.006430	43	.104170	-.028120	58	.899700	-.003440
14	.449840	.060580	29	.001250	.004770	44	.138890	-.031940	59	.949850	.000090
15	.399680	.060670	30	.000500	.003240	45	.173610	-.034860	60	.975000	.000600
									61	.987500	.000600
									62	1.000000	0.

ORDE 2) = 0

TYPE = 0
EPS = .00001

XO = 90.1
YO = 85.4
ZO = 0.
ETAX = 0.
ETAY = 0.
ETAZ = 1.00000

***** REGION = 1 *****

PARTS = 2

CODE = 1

M = 3

I	PC(I)
1	0.
2	.500
3	1.000

NP = 5

I	J	X(I,J)	Y(I,J)
1	1	111.351990	148.560000
2	1	97.669880	148.560000
3	1	83.987770	148.560000
4	1	73.042090	148.560000
5	1	64.723430	148.560000
1	2	105.385590	132.422360
2	2	95.285880	132.401850
3	2	85.186180	132.381340
4	2	76.878090	127.573620
5	2	68.570000	122.765890

UPPER SURFACE COORDINATES

NETWORK	COLUMN	ROW	X	Y	Z
1	1	1	111.351990	148.560000	7.250016
1	1	2	108.368790	140.491180	7.456585
1	1	3	105.385590	132.422360	7.655846
1	2	1	97.669880	148.560000	7.108867
1	2	2	96.477880	140.480925	7.320382
1	2	3	95.285880	132.401850	7.529916
1	3	1	83.987790	148.560000	6.259625
1	3	2	84.586985	140.470670	6.668447
1	3	3	85.186180	132.381340	7.043526
1	4	1	73.042090	148.560000	4.997056
1	4	2	74.960090	138.066810	5.861702
1	4	3	76.878090	127.573620	6.592071
1	5	1	64.723430	148.560000	3.514847
1	5	2	66.646715	135.662945	4.876176
1	5	3	68.570000	122.765890	5.946460

CODE = -1

M = 3

I	PC(I)
1	0.
2	.500
3	1.000

NP = 5

I	J	X(I,J)	Y(I,J)
1	1	64.723430	148.560000
2	1	73.042090	148.560000
3	1	83.987790	148.560000
4	1	97.669880	148.560000
5	1	111.351990	148.560000
1	2	68.570000	122.765890
2	2	76.878090	127.573620
3	2	85.186180	132.381340
4	2	95.285880	132.401850
5	2	105.385590	132.422360

LOWER SURFACE COORDINATES

NETWORK	COLUMN	ROW	X	Y	Z
2	1	1	64.723430	148.560000	-2.754221
2	1	2	66.646715	135.662945	-3.737538
2	1	3	68.570000	122.765890	-4.466285
2	2	1	73.042090	148.560000	-3.806640
2	2	2	74.960090	138.066810	-4.379037
2	2	3	76.878090	127.573620	-4.810849
2	3	1	83.987790	148.560000	-4.537959
2	3	2	84.586985	140.470670	-4.715430
2	3	3	85.186180	132.381340	-4.872007
2	4	1	97.669880	148.560000	-4.685758
2	4	2	96.477880	140.480925	-4.809304
2	4	3	95.285880	132.401850	-4.933134
2	5	1	111.351990	148.560000	-4.681387
2	5	2	108.368790	140.491180	-4.810906
2	5	3	105.385590	132.422360	-4.937546

ZERO VALUE FOR REGION READ.

INLET RELINQUISHING CONTROL.

INLET NETWORK NUMBER 10 FOR
NASA FAN - IN - WING

TITLE1 JUN 09, 1967
TITLE2

TUBE input: The input is shown below for part of the efflux tube shown in Figure 91(b). Because only part of the efflux tube was generated for this sample case, no cards were prepared for the potential-flow program. The CARD control card was, therefore, omitted. The efflux tube was computed for a velocity ratio of $U_\infty/V_j = 0.275$, and the angles of attack and yaw were zero. Sixteen initial $(x,y,z)_i$ coordinates on the wing lower surface and six s_k arc lengths were used to generate the tube. The adjustment to the shape of the wing lower surface is taken up in the first five arc-length segments. The multihorseshoe boundary points are located below the wing surface 0.05 of the distance to the first row of vortices.

TUBE printout: The printout for the tube is shown on pages 252 through 255. The printout lists the input data, the (x,y,z) coordinate output, the multihorseshoe boundary point coordinates, and the direction cosines of the normal vectors at the boundary points. No cards were printed out.

SEVEN FIELD, TEN DIGIT CRD FORMAT

1 10	11 20	21 30	31 40	41 50	51 60	61 69/70 71	72	IDENT 80
CASE								
JET EFFLUX	TUBE FOR NASA FAN - IN - WING							TITLE 1
VELOCITY RATIO = 0.275,	BETA = ALPHA = PSI = 0.							TITLE 2
TUBE								1
90. 12	85. 44	0.	0.	0.	1.			2
0.	0.	-1.						3
.275	0.	0.	62. 5					4
16.								5-M
121. 37	85. 44	-4. 5738	118. 6683	98. 1505	-4. 7934			6-1
111. 0303	108. 6633	-5. 0908	99. 7768	115. 1605	-5. 2017			6-2
86. 8535	116. 5188	-5. 2725	74. 4950	112. 5033	-5. 0832			6-3
64. 8382	103. 8083	-4. 8818	59. 5529	91. 9372	-4. 9402			6-4
59. 5529	78. 9428	-5. 3875	64. 8382	67. 0717	-5. 7273			6-5
74. 4950	58. 3767	-6. 3233	86. 8535	54. 3612	-6. 1080			6-6
99. 7768	55. 7195	-5. 9087	111. 0303	62. 2167	-5. 3923			6-7
118. 6683	72. 7295	-4. 8060	121. 37	85. 44	-4. 5738			6-8
6.								7-N
3. 125	9. 375	15. 625	21. 875	28. 125	34. 5625			8-1
5.	.1111	.05						9
TITLE SAMPLE CASE FOR SUBROUTINE TUBE			NAME			DATE	PAGE	OF

CASE CARD READ. STARTING CASE NUMBER 4

JET EFFLUX TUBE FOR NASA FAN - IN - WING
VELOCITY RATIO = 0.275, BETA = ALPHA = PSI = 0.

TUBE HAS CONTROL.

TITLE1 JUN 09, 1967
TITLE2

• • • • • • • • • • • • • • • • INPUT DATA FOR TUBE • • • • • • • • • • • • • • • •

XTUBE = 90.120000
YTUBE = 85.440000
ZTUBE = 0.
NX = 0.
NY = 0.
NZ = 1.000000

TX = 0.
TY = 0.
TZ = -1.000000

VELOCITY RATIO = .275000
ALPHA = 0.
PSI = 0.
DIAMETER = 62.500000

N = 16

I	X(I)	Y(I)	Z(I)
1	121.370000	85.440000	-4.573800
2	118.668300	98.150500	-4.793400
3	111.030300	108.663300	-5.090800
4	99.776800	115.160500	-5.201700
5	86.853500	116.518800	-5.272500
6	74.495000	112.503[illegible]	-5.083200
7	64.838200	10[illegible]	-4.881800
8	59.552900	[illegible]	-4.940200
9	59.552900	[illegible]	-5.387500
10	64.838200	[illegible]	-5.727300
11	74.495000	[illegible]	-6.323300
12	86.853500	[illegible]	-6.108000
13	99.776800	[illegible]	-5.908700
14	111.030300	[illegible]	-5.392300
15	118.668300	[illegible]	-4.806000
16	121.370000	[illegible]	-4.573800

N = 6

J	S(J)
1	3.125000
2	9.375000
3	15.625000
4	21.875000
5	28.125000
6	34.562500

NTR = 5.000000
DEL = .111100
ESP = .050000

COORDINATE OUTPUT

COLUMN	ROW	X	Y	Z
1	1	121.370077	85.440000	-7.771498
1	2	118.668397	98.150500	-7.986523
1	3	111.030428	108.663300	-8.231239
1	4	99.774941	115.160500	-8.331184
1	5	86.853650	116.518800	-8.395915
1	6	74.495127	112.503300	-8.229185
1	7	64.838306	103.808300	-8.051024
1	8	59.553012	91.937200	-8.103664
1	9	59.553066	78.942800	-8.502338
1	10	64.838416	67.071700	-8.804328
1	11	74.495328	58.376700	-9.333259
1	12	86.853784	54.361200	-9.138829
1	13	99.777046	55.719500	-8.959031
1	14	111.030466	62.216700	-8.498733
1	15	118.668398	72.729500	-7.977698
1	16	121.370077	85.440000	-7.771498
2	1	121.372675	85.440000	-13.498222
2	2	118.671189	98.150500	-13.702087
2	3	111.033600	108.663300	-14.065089
2	4	99.780465	115.160500	-14.383764
2	5	86.857592	116.518800	-14.712541
2	6	74.499256	112.503300	-14.855197
2	7	64.842526	103.808300	-14.930193
2	8	59.557415	91.937200	-15.084281
2	9	59.557844	78.942800	-15.384946
2	10	64.843335	67.071700	-15.497753
2	11	74.500459	58.376700	-15.685559
2	12	86.858359	54.361200	-15.270051
2	13	99.781085	55.719500	-14.853831
2	14	111.033831	62.216700	-14.264946
2	15	118.671198	72.729500	-13.710424
2	16	121.372675	85.440000	-13.498222
3	1	121.382979	85.440000	-19.223201
3	2	118.681944	98.150500	-19.436571
3	3	111.045448	108.663300	-19.898650
3	4	99.793759	115.160500	-20.436287
3	5	86.872475	116.518800	-21.029145
3	6	74.515480	112.503300	-21.481406
3	7	64.859736	103.808300	-21.810106
3	8	59.575305	91.937200	-22.065654
3	9	59.576126	78.942800	-22.267203
3	10	64.861259	67.071700	-22.190197
3	11	74.517657	58.376700	-22.036515
3	12	86.873849	54.361200	-21.401033
3	13	99.794831	55.719500	-20.749119
3	14	111.045867	62.216700	-20.031379
3	15	118.681960	72.729500	-19.442700
3	16	121.382979	85.440000	-19.223201

4	1	121.406433	85.440000	-24.946403
4	2	118.706151	98.150500	-25.169942
4	3	111.071789	108.663300	-25.731885
4	4	99.823251	115.160500	-26.488711
4	5	86.905590	116.518800	-27.345674
4	6	74.552064	112.503300	-28.107749
4	7	64.899028	103.808300	-28.690694
4	8	59.616079	91.937200	-29.047713
4	9	59.616994	78.942800	-29.149038
4	10	64.900532	67.071700	-28.881596
4	11	74.534176	58.376700	-28.386067
4	12	86.906916	54.361200	-27.531723
4	13	99.824287	55.719500	-26.644852
4	14	111.072196	62.216700	-25.797994
4	15	118.706167	72.729500	-25.172692
4	16	121.406433	95.440000	-24.946403
5	1	121.448599	85.440000	-30.667758
5	2	118.749412	98.150500	-30.902126
5	3	111.118518	108.663300	-31.564711
5	4	99.875488	115.160500	-32.540935
5	5	86.964212	116.518800	-33.662012
5	6	74.617210	112.503300	-34.734093
5	7	64.969394	103.808300	-35.571805
5	8	59.689012	91.937200	-36.030297
5	9	59.689012	78.942800	-36.030297
5	10	64.969394	67.071700	-35.571805
5	11	74.617210	58.376700	-34.734093
5	12	86.964212	54.361200	-33.662012
5	13	99.875488	55.719500	-32.540935
5	14	111.118518	62.216700	-31.564711
5	15	118.749412	72.729500	-30.902126
5	16	121.448599	85.440000	-30.667758
6	1	121.515420	85.440000	-36.408447
6	2	118.818423	98.150500	-36.703000
6	3	111.193717	108.663300	-37.535733
6	4	99.959804	115.160500	-38.762646
6	5	87.058997	116.518800	-40.171609
6	6	74.722008	112.503300	-41.518995
6	7	65.082016	103.808300	-42.571828
6	8	59.805915	91.937200	-43.148058
6	9	59.805915	78.942800	-43.148058
6	10	65.082016	67.071700	-42.571828
6	11	74.722008	58.376700	-41.518995
6	12	87.058997	54.361200	-40.171609
6	13	99.959804	55.719500	-38.762646
6	14	111.193717	62.216700	-37.535733
6	15	118.818423	72.729500	-36.703000
6	16	121.515420	85.440000	-36.408447

BOUNDARY POINT COORDINATES AND DIRECTION COSINES

X	Y	Z	NX	NY	NZ
120.019154	91.795250	-4.842871	.978144	-.207911	.000027
114.869306	103.609900	-5.099930	.309017	-.587785	.000029
105.403567	111.911900	-5.302906	.+00000	-.866026	.000021
93.315167	15.833660	-5.393422	.104529	-.994522	.000005
80.674267	14.511950	-5.334495	-.309016	.951057	-.000014
59.566604	103.155300	-5.140390	-.669130	.743146	-.000025
52.135555	97.877250	-5.069317	-.913547	.406733	-.000031
59.552907	89.640250	-5.320000	-1.000000	-.000001	-.000044
52.135560	3.007250	-5.712197	-.913547	-.406734	-.000056
59.566614	82.726250	-6.177675	-.669129	-.743146	-.000060
80.674265	56.368950	-6.366870	-.309016	-.951057	-.000031
93.315163	55.040350	-6.160370	.104529	-.994522	.000009
105.403560	53.963100	-5.904419	.500000	-.866026	.000033
114.449307	67.473100	-5.256103	.309017	-.587785	.000034
120.019154	79.084250	-4.869135	.978149	-.207911	.000027

TUBE RELINQUISHING CONTROL.

JET EFFLUX TUBE FOR NASA FAN - IN - WING
VELOCITY RATIO = 0.275, BETA = ALPHA = PSI = 0.

TITLE1 JUN 09, 1967
TITLE2

AXISYM input: The input is shown below for the centerbody for the NASA fan-in-wing configuration. One input table of seven $(r,z)_i$ coordinates defines the centerbody paneling arrangement. The angular panel spacing is specified by 16 θ_k values. The remaining input quantities (cards 6-12) specify the position and orientation of the centerbody and its distortion ($k_1 = k_2 = k_3 = 1.$ in this case). Card 12 sets OUTCODE = 1. so that the radii vary first on the output to form a right-hand source-panel network. The EXIT control card is used as the last card in the data deck for these five sample cases and causes execution to be returned to the computer monitor control system.

AXISYM printout: The printout for the centerbody is shown on pages 257 through 261. The printout lists the input and the (x,y,z) coordinate output. Cards were punched for this case.

SEVEN FIELD, TEN DIGIT CRD FORMAT

CASE										
AXISYMMETRIC CENTERBODY FOR NASA FAN - IN - WING										TITLE 1
CARD										
AXISYM										1
7.	1.									2-MN1
13.	-1.8	13.	1.8	12.95	5.7					3.1-1
11.5	9.2	9.2	11.5	5.5	13.5					3.1-2
0.	13.5									3.1-3
16.										4-N2
0.	24.	48.	72.	96.	120.					5-1
144.	168.	192.	216.	240.	264.					5-2
288.	312.	336.	360.							5-3
90.1.	85.44	0.								6
1	0.	0.								7
0.	1.	0.								8
0.	0.	1.								9
1.	1.	1.								10
0.	0.	0.								11
1										12
EXIT										
SAMPLE CASE FOR SUBROUTINE AXISYM				NAME			DATE		PAGE OF	

CASE CARD READ. STARTING CASE NUMBER 5

AXISYMMETRIC CENTERBODY FOR
NASA FAN - IN - WING

TITLE1 JUN 09, 1967
TITLE2

CARD OUTPUT WILL BE OBTAINED FOR THIS CASE.
AXISYM HAS CONTROL.

• • • • • • • • • • • • • • • • INPUT DATA FOR AXISYM • • • • • • • • • • • • • • • •

M = 7.0

I	R(I)	Z(I)	I
1	13.000000	-1.800000	1
2	13.000000	1.800000	2
3	12.950000	5.700000	3
4	11.500000	9.200000	4
5	9.200000	11.500000	5
6	5.500000	13.500000	6
7	0.	13.500000	7

N = 16.0

J	THETA(J)
1	0.
2	24.00000000
3	48.00000000
4	72.00000000
5	96.00000000
6	120.00000000
7	144.00000000
8	168.00000000
9	192.00000000
10	216.00000000
11	240.00000000
12	264.00000000
13	288.00000000
14	312.00000000
15	336.00000000
16	360.00000000

ORIGIN COORDINATES OF THE (X1, Y1, Z1) COORDINATE SYSTEM
WITH RESPECT TO THE (X, Y, Z) REFERENCE COORDINATE SYSTEM

XO = 90.12000
YO = 85.44000
ZO = 0.

DIRECTION COSINES FOR TRANSFORMATION TO THE
(X, Y, Z) REFERENCE COORDINATE SYSTEM

			WITH RESPECT TO		
			X	Y	Z
A	ZI	=	1.0000000	0.	0.
X	YI	=	0.	1.0000000	0.
I	ZI	=	0.	0.	1.0000000
S		=			

DISTORTION FACTORS FOR THE (X, Y, Z) COORDINATES

KI = 1.0000000
K2 = 1.0000000
K3 = 1.0000000

DISPLACEMENT FACTORS FOR THE (X, Y, Z) COORDINATES

XP = 0.
YP = 0.
ZP = 0.

OUTCODE = 1.0
RADII WILL VARY FIRST.

C O O R D I N A T E O U T P U T

I	J	X(I,J)	Y(I,J)	Z(I,J)
1	1	103.120000	85.440000	-1.800000
2	1	103.120000	85.440000	1.800000
3	1	103.070000	85.440000	5.700000
4	1	101.620000	85.440000	9.200000
5	1	99.320000	85.440000	11.500000
6	1	95.620000	85.440000	13.500000
7	1	90.120000	85.440000	13.500000
1	2	101.996091	90.727576	-1.800000
2	2	101.996091	90.727576	1.800000
3	2	101.950414	90.707239	5.700000
4	2	100.625773	90.117471	9.200000
5	2	98.524618	89.181977	11.500000
6	2	95.144500	87.677051	13.500000
7	2	90.120000	85.440000	13.500000
1	3	98.818698	95.100883	-1.800000
2	3	98.818698	95.100883	1.800000
3	3	98.785242	95.063725	5.700000
4	3	97.815002	93.986185	9.200000
5	3	96.276002	92.276932	11.500000
6	3	93.800218	89.527296	13.500000
7	3	90.120000	85.440000	13.500000
1	4	94.137221	97.803735	-1.800000
2	4	94.137221	97.803735	1.800000
3	4	94.121771	97.756182	5.700000
4	4	93.673696	96.377150	9.200000
5	4	92.962957	94.189720	11.500000
6	4	91.819594	90.670811	13.500000
7	4	90.120000	85.440000	13.500000
1	5	88.761131	98.368785	-1.800000
2	5	88.761131	98.368785	1.800000
3	5	88.746357	98.319059	5.700000
4	5	88.917923	96.877002	9.200000
5	5	89.158339	94.589601	11.500000
6	5	89.445034	90.909870	13.500000
7	5	90.120000	85.440000	13.500000
1	6	83.620001	96.698331	-1.800000
2	6	83.620001	96.698331	1.800000
3	6	83.645001	96.655029	5.700000
4	6	84.370001	95.399293	9.200000
5	6	85.520000	93.407434	11.500000
6	6	87.370050	90.203140	13.500000
7	6	90.120000	85.440000	13.500000
1	7	79.602780	93.081209	-1.800000
2	7	79.602780	93.081209	1.800000
3	7	79.643230	93.051820	5.700000
4	7	80.816305	92.199531	9.200000
5	7	82.677744	90.847625	11.500000
6	7	85.670407	88.672819	13.500000
7	7	90.120000	85.440000	13.500000

I	J	X(I,J)	Y(I,J)	Z(I,J)
1	8	77.404081	89.142853	-1.800000
2	8	77.404081	88.142853	1.800000
3	8	77.452989	88.132448	5.700000
4	8	78.871303	87.830985	9.200000
5	8	81.121042	87.352788	11.500000
6	8	84.740188	86.583515	13.500000
7	8	90.120000	85.440000	13.500000
1	9	77.404081	82.737149	-1.800000
2	9	77.404081	82.737149	1.800000
3	9	77.452988	82.747545	5.700000
4	9	78.871302	83.049017	9.200000
5	9	81.121042	83.527213	11.500000
6	9	84.740188	84.296486	13.500000
7	9	90.120000	85.440000	13.500000
1	10	79.602778	77.798793	-1.800000
2	10	79.602778	77.798793	1.800000
3	10	79.643229	77.828182	5.700000
4	10	80.816304	78.680471	9.200000
5	10	82.677043	80.032377	11.500000
6	10	85.670406	82.207182	13.500000
7	10	90.120000	85.440000	13.500000
1	11	83.619999	74.181671	-1.800000
2	11	83.619999	74.181671	1.800000
3	11	83.644999	74.224972	5.700000
4	11	84.369999	75.480709	9.200000
5	11	85.519999	77.472567	11.500000
6	11	87.369999	80.676861	13.500000
7	11	90.120000	85.440000	13.500000
1	12	88.761128	72.511216	-1.800000
2	12	88.761128	72.511216	1.800000
3	12	88.766355	72.560942	5.700000
4	12	88.917921	74.002998	9.200000
5	12	89.158937	76.290399	11.500000
6	12	89.545093	79.970130	13.500000
7	12	90.120000	85.440000	13.500000
1	13	94.137219	73.076265	-1.800000
2	13	94.137219	73.076265	1.800000
3	13	94.121768	73.123818	5.700000
4	13	93.677694	74.502850	9.200000
5	13	92.9[illegible]955	76.690280	11.500000
6	13	91.81[illegible]593	80.209189	13.500000
7	13	90.120000	85.440000	13.500000
1	14	98.818696	75.779116	-1.800000
2	14	98.818696	75.779116	1.800000
3	14	98.785240	75.816273	5.700000
4	14	97.815001	76.893833	9.200000
5	14	96.276000	78.603047	11.500000
6	14	93.800218	81.352703	13.500000
7	14	90.120000	85.440000	13.500000

I	J	X(I,J)	Y(I,J)	Z(I,J)
1	15	101.996090	80.152422	-1.800000
2	15	101.996090	80.152422	1.800000
3	15	101.950413	80.172758	5.700000
4	15	100.625772	80.762527	9.200000
5	15	98.524618	81.698021	11.500000
6	15	95.144500	83.202948	13.500000
7	15	90.120000	85.440000	13.500000
1	16	103.120000	85.439998	-1.800000
2	16	103.120000	85.439998	1.800000
3	16	103.070000	85.439998	5.700000
4	16	101.620000	85.439998	9.200000
5	16	99.320000	85.439998	11.500000
6	16	95.620000	85.439999	13.500000
7	16	90.120000	85.440000	13.500000

AXISYM RELINQUISHING CONTROL.

AXISYMMETRIC CENTERBODY FOR
NASA FAN - IN - WING

TITLE1 JUN 09, 1967
TITLE2

CONTROL WORD =EXIT = FORCES HALT.

POTENTIAL-FLOW PROGRAM SAMPLE CASE

The potential-flow program case considered is a three-dimensional lifting wing; inputs appear on page 263, and printouts appear on pages 264 through 278.

Three-dimensional lifting wing input: This sample case is for the wing and lifting system shown in Figure 107. All of the source-geometry data cards for the wing were prepared by the geometry program, as described on page 235. The multihorseshoe network coordinates were prepared by the geometry program as described on page 242.

The input to the potential-flow program is shown on page 263. The wing and the flow are symmetric about the x-z plane so ICODE = 1. on card 3. A total of 50 singularities (48 source panels and 2 multihorseshoes) were used to represent the wing and lifting system. The options for the multihorseshoe lifting system are input on card 3 of the appropriate section. The size of the multihorseshoe network is M x N = 10 x 3. There are eight weighted segments: OPTWT = 1. indicating that the weighting values are input once and do not vary spanwise, OPTBP = 10. indicating that both the boundary-point coordinates and unit normal vectors are specified, and OPTUS = 0. indicating that all normal velocities are zero. The weighting values in card set 5 were designed to be constant over the first 40 percent of the airfoil, then taper off to nearly zero at (x/c) = 0.8. The boundary point and unit normal vector components were prepared by the geometry program.

Three aerodynamic solutions were requested for α = 0, 4, and 10 degrees. The options for forces and streamlines were also exercised. Card 4 gives the quantities needed to nondimensionalize the force and moment coefficients. A streamline was requested for the second solution (α = 4 degrees), which is to start at the trailing edge of the airfoil in the first column of source panels on the right half of the wing.

Three-dimensional lifting wing printout: The printout for this sample case is shown on pages 264 through 278. The first two pages give an exact listing of the input data cards. This provides a permanent listing of the input for each run and enables the user to check a large number of input cards rapidly.

Following this is the printout from the Geometric Section. It consists of detailed geometric information describing the source panels, quadrilateral vortices, and multihorseshoe vortices (see page 144).

The Aerodynamic Section printout is next. Output quantities are described on pages 144 through 146.

SEVEN FIELD, TEN DIGIT CRD FORMAT

GEOMETRIC SECTION									1GEOM
SAMPLE WING AND LIFTING SYSTEM CASE									2GEOM
1.	50.								3GEOM
SOURCE GEOMETRY									1SOUR
NOTE: THIS GROUP OF DATA CARDS FOR THE WING IS PREPARED BY THE GEOMETRY PROGRAM									
MULTI-HORSESHOE VORTEX GEOMETRY									1MULT
1.									2MULT
10.	3.	8.	1.	10.	0.				3MULT
NOTE: THIS GROUP OF DATA CARDS FOR THE LIFTING SYSTEM IS PREPARED BY THE GEOMETRY PROGRAM									
.17	.17	.17	.17	.14	.1	.06			5MULT
.02									5MULT
NOTE: TWO CARDS PREPARED BY THE GEOMETRY PROGRAM ARE INPUT HERE, WHICH ARE THE POSITION AND NORMAL VECTOR AT THE BP									
END OF GEOMETRIC SECTION									4GEOM
AERODYNAMIC SECTION									1AERO
3.	1.			1.					2AERO
0.									3AERO
4									3AERO
10.									3AERO
.25	.0	.0	2.	1.	2.				4AERO
2.	1.	1.	1.	2.	0.5	4.			11AERO
0.001									12AERO
END OF AERODYNAMIC SECTION									13AERO

TITLE SAMPLE CASE FOR AERODYNAMIC PROGRAM NAME DATE PAGE OF

INVESTIGATION OF INLET FLOW CHARACTERISTICS OF A LIFT FAN IN A WING

DATA CARDS FOR CASE NO. 1 ARE LISTED BELOW

```
GEOMETRIC SECTION
SAMPLE  WING  AND  LIFTING  SYSTEM  CASE
1.          50.
SOURCE GEOMETRY
   1.00300
29.         3.
   1.00000    0.00000    0.00000    0.90000    0.00000    0.01256
   0.80000    0.00000    0.02699    0.70000    0.00000    0.03992
   0.60000    0.00000    0.04923    0.50000    0.00000    0.05429
   0.40000    0.00000    0.05556    0.30000    0.00000    0.05396
   0.20000    0.00000    0.04969    0.10800    0.00000    0.04104
   0.04400    0.00000    0.02849    0.01000    0.00000    0.01392
   0.00000    0.00000    0.00000    0.01000    0.00000   -0.01392
   0.04400    0.00000   -0.02849    0.10800    0.00000   -0.04104
   0.20000    0.00000   -0.04969    0.30000    0.00000   -0.05396
   0.40000    0.00000   -0.05556    0.50000    0.00000   -0.05429
   0.60000    0.00000   -0.04923    0.70000    0.00000   -0.03992
   0.80000    0.00000   -0.02699    0.90000    0.00000   -0.01256
   1.00000    0.00000   -0.00000    1.00000    0.50000    0.00000
   0.90000    0.50000    0.01256    0.80000    0.50000    0.02699
   0.70000    0.50000    0.03992    0.60000    0.50000    0.04923
   0.50000    0.50000    0.05429    0.40000    0.50000    0.05556
   0.30000    0.50000    0.05396    0.20000    0.50000    0.04969
   0.10800    0.50000    0.04104    0.04400    0.50000    0.02849
   0.01000    0.50000    0.01392    0.00000    0.50000    0.00000
   0.01000    0.50000   -0.01392    0.04400    0.50000   -0.02849
   0.10800    0.50000   -0.04104    0.20000    0.50000   -0.04969
   0.30000    0.50000   -0.05396    0.40000    0.50000   -0.05556
   0.50000    0.50000   -0.05429    0.60000    0.50000   -0.04923
   0.70000    0.50000   -0.03992    0.80000    0.50000   -0.02699
   0.90000    0.50000   -0.01256    1.00000    0.50000   -0.00000
   1.00000    1.00000    0.00000    0.90000    1.00000    0.01256
   0.80000    1.00000    0.02699    0.70000    1.00000    0.03992
   0.60000    1.00000    0.04923    0.50000    1.00000    0.05429
   0.40000    1.00000    0.05556    0.30000    1.00000    0.05396
   0.20000    1.00000    0.04969    0.10800    1.00000    0.04104
   0.04400    1.00000    0.02849    0.01000    1.00000    0.01392
   0.00000    1.00000    0.00000    0.01000    1.00000   -0.01392
   0.04400    1.00000   -0.02849    0.10800    1.00000   -0.04104
   0.20000    1.00000   -0.04969    0.30000    1.00000   -0.05396
   0.40000    1.00000   -0.05556    0.50000    1.00000   -0.05429
   0.60000    1.00000   -0.04923    0.70000    1.00000   -0.03992
   0.80000    1.00000   -0.02699    0.90000    1.00000   -0.01256
   1.00000    1.00000   -0.00000
MULTI-HORSESHOE VORTEX GEOMETRY
   1.0000
10.         3.         8.         1.        10.         0.
```

```
    0.1238   0.00000   0.00000    0.2050   0.00000   0.00000
    0.3012   0.00000   0.00000    0.4000   0.00000   0.00000
    0.4980   0.00000   0.00000    0.5967   0.00000   0.00000
    0.6953   0.00000   0.00000    0.7963   0.00000   0.00000
    1.0000   0.00000   0.00000 4000.0000   0.00000   0.00000
    0.1238   0.50000   0.00000    0.2050   0.50000   0.00000
    0.3012   0.50000   0.00000    0.4000   0.50000   0.00000
    0.4980   0.50000   0.00000    0.5967   0.50000   0.00000
    0.6953   0.50000   0.00000    0.7963   0.50000   0.00000
    1.0000   0.50000   0.00000 4000.0000   0.50000   0.00000
  0.1208   0.95000   0.00000    0.2050   0.95000   0.00000
    0.3012   0.95000   0.00000    0.4000   0.95000   0.00000
    0.4980   0.95000   0.00000    0.5967   0.95000   0.00000
    0.6953   0.95000   0.00000    0.7963   0.95000   0.00000
    1.0000   0.95000   0.00000 4000.0000   0.95000   0.00000
.17      .17      .17      .17      .14      .1       .06
.02
    1.0050   0.25000   0.00000    0.0000   0.00000   1.00000
    1.0050   0.75000  -0.00000    0.0000   0.00000   1.00000
END OF GEOMETRIC SECTION
AERODYNAMIC SECTION
3.       1.                                1.
0.
4.
10.
.25      .0       .0       2.       1.       2.
2.       1.       1.       1.       2.       0.5      4.
0.001
END OF AERODYNAMIC SECTION
```

GEOMETRIC SECTION

AUG 23, 1967

INVESTIGATION OF INLET FLOW CHARACTERISTICS OF A LIFT FAN IN A WING

SAMPLE WING AND LIFTING SYSTEM CASE

SYMMETRIC FLOW

GEOMETRIC SECTION

THE MATRIX (ORDER 50) HAS BEEN PARTITIONED 25 25

SOURCE GEOMETRY

SOURCE PANEL GEOMETRY

ACCUM. NO.	NO.	XBP / X1	YBP / Y1	ZBP / Z1	NX / X2	NY / Y2	NZ / Z2	T / X3	AREA / Y3	D / Z3	X4	Y4	Z4
1	1	.9400	.2500	.0063	.1246	0.	.9922	.5101	.050393	4.1633E-16			
		1.0000	0.	0.	.9000	0.	.0126	.9000	.5000	.0126	1.0000	.5000	0.
2	2	.8500	.2500	.0198	.1428	0.	.9897	.5101	.050519	-8.6042E-16			
		.9000	0.	.0126	.8000	0.	.0270	.8000	.5000	.0270	.9000	.5000	.0126
3	3	.7500	.2500	.0335	.1252	0.	.9917	.5101	.050416	-6.3838E-16			
		.8000	0.	.0270	.7000	0.	.0399	.7000	.5000	.0399	.8000	.5000	.0270
4	4	.6500	.2500	.0446	.0927	0.	.9957	.5100	.050216	-3.8858E-16			
		.7000	0.	.0399	.6300	0.	.0492	.6300	.5000	.0492	.7000	.5000	.0399
5	5	.5500	.2500	.0518	.0505	0.	.9987	.5099	.050064	-2.2204E-16			
		.6000	0.	.0492	.5000	0.	.0543	.5000	.5000	.0543	.6300	.5000	.0492
6	6	.4500	.2500	.0549	.0127	0.	.9999	.5099	.050004	-1.3531E-16			
		.5000	0.	.0543	.4000	0.	.0556	.4000	.5000	.0556	.5000	.5000	.0543
7	7	.3500	.2500	.0548	-.0160	0.	.9999	.5099	.050006	-1.0061E-16			
		.4000	0.	.0556	.3000	0.	.0540	.3000	.5000	.0540	.4000	.5000	.0556
8	8	.2500	.2500	.0518	-.0427	0.	.9991	.5099	.050046	2.7756E-17			
		.3000	0.	.0540	.2000	0.	.0497	.2000	.5000	.0497	.3000	.5000	.0540
9	9	.1540	.2500	.0454	-.0936	0.	.9956	.5085	.046203	2.7756E-17			
		.2000	0.	.0497	.1080	0.	.0410	.1080	.5000	.0410	.2000	.5000	.0497
10	10	.0770	.2500	.0348	-.1984	0.	.9801	.5040	.031629	-1.9429E-16			
		.1080	0.	.0410	.0460	0.	.0285	.0460	.5000	.0285	.1080	.5000	.0410
11	11	.0280	.2500	.0212	-.3752	0.	.9270	.5015	.019418	-1.1102E-16			
		.0460	0.	.0285	.0100	0.	.0139	.0100	.5000	.0139	.0460	.5000	.0285
12	12	.0050	.2500	.0070	-.8122	0.	.5834	.5003	.008570	0.			
		.0100	0.	.0139	0.	0.	0.	0.	.5000	0.	.0100	.5000	.0139
13	13	.0050	.2500	-.0070	-.8122	0.	-.5834	.5003	.008570	2.7756E-17			
		0.	0.	0.	.0100	0.	-.0139	.0100	.5000	-.0139	0.	.5000	0.
14	14	.0280	.2500	-.0212	-.3752	0.	-.9270	.5015	.019418	-1.3878E-16			
		.0100	0.	-.0139	.0460	0.	-.0285	.0460	.5000	-.0285	.0100	.5000	-.0139
15	15	.0770	.2500	-.0348	-.1984	0.	-.9801	.5040	.031629	-1.6653E-16			
		.0460	0.	-.0285	.1080	0.	-.0410	.1080	.5000	-.0410	.0460	.5000	-.0285
16	16	.1540	.2500	-.0454	-.0936	0.	-.9956	.5085	.046203	0.			
		.1080	0.	-.0410	.2000	0.	-.0497	.2000	.5000	-.0497	.1080	.5000	-.0410
17	17	.2500	.2500	-.0518	-.0427	0.	-.9991	.5099	.050046	4.1633E-17			
		.2000	0.	-.0497	.3000	0.	-.0540	.3000	.5000	-.0540	.2000	.5000	-.0497

SOURCE PANEL GEOMETRY

ACCUM. NO.	NO.	XBP / X1	YBP / Y1	ZBP / Z1	NX / X2	NY / Y2	NZ / Z2	T / X3	AREA / Y3	D / Z3	X4	Y4	Z4
18	18	.3500	.2500	-.0548	-.0160	0.	-.9999	.5099	.050006	-6.5919E-17			
		.3000	0.	-.0540	.4000	0.	-.0556	.4000	.5000	-.0556	.3000	.5000	-.0540
19	19	.4500	.2500	-.0549	.0127	0.	-.9999	.5099	.050004	-1.1102E-16			
		.4000	0.	-.0556	.5000	0.	-.0543	.5000	.5000	-.0543	.4000	.5000	-.0556
20	20	.5500	.2500	-.0518	.0505	0.	-.9987	.5099	.050064	0.			
		.5000	0.	-.0543	.6000	0.	-.0492	.6070	.5000	-.0492	.5000	.5000	-.0543
21	21	.6500	.2500	-.0446	.0927	0.	-.9957	.5100	.050216	-3.8858E-16			
		.6000	0.	-.0492	.7000	0.	-.0399	.7000	.5000	-.0399	.6000	.5000	-.0492
22	22	.7500	.2500	-.0335	.1282	0.	-.9917	.5101	.050416	-6.9389E-16			
		.7000	0.	-.0399	.8000	0.	-.0270	.8000	.5000	-.0270	.7000	.5000	-.0399
23	23	.8500	.2500	-.0196	.1428	0.	-.9897	.5101	.050518	-3.6082E-16			
		.8000	0.	-.0270	.9000	0.	-.0126	.9000	.5000	-.0126	.8000	.5000	-.0270
24	24	.9500	.2500	-.0063	.1246	0.	-.9922	.5101	.050393	-4.1633E-16			
		.9000	0.	-.0126	1.0000	0.	-0.	1.0000	.5000	-0.	.9000	.5000	-.0126

END OF PANEL COLUMN 1, OF NETWORK 1

25	1	.9500	.7500	.0063	.1246	0.	.9922	.5101	.050393	4.1633E-16			
		1.0000	.5000	0.	.9000	.5000	.0126	.9000	1.0000	.0126	1.0000	1.0000	0.
26	2	.8500	.7500	.0198	.1428	0.	.9897	.5101	.050518	-8.6042E-16			
		.9000	.5000	.0126	.8000	.5000	.0270	.8000	1.0000	.0270	.9000	1.0000	.0126
27	3	.7500	.7500	.0335	.1282	0.	.9917	.5101	.050416	-6.3838E-16			
		.8000	.5000	.0270	.7000	.5000	.0399	.7000	1.0000	.0399	.8000	1.0000	.0270
28	4	.6500	.7500	.0446	.0927	0.	.9957	.5100	.050216	-3.8858E-16			
		.7000	.5000	.0399	.6000	.5000	.0492	.6000	1.0000	.0492	.7000	1.0000	.0399
29	5	.5500	.7500	.0518	.0505	0.	.9987	.5099	.050064	-2.2204E-16			
		.6000	.5000	.0492	.5000	.5000	.0543	.5000	1.0000	.0543	.6000	1.0000	.0492
30	6	.4500	.7500	.0549	.0127	0.	.9999	.5099	.050004	-1.3531E-16			
		.5000	.5000	.0543	.4000	.5000	.0556	.4000	1.0000	.0556	.5000	1.0000	.0543
31	7	.3500	.7500	.0548	-.0160	0.	.9999	.5099	.050006	-1.0061E-16			
		.4000	.5000	.0556	.3000	.5000	.0540	.3000	1.0000	.0540	.4000	1.0000	.0556
32	8	.2500	.7500	.0518	-.0427	0.	.9991	.5099	.050046	2.7756E-17			
		.3000	.5000	.0540	.2000	.5000	.0497	.2000	1.0000	.0497	.3000	1.0000	.0540
33	9	.1540	.7500	.0454	-.0936	0.	.9956	.5085	.046203	2.7756E-17			
		.2000	.5000	.0497	.1080	.5000	.0410	.1080	1.0000	.0410	.2000	1.0000	.0497
34	10	.0770	.7500	.0348	-.1984	0.	.9801	.5040	.031629	-1.9429E-16			
		.1080	.5000	.0410	.0460	.5000	.0285	.0460	1.0000	.0285	.1080	1.0000	.0410
35	11	.0280	.7500	.0212	-.3752	0.	.9270	.5015	.019418	-1.1102E-16			
		.0460	.5000	.0285	.0100	.5000	.0139	.0100	1.0000	.0139	.0460	1.0000	.0285

SOURCE PANEL GEOMETRY

ACCUM. NO.	NO.	XBP X1	YBP Y1	ZBP Z1	NX X2	NY Y2	NZ Z2	T X3	AREA Y3	D Z3	X4	Y4	Z4
36	12	.0050	.7500	.0070	-.8122	0.	.5834	.5003	.008570	0.			
		.0100	.5000	.0139	0.	.5000	0.	0.	1.0000	0.	.0100	1.0000	.0139
37	13	.0050	.7500	-.0070	-.8122	0.	-.5834	.5003	.008570	2.7756E-17			
		0.	.5000	0.	.0100	.5000	-.0139	.0100	1.0000	-.0139	0.	1.0000	0.
38	14	.0280	.7500	-.0212	-.3752	0.	-.9270	.5015	.019418	-1.3878E-16			
		.0100	.5000	-.0139	.0460	.5000	-.0285	.0460	1.0000	-.0285	.0100	1.0000	-.0139
39	15	.0770	.7500	-.0348	-.1984	0.	-.9801	.5040	.031629	-1.6653E-16			
		.0460	.5000	-.0285	.1080	.5000	-.0410	.1080	1.0000	-.0410	.0460	1.0000	-.0285
40	16	.1540	.7500	-.0454	-.0936	0.	-.9956	.5085	.046203	0.			
		.1080	.5000	-.0410	.2000	.5000	-.0497	.2000	1.0000	-.0497	.1080	1.0000	-.0410
41	17	.2500	.7500	-.0518	-.0427	0.	-.99 .	.5099	.050046	4.1633E-17			
		.2000	.5000	-.0497	.3000	.5000	-.0540	.3000	1.0000	-.0540	.2000	1.0000	-.0497
42	18	.3500	.7500	-.0548	-.0160	0.	-.9999	.5099	.050006	-6.5919E-17			
		. 00	.5000	-.0540	.4000	.5000	-.0556	.4000	1.0000	-.0556	.3000	1.0000	-.0540
43	19	.4500	.7500	-.0549	.0127	0.	-.9999	.5099	.050004	-1.1102E-16			
		.4000	.5000	-.0556	.5000	.5000	-.0543	.5000	1.0000	-.0543	.4000	1.0000	-.0556
44	20	.5500	.7500	-.0518	.0505	0.	-.9989	.5099	.050064	0.			
		.5000	.5000	-.0543	.6000	.5000	-.0492	.6000	1.0000	-.0492	.5000	1.0000	-.0543
45	21	.6500	.7500	-.0446	.0927	0.	-.9957	.5100	.050216	-3.8858E-16			
		.6000	.5000	-.0492	.7000	.5000	-.0399	.7000	1.0000	-.0399	.6000	1.0000	-.0492
46	22	.7500	.7500	-.0335	.1282	0.	-.9917	.5101	.050416	-6.9389E-16			
		.7000	.5000	-.0399	.8000	.5000	-.0270	.8000	1.0000	-.0270	.7000	1.0000	-.0399
47	23	.8500	.7500	-.0198	.1628	0.	-.9897	.5101	.050518	-3.6082E-16			
		.8000	.5000	-.0270	.9000	.5000	-.0126	.9000	1.0000	-.0126	.8000	1.0000	-.0270
48	24	.9500	.7500	-.0063	.1246	0.	-.9922	.5101	.050393	-4.1633E-16			
		.9000	.5000	-.0126	1.0000	.5000	-0.	1.0000	1.0000	-0.	.9000	1.0000	-.0126

END OF PANEL COLUMN 2, OF NETWORK 1

CHARACTERISTICS OF NETWORK 1

LONGEST PANEL DIAGONAL ------	.510106
LARGEST PANEL AREA ----------	.050518
SMALLEST PANEL AREA ---------	.008570
TOTAL PANEL AREA ------------	2.029931
LARGEST PANEL D FACTOR ------	-8.6042E-16
SMALLEST PANEL D FACTOR -----	0.

MULTI-HORSESHOE VORTEX GEOMETRY

MULTI-HORSESHOE VORTEX GEOMETRY

ACCUM. NO.	NO.	XL	YL	ZL	XR	YR	ZR	WT
49	1							
	1	.1208	0.	0.	.1208	.5000	0.	.1700
	2	.2050	0.	0.	.2050	.5000	0.	.1700
	3	.3012	0.	0.	.3012	.5000	0.	.1700
	4	.4000	0.	0.	.4000	.5000	0.	.1700
	5	.4980	0.	0.	.4980	.5000	0.	.1400
	6	.5967	0.	0.	.5967	.5000	0.	.1000
	7	.6953	0.	0.	.6953	.5000	0.	.0600
	8	.7963	0.	0.	.7963	.5000	0.	.0200
	9	1.0000	0.	0.	1.0000	.5000	0.	
	10	4000.0000	0.	0.	4000.0000	.5000	0.	

SPECIFIED BOUNDARY POINT XBP= 1.0050 YBP= .2500 ZBP= 0. NX= 0. NY= 0. NZ= 1.0000

ACCUM. NO.	NO.	XL	YL	ZL	XR	YR	ZR	WT
50	2							
	1	.1208	.5000	0.	.1208	.9500	0.	.1700
	2	.2050	.5000	0.	.2050	.9500	0.	.1700
	3	.3012	.5000	0.	.3012	.9500	0.	.1700
	4	.4000	.5000	0.	.4000	.9500	0.	.1700
	5	.4980	.5000	0.	.4980	.9500	0.	.1400
	6	.5967	.5000	0.	.5967	.9500	0.	.1000
	7	.6953	.5000	0.	.6953	.9500	0.	.0600
	8	.7963	.5000	0.	.7963	.9500	0.	.0200
	9	1.0000	.5000	0.	1.0000	.9500	0.	
	10	4000.0000	.5000	0.	4000.0000	.9500	0.	

SPECIFIED BOUNDARY POINT XBP= 1.0050 YBP= .7500 ZBP= -0. NX= 0. NY= 0. NZ= 1.0000

END OF NETWORK 1

END OF GEOMETRIC SECTION

AERODYNAMIC SECTION

INVESTIGATION OF INLET FLOW CHARACTERISTICS OF A LIFT FAN IN A WING

AUG 23, 1967

SAMPLE WING AND LIFTING SYSTEM CASE

SYMMETRIC FLOW

A E R O D Y N A M I C S E C T I O N

271

[illegible] PROGRAM DATED 08/23/67 IS IN EXECUTION.

SOLUTION NUMBER 1

ALPHA = 0. DEGREES
PSI = -0. DEGREES

FLOW PROPERTIES AT SOURCE PANEL BOUNDARY POINTS

ACCUM. NO.	NO.	XBP	YBP	ZBP	VX	VY	VZ	V	CP	SIGMA	VRN
1	1	.95000	.25000	.00628	.92202	-.00263	-.11581	.92926	.13647	-.00966	1.6431E-14
2	2	.85000	.25000	.01977	.98201	-.00244	-.14170	.99218	.01557	-.01250	-9.3291E-15
3	3	.75000	.25000	.03345	1.04026	-.00207	-.13451	1.04892	-.10023	-.01228	0.
4	4	.65000	.25000	.04457	1.08596	-.00153	-.10110	1.09066	-.18954	-.00920	2.2204E-15
5	5	.55000	.25000	.05176	1.11106	-.00083	-.05622	1.11249	-.23762	-.00491	1.5543E-15
6	6	.45000	.25000	.05492	1.11811	-.00004	-.01420	1.11820	-.25037	-.00108	3.8858E-16
7	7	.35000	.25000	.05476	1.11794	.00077	.01789	1.11809	-.25012	.00140	-1.1102E-16
8	8	.25000	.25000	.05182	1.12295	.00153	.04795	1.12397	-.26331	.00320	0.
9	9	.15400	.25000	.04536	1.13102	.00217	.10634	1.13601	-.29052	.00764	0.
10	10	.07700	.25000	.03476	1.11128	.00256	.22494	1.13382	-.28555	.01834	-8.8818E-16
11	11	.02800	.25000	.02120	.99306	.00276	.40191	1.07132	-.14772	.03578	0.
12	12	.00500	.25000	.00696	.38200	.00283	.53175	.65475	.57131	.08733	0.
13	13	.00500	.25000	-.00696	.38200	.00283	-.53175	.65475	.57131	.08733	1.7764E-15
14	14	.02800	.25000	-.02120	.99306	.00276	-.40191	1.07132	-.14772	.03578	0.
15	15	.07700	.25000	-.03476	1.11128	.00256	-.22494	1.13382	-.28555	.01834	-2.6645E-15
16	16	.15400	.25000	-.04536	1.13102	.00217	-.10634	1.13601	-.29052	.00764	-1.7764E-15
17	17	.25000	.25000	-.05182	1.12295	.00153	-.04795	1.12397	-.26331	.00320	0.
18	18	.35000	.25000	-.05476	1.11794	.00077	-.01789	1.11809	-.25012	.00140	-3.3307E-16
19	19	.45000	.25000	-.05492	1.11811	-.00004	.01420	1.11820	-.25037	-.00108	4.9960E-16
20	20	.55000	.25000	-.05176	1.11106	-.00083	.05622	1.11249	-.23762	-.00491	6.6613E-16
21	21	.65000	.25000	-.04457	1.08596	-.00153	.10110	1.09066	-.18954	-.00920	1.7764E-15
22	22	.75000	.25000	-.03345	1.04026	-.00207	.13451	1.04892	-.10023	-.01228	8.8818E-16
23	23	.85000	.25000	-.01977	.98201	-.00244	.14170	.99218	.01557	-.01250	-8.8818E-16
24	24	.95000	.25000	-.00628	.92202	-.00263	.11581	.92926	.13647	-.00966	1.5987E-14
					END OF PANEL COLUMN 1. OF NETWORK 1						
25	1	.95000	.75000	.00628	.92429	-.02007	-.11609	.93177	.13181	-.00970	-4.4409E-16
26	2	.85000	.75000	.01977	.98039	-.02178	-.14147	.99078	.01835	-.01257	8.8818E-16
27	3	.75000	.75000	.03345	1.03389	-.02053	-.13368	1.04270	-.08722	-.01235	0.
28	4	.65000	.75000	.04457	1.07522	-.01631	-.10010	1.08000	-.16639	-.00926	-4.4409E-16
29	5	.55000	.75000	.05176	1.09719	-.00987	-.05552	1.09864	-.20701	-.00497	-2.2204E-16
30	6	.45000	.75000	.05492	1.10267	-.00215	-.01400	1.10276	-.21607	-.00110	-5.5511E-17
31	7	.35000	.75000	.05476	1.10243	.00612	.01764	1.10259	-.21570	.00144	0.
32	8	.25000	.75000	.05182	1.10889	.01429	.04735	1.10999	-.23208	.00331	0.
33	9	.15400	.75000	.04536	1.12022	.02113	.10532	1.12536	-.26443	.00776	-4.4409E-16
34	10	.07700	.75000	.03476	1.10461	.02472	.22359	1.12729	-.27077	.01841	-8.8818E-16
35	11	.02800	.75000	.02120	.98966	.02560	.40054	1.06795	-.14052	.03578	0.
36	12	.00500	.75000	.00696	.38114	.02559	.53055	.65376	.57260	.08719	-7.1054E-15
37	13	.00500	.75000	-.00696	.38114	.02559	-.53055	.65376	.57260	.08719	-5.3291E-15
38	14	.02800	.75000	-.02120	.98966	.02560	-.40054	1.06795	-.14052	.03578	3.5527E-15
39	15	.07700	.75000	-.03476	1.10461	.02472	-.22359	1.12729	-.27077	.01841	0.
40	16	.15400	.75000	-.04536	1.12022	.02113	-.10532	1.12536	-.26443	.00776	-8.8818E-16
41	17	.25000	.75000	-.05182	1.10889	.01429	-.04735	1.10999	-.23208	.00331	0.
42	18	.35000	.75000	-.05476	1.10243	.00612	-.01764	1.10259	-.21570	.00144	-1.1102E-16
43	19	.45000	.75000	-.05492	1.10267	-.00215	.01400	1.10276	-.21607	-.00110	1.6653E-16

FLOW PROPERTIES AT SOURCE PANEL BOUNDARY POINTS

ACCUM. NO.	NO.	XBP	YBP	ZBP	VX	VY	VZ	V	CP	SIGMA	VRN
44	20	.55000	.75000	-.05176	1.09719	-.00987	.05552	1.09864	-.20701	-.00497	-2.2204E-16
45	21	.65000	.75000	-.04457	1.07522	-.01631	.10010	1.08000	-.16639	-.00926	4.4409E-16
46	22	.75000	.75000	-.03345	1.03389	-.02053	.13368	1.04270	-.08722	-.01235	-8.8818E-16
47	23	.85000	.75000	-.01977	.98039	-.02178	.14147	.99078	.01835	-.01257	8.8818E-16
48	24	.95000	.75000	-.00628	.92429	-.02007	.11609	.93177	.13181	-.00970	0.

END OF PANEL COLUMN 2, OF NETWORK 1

FLOW PROPERTIES AT MULTI-HORSESHOE VORTEX BOUNDARY POINTS

ACCUM. NO.	NO.	XBP	YBP	ZBP	VX	VY	VZ	V	CP	SIGMA	VRN
49	1	1.00500	.25000	0.	.83316	-.00265	.00000	.83317	.30583	.00000	3.2700E-16
50	2	1.00500	.75000	-0.	.83657	-.01827	.00000	.83676	.29983	.00000	9.5302E-17

END OF NETWORK 1

FORCE AND MOMENT COEFFICIENTS ON SOURCE PANELS

FORCE AND MOMENT COEFFICIENTS PER PANEL COLUMN

COL.	CFX	CFZ	CMY	CL	CD	NET STRENGTH	AREA
1	.000411	.000000	.000000	.000000	.000411	.000214	1.0150
2	.000481	.000000	.000000	.000000	.000481	.000211	1.0150

END OF NETWORK 1

TOTAL FORCE AND MOMENT COEFFICIENTS

CFX	CFZ	CMY	CL	CD	NET STRENGTH	AREA
.001784	.000000	.000000	.000000	.001784	.000850	4.0599

REFERENCE GEOMETRY

XR	YR	ZR	SR	CR	BR
.2500	0.	0.	2.0000	1.0000	2.0000

SOLUTION NUMBER 2

ALPHA = 4.0000 DEGREES
PSI = -0. DEGREES

FLOW PROPERTIES AT SOURCE PANEL BOUNDARY POINTS

ACCUM. NO.	NO.	XBP	YBP	ZBP	VX	VY	VZ	V	CP	SIGMA	VRN
1	1	.95000	.25000	.00628	.92303	-.00312	-.11593	.93028	.13457	-.00776	0.
2	2	.85000	.25000	.01977	.98733	-.00396	-.14247	.99757	.00486	-.00922	-7.1054E-15
3	3	.75000	.25000	.03345	1.04939	-.00450	-.13569	1.05813	-.11964	-.01061	-7.1054E-15
4	4	.65000	.25000	.04457	1.10214	-.00453	-.10261	1.10691	-.22526	-.01145	-6.2172E-15
5	5	.55000	.25000	.05176	1.13609	-.00401	-.05749	1.13755	-.29402	-.01239	1.1102E-15
6	6	.45000	.25000	.05492	1.15403	-.00305	-.01466	1.15412	-.33200	-.01545	3.3307E-15
7	7	.35000	.25000	.05476	1.16490	-.00183	.01864	1.16505	-.35735	-.02133	-2.1094E-15
8	8	.25000	.25000	.05182	1.18546	-.00051	.05062	1.18654	-.40788	-.02780	-4.4409E-16
9	9	.15400	.25000	.04536	1.22581	.00074	.11525	1.23121	-.51589	-.03268	0.
10	10	.07700	.25000	.03476	1.24664	.00170	.25234	1.27192	-.61778	-.03454	5.3291E-15
11	11	.02800	.25000	.02120	1.21554	.00231	.43196	1.31132	-.71956	-.01612	3.5527E-15
12	12	.00500	.25000	.00696	.67380	.00269	.93793	1.15487	-.33373	.05143	-7.1054E-15
13	13	.00500	.25000	-.00696	.08835	.00296	-.12298	.15145	.97706	.12280	8.8818E-16
14	14	.02800	.25000	-.02120	.76575	.00319	-.30992	.82609	.31757	.08751	-7.1054E-15
15	15	.07700	.25000	-.03476	.97051	.00342	-.19645	.99020	.01951	.07112	2.6645E-15
16	16	.15400	.25000	-.04536	1.03073	.00358	-.09691	1.03528	-.07180	.04792	-8.8818E-16
17	17	.25000	.25000	-.05182	1.05496	.00357	-.04505	1.05593	-.11498	.03418	-3.1086E-15
18	18	.35000	.25000	-.05476	1.06554	.00336	-.01705	1.06568	-.13567	.02412	-1.5543E-15
19	19	.45000	.25000	-.05492	1.07675	.00296	.01367	1.07684	-.15958	.01329	-4.996UE-16
20	20	.55000	.25000	-.05176	1.08063	.00235	.05468	1.08201	-.17075	.00259	-2.6645E-15
21	21	.65000	.25000	-.04457	1.06450	.00149	.09910	1.06910	-.14298	-.00690	3.1086E-15
22	22	.75000	.25000	-.03345	1.02606	.00037	.13267	1.03460	-.07039	-.01388	8.8818E-16
23	23	.85000	.25000	-.01977	.97190	-.00091	.14024	.98197	.03574	-.01572	-3.5527E-15
24	24	.95000	.25000	-.00628	.91651	-.00212	.11511	.92372	.14675	-.01151	2.6645E-15

END OF PANEL COLUMN 1, OF NETWORK 1

25	1	.95000	.75000	.00628	.92373	-.02248	-.11602	.93126	.13276	-.00871	-8.8818E-16
26	2	.85000	.75000	.01977	.98180	-.02925	-.14167	.99240	.01514	-.01097	8.8818E-16
27	3	.75000	.75000	.03345	1.03696	-.03263	-.13408	1.04610	-.09633	-.01237	-8.8818E-16
28	4	.65000	.75000	.04457	1.08267	-.03139	-.10080	1.08781	-.18332	-.01268	-1.7764E-15
29	5	.55000	.75000	.05176	1.11088	-.02592	-.05621	1.11260	-.23788	-.01280	2.2204E-16
30	6	.45000	.75000	.05492	1.12464	-.01737	-.01428	1.12487	-.26532	-.01465	2.3315E-15
31	7	.35000	.75000	.05476	1.13339	-.00701	.01813	1.13355	-.28495	-.01897	2.2204E-15
32	8	.25000	.75000	.05182	1.15313	.00408	.04924	1.15419	-.33216	-.02392	-2.2204E-16
33	9	.15400	.75000	.04536	1.19236	.01422	.11211	1.19770	-.43448	-.02704	0.
34	10	.07700	.75000	.03476	1.21436	.02068	.24581	1.23916	-.53552	-.02619	8.8818E-16
35	11	.02800	.75000	.02120	1.17636	.02357	.47610	1.26928	-.61106	-.00836	-3.5527E-15
36	12	.00500	.75000	.00696	.62936	.02495	.87606	1.07898	-.16420	.05691	-1.0658E-14
37	13	.00500	.75000	-.00696	.13107	.02611	-.18244	.22615	.94885	.11745	-1.9984E-14
38	14	.02800	.75000	-.02120	.79814	.02751	-.32302	.86147	.25788	.07976	3.5527E-15
39	15	.07700	.75000	-.03476	.98948	.02863	-.20029	1.00996	-.02001	.06291	0.
40	16	.15400	.75000	-.04536	1.04262	.02793	-.09803	1.04759	-.09745	.04253	-5.3291E-15
41	17	.25000	.75000	-.05182	1.05924	.02644	-.06523	1.06048	-.12463	.03053	-1.5543E-15
42	18	.35000	.75000	-.05476	1.06610	.01922	-.01706	1.06641	-.13724	.02185	-4.6613E-16
43	19	.45000	.75000	-.05492	1.07532	.01309	.01366	1.07549	-.15667	.01245	-3.8531E-15

FLOW PROPERTIES AT SOURCE PANEL BOUNDARY POINTS

ACCUM. NO.	NO.	XBP	YBP	ZBP	VX	VY	VZ	V	CP	SIGMA	VRN
44	20	.55000	.75000	-.05176	1.07817	.00622	.05456	1.07956	-.16546	.00289	4.4409E-16
45	21	.65000	.75000	-.04457	1.06254	-.00114	.09892	1.06713	-.13877	-.00580	-2.6645E-15
46	22	.75000	.75000	-.03345	1.02579	-.00833	.13263	1.03436	-.06990	-.01227	-2.6645E-15
47	23	.85000	.75000	-.01977	.97420	-.01420	.14058	.98439	.03097	-.01410	1.7764E-15
48	24	.95000	.75000	-.00628	.92035	-.01758	.11560	.92775	.13928	-.01065	0.

END OF PANEL COLUMN 2, OF NETWORK 1

FLOW PROPERTIES AT MULTI-HORSESHOE VORTEX BOUNDARY POINTS

ACCUM. NO.	NO.	XBP	YBP	ZBP	VX	VY	VZ	V	CP	SIGMA	VRN
49	1	1.00500	.25000	0.	.83113	-.00265	0.	.83114	.30921	.11329	0.
50	2	1.00500	.75000	-0.	.83453	-.01822	.00000	.83473	.30323	.08393	1.7764E-15

END OF NETWORK 1

FORCE AND MOMENT COEFFICIENTS ON SOURCE PANELS

FORCE AND MOMENT COEFFICIENTS PER PANEL COLUMN

COL.	CFX	CFZ	CMY	CL	CD	NET STRENGTH	AREA
1	-.001943	.057325	.000890	.057321	.002060	.000213	1.0150
2	-.001202	.042036	.001803	.042017	.001734	.000211	1.0150

END OF NETWORK 1

TOTAL FORCE AND MOMENT COEFFICIENTS

CFX	CFZ	CMY	CL	CD	NET STRENGTH	AREA
-.006290	.198722	.005387	.198676	.007588	.000848	4.0599

REFERENCE GEOMETRY

XR	YR	ZR	SR	CR	BR
.2500	0.	0.	2.0000	1.0000	2.0000

SOLUTION NUMBER 3

ALPHA = 10.0000 DEGREES
PSI = -0. DEGREES

FLOW PROPERTIES AT SOURCE PANEL BOUNDARY POINTS

ACCUM. NO.	NO.	XBP	YBP	ZBP	VX	VY	VZ	V	CP	SIGMA	VRN
1	1	.95000	.25000	.00628	.91612	-.00383	-.11506	.92332	.14748	-.00485	-2.8422E-14
2	2	.85000	.25000	.01977	.98630	-.00620	-.14232	.99654	.00691	-.00421	-9.7700E-15
3	3	.75000	.25000	.03345	1.05349	-.00811	-.13622	1.06229	-.12846	-.00802	-1.2434E-14
4	4	.65000	.25000	.04457	1.11632	-.00900	-.10393	1.12118	-.25704	-.01473	-5.7732E-15
5	5	.55000	.25000	.05176	1.16322	-.00874	-.05886	1.16474	-.35662	-.02348	5.9952E-15
6	6	.45000	.25000	.05492	1.19731	-.00753	-.01521	1.19743	-.43384	-.03683	1.1935E-14
7	7	.35000	.25000	.05476	1.22464	-.00571	.01959	1.22481	-.50016	-.05520	4.3299E-15
8	8	.25000	.25000	.05182	1.26832	-.00357	.05416	1.26948	-.61158	-.07399	2.2204E-16
9	9	.15400	.25000	.04536	1.35665	-.00139	.12755	1.36264	-.85678	-.09280	9.7700E-15
10	10	.07700	.25000	.03476	1.43809	.00039	.29110	1.46729	-1.15283	-.11346	3.5527E-15
11	11	.02800	.25000	.02120	1.53782	.00162	.62239	1.65899	-1.75226	-.09374	0.
12	12	.00500	.25000	.00696	1.10490	.00246	1.53802	1.89376	-2.58432	-.00282	7.1054E-15
13	13	.00500	.25000	-.00696	-.35250	.00312	.49068	.60618	.63497	.17482	3.5527E-15
14	14	.02800	.25000	-.02120	.61814	.00381	-.16923	.45110	.79651	.16422	-1.3323E-14
15	15	.07700	.25000	-.03476	.75071	.00466	-.15196	.76595	.41333	.14957	1.0658E-14
16	16	.15400	.25000	-.04536	.87103	.00566	-.08190	.87689	.23457	.10784	-8.4377E-15
17	17	.25000	.25000	-.05182	.94345	.00659	-.04029	.94434	.10823	.08030	-1.3323E-15
18	18	.35000	.25000	-.05476	.97728	.00722	-.01944	.97743	.04463	.05795	-1.2212E-15
19	19	.45000	.25000	-.05492	1.00494	.00745	.01276	1.00504	-.01011	.03470	2.9421E-15
20	20	.55000	.25000	-.05176	1.02515	.00711	.05107	1.02649	-.05368	.01380	2.2204E-15
21	21	.65000	.25000	-.04457	1.02261	.00599	.09521	1.02705	-.05483	-.00339	2.2204E-15
22	22	.75000	.25000	-.03345	.99541	.00402	.12871	1.00371	-.00743	-.01616	-6.2172E-15
23	23	.85000	.25000	-.01977	.94788	.00138	.13678	.95770	.08282	-.02041	-1.4211E-14
24	24	.95000	.25000	-.00628	.89990	-.00134	.11303	.90697	.17740	-.01418	-1.9540E-14
					END OF PANEL COLUMN 1, OF NETWORK 1						
25	1	.95000	.75000	.00628	.91445	-.02587	-.11486	.92200	.14992	-.00713	8.8818E-16
26	2	.85000	.75000	.01977	.97495	-.04018	-.14069	.98587	.02807	-.00847	8.8818E-16
27	3	.75000	.75000	.03345	1.03209	-.05047	-.13345	1.04191	-.08557	-.01229	7.1054E-15
28	4	.65000	.75000	.04457	1.08305	-.05371	-.10092	1.08996	-.18801	-.01768	-2.6645E-15
29	5	.55000	.75000	.05176	1.12124	-.04973	-.05673	1.12377	-.26286	-.02442	-4.8850E-15
30	6	.45000	.75000	.05492	1.14730	-.04003	-.01457	1.14809	-.31812	-.03481	2.8866E-15
31	7	.35000	.75000	.05476	1.16943	-.02663	.01871	1.16988	-.36863	-.04938	2.2204E-15
32	8	.25000	.75000	.05182	1.20891	-.01127	.05162	1.21007	-.46426	-.06451	3.1086E-15
33	9	.15400	.75000	.04536	1.28957	.00375	.12125	1.29526	-.67770	-.07895	-3.5527E-15
34	10	.07700	.75000	.03476	1.36773	.01444	.27685	1.39594	-.94793	-.09278	5.3291E-15
35	11	.02800	.75000	.02120	1.44540	.02031	.58498	1.55962	-1.63179	-.07442	-3.5527E-15
36	12	.00500	.75000	.00696	.99556	.02375	1.38582	1.70652	-1.91220	.01001	0.
37	13	.00500	.75000	-.00696	-.24486	.02665	.34085	.42053	.82316	.16172	-3.1974E-14
38	14	.02800	.75000	-.02120	.50386	.03012	-.20392	.54439	.70364	.14489	8.8818E-16
39	15	.07700	.75000	-.03476	.80793	.03424	-.16354	.82503	.31933	.12903	2.6645E-15
40	16	.15400	.75000	-.04536	.91683	.03786	-.08620	.92165	.15055	.09424	-4.4409E-15
41	17	.25000	.75000	-.05182	.97517	.03943	-.04164	.97685	.04575	.07103	4.4629E-15
42	18	.35000	.75000	-.05476	1.00193	.03867	-.01603	1.00281	-.00563	.05222	1.7764E-15
43	19	.45000	.75000	-.05492	1.02493	.03581	.01301	1.02524	-.05111	.03265	-3.0531E-15

FLOW PROPERTIES AT SOURCE PANEL BOUNDARY POINTS

ACCUM. NO.	NO.	XBP	YBP	ZBP	VX	VY	VZ	V	CP	SIGMA	VRN
44	20	.55000	.75000	-.05176	1.03981	.03028	.05261	1.04158	-.08490	.01464	-4.4409E-15
45	21	.65000	.75000	-.04457	1.03383	.02159	.09625	1.03852	-.07853	-.00056	1.3323E-15
46	22	.75000	.75000	-.03345	1.00428	.01003	.12985	1.01269	-.02554	-.01203	-1.7764E-15
47	23	.85000	.75000	-.01977	.95604	-.00272	.13796	.96594	.06695	-.01628	2.6645E-15
48	24	.95000	.75000	-.00628	.90605	-.01367	.11380	.91327	.16994	-.01198	-2.2204E-15

END OF PANEL COLUMN 2, OF NETWORK 1

FLOW PROPERTIES AT MULTI-HORSESHOE VORTEX BOUNDARY POINTS

ACCUM. NO.	NO.	XBP	YBP	ZBP	VX	VY	VZ	V	CP	SIGMA	VRN
49	1	1.00500	.25000	0.	.82051	-.002(	.00000	.82051	.32676	.28202	9.7700E-15
50	2	1.00500	.75000	-0.	.82386	-.01799	.00000	.82405	.32094	.20894	2.6645E-15

END OF NETWORK 1

FORCE AND MOMENT COEFFICIENTS ON SOURCE PANELS

FORCE AND MOMENT COEFFICIENTS PER PANEL COLUMN

COL.	CFX	CFZ	CMY	CL	CD	NET STRENGTH	AREA
1	-.014176	.146877	.002189	.141199	.010502	.000210	1.0150
2	-.009947	.103304	.004432	.103462	.008142	.000208	1.0150

END OF NETWORK 1

TOTAL FORCE AND MOMENT COEFFICIENTS

CFX	CFZ	CMY	CL	CD	NET STRENGTH	AREA
-.048247	.488362	.013240	.489320	.037289	.000837	4.0599

REFERENCE GEOMETRY

XR	YR	ZR	SR	CR	BR
.2500	0.	0.	2.0000	1.0000	2.0000

STREAMLINE NO. 1

SOLUTION NO. 2 (ALPHA = 4.0000 DEG. PSI = -0. DEG.)

ACCUM. NO.	I	J	K	NO.	XS	YS	ZS	VX	VY	VZ	V	DS	EE	DDE	EX	DCX
1	1	1	1	1	.9500	.2502	.0063	.9230	-.0031	-.1159	.9303	.1008	4	.5000	2	.500
2	2	1	1	2	.8500	.2505	.0198	.9873	-.0040	-.1625	.9976	.1010	4	.4993	2	.501
3	3	1	1	3	.7500	.2510	.0335	1.0494	-.0045	-.1357	1.0581	.1008	4	.4985	2	.502
4	4	1	1	4	.6500	.2514	.0446	1.1021	-.0045	-.1026	1.1069	.1004	4	.4977	2	.503
5	5	1	1	5	.5500	.2518	.0518	1.1361	-.0040	-.0575	1.1375	.1001	4	.4968	2	.503
6	6	1	1	6	.4500	.2521	.0549	1.1540	-.0031	-.0147	1.1541	.1000	4	.4961	2	.504
7	7	1	1	7	.3500	.2523	.0548	1.1649	-.0018	.0186	1.1651	.1000	4	.4956	2	.504
8	8	1	1	8	.2500	.2524	.0518	1.1855	-.0005	.0506	1.1865	.1001	4	.4953	2	.504
9	9	1	1	9	.1540	.2524	.0454	1.2258	.0007	.1153	1.2312	.0924	4	.4952	2	.504
10	10	1	1	10	.0770	.2523	.0348	1.2466	.0017	.2523	1.2719	.0633	4	.4953	2	.504
11	11	1	1	11	.0280	.2522	.0212	1.2155	.0023	.4920	1.3113	.0388	4	.4955	2	.504
12	12	1	1	12	.0050	.2522	.0070	.6738	.0027	.9379	1.1549	.0171	4	.4956	2	.504

END OF STREAMLINE

STREAMLINE HAS REACHED A NEAR STAGNATION REGION

ACCUM. NO.	I	J	K	XBP	YBP	ZBP	VX	VY	VZ	V	
12	12	1	1	.0050	.2500	.0070	.6738	.0027	.9379	1.1549	LAST PANEL TRAVERSED
13	13	1	1	.0050	.2500	-.0070	.0883	.0030	-.1230	.1514	PANEL S.L. FAILED TO ENTER

STREAMLINE NO. 1

VELOCITY DERIVATIVE AT POINT 80 VS. DISTANCE ALONG STREAMLINE

NO.	X80	Y80	Z80	VX80	VY80	VZ80	V80.S	DVTDST	S
1	.95000	.25051	.00628	.92910	-.00313	-.06760	-.0000086	-.0169	.0504
2	.85000	.25051	.01977	.99560	-.00397	-.08519	-.0000128	-.0251	.1513
3	.75000	.25051	.03345	1.05793	-.00452	-.06958	-.0000160	-.0313	.2522
4	.65000	.25051	.04457	1.10880	-.00455	-.03099	-.0000170	-.0334	.3529
5	.55000	.25051	.05176	1.14002	-.00403	.02023	-.0000159	-.0312	.4532
6	.45000	.25051	.05492	1.15525	-.00307	.08237	-.0000131	-.0256	.5532
7	.35000	.25051	.05476	1.16275	-.00184	.15264	-.0000091	-.0179	.6532
8	.25000	.25051	.05183	1.17801	-.00051	.22509	-.0000047	-.0091	.7533
9	.15400	.25051	.04536	1.20658	.00074	.31970	-.0000002	-.0005	.8495
10	.07700	.25051	.03476	1.20358	.00170	.46503	.0000032	.0063	.9274
11	.02800	.25051	.02120	1.17754	.00232	.58582	.0000054	.0105	.9784
12	.00500	.25051	.00696	.93622	.00270	.74937	.0000067	.0132	1.0064

END OF AERODYNAMIC SECTION

EXIT

BOUNDARY-LAYER PROGRAM SAMPLE CASE

The data input sheet for the analysis of the Rotta body boundary layer and the computer output from this analysis are shown on the following pages. The first line on the input sheet contains the title; the second line contains the constants and control numbers of the problem. The format for this second line is floating point without an exponential. The remaining lines on the input sheet contain the tabulated velocity and divergence data for the streamline. The format for these cards is floating point, with or without an exponential. If an exponential expression is used, the exponential number must be right-adjusted in the field.

The computer output presents the input data, followed by the boundary-layer solution. The solution values are all printed in exponential format, whereas the data cards are printed as they appear on the input sheet. An error message may be printed after the last solution. This indicates the method by which the program left the computer and should be disregarded. An error message preceded by a statement in the solution concerning the nature of the boundary-layer parameters indicates a boundary-layer growth that has reached an impossible condition (negative shape factor or momentum thickness). The output for that analysis contains the solution up to the point at which the faulty parameter was recognized. The step size of such an output is always the integration step size, regardless of the prescribed value of STEP.

In the sample case presented here, only one streamline was analyzed. Since the boundary-layer analysis was completed, no error statement occurred.

SEVEN FIELD, TEN DIGIT CRD FORMAT

1 10	11 20	21 30	31 40	41 50	51 60	61 69/70 71 72	IDENT 80
ROTTA BODY							TITLE
.0001	20.	9660000.	0.01	1.04	1.0		
0.	1.046	1.569					1
.055	.982	1.56138					2
.11	.954	1.5359					3
.163	.945	1.52145					4
.215	.93	1.488					5
.267	.912	1.2768					6
.321	.914	-1.0968					7
.375	.935	-1.24355					8
.428	.947	-1.29739					9
.482	.961	-1.29735					10
.535	.979	-1.2727					11
.586	1.025	-1.148					12
.64	1.09	-.763					13
.695	1.13	-.0565					14
.748	1.14	.7866					15
908	1.109	1.68568					16
.855	1.036	2.4864					17
.908	.953	3.2402					18
95	897	3.80328					19
1.006	.828	4.6368					20
TITLE SAMPLE CASE FOR BOUNDARY LAYER PROGRAM			NAME		DATE	PAGE 1 OF 1	

ROTTA BODY

A= .00010 XM= 20 RINF= 9660000 STEP= .01000 SL= 1.04000 FLAG= 1

S	V	DVT/DST
0.	1.04600	1.56900
.05500	.98200	1.56138
.11000	.95400	1.53590
.16300	.94500	1.52145
.21500	.93000	1.48800
.26700	.91200	1.27680
.32100	.91400	-1.09680
.37500	.93500	-1.24355
.42800	.94700	-1.29739
.48200	.96100	-1.29735
.53500	.97900	-1.27270
.58600	1.02500	-1.14800
.64000	1.09000	-.76300
.69500	1.13000	-.05650
.74800	1.14000	.78660
.80800	1.10900	1.68508
.85500	1.03600	2.40640
.90800	.95300	3.24020
.95000	.89700	3.80328
1.00600	.82800	4.63680

S	CF	THETA	M	V	DV/DS	K1
3.40000E-02	3.94393E-03	1.00000E-04	1.50000E+00	8.28000E-01	1.26344E+00	-5.60000E+00
4.40000E-02	4.07132E-03	1.08846E-04	1.46249E+00	8.40700E-01	1.27655E+00	-5.34363E+00
5.40000E-02	4.13219E-03	1.17550E-04	1.43716E+00	8.53531E-01	1.28966E+00	-5.09403E+00
6.40000E-02	4.15953E-03	1.25945E-04	1.41851E+00	8.66493E-01	1.30276E+00	-4.85100E+00
7.40000E-02	4.17029E-03	1.33975E-04	1.40367E+00	8.79586E-01	1.31587E+00	-4.61437E+00
8.40000E-02	4.17198E-03	1.41646E-04	1.39129E+00	8.92810E-01	1.32898E+00	-4.38396E+00
9.40000E-02	4.16956E-03	1.48981E-04	1.38060E+00	9.06174E-01	1.34587E+00	-4.15965E+00
1.04000E-01	4.16247E-03	1.55993E-04	1.37109E+00	9.19725E-01	1.36297E+00	-3.94162E+00
1.14000E-01	4.15399E-03	1.62750E-04	1.36258E+00	9.33406E-01	1.37211E+00	-3.72932E+00
1.24000E-01	4.14311E-03	1.69329E-04	1.35495E+00	9.47141E-01	1.37332E+00	-3.52202E+00
1.34000E-01	4.12996E-03	1.75797E-04	1.34806E+00	9.60856E-01	1.36850E+00	-3.31891E+00
1.44000E-01	4.11546E-03	1.82161E-04	1.34163E+00	9.74574E-01	1.37110E+00	-3.11944E+00
1.54000E-01	4.10011E-03	1.88443E-04	1.33597E+00	9.88310E-01	1.37538E+00	-2.92344E+00
1.64000E-01	4.08416E-03	1.94662E-04	1.33052E+00	1.00207E+00	1.37588E+00	-2.73273E+00
1.74000E-01	4.06756E-03	2.00851E-04	1.32542E+00	1.01582E+00	1.37472E+00	-2.54621E+00
1.84000E-01	4.05023E-03	2.07045E-04	1.32063E+00	1.02954E+00	1.37151E+00	-2.36477E+00
1.94000E-01	4.03596E-03	2.12981E-04	1.31570E+00	1.04367E+00	1.43934E+00	-2.18718E+00
2.04000E-01	4.02372E-03	2.18697E-04	1.31072E+00	1.05822E+00	1.45656E+00	-2.01312E+00
2.14000E-01	4.00775E-03	2.24654E-04	1.30635E+00	1.07253E+00	1.39406E+00	-1.84302E+00
2.24000E-01	3.98364E-03	2.31328E-04	1.30307E+00	1.08585E+00	1.25762E+00	-1.68069E+00
2.34000E-01	3.94595E-03	2.39123E-04	1.30115E+00	1.09749E+00	1.09039E+00	-1.52390E+00
2.44000E-01	3.91108E-03	2.47557E-04	1.29973E+00	1.10806E+00	1.02314E+00	-1.37182E+00
2.54000E-01	3.87239E-03	2.56473E-04	1.29853E+00	1.11781E+00	9.34556E-01	-1.22353E+00
2.64000E-01	3.83901E-03	2.66208E-04	1.29788E+00	1.12630E+00	7.73510E-01	-1.07900E+00
2.74000E-01	3.79219E-03	2.77085E-04	1.29801E+00	1.13314E+00	5.86001E-01	-9.37032E-01

2.84000E-01	3.72723E-03	2.89475E-04	1.29915E+00	1.13793E+00	3.62029E-01	-8.00238E-01
2.94000E-01	3.66356E-03	3.03808E-04	1.30155E+00	1.14024E+00	8.92671E-02	-6.65032E-01
3.04000E-01	3.58977E-03	3.20575E-04	1.30544E+00	1.13971E+00	-1.83181E-01	-5.30359E-01
3.14000E-01	3.50984E-03	3.39590E-04	1.31040E+00	1.13681E+00	-3.85502E-01	-3.95504E-01
3.24000E-01	3.42836E-03	3.60469E-04	1.31590E+00	1.13224E+00	-5.17735E-01	-2.61163E-01
3.34000E-01	3.34910E-03	3.82749E-04	1.32143E+00	1.12669E+00	-5.79880E-01	-1.27995E-01
3.44000E-01	3.27564E-03	4.05843E-04	1.32646E+00	1.12088E+00	-5.72747E-01	2.69047E-03
3.54000E-01	3.20576E-03	4.30031E-04	1.33129E+00	1.11470E+00	-6.73288E-01	1.33486E-01
3.64000E-01	3.13402E-03	4.56366E-04	1.33670E+00	1.10750E+00	-7.60882E-01	2.67154E-01
3.74000E-01	3.06194E-03	4.84673E-04	1.34250E+00	1.09959E+00	-8.16424E-01	3.99620E-01
3.84000E-01	2.99103E-03	5.14828E-04	1.34844E+00	1.09128E+00	-8.30841E-01	5.26996E-01
3.94000E-01	2.92285E-03	5.46956E-04	1.35431E+00	1.08287E+00	-8.25548E-01	6.44387E-01
4.04000E-01	2.85863E-03	5.79247E-04	1.35965E+00	1.07464E+00	-8.31528E-01	7.47313E-01
4.14000E-01	2.79474E-03	6.14040E-04	1.36508E+00	1.06615E+00	-8.64291E-01	8.38292E-01
4.24000E-01	2.73106E-03	6.50928E-04	1.37104E+00	1.05742E+00	-8.77967E-01	9.19186E-01
4.34000E-01	2.66876E-03	6.89636E-04	1.37813E+00	1.04867E+00	-8.69156E-01	9.91329E-01
4.44000E-01	2.60890E-03	7.29851E-04	1.38435E+00	1.04007E+00	-8.35554E-01	1.05584E+00
4.54000E-01	2.55188E-03	7.71320E-04	1.39039E+00	1.03174E+00	-8.09861E-01	1.11246E+00
4.64000E-01	2.49787E-03	8.13983E-04	1.39619E+00	1.02371E+00	-8.01842E-01	1.16114E+00
4.74000E-01	2.44497E-03	8.58361E-04	1.40213E+00	1.01576E+00	-7.85689E-01	1.19944E+00
4.84000E-01	2.39414E-03	9.04082E-04	1.40800E+00	1.00804E+00	-7.56515E-01	1.23003E+00
4.94000E-01	2.34627E-03	9.50664E-04	1.41357E+00	1.00067E+00	-7.14242E-01	1.25559E+00
5.04000E-01	2.30236E-03	9.97533E-04	1.41858E+00	9.93799E-01	-6.58824E-01	1.27917E+00
5.14000E-01	2.26233E-03	1.04456E-03	1.42301E+00	9.87433E-01	-6.15823E-01	1.29970E+00
5.24000E-01	2.22543E-03	1.09187E-03	1.42698E+00	9.81479E-01	-5.75092E-01	1.31478E+00
5.34000E-01	2.19158E-03	1.13931E-03	1.43047E+00	9.75933E-01	-5.34003E-01	1.32573E+00
5.44000E-01	2.16074E-03	1.18671E-03	1.43345E+00	9.70799E-01	-4.92714E-01	1.33417E+00
5.54000E-01	2.13298E-03	1.23390E-03	1.43588E+00	9.66077E-01	-4.51764E-01	1.34211E+00
5.64000E-01	2.10872E-03	1.28042E-03	1.43781E+00	9.61838E-01	-3.93014E-01	1.35028E+00
5.74000E-01	2.08877E-03	1.32558E-03	1.43840E+00	9.58189E-01	-3.38356E-01	1.35770E+00
5.84000E-01	2.07204E-03	1.36974E-03	1.43849E+00	9.54998E-01	-3.02688E-01	1.36370E+00
5.94000E-01	2.05711E-03	1.41372E-03	1.43823E+00	9.52085E-01	-2.85844E-01	1.36801E+00
6.04000E-01	2.04219E-03	1.45853E-03	1.43806E+00	9.49217E-01	-2.88033E-01	1.37017E+00
6.14000E-01	2.02636E-03	1.50484E-03	1.43821E+00	9.46265E-01	-3.02786E-01	1.37078E+00
6.24000E-01	2.01003E-03	1.55250E-03	1.43858E+00	9.43292E-01	-2.92805E-01	1.38389E+00
6.34000E-01	1.99398E-03	1.60113E-03	1.43895E+00	9.40403E-01	-2.85382E-01	1.40413E+00
6.44000E-01	1.97811E-03	1.65086E-03	1.43933E+00	9.37586E-01	-2.78656E-01	1.41668E+00
6.54000E-01	1.96250E-03	1.70129E-03	1.43975E+00	9.34827E-01	-2.73102E-01	1.40162E+00
6.64000E-01	1.94713E-03	1.75210E-03	1.44023E+00	9.32109E-01	-2.73022E-01	1.34287E+00
6.74000E-01	1.93123E-03	1.80329E-03	1.44106E+00	9.29288E-01	-2.97631E-01	1.22814E+00
6.84000E-01	1.91429E-03	1.85450E-03	1.44246E+00	9.26256E-01	-3.03512E-01	1.06361E+00
6.94000E-01	1.89879E-03	1.90276E-03	1.44380E+00	9.23312E-01	-2.80610E-01	8.67747E-01
7.04000E-01	1.88679E-03	1.94551E-03	1.44453E+00	9.20721E-01	-2.29064E-01	6.57693E-01
7.14000E-01	1.88087E-03	1.97980E-03	1.44390E+00	9.18829E-01	-1.48082E-01	4.56211E-01
7.24000E-01	1.88235E-03	2.00391E-03	1.44150E+00	9.17829E-01	-5.58337E-02	2.72206E-01
7.34000E-01	1.89064E-03	2.01826E-03	1.43749E+00	9.17663E-01	1.83399E-02	9.31968E-02
7.44000E-01	1.90411E-03	2.02429E-03	1.43234E+00	9.18130E-01	7.17458E-02	-8.52158E-02
7.54000E-01	1.92113E-03	2.02364E-03	1.42653E+00	9.19017E-01	1.02816E-01	-2.60285E-01
7.64000E-01	1.94028E-03	2.01784E-03	1.42046E+00	9.20136E-01	1.08100E-01	-4.30115E-01
7.74000E-01	1.96083E-03	2.00787E-03	1.41433E+00	9.21391E-01	1.19754E-01	-5.98142E-01
7.84000E-01	1.98251E-03	1.99409E-03	1.40822E+00	9.22742E-01	1.49966E-01	-7.65434E-01
7.94000E-01	2.00652E-03	1.97535E-03	1.40183E+00	9.24342E-01	1.73358E-01	-9.33689E-01
8.04000E-01	2.03243E-03	1.95227E-03	1.39529E+00	9.26189E-01	1.90398E-01	-1.09467E+00
8.14000E-01	2.05963E-03	1.92596E-03	1.38874E+00	9.28152E-01	2.01190E-01	-1.23801E+00
8.24000E-01	2.08763E-03	1.89732E-03	1.38229E+00	9.30169E-01	2.06529E-01	-1.35531E+00
8.34000E-01	2.11623E-03	1.86705E-03	1.37594E+00	9.32299E-01	2.10984E-01	-1.44234E+00
8.44000E-01	2.14561E-03	1.83548E-03	1.36963E+00	9.34528E-01	2.28805E-01	-1.50416E+00
8.54000E-01	2.17557E-03	1.80316E-03	1.36336E+00	9.36873E-01	2.40200E-01	-1.54750E+00
8.64000E-01	2.20601E-03	1.77044E-03	1.35716E+00	9.39334E-01	2.53158E-01	-1.57857E+00
8.74000E-01	2.23671E-03	1.73766E-03	1.35105E+00	9.41888E-01	2.62016E-01	-1.60220E+00

8.84000E-01	2.26746E-03	1.70514E-03	1.34507E+00	9.44510E-01	2.62520E-01	-1.62102E+00
8.94000E-01	2.29784E-03	1.67334E-03	1.33929E+00	9.47152E-01	2.67810E-01	-1.62683E+00
9.04000E-01	2.32832E-03	1.64195E-03	1.33361E+00	9.49897E-01	2.82509E-01	-1.62360E+00
9.14000E-01	2.35930E-03	1.61065E-03	1.32791E+00	9.52823E-01	3.07118E-01	-1.61550E+00
9.24000E-01	2.39129E-03	1.57898E-03	1.32212E+00	9.56037E-01	3.37992E-01	-1.60818E+00
9.34000E-01	2.42393E-03	1.54726E-03	1.31630E+00	9.59489E-01	3.49632E-01	-1.60482E+00
9.44000E-01	2.45633E-03	1.51802E-03	1.31102E+00	9.62677E-01	3.06346E-01	-1.60367E+00
9.54000E-01	2.48388E-03	1.48993E-03	1.30600E+00	9.65840E-01	3.36542E-01	-1.60223E+00
9.64000E-01	2.51617E-03	1.45985E-03	1.30059E+00	9.69593E-01	4.24744E-01	-1.59965E+00
9.74000E-01	2.55407E-03	1.42548E-03	1.29419E+00	9.74493E-01	5.70953E-01	-1.59492E+00
9.84000E-01	2.60095E-03	1.38427E-03	1.28641E+00	9.81223E-01	7.77618E-01	-1.58708E+00
9.94000E-01	2.65576E-03	1.33741E-03	1.27749E+00	9.89716E-01	9.20537E-01	-1.57616E+00
1.00400E+00	2.71551E-03	1.28768E-03	1.26804E+00	9.99572E-01	1.05086E+00	-1.56304E+00
1.01400E+00	2.77929E-03	1.23603E-03	1.25829E+00	1.01074E+00	1.18354E+00	-1.54791E+00
1.02400E+00	2.84455E-03	1.18308E-03	1.24838E+00	1.02324E+00	1.31621E+00	-1.53086E+00
1.03400E+00	2.91647E-03	1.12961E-03	1.23847E+00	1.03707E+00	1.44889E+00	-1.51207E+00
1.04400E+00	2.98858E-03	1.07608E-03	1.22867E+00	1.05222E+00	1.58156E+00	-1.49164E+00
1.05400E+00	3.06264E-03	1.02267E-03	1.21901E+00	1.06870E+00	1.71424E+00	-1.46961E+00
1.06400E+00	3.13068E-03	9.69376E-04	1.20949E+00	1.08650E+00	1.84691E+00	-1.44598E+00

UNCLASSIFIED
Security Classification

DOCUMENT CONTROL DATA - R & D
(Security classification of title, body of abstract and indexing annotation must be entered when the overall report is classified)

1 ORIGINATING ACTIVITY (Corporate author) THE BOEING COMPANY Commercial Airplane Division P.O. Box 707, Renton, Washington 98055	2a. REPORT SECURITY CLASSIFICATION Unclassified 2b GROUP

3. REPORT TITLE

A General Method for Determining the Aerodynamic Characteristics of Fan-in-Wing Configurations–
Volume I, Theory and Application

4 DESCRIPTIVE NOTES (Type of report and inclusive dates)

Final Report

5. AUTHOR(S) (First name, middle initial, last name)

Paul E. Rubbert
Gary R. Saaris
Michael B. Scholey
Neil M. Standen
Richard E. Wallace

6 REPORT DATE	7a TOTAL NO. OF PAGES	7b NO OF REFS
December 1967	302	14

8a CONTRACT OR GRANT NO.	9a ORIGINATOR'S REPORT NUMBER(S)
DA 44-177-AMC-323(T) b PROJECT NO c. Task 1F125901A14234 d.	USAAVLABS Technical Report 67-61A 9b. OTHER REPORT NO(S) (Any other numbers that may be assigned this report) None

10 DISTRIBUTION STATEMENT

This document has been approved for public release and sale; its distribution is unlimited.

11 SUPPLEMENTARY NOTES	12. SPONSORING MILITARY ACTIVITY
None	Department of the Army U.S. Army Aviation Materiel Laboratories Fort Eustis, Virginia 23604

13 ABSTRACT

A general method is presented for the determination of aerodynamic characteristics of fan-in-wing configurations by means of incompressible potential-flow theory. The method is applicable to wings, flapped or unflapped, and to a wide variety of other potential-flow boundary-value problems. Arbitrary wing and inlet geometry, fan inflow distribution, thrust vectoring, angle of attack, angle of yaw, and flight speeds from hover through transition can be treated. The theoretical model is completely three dimensional, with no linearization of boundary conditions. The calculated results include pressure distributions, lift, induced drag and side force, pitching moment, rolling moment and yawing moment. The numerical potential-flow solution is obtained with source and vortex distributions on the boundary surfaces. The representation is composed of small, constant strength source sheet panels distributed over the exterior wing surfaces, internal vortex filaments which emanate from the wing trailing edge to provide circulation and to produce the trailing vortex sheet, and a vortex lattice across the fan face and along the periphery of the fan efflux. Source and vortex strengths are obtained by satisfying boundary conditions at discrete points on the boundary surfaces. Velocities and surface pressures are calculated from the induced effects of the source and vortex distributions. Internal fan loads, based on pressure and momentum relations across the fan and an assumed fan exit flow distribution, are added to integrated wing surface pressures to determine total forces and moments on a fan-in-wing configuration. The method has been programmed for use with a high-speed digital computer.

DD FORM 1 NOV 65 1473

UNCLASSIFIED
Security Classification

14 KEY WORDS	LINK A		LINK B		LINK C	
	ROLE	WT	ROLE	WT	ROLE	WT
Potential Flow Incompressible Flow VSTOL VTOL Lifting Wing						